



PB99-134496



*Excellence With Caring*

## FINAL REPORT



# RECYCLED AND VIRGIN PLASTICS IN

# FIBER REINFORCED CONCRETE

**FDOT State Job # 99700-7615**

**Contract # B-9118**

**WPI # 0510711**

**FAMU Project # 11-1902-129**

**By**

**Kamal S. Tawfiq, Ph.D., P.E.**

**DEPARTMENT OF CIVIL ENGINEERING  
FAMU-FSU COLLEGE OF ENGINEERING  
Tallahassee, Florida 32310-6046**

**Submitted to  
State of Florida  
Department of Transportation**

**August 30, 1998**



**FINAL REPORT**

**RECYCLED AND VIRGIN PLASTICS**  
**IN**  
**FIBER REINFORCED CONCRETE**

**FDOT State Job # 99700-7615**  
**Contract # B-9118**  
**WPI # 0510711**  
**FAMU Project # 11-1902-129**

**Submitted to**  
**State of Florida**  
**Department of Transportation**

**By**  
**Kamal S. Tawfiq, Ph.D., P.E.**


**DEPARTMENT OF CIVIL ENGINEERING**  
**FAMU-FSU COLLEGE OF ENGINEERING**  
**Tallahassee, Florida 32310-6046**

**PROTECTED UNDER INTERNATIONAL COPYRIGHT**  
**ALL RIGHTS RESERVED.**  
**NATIONAL TECHNICAL INFORMATION SERVICE**  
**U.S. DEPARTMENT OF COMMERCE**

**August 30, 1998**





1. Report No.		 PB99-134496		3. Recipient's Catalog No.	
4. Title and Subtitle Recycled and Virgin Plastic in Fiber Reinforced Concrete				5. Report Date	
				6. Performing Organization Code	
7. Author(s)				8. Performing Organization Report No.	
9. Performing Organization Name and Address FAMU/FSU College of Engineering Department of Civil Engineering 2525 Pottsdamer Street Tallahassee, FL 32316				10. Work Unit No.	
				11. Contract or Grant No.	
12. Sponsored Agency Name and Address State of Florida Department of Transportation Research Center 605 Suzanne Street, M.S. 30 Tallahassee, FL 32301				13. Type of Report and Period Covered Final Report October 1994 to August 1997	
				14. Sponsoring Agency Code	
15. Supplementary Notes Prepared in cooperation with the Federal Highway Administration					
16. Abstract <p>Microcracking is an unavoidable occurrence in concrete structures subjected to various environmental and loading conditions. Its presence may be due to the inherent voids and discontinuities in concrete matrix or may develop as a result of stress concentration in weak zones in concrete. However, the severance of the development and progression of microcracking in concrete can be restrained and controlled by using concrete admixtures, and/or appropriate design and curing practices. Additionally, plastic and structural cracking can be eased off by strengthening the concrete paste with ductile inclusions such as steel or plastic fiber. Fiber with large aspect ratio has proven to improve the mechanical properties of concrete material. Because of some environmental constrained, plastic fiber has been favored over steel fiber. Plastic fiber is commercially produced from different polymers and shaped in different forms to serve certain concrete applications. The availability of various types of plastic fibers in the market today has caused some confusion over the suitability of one fiber over another. Many different commercial brands have been utilized on the trial and error basis in various concrete applications without tabulating the short and long term performances of the concrete. Research studies on the fiber reinforced concrete are spread out in literature in a way that became difficult for engineers to include the findings in any concrete design methodology. Adding to these difficulties is the fact that studies have been initiated on determining the index and basic properties of fiber reinforced concrete (FRC). The constitutional properties of FRC such as fatigue fracture behavior has been dealt with ambiguity. Most of these studies describe the effectiveness of plastic fiber in withholding macro-cracking or post-cracking. At that stage, unfortunately, the concrete structure is unusable. Thus, designers have hardly benefitted from the improved performance of plastic fiber. The question that still remains to be answered is which fiber would provide the best fatigue performance. This question has drawn the shade on the definition of fatigue performance of concrete. If the answer was to reduce the fatigue cracking and to prolong the fatigue life expectancy of concrete, the subsequent inquiry would be at what stage of cracking the inclusion of plastic fiber can add the performance of the structure. Moreover, does the improved performance justifies the increased cost of the FRC. The applicability of the plastic fiber in concrete especially in pavement structures and the answer to all of these questions have promoted the Florida Department of Transportation to initiate an investigation on the performance of plastic fiber in concrete specifically the feasibility of reducing the cost of FRC by adding fibers from recycled plastic and compare the performance with those prepared from fibers produced from virgin plastic. The results of this study is presented herein. In summary, although the performance of concrete has slightly been improved, the possibility of using recycled plastic in concrete pavement has economically been discounted after the added cost of reclassifying and preparing the plastic fibers has surpassed the cost of producing and acquiring virgin plastic fibers. The reason for that is simply due to the lack of an efficient technology that can mass produce the recycled fiber in a cost effective manner. Other economical factors have brought out during the fate of this study that reduced the cost of the virgin plastic and made it more cost-effective. Fatigue behavior of fiber reinforced concrete significantly improved by using mono-filament plastic fiber. For structural performance the choice should be a mono-filament plastic fiber with aspect ratio of 50 or more. Scanning Electron Microscope (SEM) investigation performed in this study indicated that, the higher the aspect ratio of the plastic fibers the denser is the accumulation of calcium hydroxide (CH) deposits and the higher is the chemical (adhesion) bonding between fiber and concrete paste. From the notched and unnotched beam samples prepared from different FRC mixes and tested in the laboratory under various stress ratios. Strain measurements versus number of cycles it was found that the addition of plastic fibers to the concrete matrix, in general, extended Stage I of crack initiation by about 18%, and prolonged Stage II of the crack propagation by 60%. Results from the finite element analysis (FEA) on fiber reinforced concrete have conformed to the laboratory test results. It is suggested that Stage III of fatigue cracking be neglected when estimating the total fatigue life expectancy of concrete structures. With the improved fatigue performance of the FRC, it would be advantageous to incorporate plastic fiber in pavement applications subjected to repetitive cyclic loading such as concrete pavement overlay and to reduce the overlay thickness taking advantage also from the increased ductility of the FRC. The Ultrathin White-Topping (UTW) concrete overlay would be the prime candidate for such FRC applications. Results obtained from this study can be used to set guidelines for the required plastic fiber in concrete.</p>					
17. Key Words Fiber Reinforced Concrete, Fatigue Fracture, Recycled Plastic			18. Distribution Statement No restriction. This document is available to the public through the National Technical Information Service, Springfield Va. 22161		
19. Security Classif. (of this report) Unclassified		20. Security Classif. (of this page) Unclassified		21. No. of Pages 223 Pages	



## **DISCLAIMER**

The opinions, findings and conclusions expressed in this publication are those of the authors and not necessarily those of the Florida Department of transportation and the Federal Highway Administration.

Prepared in cooperation with the Florida Department of Transportation and the Federal highway Administration.



## ACKNOWLEDGMENTS

The Principal Investigator would like to express his sincere regards to the Florida Department of Transportation represented by Dr. Jamshid Armaghani, State Pavement Evaluation Engineer, for managing this project and for providing his assistant and guidance to successfully complete this study. Many thanks also to Mr. Rodolfo Ruiz , a graduate research assistant, who prepared the required testing specimens and conducted the back-breaking laboratory fatigue testing on concrete beams. Financial support was provided by the Florida Department of Transportation, this support is gratefully acknowledged. The Department of Civil Engineering at FAMU-FSU College of Engineering has made it possible by providing the laboratory facilities for this project. Thanks to Dr. Peter Gillisy for allowing our team to use his valuable Scanning Electron Microscope (SEM) to instigate the deposition of the CH precipitants on plastic fibers.



# METRIC CONVERSION FACTORS

## Approximate Conversions to Metric Measures

Symbol	When You Know	Multiply by	To Find	Symbol
<b>LENGTH</b>				
in	inches	2.5	centimeters	cm
ft	feet	30	centimeters	cm
yd	yards	0.9	meters	m
mi	miles	1.6	kilometers	km
<b>AREA</b>				
sq in	square inches	6.5	square centimeters	cm <sup>2</sup>
sq ft	square feet	0.09	square meters	m <sup>2</sup>
sq yd	square yards	0.8	square meters	m <sup>2</sup>
sq mi	square miles	2.6	square kilometers	km <sup>2</sup>
acre	acres	0.4	hectares	ha
<b>MASS (weight)</b>				
oz	ounces	28	grams	g
lb	pounds	0.45	kilograms	kg
	short tons (2000 lb)	0.9	tonnes	t
<b>VOLUME</b>				
teaspoon	teaspoons	5	milliliters	ml
tablespoon	tablespoons	15	milliliters	ml
fluid ounce	fluid ounces	30	milliliters	ml
cup	cups	0.24	liters	l
pint	pints	0.47	liters	l
quart	quarts	0.95	liters	l
gallon	gallons	3.8	liters	l
cu ft	cubic feet	0.03	cubic meters	m <sup>3</sup>
cu yd	cubic yards	0.76	cubic meters	m <sup>3</sup>
<b>TEMPERATURE (exact)</b>				
°F	Fahrenheit temperature	5/9 (after subtracting 32)	Celsius temperature	°C

\* 1 in = 2.54 centimeters. For other exact conversions and more detailed tables, see NBS Spec. Publ. 286, Units of Weights and Measures, Part 2, 25, 50, 100, 150, 200, 250, 300, 350, 400, 450, 500, 550, 600, 650, 700, 750, 800, 850, 900, 950, 1000.

## Approximate Conversions from Metric Measures

Symbol	When You Know	Multiply by	To Find	Symbol
<b>LENGTH</b>				
mm	millimeters	0.04	inches	in
cm	centimeters	0.6	inches	in
m	meters	3.3	feet	ft
km	kilometers	1.1	yards	yd
		0.6	miles	mi
<b>AREA</b>				
cm <sup>2</sup>	square centimeters	0.16	square inches	sq in
m <sup>2</sup>	square meters	1.2	square yards	sq yd
ha	hectares (10,000 m <sup>2</sup> )	0.4	square miles	sq mi
		2.5	acres	acre
<b>MASS (weight)</b>				
g	grams	0.035	ounces	oz
kg	kilograms	2.2	pounds	lb
t	tonnes (1000 kg)	1.1	short tons	ton
<b>VOLUME</b>				
ml	milliliters	0.03	fluid ounces	fl oz
l	liters	2.1	pints	pt
		1.06	quarts	qt
		0.26	gallons	gal
m <sup>3</sup>	cubic meters	35	cubic feet	cu ft
		1.3	cubic yards	cu yd
<b>TEMPERATURE (exact)</b>				
°C	Celsius temperature	9/5 (then add 32)	Fahrenheit temperature	°F

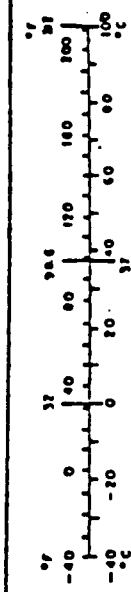


FIGURE 1. METRIC CONVERSION FACTORS





## TABLE OF CONTENTS

SECTION	Page
LIST OF TABLES	vii
LIST OF FIGURES	viii
EXECUTIVE SUMMARY	xii
 <b>CHAPTER I</b>	
<b>INTRODUCTION</b>	1
1.1 General	1
1.2 Problem Statement	3
1.3 Objectives	5
1.4 Scope	7
1.5 Report Organization	9
 <b>CHAPTER II</b>	
<b>LITERATURE REVIEW</b>	18
2.1 Fiber Reinforced Concrete (FRC)	18
2.2 Plastic Fibers	22
2.3 Fatigue Fracture of Concrete	23
2.4 Influence of Laboratory Loading Conditions	26
2.5 Fatigue Data Representation	32
2.6 Ultra-Thin Pavement Overlays	33
2.7 Finite Element Modeling (FEM)	34
 <b>CHAPTER III</b>	
<b>EXPERIMENTAL PROGRAM METHODOLOGY</b>	37
3.1 Introduction	37
3.2 Sample Size Selection	39
3.3 Mix Design	40
3.4 Sample Preparation	41
3.4.1 Mixing Procedures	42
3.4.2 Sample Curing	43
3.5 Sample Testing and Instrumentation	44
3.5.1 Strain Gauges	44
3.5.2 Testing Equipment	47
3.5.3 Data Acquisition System	48
3.6 Testing Procedures	49
3.6.1 Static Testing	51
3.6.2 Fatigue Testing	52
3.7 Field Testing	54

<b>SECTION</b>	<b>Page</b>
3.8 Finite Element Modeling (FEM)	55
<b>CHAPTER IV</b>	
<b>TEST RESULTS AND ANALYSIS</b>	72
4.1 Introduction	72
4.2 Fresh Properties of FRC	73
4.3 Compressive and Tensile Strength of FRC	76
4.4 Flexural Strength of FRC	77
4.5 Fatigue Strength of FRC	82
4.5.1 Hysteretic Behavior of FRC	82
4.5.2 Strain Analysis and Stiffness Degradation	84
4.5.3 Maximum Stress Ratio and Cycles Endured	87
4.6 Electronic Scanning Microscopy	89
4.7 Finite Element Analysis	91
4.7.1 Three-Dimensional Notched Beam F.E. Model	92
4.7.2 Ultra Thin Pavement Overlay Pavement F.E. Model	95
4.8 Ultra-Thin Pavement Overlay Field Results	96
<b>CHAPTER V</b>	
<b>CONCLUSION AND RECOMMENDATIONS</b>	214
5.1 Conclusions	214
5.2 Recommendations	218
<b>REFERENCES</b>	220

## LIST OF TABLES

<u>Table</u>	<u>Page</u>
2.1 Various Forms of Polypropylene Fibers Used to Reinforce Concrete	36
3.1 Concrete Mix Design	57
3.2 Physical Properties of Plastic Fibers	58
4.1 Fresh Properties of Fiber Reinforced Concrete	98
4.2 Stress Ratio (S), Number of Cycles Endured (N), and Speed of Cracking	99
4.3 Summary of Materials Properties Used in FEA	100



## LIST OF FIGURES

Figure	Page
1.1 Virgin Plastic Fibers	11
1.2 Recycled Post-Consumer PET fibers	12
1.3 Fiber Bridging Across a Crack	13
1.4 Vertical Mixing for the Fiber Reinforce Concrete	14
1.5 Horizontal Mixing for the Fiber Reinforce Concrete	15
1.6 Three-Dimensional FE Model for the Notched Beam	16
1.7 Three-Dimensional FE Model of Pavement Overlay	17
3.1 Beam Form Details	59
3.2 Flowchart Diagram of Experimental Program	60
3.3 Notched Concrete Beam Subjected to Cyclic Loading	61
3.4 Wheatstone Bridge Circuit	62
3.5 Unnotched Concrete Beam Under Cyclic Loading	63
3.6 Tensile Strength Test Setup	64
3.7 Typical Loading Configuration of Concrete Beam	65
3.8 Schematic Diagram of Test Setup	66
3.9 Schematic for Deflection Measurements	67
3.10 Schematic of Test Track	68
3.11 Test Track Strain Gage Locations	69
3.12 Three-Dimensional Loading of FE Beam Model	70
3.13 Loading Conditions of 3-D FE Pavement Overlay Model	71
4.1 Concrete Temperature Results	101
4.2 Slump of Concrete Test Results	102
4.3 Air Content of Concrete Test Results	103
4.4 Unit Weight of Concrete Test Results	104
4.5.a Preliminary Compression Test Results of Recycled HDPE	105
4.5.b Preliminary Compression Test Results of Recycled PET	106
4.6.a Compression Strength Development for FRC, FRB1 and FBR2	107
4.6.b Compression Strength Development for FRC, FBR3M	108
4.6.c Compression Strength Development for FRC and FBRME	109
4.6.d Compression Strength Development for FRC, FRB1 and FBR2	110
4.6.e Compression Strength Development for FRC, FBR3M	111
4.6.f Compression Strength Development for FRC and FBRME	112
4.7 Static Modulus of Elasticity Results	113
4.8 Tensile Strength Results for FBR1 and FBR2	114

<b>Figure</b>	<b>Page</b>
4.9 Tensile Strength Results for FBRME	115
4.10 Tensile Strength results for FBR3M	116
4.11 Flexural Strength Results for FBRC	117
4.12 Flexural Strength Results for FBRC	118
4.13 Flexural Strength Results for FBRC	119
4.14 Flexural Strength Results for FBRC	120
4.15 Flexural Strength Results for FBR1	121
4.16 Flexural Strength Results for FBR1	122
4.17 Flexural Strength Results for FBR2	123
4.18 Flexural Strength Results for FBR2	124
4.19 Flexural Strength Results for FBR2	125
4.20 Flexural Strength Results for FBR2	126
4.21 Flexural Strength Results for FBR2	127
4.22 Flexural Strength Results for FBRCNT	128
4.23 Flexural Strength Results for FBRCNT	129
4.24 Flexural Strength Results for FBRCNT	130
4.25 Flexural Strength Results for FBRCNT	131
4.26 Flexural Strength Results for FBRCNT	132
4.27 Flexural Strength Results for FBRME	133
4.28 Flexural Strength Results for FBRME	134
4.29 Flexural Strength Results for FBRME	135
4.30 Flexural Strength Results for FBR3M	136
4.31 Flexural Strength Results for FBR3M	137
4.32 Stress-Strain Relationship for FRC and Plain Concrete	138
4.32.a Strain Distribution in the Z direction of Plain Concrete Sample	139
4.32.b Strain Distribution in the Z direction of Fiber Reinforced Concrete	140
4.33 Schematic of Crack Development Stages	141
4.34 Delay of Crack Initiation at First Stage	142
4.35 Hysteresis Loops for FBR3M (S = 60% )	143
4.36 Hysteresis Loops for FBR3M (S = 73% )	144
4.37 Hysteresis Loops for FBR3M (S = 82% )	145
4.38 Hysteresis Loops for FBR1 (S = 67% )	146
4.39 Hysteresis Loops for FBR1 (S = 71% )	147
4.40 Hysteresis Loops for FBR1 (S = 74% )	148
4.41 Hysteresis Loops for FBR1 (S = 84% )	149
4.42 Hysteresis Loops for FBRME (S = 75%)	150
4.43 Hysteresis Loops for FBRME (S = 84%)	151
4.44 Hysteresis Loops for FBRME (S = 93%)	152
4.45 Strain Development for FBR3M (S = 60% )	153
4.46 Strain Development for FBR3M (S = 73% )	154
4.47 Strain Development for FBR3M (S = 82% )	155

Figure		Page
4.48	Strain Development for FBR1 (S = 67% )	156
4.49	Strain Development for FBR1 (S = 71% )	157
4.50	Strain Development for FBR1 (S = 74% )	158
4.51	Strain Development for FBR1 (S = 84% )	159
4.52	Strain Development for FBRME (S = 75%)	160
4.53	Strain Development for FBRME (S = 84%)	161
4.54	Strain Development for FBRME (S = 93%)	162
4.55	Stiffness Degradation for FBR1 (S = 67% )	163
4.56	Stiffness Degradation for FBR1 (S = 71% )	164
4.57	Stiffness Degradation for FBR1 (S = 74% )	165
4.58	Stiffness Degradation for FBR1 (S = 84% )	166
4.59	Stiffness Degradation for FBR3M (S = 60% )	167
4.60	Stiffness Degradation for FBR3M (S = 73% )	168
4.61	Stiffness Degradation for FBR3M ( S = 82% )	169
4.62	Stiffness Degradation for FBRME (S = 75%)	170
4.63	Stiffness Degradation for FBRME (S = 84%)	171
4.64	Stiffness Degradation for FBRME (S = 93%)	172
4.65	S-N curves for Plain Concrete and FRC	173
4.66	Calcium Formation on Fibrillated Fiber Surface	174
4.67	Fibrillated Fiber After Failure	174
4.68	Monofilament Fiber Bonded to Concrete	175
4.69	Monofilament Fiber Failed in Tension	175
4.70	Monofilament Fiber After Failure	176
4.71	Random Orientation of Fibers	176
4.72	Major Principal Stress ( $\sigma_1$ ) in a Plain Concret Notched Beam	177
4.73	Major Principal Stress ( $\sigma_1$ ) along the Notch Section A-A	178
4.74	Stress Distribution Across The Notch Section B-B	179
4.75	Crack Distribution in FRC at 45° Fiber Orientation (FEA)	180
4.76	Stress Distribution in FRC at 45° Fiber Orientation (FEA)	181
4.77	Crack Distribution in FRC at 90° Fiber Orientation (FEA)	182
4.78	Stress Distribution in FRC at 90° Fiber Orientation (FEA)	183
4.79	FEM Stress vs. Deflection Curve with 0° Fiber Orientation	184
4.80	FEM Stress vs. Deflection Curve with 0° Fiber Orientation	185
4.81	FEM Stress vs. Deflection Curve with 45° Fiber Orientation	186
4.82	FEM Stress vs. Deflection Curve with 90° Fiber Orientation	187
4.83	Stress Distribution On The Pavement Overlay (FEA)	188
4.84	Stress Distribution At The Overlay Edge (FEA)	189
4.85	Stress Distribution At The Middle Section (FEA)	190
4.86	Stress Distribution In Concrete Overlay at Middle Section (FEA)	191
4.87	Vertical Deflection At Middle Underneath Middle Tandem (FEA)	192
4.88	Vertical Deflection Along The Pavement From FEA	193

<b>Figure</b>		<b>Page</b>
4.89	Results from Pavement Overlay Field Testing (Pass #2, Gage #1)	194
4.90	Results from Pavement Overlay Field Testing (Pass #2, Gage #2)	195
4.91	Results from Pavement Overlay Field Testing (Pass #2, LVDT #1)	196
4.92	Results from Pavement Overlay Field Testing (Pass #2, LVDT #2)	197
4.93	Results from Pavement Overlay Field Testing (Pass #2, LVDT #4)	198
4.94	Results from Pavement Overlay Field Testing (Pass #5, Gage #1)	199
4.95	Results from Pavement Overlay Field Testing (Pass #5, Gage #2)	200
4.96	Results from Pavement Overlay Field Testing (Pass #5, LVDT #1)	201
4.97	Results from Pavement Overlay Field Testing (Pass #5, LVDT #2)	202
4.98	Fiber Reinforced Concrete Placing Over Crack Relief Layer	203
4.99	Placing of Plain Concrete	204
4.100	Preparation of Control Ultra-Thin Concrete Slab	205
4.101	Screeding of Fiber Reinforced Concrete	206
4.102	Screeding of Fiber Reinforced Concrete	207
4.103	Ultra-Thin Pavement Overlay Surface Finishing	208
4.104	Joint Cutting 8 Hours After Placing Concrete	209
4.105	Ultra-Thin Pavement Top View and Thermocouple Leadwire	210
4.106	Instrumentation of Ultra-Thin Surface Using Strain Gauges	211
4.107	Loading of Ultra-Thin Pavement Using 20-kip Per Axle Truck	212
4.108	Truck Loading Overlay Pavement and Outside Strain Gage	213



## EXECUTIVE SUMMARY

Concrete is one of the most common construction materials and is used in a wide variety of applications, ranging from piles to multistory buildings and from railroad ties to highway pavements. Ordinary concrete contains numerous micro-cracks, which are responsible for its low tensile strength. Reinforcement of concrete with discontinuous discrete plastic fibers offers a solution to this problem by enhancing its mechanical properties.

The experimental work was aimed to quantify the delay of fatigue crack initiation and further propagation in the concrete matrix due to the addition of plastic fibers. Virgin and Post-Consumer Recycled In-House made plastic fibers were used. For this purpose, cylinders as well as notched and unnotched specimens were prepared from different Fiber-Reinforced Concrete (FRC) mixes. Also, three full scale Ultra-Thin Pavement Overlays (Whitetopping) were prepared using different fibers and joint spacing. Concrete mixing for the cylinders and beams was done in the laboratory. FRC used on overlays was batched at a local concrete plant and delivered by a concrete mixing truck. All the specimens were cast and cured in the laboratory.

Fatigue test was performed on the beam specimens using reversed constant cyclic loading. Different Stress Ratios were applied for different specimens. Number of cycles (N) and strain data, obtained using strain gauges, was acquired until specimen failure. Furthermore, the study includes the strain evolution of FRC compared to ordinary concrete, correlation between strain rate and cycles to failure, stiffness degradation to cycles to failure and a hysteretic behavior analysis. Reinforcement of the analytical investigation was made using finite element analysis where different materials and geometrical parameters were

incorporated in different three-dimensional numerical models.

The background literature review covers only relevant aspects related to this study such as concrete fiber matrix composition, loading conditions, applications, use of recycled plastic material and application of numerical models to FRC.

Part of this manuscript was dedicated to the testing and experimental procedures for the different FRC mixes under cyclic loading. The effects of loading application from beginning to failure of the specimen was study. The damage occurred on the specimen due to different loading histories was examined through analysis of data and numerical models.

The experimental results and analysis indicated three main stages for the fatigue life of the specimen. **Stage I** or *crack initiation* period, starts immediately after the load is applied, the rate of strain is very high and gets stable before reaching **Stage II** or *crack propagation* stage. During this period the strain accumulation is very much constant. The last part of the fatigue life is **Stage III** or *rapid crack propagation*, the strain rate becomes significantly higher and takes the matrix rapidly into failure.

It was found that the addition of plastic fibers to the concrete produces an extension of **Stage I** of about 18% and prolongs **Stage II** of the crack propagation by about 60%. The results from the numerical models conformed the laboratory test results. Finally, it is suggested to eliminate **Stage III** when estimating the fatigue life of concrete.

# CHAPTER 1

## INTRODUCTION

### **1.1 General**

The durability of brittle material has been the concern of engineers since ancient times when bricks were reinforced using straw. In the last five decades increased efforts have been made by researchers to better understand the underlying mechanics of concrete, specially its durability. Many structures such as bridges, airfields, highway pavements, dams and many other man-engineered structures are erected using concrete. These structures undergo repeated load application during their life span which produces a strength and stiffness degradation decay of concrete better known as *fatigue*. In fact, fracture of concrete as a result of fatigue is the most predominant cause of structural failure due to its inherent low tension handling capacity. This limitation of concrete yields to easier fracture or cracking even before the loading process starts. The incorporation of discrete discontinues virgin or post-consumer recycled plastic fibers to concrete help to control this disadvantage. The plastic fibers behaves similarly to any aggregate which is a crack arrestor. The crack travels around the aggregate thus requiring more energy to continue its growth. Once the crack has passed the aggregate, it does not offer more crack arresting capabilities.

However, plastic fibers do offer this capability even after a micro-crack formation exist without losing any of their material properties. The fibers will hold the crack walls together by virtue of their tensile strength and the mechanical bond strength from the concrete matrix and the fiber. Hence, fibers not only require to be an increase of energy for a crack initiation to take place, but also there must be an increase for the energy needed to propagate the crack. Thus, the crack initiation stage is controlled and the crack propagation stage is prolonged with the addition of low percentage by volume (0.5% to 1.6%) of discrete virgin or post-consumer recycled plastic fibers to the concrete.

The improved toughness resistance, tensile strength, flexural strength, plastic shrinkage control as well as fatigue strength increase are also amongst the advantages offered by the integration of plastic fibers to the concrete. The improvements offered by fiber-reinforced concrete have led to a wide spread use in applications such as ultra-thin white topping, highway pavements, airfields, and repair of infrastructure facilities. These improvements would suggest a widely acceptance of this important structural material, however, it is not the case due to the lack of design guidelines and engineering experience with this concrete technology.

A fiber is defined as a thin plastic strand of varying cross-sectional shape and length. In the case of fibers used for concrete reinforcement the length is from  $\frac{1}{2}$ " to  $2\frac{1}{2}$ " and a diameter which will be in the order of 5 to 20 mils. The ratio of the width to the length of the fiber is defined as the aspect ratio and is a very important factor which will be consider

later on this manuscript. The most common materials used for manufacturing fiber for concrete reinforcement are steel, glass and synthetic fibers. The latter has gain the most popularity because of the excellent properties it offers, namely high modulus of elasticity, high yield strength, alkaline resistant, and ultraviolet rays resistance to name a few. Fibers distribute randomly during concrete mixing and are only effective to the extent that they are parallel to the tensile force and perpendicular to the crack. However, cracks not always run perpendicular to the tensile forces and fibers are needed to prevent fracture in any direction.

The purpose of this project is to investigate the fresh and harden properties of plastic fiber-reinforced concrete (FRC) in order to have a comprehensive and reliable data base to be able to fully comprehend the mechanical and damage accumulation processes which are complicated by the addition of fibers. This data would help building finite element numerical models to better understand the stress and strain behavior of this structural material and the effects of fiber orientation. Furthermore, to help establish data for future design guidelines which in fiber-reinforced concrete is all but non existent.

## **1.2 Problem Statement**

In the state of Florida there exist about 2000 lane miles of concrete pavements and about 8100 bridges made of concrete. Approximately, 1500 of these structures are functionally obsolete and 250 of them are structurally deficient. The biggest weakness of these structures are primarily related to the concrete material performance. The **Florida Department of Transportation (FDOT)**, has involved in extensive research, investigation

and condition evaluation of these structures. The main objective has been to develop better performance and durability of the concrete materials.

The performance and durability of various concretes under repeated fluctuated loading are mainly affected by cracking (crack initiation and crack propagation) and premature distress. The control of early cracking as well as post loading cracking can result in improved efficiency and longer life span of the concrete materials. These goals can be achieved by improving the quality of concrete materials, mechanical properties of the concrete and construction procedures.

The addition of discrete discontinuous virgin and/or post-consumer recycled plastic fibers to the concrete materials would improve the low tensile strain capacities and their low tensile strength. The different types of fiber are presented on Fig. 1.1 and Fig. 1.2. The incorporation of these randomly distributed fibers help the pre-loading and post-loading crack control. The fibers bridge across the concrete matrix (Fig. 1.3) helping to control the shrinkage cracking during the plastic stage and matrix micro cracks that occur as the concrete is loaded and so providing post-cracking ductility. If the fibers develop sufficient bond strength with the matrix and by virtue of their high tensile strength capability, they will ensure both that the crack remains small and that the composite material can still withstand significant stress in the strain-softening stage. The addition of low percentage by volume (maximum of 1%), will produce modest increase in the strength of the resulting composite. However, at much higher rates (up to 3%), by volume considerable increases in strength and strain capacity will be developed by concrete.

The mechanical properties and durability of the concrete used in the state of Florida can be improved with the addition of high-strength plastic fibers which will at the end improve the ultimate strength and fatigue strength properties. The use of fibers made out of virgin or post-consumer recycled synthetic materials would be the proper selection as they would be able to resist high alkaline environment, possess ultra-violet ray resistance, possess long-term durability and exhibit high tensile strength. The use of post-consumer recycled Polyethylene Terephthalate (PET) has shown satisfactory results compared to FRC reinforced with virgin synthetic materials such as Polypropylene. The addition of post-consumer recycled materials to concrete will both help improve the mechanical properties of concrete and also help Florida's environment by reducing plastic wastes.

The main goal of this research will be to evaluate and select the best synthetic fibers that will reduce plastic shrinkage cracking, temperature cracking, energy absorption and increase fatigue strength by prolonging the crack propagation stage in concrete pavements.

### **1.3 Objectives**

The primary objectives of this study is to conduct a laboratory investigation to evaluate the intrinsic stress that can cause cracking of concrete mixes recommended by the Florida Department of Transportation with the addition of monofilament and fibrillated polypropylene and monofilament polyolefin fibers, subjected to highly cyclic loading. In addition, the flexural behavior of concrete reinforced with recycled post-consumer in-house made fibers will be studied and Finite Element Methods (FEM) following laboratory work

would be used to establish comparable numerical models for the flexural test and pavement overlays.

The aforementioned objectives are constituted as follows:

- Concrete pavement premature failure and fatigue cracking assessment in single-edge notched-beam (SENB) and unnotched beams under high cyclic constant amplitude loading. The assessment herein involved studying the influence of damage accumulation, stiffness degradation and life span of the beam through the number of cycles endured until failure.
- Behavioral comparison of the resulting composite, namely fiber-reinforced concrete (FRC), with the incorporation of different virgin (monofilament and fibrillated) synthetic fibers under cyclic loading.
- Defining the effect of various parameters on the fatigue life of fiber-reinforced concrete, and formulating these effects in a functional expression to facilitate the prediction of damage accumulation and stiffness degradation on the fatigue life expectancy of FRC used in the state of Florida.
- Study of the flexural behavior of fiber reinforced concrete using recycled post-consumer in-house made Polyethylene Terephthalate (PET) fibers.



- Incorporating the geometrical and material strength parameters to create and calibrate numerical models using Finite Element Methods in order to evaluate the effect of fiber orientation and facilitate the prediction of stress and strain values of fiber-reinforced concretes used in Florida.
- Field evaluation of Ultra-Thin Fiber Reinforced Pavement Overlays using different fibers, overlay thicknesses and slab dimensions.

#### **1.4 Scope**

The proposed research will study the fresh and mechanical properties of fiber-reinforced concrete, FRC. This work will extend the understanding of the structural properties of concrete materials used in Florida with the addition of virgin and post-consumer recycled synthetic fibers. The fatigue fracture parameters of fiber-reinforced concrete will be first study using notched and unnotched beams under flexure and constant cyclic loading. The understanding of these various parameters could help controlling the stress intensity factor, microstructural defects, crack intensity, crack length, crack growth rate and crack mouth opening to name a few. The use of classical linear elastic fracture mechanics cannot be used in concrete since it is a elasto-plastic-plastic material and not a linear plastic material. Thus, the use of modern computer programs, such as ANSYS 5.2, takes advantage of Finite Element Method (FEM) theory to analyze non-linear elasto-plastic

material such as concrete. Furthermore, the fracture parameters, namely the J-integral, crack intensity factor, and fatigue life of concrete can be analyzed using FEM methods.

Several representative parameters that influence the fatigue strength of FRC were identified and selected for this study. The parameters selected for this research project were thought of as the most influential parameters in concrete pavements used in Florida.

The selected parameter for this study included the following:

- Aggregate type and size
- Composite material properties
- Stress ratio applied during constant cycling loading
- Number of cycles
- Crack configuration (Notched or Unnotched beams)
- Type of synthetic material (Polypropylene, Nylon, Polyethylene, PET)
- Type of fiber (Monofilament, Collated Fibrillated fiber)
- Percentage of fiber addition (by volume)

The effect of fiber addition to the plastic properties of the concrete matrix will be investigated by measuring the changes in slump, temperature, unit weight and air content for each batch prepared. Furthermore, the effect of using an standard vertical rotation gravity mixer versus a “pan” or horizontal rotation mixer as well as workability of the mix and setting time will be assessed. The types of mixer used for this projects are presented on Figure 1.5 and 1.6, respectively

The crack initiation, propagation and rapid propagation stage will be measured during the constant cycle loading test or fatigue test. The data will be obtained by using strain gages placed below the tip of the notched, Fig. 1.4. Furthermore, the speed with which the crack travels in FRC will be measured by using the predetermined distance of the strain gauges 1 and 2 and measuring the time it takes a crack to travel from the first to the second gage.

Finally, the geometrical parameters as well as strength parameters of the concrete matrix and the synthetic fibers will be used to develop a single-edge-notch-beam and pavement model to investigate the effect of orientation of fibers. The beam will be used as a comparative model to the data developed in the laboratory. The pavement model will be used to help understand the effects of temperature, curling and different joint spacing on Ultra-thin pavement overlays. Both the beam and pavement overlay model are presented on Figure 1.7 and 1.8, respectively.

## **1.5 Report Organization**

This report is composed of five chapters. The first chapters is an introduction of the fiber-reinforced subject, a summary of this investigation and the scopes and goals to be achieved at the end of the project. The second chapter is a literature review for the different and most relevant research work that have taken place during the last three decades on fiber-reinforced concrete (FRC) . The review includes work performed on fresh material properties of FRC, mechanics of concrete fatigue fracture, fatigue cracking of FRC, and

efforts on numerical modeling of FRC using finite element methods.

The third chapter, presents the experimental details and the test set-up. This chapter is subdivided into four sections. First, on this chapter is presented the mix design, mixing procedures, specimen type and curing procedures. Secondly, coverage of the testing and instrumentation of the various specimens takes place. Next, it covers problems overcame and precautions taken to test FRC beam specimens under static and dynamic loading. The parametric considerations and developing of numerical model is cover in the last section of this chapter.

Chapter four describes the methods of analysis and explains the effect of testing and material parameters on fatigue fracture of FRC. Furthermore, the mathematical formulas developed based on the testing and numerical modeling findings are presented herein. The conclusions and recommendations are presented on the last chapter of this manuscript.

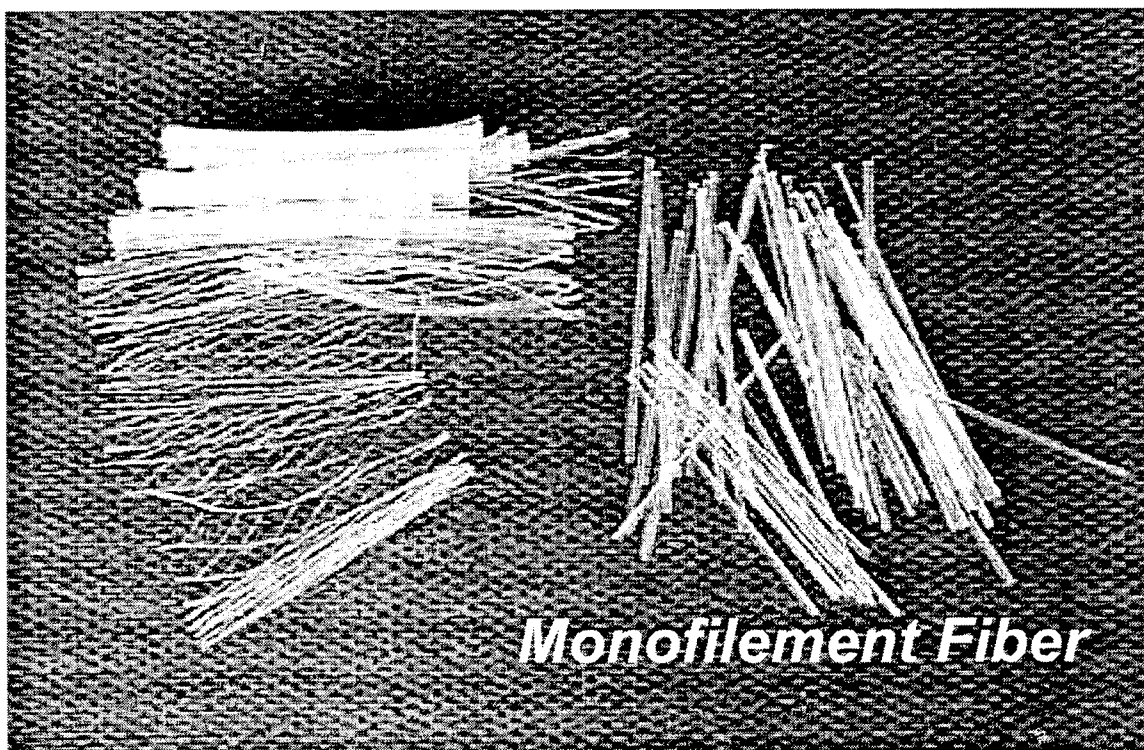


Figure 1.1 Virgin Plastic Fiber Used in the Study

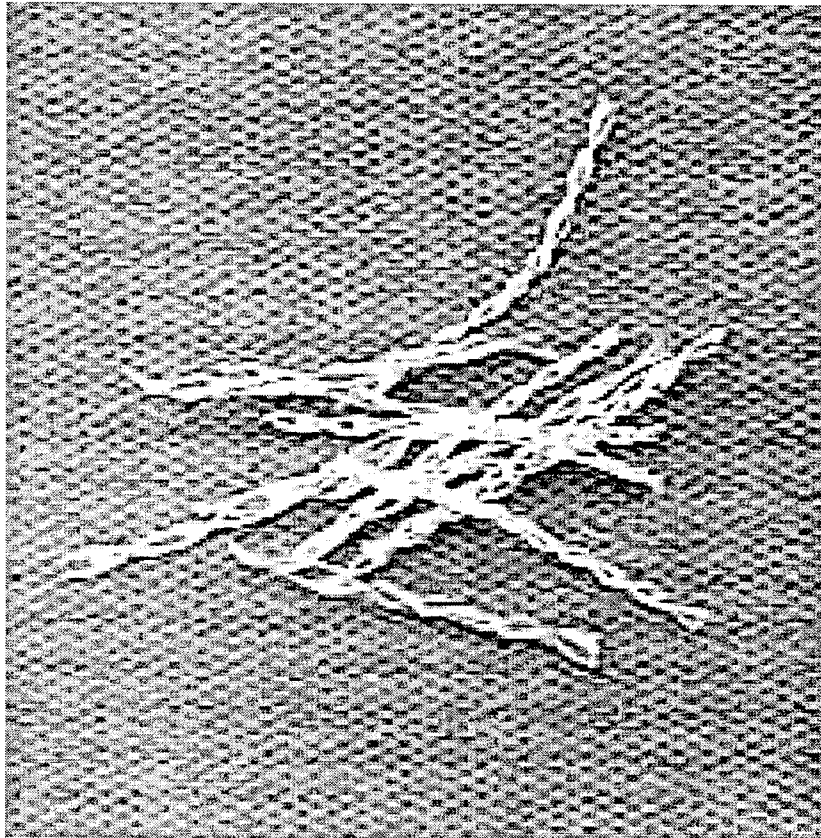
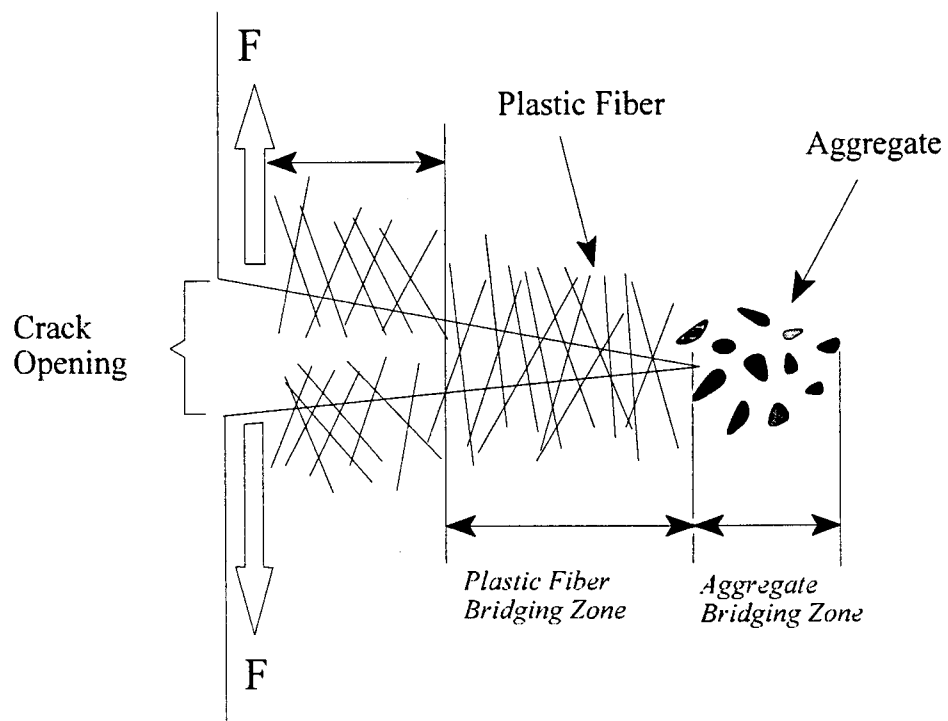
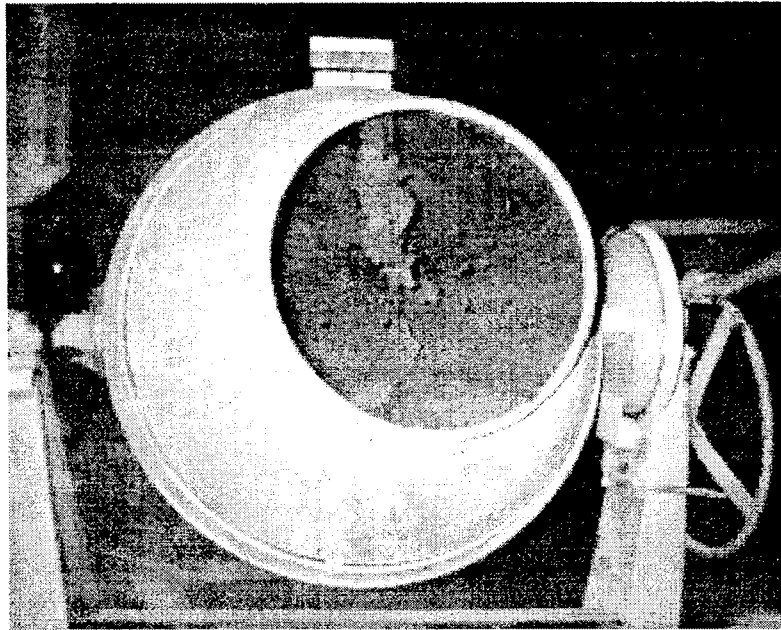


Figure 1.2 Recycled Post-Consumer PET Fiber

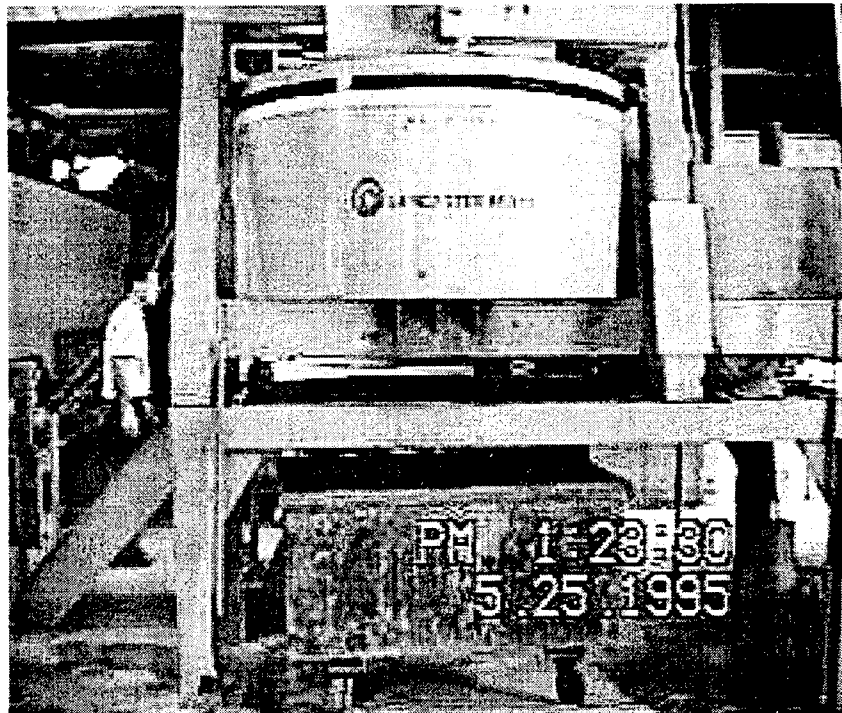


**Figure 1.3 Fiber Bridging Across a Crack**



**Figure 1.4 Vertical Mixing For Fiber Reinforced Concrete**





**Figure 1.5 Horizontal Mixing For Fiber Reinforced Concrete**

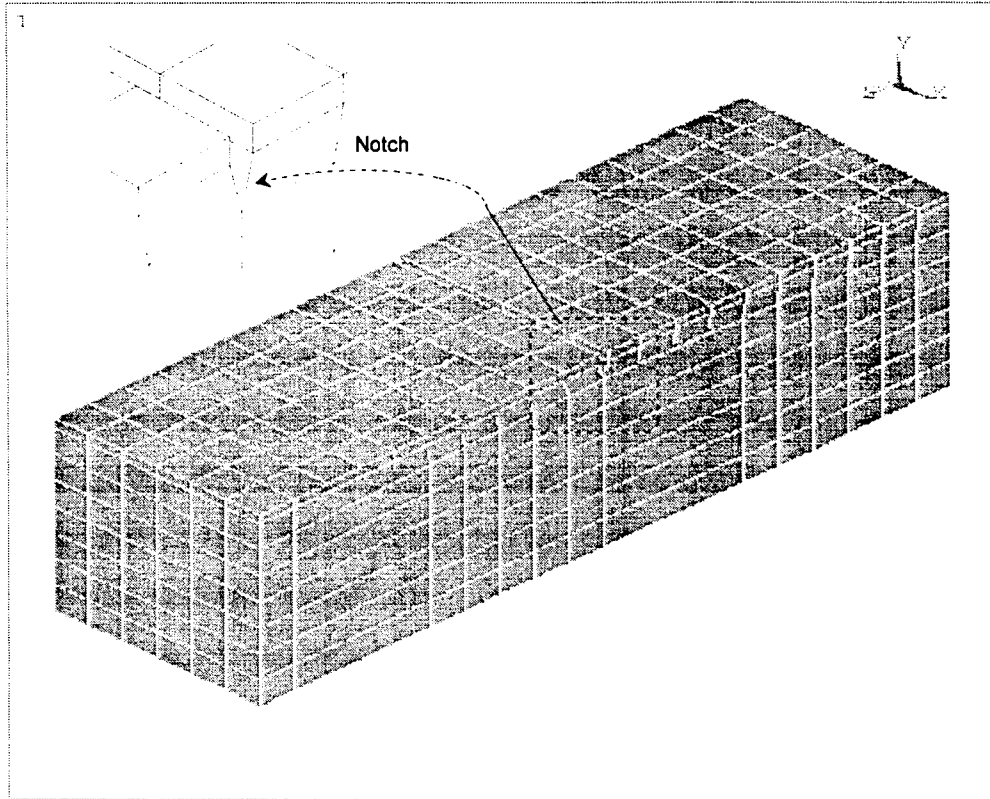


Figure 1.6 Three Dimensional FE Model for the Notched Beams

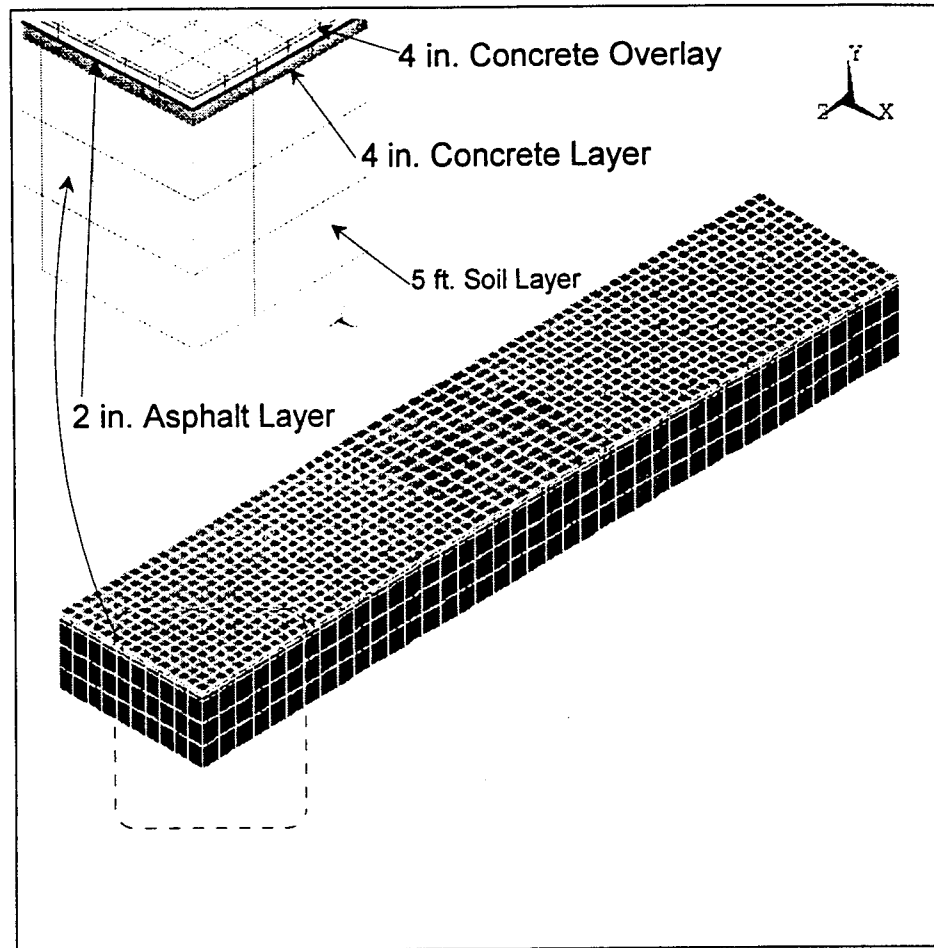


Figure 1.7 Three Dimensional FE Model of Pavement Overlay



## **CHAPTER II**

### **LITERATURE REVIEW**

#### **2.1 Fiber Reinforced Concrete (FRC)**

The incorporation of monofilament or collated fibrillated discrete discontinues fibers into a cement brittle matrix serve to increase the fracture toughness of the reinforced concrete by the result of the crack arresting process and increase of the flexural and tensile strength.

The fibers used as reinforcement exist in various types of materials, size, shapes and colors. The Egyptians during ancient times used straw to reinforce sun-baked bricks and horse hair to reinforce mortars. Also, natural fiber as bamboo were used for reinforcement of mortars. The main purpose of adding fiber to form a new composite was to keep brittle materials together. The modern manufacturing process and advanced technology have led the production of more sophisticated fibers made out of steel, synthetics material, glass and carbon materials. The last two decades there has been a wide-spread use of plastic fibers, particularly polypropylene fibers. In 1965 Shell Chemical Co. started investigations of Polypropylene (PP) to be used in concrete (Zonsveld, 1975). They realized that developments designed to utilize the mechanical bonding of the reinforcement were likely to be successful; thus, the production and marketing of a yarn with a net structure of fibrillated fibers, Figure 1.1, created to enhanced mechanical bonding with concrete matrix was the end

result. Shell Company was granted a U.S. patent in 1971 which claimed improved bending strength in concrete matrix with the incorporation of polypropylene fibers up to 2% by weight of cement (Zonsveld et al, 1971). Another U.S. patent in 1972 claimed that a great increase of impact strength can be obtained by incorporating less than 3% by weight of PP fibers (Ball et al, 1972). Since the early 1970's there has been more than twenty U.S. patents applications regarding the production of concrete products with superior properties as a result of incorporating polypropylene fibers. The main reason to select these fibers are: high strength, high Young's modulus, low weight (ACI Committee 544), alkali resistant, ultra-violet ray resistance, posses long term durability, fire resistance, abrasion resistance and unsusceptible to harsh environments.

The aspect ratio of straight fibers, as it is well known, has a considerable effect on the performance of fresh and hardened concrete. Paramasivan et al (1974) studied the effects of steel and nylon fiber addition to regular mesh reinforced concrete matrix. It was reported that fiber aspect ratio and spacing have a sound effect on the strength and toughness of the fiber-reinforced concrete. If both the volume of fibers and aspect ratio are increased, the fiber spacing will not decrease as much as it would have if the aspect ratio remains the same. An increase in fiber spacing was reported to decrease the crack arresting capabilities and therefore cause a loss in strength.

The use of plastic fibers have a significant effect on the rheological properties of fresh concrete. The slumps test (ASTM C143) used to evaluate the workability of fresh concrete mixes, have a nonlinear decrease with the volume concentration of fibers (Beaudion, 1990). The slump of typical concretes is decreased almost 30-50% with the addition of 0.1% PP

fibers. Furthermore, other workability tests, namely Vebe time and Compacting Factor, have shown that internal resistance of concrete mixes is increased steadily as the fiber volume addition is increased. The addition of fibers also has an effect on the amount of water that reaches the surface of the concrete, better known as bleeding, it is reduced by 50% or more. The amount of water that is bleed is probably collected by the fibers which may have a negative effect on their intrinsic efficiency.

The failure of fiber-reinforced matrix can be of various modes, including matrix or fiber failure in tension, fiber pull-out, and failure due to flawed fibers. Fiber pull-out is in direct relation to the bond strength of the fiber and the matrix. Similarly, bond strength which is an important factor for effective fiber-reinforced structural component design, it is directly related to the aspect ratio of the fiber. The cracking of the FRC matrix represents either a total failure or the load transferring to the fibers which will carry the additional load. In order for a composite reinforced with fiber to resist a load after matrix fracture, a minimum critical volume needs to be met which is a ratio of the ultimate strength of the matrix and fiber as well as the stress of the fiber, according to Bendouis, 1990. The critical volume of plastic fiber to be used as reinforcement to concrete is 0.75% by volume according to Mindess (1977). This percentage of fiber addition to concrete is the minimum amount need to be able to improve the tensile properties of the concrete. The maximum amount of fiber to be added it has been suggested as 3% by volume or more due to the concrete mixing limitations. However, percentages by volume of up to 15% have been used (Shah, 1991).

The aggregate size and the percentage of fibers are factors that have a bearing effect on the fiber orientation, which is very important in order to keep a high efficiency on the

crack arresting process of the fibers. In addition, the fiber type is another factor that affects fiber-reinforced concrete. The parameter affecting the strength and toughness of fiber-reinforced concrete were study by Swamy (1974). He makes relevance to the length of the fiber which significantly affects the strength of the composite. Also, the orientation of the fiber affect the stress on it, that is, if not properly oriented the stress is not constant along the entire length of the fiber, hence the total length is not being efficiently used to arrest the cracks. Depending on the orientation of the fiber, it could have little or no effect or it could have an efficiency of one. The fiber which are aligned perpendicular to the applied stress will not have any effect on the composite; however, if fibers are aligned and parallel to the applied stress they will be one-hundred percent efficient, as it is demonstrated by Cox's analysis (1952).

The surface treatment of fiber with a solution of alcohol alkoxylates has been used and reported to increase the bonding strength, which was also reflected on the prevention of massive crack propagation through the composite (Fahmy et al, 1988). Other studies have also show that the use of sulfur infiltrated and polymer impregnated fiber used as reinforcement exhibit better bonding as well as improvements on the overall strength of the concrete composite.

Ramakrishnan et al (1980) used different type of fibers and procedures when incorporating the fibers to the concrete matrix. Increase in pull-out strength of hooked end fibers compared to straight fibers were reported. Furthermore, it has been established on this report that addition of fiber to concrete considerably improves static flexural strength, impact strength, and fatigue strength. Johnston (1982) and Patton et al (1983) researched the



factors influencing flexural strength measurements. Johnston concluded that because of possible twisting the length of the beam has a significant effect on the flexural strength. The effects of loading due to the inhomogeneities of concrete were also studied. The beam size will have a great effect on fiber-reinforced concrete, since the fiber will orient differently depending on the beam size. The larger the beam the better and more randomly the fiber will distribute and be able to orient in all directions.

## **2.2 Plastic Fibers**

The use of polypropylene fibers to be used as reinforcement for concrete started in the 1960's (Goldfein, 1963). Since then several forms of polypropylene fibers have been used for concrete reinforcement, Table 2.1. The Polypropylene (PP) fibers became stronger as a result of more developed plastic materials which offered a potentially low priced polymer. The use of intrusion and stretching of melted polypropylene pellets produces thin films with molecular orientation and consequently the mechanical strength is develop parallel to the direction of stretching. Modification of this thin film produces the modern Collated Fibrillated Polypropylene fibers. The network structure of fibrillated polypropylene fibers before mixing consists of oriented fibrils linked together. After mixing, the fibrils will filamentize into multi-filament strands due to the mixing action (shear forces) exerted by the aggregates (Bentur, 1989) which will help reinforcement on all directions. The advantage of these fibers in concrete applications include: high chemical resistance to alkalis, high strength after stretching, high resistance to oxidation, fire resistant, easy to mix with concrete and ultraviolet resistance to name a few.

Polyethylene terephthalate (PET), which is recovered from scrap beverage bottles is one of the biggest source for recycled plastic. Polymer Concrete (PC) which is made with unsaturated polyester resins using recycled PET has been the only use that recycled materials have had in concrete. The PET resins have some success with concrete, however, the main difficulty is the cost of recycling the scrap materials. So far there is no existence for any kind of fibers made out of recycled plastic. PC has had comparative results to Portland Cement Concrete, which is also 5% to 10% more expensive (Rebeiz 1991).

Others efforts have geared toward the recycling of PET obtained from carpet industrial wastes. Younjiang (1994) used 1 and 2% volume fractions of PET recycled fibers from carpet. The fibers used were from hard carpet wastes, disassembled mechanically which would give a fiber with a length of 12-25 mm. The results indicate that a reduction was obtained in the 28<sup>th</sup> day compressive strength for the mix with 2% by volume of recycled carpet waste. The split tensile test shows no difference from the control sample, however, the flexural strength was as high as 40% of the results obtained from the control mix. The results obtained from this research show that results obtained from recycled materials are comparable to or better than plain concrete.

### **2.3 Fatigue Fracture of Concrete**

The fatigue strength of a material is a very important factor, especially when dealing with concrete. Gerwick (1981) evaluated a series of structures to see their ability to withstand repetitive loadings. One of his conclusion was that for high cycle loading typical FRC concrete had superior endurance over plain concrete. Furthermore, at large amplitude

the resistance decreased considerably because the concrete experienced tensile loads and cracking occurred. Taylor and Sharp (1978) found that the compression strength did not vary considerably during the fatigue and static mode of various platforms they studied. In tension, fatigue failure was associated with rapid crack growth.

The fatigue strength decreases slightly, concluded Nordby (1958), when high water-cement (W/C) ratio is used. He also listed age and curing time have a considerable effect on the fatigue strength. The fatigue strength was less for those specimens which were not aged and cured properly as opposed to those specimens which received the correct amount of curing time. Antrim (1967), in his research of fatigue fracture of concrete concluded that natural aggregate concrete made with a W/C equal to 0.7 has higher endurance than concrete with W/C equal to 0.45. In addition, Klaiber and Lee (1982) tested over 350 beams in flexural fatigue loading, using W/C ratio, air content, coarse and fine aggregates type as the major variables. These researchers were not able to infer a good relationship between the effect of W/C ratio on the fatigue strength of plain concrete primarily because of the effects produced by the air content and aggregate size on the flexural fatigue strength. However, they concluded that the fatigue strength decreases as the air content increases. Furthermore, they found that at high stress ratios, the concrete made with gravel tended to have higher fatigue strength than concretes prepared with limestone. However, for low stress ratios the fatigue strength had no significance difference.

The behavior of plain and fiber-reinforced mortars was studied by Morris and Garrant (1981) and compared for cases of compression and tensile loads applied statically and dynamically. Their analysis included ultrasonic reading to determine the dynamic modulus

of elasticity for the different materials along with the standard stress-strain and S-N curves. Their test were carried out using square prism which used slender centers sections for the tensile test. They concluded that no significant changes were shown in the mortars loaded in compression. However, the strength of the mortar was significantly increased when fibers were present during the tensile test. The aforementioned ultrasonic monitoring helped determine that opening and closing of the micro cracks in the matrix were occurring, thus , leaving the fibers to carry all the load.

The addition of fibers to concrete increases its fatigue life according to various researchers. Also, it has been noticed that during crack propagation of fiber-reinforced concrete there is a redistribution of stress along the fibers which slows down the propagation of cracks. Ramakrishnan et al (1989), concluded that the addition of low percentage by volume of fibers improved the fatigue strength. The research used flexural fatigue using rectangular beams which were tested for an endurance limit of two million cycles. He concluded that the addition of polypropylene fibers increased the endurance limit which would be beneficial when applied to pavement slabs, which in turn would substantially increase the life of highways. Meyer et al (1990) studied the effects of fatigue and damage accumulation on fiber-reinforced concrete using cube prisms. He concluded that the use of Miner's rule which assumes a linear accumulation of damage, is not generally applicable to either plain or fiber-reinforced concrete. It was shown than other than specimens reinforced with volume percentages of 0.25 and stress ratios of 0.75 exhibit damage accumulation with a degree of non-linearity, which increased consistently with the increasing stress ratio. Also, it was concluded on this research that adding fibers to concrete had a twofold beneficial effect on

the cyclic behavior of concrete by bridging micro-cracks and retard crack growth. The combination of these two effects was shown to have a net increase in the cyclic strength. However, by increasing the volume percentage of reinforcement more than 0.25 the aforementioned effects become increasingly insignificant.

## **2.4 Influence of Laboratory Loading Conditions**

Kessler (1953), investigated the effect of frequency of loading. He conclude that a rate of between 70 cycles-per-minute (cpm) and 440 cpm had insignificant effect on the fatigue strength. However, he details that 10 cpm seemed to decrease the fatigue strength.

Tests using 240 and 1200 cpm were conducted by Galloway et al (1973) determining that no significant effect on fatigue performance was found. In the same manner, ACI Committee 215 (1986) concluded that between 70 and 900 cpm had insignificant effect on the fatigue strength, provided that the maximum stress level is less than 75% of the modulus of rupture.

Hsu (1981) concluded that in contrast to low cycle fatigue, loading rate is a factor on high cycle fatigue. He uses the  $f$ - $N$ - $R$  curve, where he defines,  $f$ , as the maximum stress, and  $N$  the number of cycles which are plotted on a log scale. The third factor,  $R$ , is defined as the ratio of the minimum applied force to the maximum applied force. These curves were constructed for concrete. However, they do not show the effect of loading rate. To introduce the parameter of loading rate, he included a third axis. He graphically represented the different parameters using plots of  $f$ - $N$ - $T$ - $R$ ; where  $T$  represented the loading rate. He derived equations for the fatigue strength estimation of concrete. Two equations were derived to be used with high cycle fatigue and low cycle fatigue. The effects of loading rate

were also studied by Weeheim and Karthaus (1984) which concluded that increasing the loading rate increases the tensile strength. It was shown that increasing the loading rate from 1.45 psi/sec to 14,503 psi/sec causes a 75% increase in the tensile strength.

The strength criteria used in studies where concrete is subjected to cyclic loading used stress as a basis for crack propagation. The fatigue strength and fatigue life of concrete is considerably affected by the range of stresses used. The larger the difference between maximum stress ratio and minimum stress ratio, the lower fatigue life is obtained. Hilsdorf and Keler (1966) concluded that the smaller the stress range between the maximum stress and minimum stress, the higher the fatigue endurance enhancement was observed. Thus, increasing the fatigue stress range, decreases the fatigue life of concrete. The fatigue behavior of concrete under variable stress levels was also studied by Hilsdorf and Keler. The experiment used varied the maximum and minimum stress level during the test or at rest periods. The result was an enhancement of the fatigue strength. They also concluded, that the sequence of repeated loading applying low stress levels followed by high stress levels decreases the fatigue life of concrete dramatically and the opposite effect is observed if the sequence is reversed.

In the other hand, Sha et al (1970) observed that for load ratios of 70% and below stable and uniform crack growth developed. However, for rates of 80% and above, a rapid cracking increase was observed prior to failure. They concluded that micro cracking was the primary factor leading to failure, which was quantify by the length, width and number of cracks during the testing. In the same manner, Hsiang (1986) stated that between 60% and 80% of total cycle to failure, micro cracking development was slow and stable. The micro

cracking of concrete involved in the loading and fatiguing of concrete was studied by Hsu (1984). He defines three stages of cracking. The formation of insignificant cracks are reported to be observed at loads under 30% of the flexural strength. A non-linear stress-strain behavior was reported between 30 and 70% of the flexural strength which was characterized by a rapid increase in micro crack. After 70% of the flexural strength is reached, crack started to increase noticeably.

Norby (1958) represented graphically using a two axis plot to establish the relationship observed between stress and strain during the cyclic loading. He called this stress-strain relationship hysteresis loops. It was stated that the slope of the curve changes from initially convex upward for the first 10% of the cycle to failure followed by an almost straight or constant behavior to finally become concave upward near failure. Aziz (1987) studied the same relationship concluding that as the degree of concavity increases, the spaces between successive cycles become much farther apart during the final loading. It was generalized that strain increases rapidly at the beginning of the experiment, and was followed by a period of instability without visible cracking for each cycle leading to failure (Aziz et al, 1987; Alliche et al, 1987; Hsiang, 1986). This relationship showing the longitudinal strain development with time under minimum load was observed to have three main stages:

- **Stage I** or crack initiation period was the rapid increase of strain up to 10% of the life;
- **Stage II** crack propagation phase or stabilization stage between 10 and 80% of the life;
- **Stage III** the rapid crack propagation stage.

Do et al (1993) observed similar behavior in concretes under cyclic fatigue loading.

The extent of damage in concrete can be evaluated by the decrease in the material stiffness (Holmen, 1982). Aziz (1987) stated that the material stiffness has a high decrease during the initial load applications, changes to a small and uniform stiffness decrease and decreases significantly prior to failure.

The criteria for damage accumulation has been suggested in literature (Loland, 1985). The majority of the criteria has been developed combining the concepts of fracture mechanics and the damage mechanics to characterize the irreversible degradation of a concrete volume. Binsheng, Zhaohong and Keru (1987) used the fracture mechanics and modulus of elasticity to predict the fatigue life of concrete. Alliche and Francois (1987) used the damage mechanics, taking advantage of the stress concentration, the strain and the damage parameter to obtain the life at every cycle. Meyer (1990) used an energy-based index, which was well suited to quantify concrete's residual strength and predict its remaining life.

The effect of notch has been study by several authors. The notched was used as a crack initiator. However, the crack propagation pattern followed a normal pattern in concrete. Brown et al, (1967) used the linear-elastic fracture mechanics (LEFM), which deals with ideal, homogeneous, elastic materials to find a stress intensity factor,  $k$ , for single-edge fractured specimens subjected to bending. Later, Naus et al, (1969) implemented the same method. However, taking some precaution since concrete is a heterogeneous material and  $k$  is value which depends of instantaneous crack depth, hence, they used an effective stress intensity factor,  $k'$ . When considering the maximum moment for a given load configuration the effective stress,  $k'$ , becomes a critical stress intensity factor,  $KC'$ . The critical stress intensity factor was expressed as :



$$KC' = ya^{1/2}\sigma$$

2-1

where:

- KC' = critical stress intensity factor for single-edge cracked specimen in bending, given in psi
- y =  $1.99 - 2.47(a/d_u) + 12.97(a/d_u)^2 - 23.17(a/d_u)^3 + 24.80(a/d_u)^4$
- a = notch depth given in inches
- d<sub>u</sub> = average gross depth of specimen in inches
- σ = gross stress calculated based on elastic analysis (Mc/I)

The specimen's geometry, y, used on equation 2. 1 was constant for all the specimens.

This equation can then be substituted by the effective Griffith crack. Jen et al, (1985) used a two parameter fracture model using the critical stress intensity, k<sub>i</sub>, which is equivalent to KC' as mentioned above and the critical tip opening displacement (CTOd<sub>c</sub>) expressed as :

$$\sigma_y = KC' / (2\pi x)^{1/2}$$

2-2

where:

- σ<sub>y</sub> = effective stress given in psi
- KC' = same as equation 2.1
- x = distance from the notch to the point of interest in inches

The fatigue life of concrete has been proposed to ensure a more accurate prediction due to the scatterness of data obtained based on models that relay upon probability approaches. The McCall model has been used to predict the fatigue life of normal concrete (Holmen, 1979). This model uses the number of samples represented by a parameter called the probability of survival and is based on a nonlinear relationship between S<sub>max</sub> and logN<sub>f</sub> (Mc Call, 1958) and has been also used by Ople and Hulsbos (1966) and Do et al, (1993) to

investigate the fatigue behavior of normal and high strength concretes. A four dimensional diagram was used by Ople and Hulsbos that represented the stress level, S, fatigue life, N, probability of failure, P, and stress gradient,  $\theta$ , or also know as the S-N-P- $\theta$  diagram. Do et al, introduced the probability of survival number, L. This number has been correlated with the maximum applied stress and the total fatigue life of the concrete and present as follows:

$$L = 10^{-a(S_{\max})^b (\log N)^c} \quad 2-3$$

where:

- L = 1-P
- $S_{\max}$  = maximum applied stress, expressed as a fraction of the static compressive strength
- $N_f$  = number of cycles to failure; and
- a, b, c = experimental constants characterize the concrete type.

Similarly, another approach was used to estimate the fatigue life expectancy of normal and high strength concrete beams, Tawfiq (1994). This approach was based on the S-N relationship with the compressive strength of the concrete,  $f'_c$ , included as one of independent variables. He expressed the fatigue life of different mixes as follows:

$$\log (N) = 1/a [b - S - c \log (f'_c)] \quad 2-4$$

where :

- N = fatigue life of concrete
- S = stress ratio (%)
- a,b,c = material parameters.

These methods represent means to predict the fatigue life of plain concrete. However, their validity to predict fatigue behavior of fiber-reinforced concrete is different from normal concrete. Fibers are used as secondary reinforcement to delay the crack initiation of fatigue cracking and to arrest the extend cracks. Since the pre-cracking and post-cracking behavior of fiber-reinforced concrete is different from that of normal concrete, these variation will influence the concepts of analyzing and designing concrete structures, such as pavements.

## **2.5 Fatigue Data Representation**

The relationship between fatigue strength of concrete,  $S$ , and the number of cycles of repeated loading,  $N$ , is usually configured as an S-N curve or better know as Wholer's diagram. Plotting the number of cycles in abscissa in a logarithmic scale and the maximum fatigue stress in a linear scale, the S-N curve will constitute a linear relationship in the high cycle region. The maximum stress,  $S_{max}$ , and the peak static strength,  $f'_r$ , were normalized, since it has been found that this relationship is independent of the specimen geometry. This S-N relationship still represents a unique characterization of the fatigue behavior of a particular material. Although, a small variation in the physical or mechanical properties of the material will produce a different S-N relationship, using the Wholer's diagram, the concepts of continuous defect field of the damage theory can be incorporated to obtain the cumulative fatigue damage of the concrete. It was stated earlier in this chapter that is known that decreasing the range of the stress ratio results in an increase of the fatigue life. Ranges from 50% to 90% were tested using the different fibers and compared among them by means of the Wholer's diagram. This relationship predicted the mean life of the concrete.

Three and four dimensional diagrams have been used by different researchers. McCall (1958), Ople and Hulsbos (1966) produced a three dimensional diagram which was represented by S-N-P diagram, where, P, represents the probability of failure. This diagram was used to represent data from tests performed on plain concrete under reversed bending. In an extend to their research, Ople and Hulsbos, presented a four dimensional diagram that represented the stress level, S, fatigue life, N, probability of failure, P, and stress gradient,  $\theta$ , or better know as the S-N-P- $\theta$  Diagram.

All the aforementioned methods for representing fatigue data used statistical analysis. The variability associated with the scatter data which is obtained from fatigue testing of plain concrete makes analytical analysis a must. The most common form of statistical analysis used is the linear regression methods, which were used on this research project.

## **2.6 Ultra-Thin Pavement Overlays**

Ultra-Thin Concrete Overlay is a two to four inches fiber reinforced high strength concrete design to be open to traffic within 24 hours. This thin overlays use the fast-track method of construction. A compressive strength of 3,000 psi must be achieved in order to open traffic within the required time. This technique has become popular in the United States during the last decades. Thin overlays have been successfully placed throughout the United States using fast-track methods (Grove et al, 1993).

The main problem of thin overlays is that they rest on Asphalt Cement Concrete which creates a problem of design. If asphalt is considered to give any structural contribution to the overall pavement system, then there must be a strong bond between the Portland Cement

Concrete (PCC) and Asphalt Cement Concrete (ACC). The bonding between the layers can be achieved by milling the asphalt surface before placing the FRC layer. If no bond is created, then the ACC should be considered as a base and thickness of PCC can not be reduced.

## **2.7 Finite Element Modeling (FEM)**

The efforts to model three-dimensional fiber-reinforced concrete using finite element methods are merely non-existent. The majority of the finite element models have been geared towards analysis of the tensile strength, flexural strength and crack growth in fiber-cement composites (Soroushian et al, 1987; Foote et al 1987; Maalej and Li, 1994). Liu (1992) has developed an elaborate constitutive model for fiber-reinforced concrete. The model combined concepts from both the continuum theory and plasticity theory. The model described stresses from an applied strain path. Efforts were made by Liu to modify the uniaxial stress represented by the William and Warkle model to be expressed by the Soroushian and Bayasi equation for the fiber-reinforced concrete:

$$\sigma_{cu} = 2 \alpha \beta \tau_u (l_f / d_f) V_f + \gamma \sigma_m (1 - V_f) \quad 2-5$$

where:

- $\sigma_{cu}$  = ultimate tensile strength
- $\tau_u$  = average interfacial bond stress at ultimate condition
- $l_f$  = fiber length
- $d_f$  = fiber diameter
- $\alpha$  = efficiency factor for the random orientation (0.41)
- $\beta$  = efficiency factor accounting for the random crack location (0.41 to 1.0)
- $\gamma$  = a factor representing the fraction of the matrix strength contributing to the tensile strength (0 to 1.0)

The shear transfer coefficient in William and Warkle model was taken as 1.0 for the fiber-reinforced concrete, representing a rough crack or no loss of shear transfer which is a typical behavior for the fiber reinforced concrete.

**Table 2.1 Various forms of polypropylene fibers used to reinforce concrete.**

<b>Polypropylene Type</b>	<b>Reference</b>
Smooth Monofilaments*	Dave and Ellis (1979)
Fibrillated Monofilaments*	Baggot (1983)
Fibrillated Film-Woven Mesh	Hannant et al (1978)
Fibrillated Tapes	Hannant (1981)
Smooth Yarn	Goldfein (1965)
Fibrillated Yarn**	Hughes and Fattuhi (1977)
Twisted Ribbon Yarn	Naaman et al (1984)
Collated Fibrillated Mesh	Zollo (1984)
Woven Fabric	Gardner et Currie (1983)

\* Generally up to 1500 denier; 30-150  $\mu\text{m}$  diameter and 50 mm long.

\*\* 1000-12,000 denier. 1 denier = mass in g of 9000 m of yarn.





## **CHAPTER III**

### **EXPERIMENTAL PROGRAM METHODOLOGY**

#### **3.1 Introduction**

This project involved extensive laboratory testing and investigation of the Florida's concrete reinforced with discrete and discontinuous plastic fibers under reversed constant cyclic loading until failure. The aim of this project was to evaluate the effect of virgin and recycled plastic fiber addition to the fresh and hardened properties of Florida's concrete. Furthermore, to quantify crack initiation and propagation periods as a result of fatigue strength.

Preliminary test were done at the FAMU/FSU laboratory using different commercially available virgin plastic fibers in addition to in-house made fibers made using recycled plastic materials. The fibers range from monofilament fiber to collated fibrillated fibers. Each of the aforementioned fibers is available in different kinds of plastic. The fibers used during the preliminary test were Monofilament Polypropylene fiber, Monofilament Nylon fiber, virgin recycled plastic and finally different In-house made post-consumer recycled fiber using HDPE and PET were used on the first phase of the preliminary test. The second phase consisted of selecting one or two fibers among the different collated fibrillated and upcoming Monofilament Polyolefin fibers. Different length of Polypropylene collated fibrillated, and

Nylon collated fibrillated fibers were tested.

Based on the results obtained three fibers were selected for the extensive investigation program coordinated by FDOT State Materials Office. The 3/4" polypropylene monofilament, 2" polypropylene collated fibrillated, and 1 1/2" to 2" PET in-house made spiral recycled plastic fiber. Later on the project a new 2" Polyolefin monofilament fiber was used. The personnel at the FDOT State Material Office in conjunction with FAMU/FSU research assistant did the concrete mixing, casting and curing of all samples. For this purpose, 110 cylinders (6"x12"), 8 unnotched beams (6"x6"x21") and 41 notched beams (6"x6"x21") were prepared for the research to be executed at the FAMU/FSU research lab. Six batches were prepared at the FDOT Materials Office laboratory and one batch was prepared at a local mixing plant in Gainesville, Florida. The plastic properties such as: air content, slump and unit weight were evaluated in the laboratory at FDOT. Also, FDOT personnel evaluated the compressive strength, split tensile strength and modulus of elasticity for the different mixes. The flexural strength and fatigue strength were evaluated at the FAMU/FSU research facilities.

All the aforementioned test comply with the most current specifications of the American Society for Testing and Materials (ASTM). The frequency of cycling, the location of the strain gauges, the maximum and minimum stress levels, Data Acquisition System (DAS), Material Testing System (MTS), amplifier system and computer software which are criteria for fatigue testing were studied a little further in order to be applied correctly.

### **3.2 Sample Size Selection**

The 6" x 12" size used for cylinders specimens was followed using ASTM (C39 - 86) and ASTM (C496 -90) standards for compression and split tensile strength, respectively. This size also satisfied FDOT regulations for cylinder size used for compression and split tensile tests.

The beam size was selected base on ASTM standards and fatigue test criteria and available testing equipment, Figure 3.1. Flexural strength ASTM C78-84, and fatigue strength required the specimen size to be 6"x 6"x 21". FDOT selected the 6"x 6"x 30" beam size to cast specimens needed for their own research purpose. The former size gives an overall size that is at least ten times the maximum aggregate size. The span gives a length that is still within a range that does not give handling problems. The width selected satisfies strength and structural stability needed from the specimen to withstand handling during curing and testing at the FDOT lab, as well as, handling during transportation from the FDOT lab to the FAMU/FSU research lab. This criteria would satisfy the former ASTM standard, however, there are other factors to be taken into account for fatigue testing.

In the fatigue test, the researcher needs to monitor the crack growth on concrete. This is not a simple task to perform, therefore, a single-edge-notched-beam (SENB) was looked upon as a solution to this problem. According to Kelly (1981) and Slate et. al. (1984) concrete has inherited defects and micro-cracks before loading takes place. Temperature changes, volume changes during the plastic range (Shrinkage), water loss, settling of coarser aggregate and volume changes during the hardened stage (Creep) are some of the reasons for these pre-loading micro-cracks. Therefore, fracture of the concrete matrix can start at

anytime, anywhere on the specimen. Hence, a point with greater stress and strain concentration at the middle span, created with a notch, forced a crack to develop through the middle third of the specimen and by the same token facilitated the acquisition of data through the strain gauges and made all fatigue testing to be consistent. The resulting steel notch and the beam form details are presented in Fig 3.1.

### **3.3 Mix Design**

There were five batches prepared at the Florida Department of Transportation, FDOT, Materials lab and one prepared at local mixing plant in Gainesville. The batch method was used during this project to obtain the best mix. The mixes were design to reach a 4000 to 6000 psi compressive strength by the 28<sup>th</sup> day. The mix used for the test tracks was required to develop 3000 psi compressive strength after 24 hours in order to satisfy fast track construction techniques, which open traffic 24 hours after placement of concrete. Other parameters included in the design were a water/cement ratio of 0.45, slump of 3.5 in. used for pavements and air content of 3-5%. The mix batch designs used on this project are presented on Table 3.1. The names used for each batch are also given in this table.

The fiber-reinforced concrete composite was integrated mainly of five ingredients. Portland cement Type I (ASTM C 150-89), Florida's coarse and fine aggregate, Gainesville tap water and plastic fiber reinforcement. Air entraining and super plasticizers were used for unworkable mixes in order to maintain water/cement and slump limits. In the mix used for the pavement overlays, there was up to 20% partial cement substitution with Fly Ash class F (ASTM C 618-89) as pozzolanic material. Four different plastic fiber were selected to be

evaluated on this project.

The coarse aggregate used was crashed lime stone with a maximum aggregate size of 0.75 in. (0.19 mm). The fine aggregate was natural sand with a specific gravity of 2.64, and absorption of 3.5%. Both coarse and fine aggregate complied with ASTM-33 standard gradation requirements.

Two of the four fibers used on this project were made of virgin Polypropylene material. The first fiber manufactured by FORTA corporation was the 3/4" Monofilament type and used at a rate of 1 1/2 lb. per cubic yard. The second fiber used was the 2" Collated Fibrillated kind manufactured by Fibermesh company and used at a rate of 1 1/2 lb per cubic yard. The third fiber was made out of virgin Polyolefin material. This monofilament 2 in. fiber is manufactured by 3M and was applied at a 1.6% by volume or 25 lbs. per cubic yard. The last fiber used on this project was the 1.5 in. in-house made post-consumer recycled PET plastic. This fiber had a spiral cross sectional shape and was added at a 0.6% by volume. The physical properties of these fibers are presented on Table 3.2 and the geometrical appearance are presented on Fig 1.1 and 1.2.

### **3.4 Sample Preparation**

Two groups of samples were included in this project in order to obtain a meaningful comparison of the behavior of plain and fiber reinforced concrete. The first group consisted of the control samples and the second group consisted of the same mix design with the addition of discontinuous discrete plastic fibers. All the mix designs were recommended by the **Florida Department of Transportation, FDOT**. Fly ash class F was used on mix

FBRME. Mix proportions and material properties are presented in Table 3.1 under FRBME. A total of 42 6"x6"x21" single-edge-notch-beams, SENB, and seven unnotched beams of the same size were prepared for static and dynamic testing.

### **3.4.1 Mixing Procedures**

Four of the mixtures were mixed in a conventional vertical rotary drum concrete mixer (Fig. 1.5) with a 15 ft<sup>3</sup> capacity inside the FDOT Materials laboratory. The mixing procedure followed ASTM C 192-90. The mixer was first coated with a paste of water and fine aggregate to assure wetness on the inside surface of the mixer. Thereafter, the coarse and fine aggregates were loaded in layers using ½ coarse aggregate then ½ fine aggregate until all the weighed material was put in the mixer. The next step was to load ½ of the water and mix it for one minute. After the mixer was started, the cement and the rest of the water were added and mixed for 3 minutes. This was followed by a 3 minutes rest period and a subsequent 2 minutes final mixing. The fibers were then added and the mixture was mixed for an extra 3 minutes. The admixtures (air entraining agent and/or superplasticizer) were added to the mixing water.

One of the mixtures was prepared on a horizontal (pan) rotary drum concrete mixer with a capacity of 1 cubic yard, Fig. 1.6. The mixing procedure was similar to the procedure mentioned above. However, problems arose in this particular mix, hence the same mix had to be prepared on a conventional vertical rotation drum mixer.

The steel beam molds were coated with oil for easy demolding prior to the mixing process. The fresh properties of concrete were being evaluated at the same time that samples were being prepared. The temperature of the matrix was measured using a pocket

thermometer. In addition slump (ASTM C143-90), air content (ASTM C173-78) and unit weight (ASTM C138-81) were tested.

The steel beam mold was filled using two lifts. The first lift was pour in and compaction was done using an adjustable frequency vibrating table for about 45 seconds, then the second lift was pour in followed by 45 seconds in the vibrating table. Surface finishing was done using wooden and/or steel float and/or trowel. The cylinders were prepared using the same techniques as above, but three lifts were used instead. To retain the moisture during the first 24 hours until demolding, all the beam specimens were covered with plastic sheets after casting and the cylinders were covered with plastic lids.

The first three batches mixed were FBR1, FBR2 and FBRC. Polypropylene 3/4" monofilament fiber and Polyethylene Terephthalate (PET) in-house post-consumer recycled plastic fiber were added to the first two mixes, respectively. The latter mixed was the control mix for the other two above mentioned mixes. Then, FBR3M and FBRCNT were casted. Monofilament Polyolefin fibers were used on the former mix and the control mix was constituted by the latter mix. Finally, FBRME using 2" collated fibrillated fiber was prepared at the mixing plant and used on the first test track.

#### **3.4.2 Sample Curing**

The curing was carried out according to ASTM C192-81. Following the 24 hours setting period, the plastic sheet was removed, the specimens were taken out of their molds and then put in the curing room where temperature was maintained at  $70\pm3$  °F and  $95\pm4\%$  humidity. Thereafter, all the beam molds were cleaned, washed, assembled back and coated with oil for future use.

After the 28th day of curing, the specimens to be tested by FDOT were removed from the tank and air dry for twenty to forty minutes . The specimens needed for the FAMU/FSU research were also transported to the FAMU/FSU research facility the same day. The specimens were back into the controlled temperature curing tank upon arrival to the college of engineering. They remained in the curing tank until the specimen needed to be taken out for instrumentation prior to testing. The curing time range went from 35 to 90 days.

### **3.5 Sample Testing and Instrumentation**

Most of the hardened concrete test were performed by the FDOT Materials Office in Gainesville, Florida. At the age of 1, 3, 7, 14 and 28 days Compressive Strength test,  $f'_c$ , (ASTM C39-86) was performed using two cylinder samples per testing day. At the ages of 7 and 28 days Split Tensile test,  $f'_t$ , (ASTM C496-90) was performed using two specimens per testing day. Modulus of Elasticity test,  $E$ , (ASTM C469-87a) was performed at 28 days using two samples per testing day. Finally, the Modulus of Rupture, M.O.R., or Flexural strength test (ASTM C78-84) was performed at the FAMU/FSU research facility using two samples from each mix at the age of 28 days. FDOT tested for their own purpose two (2) 6"x6"x30" beams from the FBRME mix. The Fatigue test were performed at the FAMU/FSU facilities. A summary of the experimental program is presented on Figure 3.2. The test arrangements for a notched concrete beam is presented on Fig. 3.3.

#### **3.5.1 Strain Gauges**

The following step after completion of the curing period was instrumenting the specimen. The specimen was taken out of the curing tank at least twenty four hours before



gauge installation in order for it to air dry. Each beam for the static and dynamic test was instrumented using Self Temperature Compensated (STC) foil gages model MM-EA-13-240UZ-120.

The strain gauge itself is the starting point of the measuring system used in this project. This device is essentially a simple electrical resistor, but it has been specially design to be bonded to the surface of a solid object such as concrete and undergo a change in resistance when a strain is encountered in the direction of the sensing grids, Fig. 1.4.

The gage installation was done using standard procedures from the Micro measurements Manual for Strain Gauge Technology, 1993. First, the beam's top side was grinded in order to level it because of the unevenness left behind by the non-uniform trowel strokes. The next step was to remove all contamination from oil and dust that would accumulate after the grinding was performed, this was done by scrubbing, brushing and finally washing the beam. Afterwards, the 18" shear span and the middle third were marked on either side of the beam using a No. 2 pencil.

The middle third of the beam underwent extra treatment prior to gage installation. This portion of the beam was abraded using grit silicone carbide sand paper, and acid conditioner and neutralizer were applied. The strain gauge location were again brushed and rinsed to remove any residual from the conditioner and neutralizer solutions. Following was the drying of this zone using a commercial hair dryer.

Strain gauge installation was done after finishing the aforementioned process. The strain gauges were bonded to the concrete surface using a special mix of epoxy which is a mixture of AE-10 curing agent and M-200 bonding agent. This mixture helped filling the

voids found on the concrete surface and creating a smooth plane for the gauge to be installed. This process need to be done carefully and rapidly because of the short mixture pot life of 20 minutes. Prior to bonding the gauge to the concrete surface, it was removed from its cover using tweezers and place on a chemically cleaned glass plate assuring that the bonding side of the gauge would be facing the glass plate. A clear tape was then used to cover the strain gauge by pressing gently the tape against the glass. The tape was remove by holding one end of the tape and pulling the other end making sure a 45° angle was kept between the tape and the glass plate. Then, the middle of the gage was placed to intersect with the vertical line below the tip of the notch. A gentle stroke over and across the gauge was executed after the gauge had been properly located to remove any bonding mixture excess. Afterwards, a 4 x 8 cm rubber pad and a aluminum pad of the same size were placed on top of each strain gauge. Weights were left on top the pads to create pressure during a 24 hours curing period. The following day, the tape was removed and a three lead wire connection was soldered to the gauge. This gauge when connected to the rest of the sensing circuit completed the Wheatstone Bridge, presented on Fig. 3.4. This arrangement using the STC single active gauge formed a quarter bridge system, used for each gauge and throughout the project. The analog signal coming out of the Wheatstone Bridge was send to a multichannel system where the signal was conditioned and amplified before being changed to a digital signal to be displayed on the computer monitor and saved into the computer's hard drive.

The notched concrete beam were instrumented with four gages located on the middle third or maximum stress zone. The gage arrangement is presented on Fig 3.3. Gauge #1 located below the tip of the notched to capture the stress concentration on the top fiber.

Gauge #4 was used to obtain data from the lower fiber or compression fiber. The other two gauges were used to monitor the areas above and below the neutral axis. The gauges were scanned 30 times per second and data acquired continuously through the different stress levels on the experiment.

### **3.5.2 Testing Equipment**

All the compression test and split tensile test were done by FDOT using a 500 kip Forney testing machine. The machine has a steel platen base and a steel loading platen. The compressive force was applied to the cylinder through the top platen. The geometrical information averages, namely diameter and height of the cylinder were input before loading the specimen. The maximum strength value was stored and then transferred to the computer.

The same equipment was used for the tensile strength test, however, instead of circular steel platens two 12" by 8" surface area steel platens were used, Fig. 3.6.

The flexural and fatigue test were performed using a 50-kip servo-controlled electro-hydraulic, closed loop Material Testing System (MTS) was used throughout the project. This system is composed of a loading frame, hydraulic system and control module. A steel bench is the base of the loading frame which consists of two steel columns with a cross beam bolted to them. This cross beam was the support for the load cell and the two 60" I-shaped steel beams supporting the specimen. The specimen was resting on movable rollers connected to the flange of the I-beams. This test set up is presented on Fig. 3.7.

The hydraulic system was a double-acting cylinder, water-heated exchanger, servo valve and pressure power supply maintained at a pressure and temperature of 3000 psi and 45 °C temperature, respectively. The 407 controller module was used for the static and

fatigue testing. This electronic module allowed for stroke and load control testing. The stroke control which applies a control displacement of 0.0003 in/min was used during the static test. Load control, is the opposite of stroke control, the load applied by the servo valve is being control throughout the test. This was used for the fatigue test to maintain the constant upper and lower stress levels. It also allowed to set an upper and lower limits on the signal feedback to maintain the maximum and minimum loads within a minimum deviation from the commanded loads. Furthermore, the 407 controller is equipped with a cycle counter which was preset to two million cycles as the maximum amount. The Material Testing System stopped automatically whenever the built-in cycle counter on the 407 controller would reach the preset amount of two millions ( $2 \times 10^6$ ) cycles.

### **3.5.3 Data Acquisition System**

The data acquisition system used was a Omegabyte Model  $\mu$ CDAs-16G. This was a multi-function high speed programmable gain analog-to-digital converter with signal conditioning for 16 channels at rates of 75 kHz with 12 bit resolution. This board minimized noise and cross-talk at high frequencies. The analog signal was coming from the Wheatstone Bridge built-in the 2100 Micro Measurement System. This system used one power supply for up to ten amplifiers and a digital readout unit. The excitation ranged from 0.5 to 12 Vdc but kept at 5 Vdc during the testing. The gain range was of unity to 2100 and a bandpass of dc to 50 kHz at -3 db. The analog output was of  $\pm 10$  Vdc. This signal conditioning amplifier system was used during both the static and dynamic testing. The schematics for this setup is presented in Fig. 3.8.

### **3.6 Testing Procedures**

Trial beam samples were prepared before the actual testing began. The pre-test operation helped to familiarized with the whole systems, namely, MTS machine and data Acquisition System. The whole system was calibrated prior to executing any test.

The MTS machine was calibrated by an MTS licensed engineer. This calibration included the stroke and load control from a range of 1/2" to 5" as well as 5000 Lbs. to 50 Kips, respectively. The data acquisition and strain gage conditioner outputs were calibrated using a Micro Measurement Strain Gage readout box. The output from the DAS were compared to readings obtained from a gage installed on a test aluminum bar using an OPTIM DAS. Labtech Notebook software was the main computer package used in combination with a Pentium-60 Personal Computer. The software was programmed to sample automatically at a rate of 30 Hz. This rate allowed a good programming without overloading the number of blocks, buffer size and test duration which are the key to execute a good program using this software package.

The load conversion from an analog DC signal sent by the load cell through the 407 controller and feed to the computer changed to engineering units using the following equations:

- a) Using the Material Testing System at the full scale of 50 Kips

$$P = 5000X$$

3-1

- b) Using the Material Testing system at the secondary scale of 5 Kips

$$P = 500X$$

3-2

where:

P = load applied by MTS in pounds

X = analog signal value from 407 controller in Vdc.

The strain conversion from an amplified and conditioned dc digital signal to engineering units was done using the following formulas:

$$E_o = \frac{E_i}{4} * GF * \epsilon * G \quad 3-3$$

where:

$E_o$  = voltage out from Wheatstone Bridge, equivalent to 527.5μ Vdc

$E_i$  = voltage in to the Wheatstone Bridge, equivalent to 5Vdc

GF = strain gage factor, equivalent to 2.11

$\epsilon$  =  $1 \times 10^{-6}$  strain

G = amplification gain, equivalent to 200

$$\epsilon_{act} = \Delta E_o \div E_o \quad \text{and} \quad 3-4$$

where:

$\epsilon_{act}$  = strain in micro in/in

$\Delta E_o$  = change in output voltage due to load application to specimen

$E_o$  = voltage out from Wheatstone Bridge, equivalent to 527.5  $\mu$  Vdc

The maximum value coming out of a Wheatstone Bridge is  $\pm 10$  Vdc which represents a maximum strain of 18,957  $\mu$  strain or gauge failure.

The testing procedure started by placing the specimen on the loading frame and aligning with the load and reaction rollers was done after, (Fig. 3.7). Overall checking of the system followed and included:

- check the resistance of each gauge and make sure equaled 120  $\Omega$
- check all connections as well as lead wires
- balance all four channels

after, the beam was raised to make contact with the rollers. Once contact was established a setting load of 50 lbs. was applied before starting the 4 Hz cycling program. The layout of this data acquisition system and loading setup was presented in Fig 3.8.

### **3.6.1 Static Testing**

A series of static test were conducted to determine the modulus of rupture,  $f_r$ , of concrete and to obtain the load-deflection curve. The test were performed using the Flexural Strength of Concrete procedure according to ASTM C78-84. In addition, strain measurements were recorded from gages placed in the same order as the fatigue specimens presented in Fig 3.3 and Fig 3.5. The set-up procedure explained on the previous section was followed by connecting the Linear Voltage Displacement Transducer (LVDT) to the data acquisition system. The LVDT was used with a resolution of 1/10000 of an inch and

maximum outputs were displayed and recorded digitally by the readout unit. The schematics of this test is presented on Fig 3.9.

To be able to perform a fatigue test, static flexural strength results must be available. Fatigue test data is graphed by plotting different stress ratios versus number of cycles, S-N, diagrams. This relationship allows for estimating the fatigue life of concrete. The stress ratio,  $S$ , is the ratio of the maximum applied stress,  $S_{max}$ , to the static flexural strength,  $f'_r$ . The abscissa in this diagram is represented by the number of cycles,  $N$ , plotted on a logarithmic scale.

The static flexural strength test was performed using the stroke control program. The ramp function which allow for a linear displacement was controlled through the 407 controller. The actuator of the MTS was set to apply a force with variable magnitude during the test with a displacement that strictly followed the 0.003 in/sec displacement rate set on the program.

### **3.6.2 Fatigue Testing**

Seven notched beams from each batch were tested under constant cyclic loading. Four gages were located on the high stress zone and a four-point bending test set-up was used, as presented on Fig. 3.3 and Fig. 3.5. The loading was applied by a 55 kip Material Testing System (MTS) under a load control program. A haversine function with a frequency of 4 Hz from the 407 controller that produces a sinusoidal wave was sent by the 407 controller to the MTS. The stability of uneven samples due to strong trowel strokes during the specimen surface finishing, was achieved using leader shims where needed. The minimum and maximum loads were monitored thru the 407 controller display and Data Acquisition



System. The minimum load was kept at 50 psi regardless of the maximum load.

The maximum stress ratios used for this project ranged from 50% to 90% of the static flexural strength. The use of these stress ratios would assure the simulation of a truck running over a graded pavement during the high stress loading and achievement of an impact free test during the low stress loading. The latter, furthermore, simulates a situation when the only acting load is a dead load due to the self weight and thermal expansion of fiber reinforced concrete. The maximum and minimum loads were applied without interruption until failure of the specimen.

According to Kesler (1953) a cycling rate of 70 cycles per minute and 440 cycles per minute had no effect on the fatigue life of concrete. A cycling rate of 110 cycles per minute would constitute an axle load moving at 55 mph or traveling a 22' slab in nine thousands of a minute ( Espiritu, 1993). A rate of 240 cycles per minute (4 Hz) was recommended for fatigue testing of Florida's concrete (Tawfiq, 1994) and was used in this project.

In order to detect the onset of a crack, the specimen was monitored for cracks using a magnifying glass to survey the tip of the notch and checking the value displayed by the first gage on the DAS, as presented on Fig. 3.5, making sure it would not display the maximum voltage allowed out from the Wheatstone Bridge. This technique would allow for determining the first stage of cracking, namely Crack Initiation or Stage I. After, crack initiation, crack propagation or Stage II of cracking was monitored using the magnifying glass until failure of the specimen occurred. Failure occurred on some specimens before the maximum number of cycles set to two millions ( $2 \times 10^6$ ). Furthermore, the speed of cracking was determined by using the known distance in between gauges and measuring the time it

would take for a crack to travel from gauge 1 to gauge 2. Table 4.2 shows the stress ratio used on the different mixes, the number of cycles endured by each specimen and the traveling time between gauges.

### **3.7 Field Testing**

The Florida Department of Transportation State Materials Office decided to build three full scale Ultra-Thin Overlays using fiber-reinforced concrete. Figures 3.10 shows the details of these tracks. Ultra-Thin Overlays or Whitetopping is a paving process in which a thin layer of fiber reinforced concrete is placed over a distress asphalt surface. The thickness of the layer were from two inches (2") to four inches (4").

The test tracks were built on FDOT's test yard. Two of the fibers were selected for testing, namely, 2" collated fibrillated polypropylene fiber manufactured by Fibermesh and the 2" monofilament polyolefin fiber. The first step was to prepare the asphalt surface where the concrete was placed. Three types of contact surfaces were prepared as follows: grinded or milled surface, ungrinded or unmilled surface and crack-relief layer. The mixes were designed by the FDOT's state material engineer and presented on Table 3.1. The concrete was delivered to FDOT testing yard from a local Gainesville concrete plant. During concrete placing, all the fresh properties of concrete were evaluated in the same manner as described earlier in this chapter. The compressive strength and flexural strength of the fiber-reinforced concrete were tested at the FDOT Material Office. One important requirement for these mixes was to gain an strength of 3,000 psi at 24 hours to be able to use it on fast track maintenance jobs.

The slabs were instrumented by member of both teams. Temperatures gauges or thermocouples were installed to monitor the changes in temperature during the early morning and midday. Furthermore, deflection gauges or LVDT were installed vertically at the midspan of a 6'x6' slab and at the expansion joint. Also, a horizontal LVDT was used at the joint to monitor the horizontal movement of the slab during the testing done as explained later on this section. In addition, strain gages were located as shown in Fig. 3.11.

### **3.8 Finite Element Modeling (FEM)**

The Finite Element (FE) models were constructed to better understand the time, origin and location of cracks as well as strain evolution during the different cracking stages. This analysis along with the laboratory and field testing allowed to better comprehend the effect of material properties, boundary conditions and geometrical characteristics on the fatigue behavior of structures, such as Ultra-Thin pavement overlays. The numerical modeling consisted of a third dimensional beam and pavement overlay.

The first numerical model was a single-edge-notch beam using the same dimensions used for the static and fatigue testing according to ASTM C78-84. The second model used the same geometry and dimensions as the first full test track. Different parameters like fiber orientation, aspect ratio of the fiber and ratio of the fiber to the total volume were included to study their effects. The loading configuration of the numerical models are presented on Fig 3.12 and Fig. 3.13, respectively.

The FE models were calibrated using the laboratory results obtained from the static and fatigue tests performed during this project. ANSYS 5.2 Finite Element program was

used to build the different models. It was chosen because of the wide range of elements available, including a concrete element which can be used with and without reinforcement. The fiber was modeled by using the smearing technique in the global coordinate system.

**SOLID65 3-D** reinforced concrete element was used for the two models. SOLID65 element is used for three-dimensional modeling of concrete with or without reinforcement. The element is capable of cracking in tension and crushing in compression. The element is defined by eight nodes having three degrees of freedom at each node; translations in the nodal x,y, and z directions. A maximum of three different rebar specifications can be used (x, y,z). The material was assumed to be isotropic for both of the models. The plastic reinforcement was used using the smeared method. The stress-strain matrix [D] used for this element is modeled as follows:

$$[D]=[1-\sum^{Nr}V^r][D^c]+\sum^{Nr}V^R[D^r]_i \quad 3-5$$

where:

- Nr = number of reinforcing materials
- Vr = ratio of reinforcing material to the total volume of the element
- [D<sup>c</sup>] = stress-strain matrix for concrete
- [D<sup>i</sup>] = stress-strain matrix for reinforcement

The stress-strain matrices are function of stiffness and poisson's ratio of the materials used in each element.

**Table 3.1 Concrete Mix Design**

<b>MIX PROPORTION</b>					
<b>TYPE OF MATERIALS</b>	<b>As designed per cubic yard</b>				
<b>(Units)</b>	<b>FBRC</b>	<b>FBR1</b>	<b>FBR2</b>	<b>FBR3M</b>	<b>FBRME</b>
<b>1. Total Cementitious (lb)</b>	658	658	658	658	740
a. Cement (Lb.)	658	658	658	658	590
b. Fly ash (Lb.)	0	0	0	0	150
<b>2. Mixing Water (lb)</b>	270	270	270	270	267
<b>3. Fine Aggregate (lb)</b>	1229	1229	1229	1226	1010
a. Specific Gravity	2.63	2.63	2.63	2.63	2.63
b. Absorption (%)	0.32	0.32	0.32	0.50	0.32
c. Total Moisture	0.50	0.50	2.36	5.22	2.36
d. Free Moisture	0.18	0.18	2.04	4.72	2.04
<b>4. Coarse Aggregate (lb)</b>	1644	1644	1644	1642	1750
a. Specific Gravity	2.40	2.40	2.40	2.40	2.40
b. Absorption (%)	3.97	3.97	3.97	4.15	3.97
c. Total Moisture	4.15	4.15	5.27	5.08	5.27
d. Free Moisture	0.18	0.18	1.30	0.93	1.30
<b>5. WR (WRDA79) (oz)</b>	49	49	49	49	40
<b>6. Air Entraining Admixture (ml)</b>	50	200	120	300	296
<b>7. Water/cement Ratio</b>	0.41	0.41	0.41	0.41	0.36
<b>8. Cement Type</b>	I	I	I	I	I
<b>9. Fiber (%)</b>	0.0	0.5	0.6	1.6	0.5

**Unit Conversion:**

1 in = 25.4 mm

1 lb = 0.00444822 kN

1 oz = 29.57

1 psi = 6.89476 kPa

Fahrenheit (F) = (C x 1.8)+32

**Mix desig Labels:**

FBRC - CONTROL

FBR1 - FORTA 3/4" VIRGIN, MONOFILAMENT, POLYPROPYLENE

FBR2 - RECYCLED PLASTIC (PET)

FBR3M - 3M POLYOLEFIN FIBER

FBRME - 2" COLLATED FIBRILLATED FIBERMESH

**Admixtures & Superplasticizers:**

WR (WRDA 79) Water Reducing and Retarder admixture. ASTM C494; Type A & D

HRWR (WRDA 19) High Range Water Reducer and Superplasticizer. ASTM C494; Type A & F

**Table 3.2 Physical properties of plastic fibers.**

Property	Synthetic Fibers Manufacturer		
	Forta Co.	Fibermesh Co.	3M
Synthetic Material Type	<b>Polypropylene</b>	<b>Polypropylene</b>	<b>Polyolefin</b>
Tensile Strength	80-110 Ksi	80-110 Ksi	43 Ksi
Young' Modulus	500 Ksi	500 Ksi	384 Ksi
Specific Gravity	0.9	0.9	0.9
Melting Point	320-340 F	320-340 F	320 F
Ignition Point	1100 F	1100 F	1100 F
Thermal Conductivity	Low	Low	Low
Electrical Conductivity	Low	Low	Low
Acid and Salt Resistance	Excellent	Excellent	Excellent

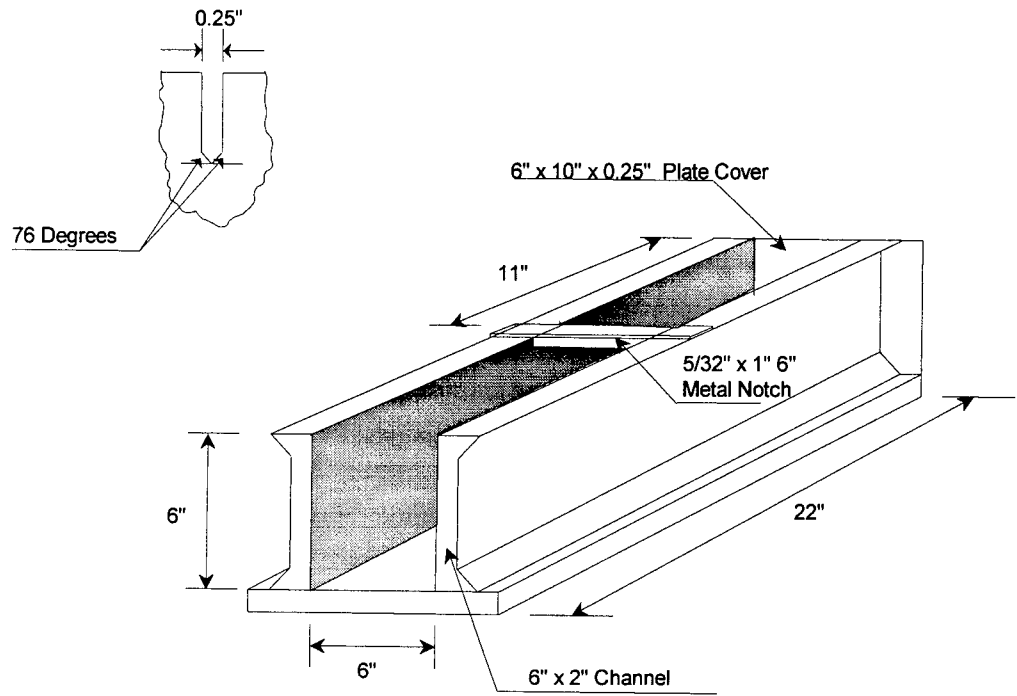


Figure 3.1 Beam Form Detail

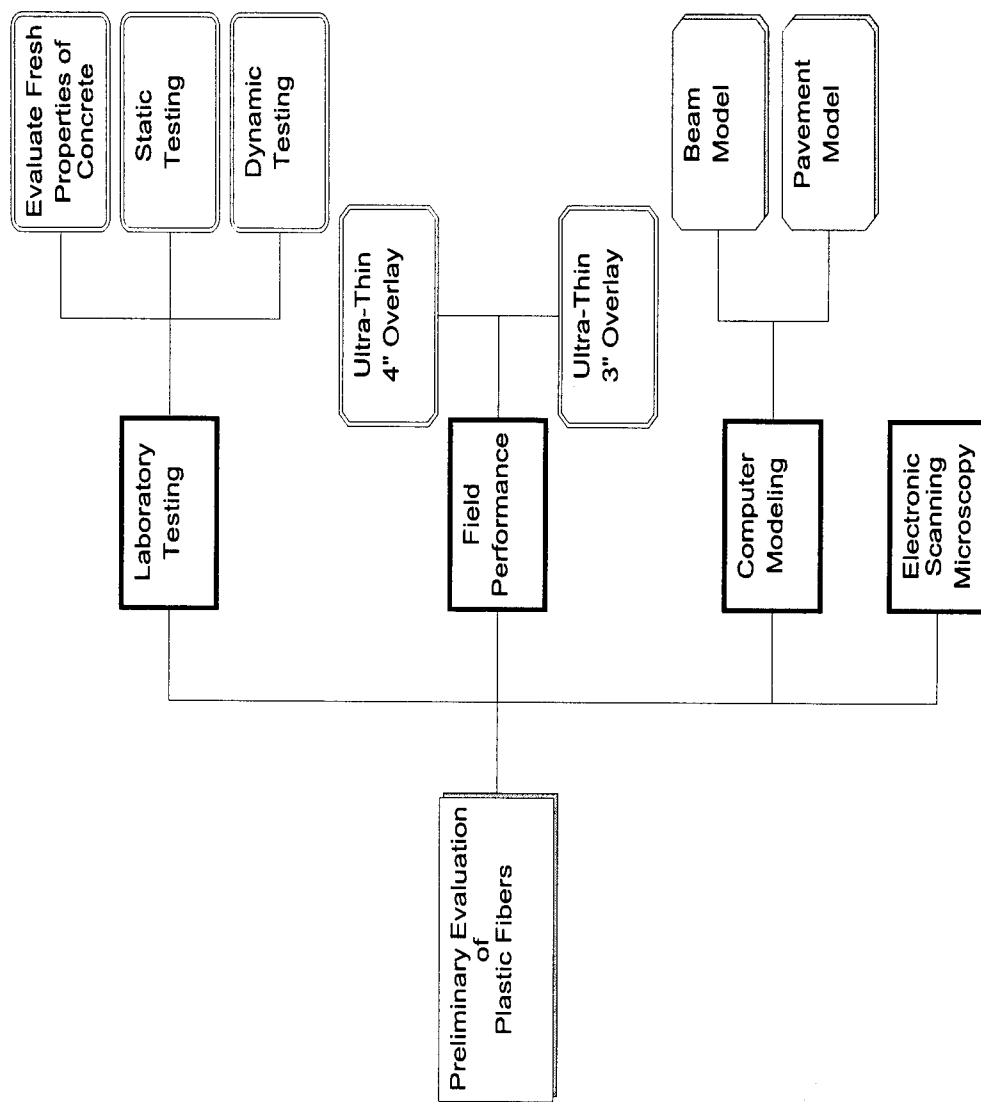
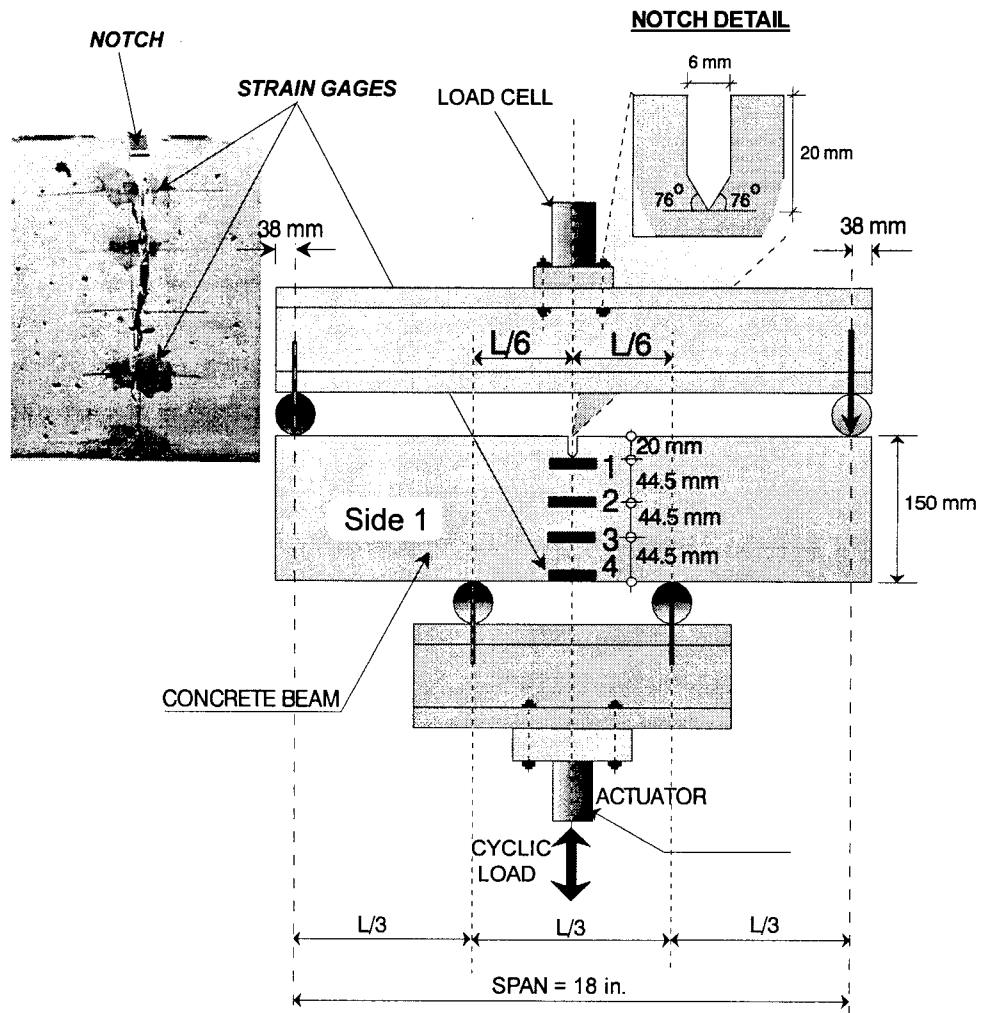


Figure 3.2 Flowchart Diagram of Experimental Program





**Figure 3.3 Fatigue Testing of Notched Beams**

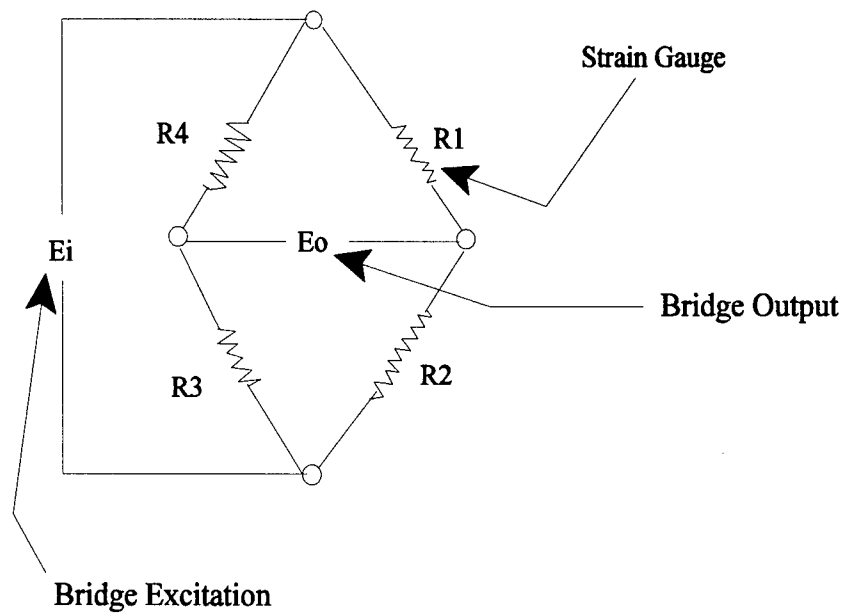
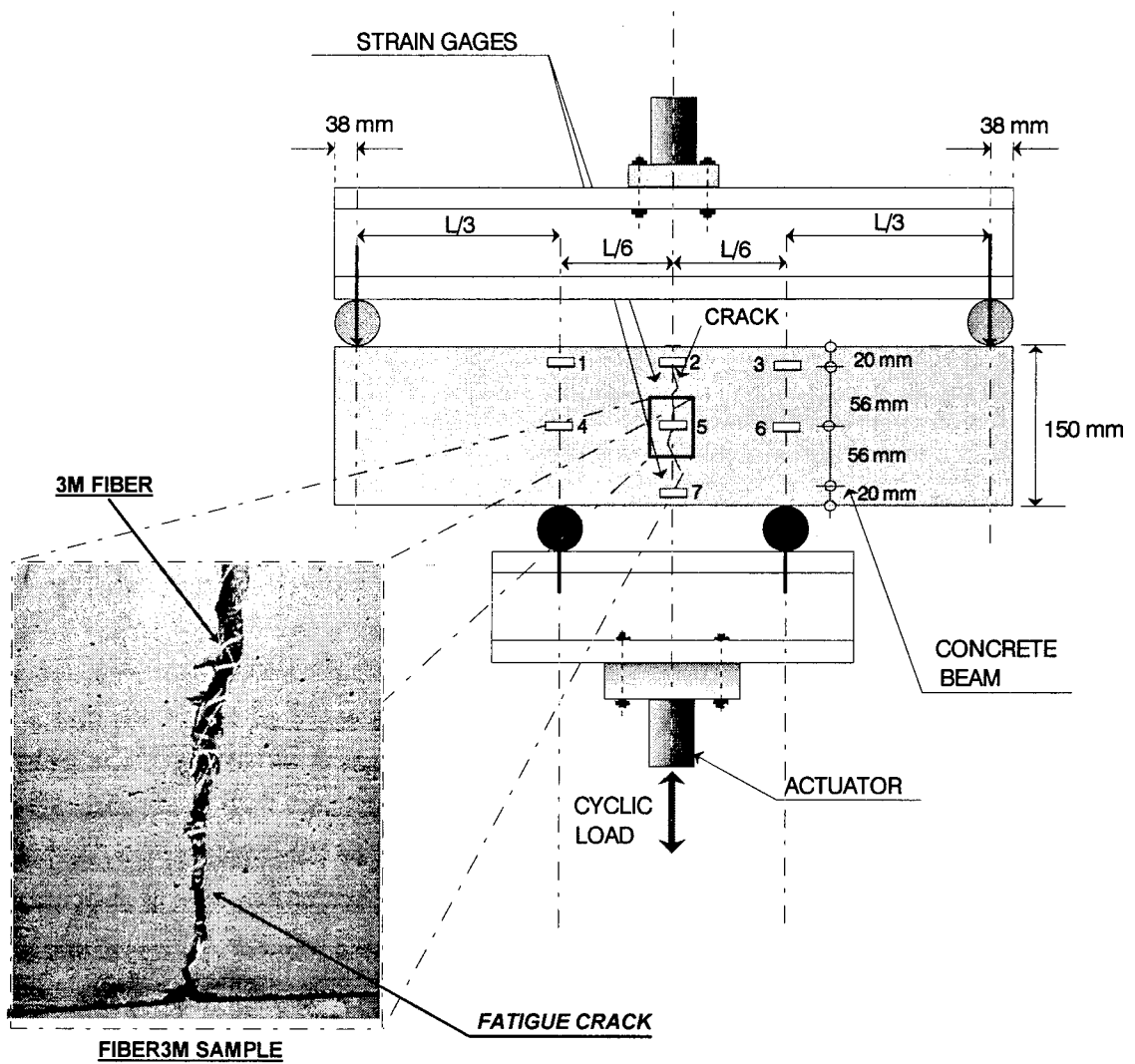
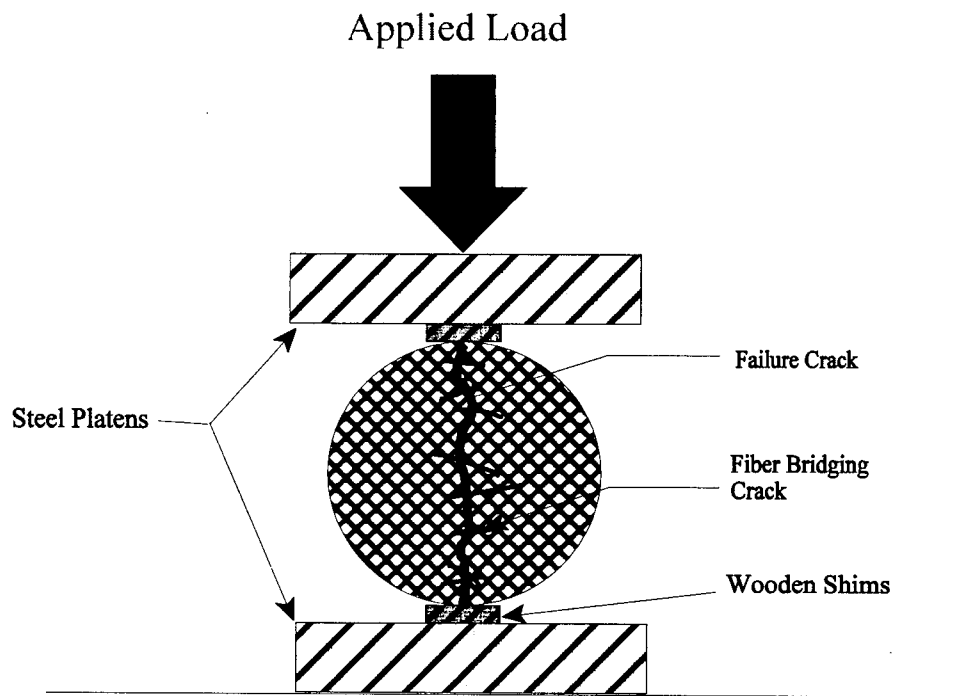


Figure 3.4 Wheatstone Bridge Circuit



**Figure 3.5 Fatigue Testing of Unnotched Beams**



**Figure 3.6 Tensile Strength Test Setup**

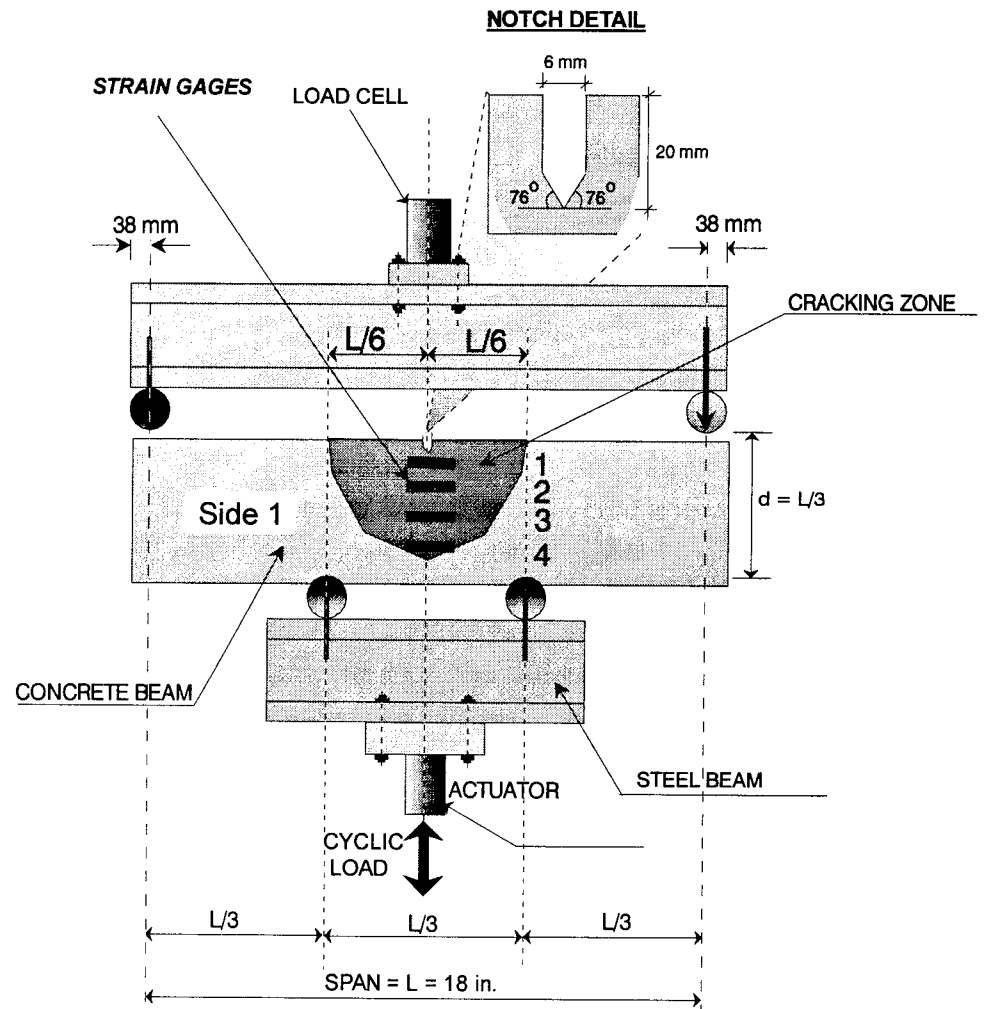
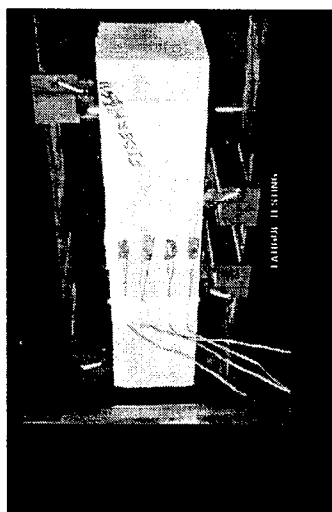
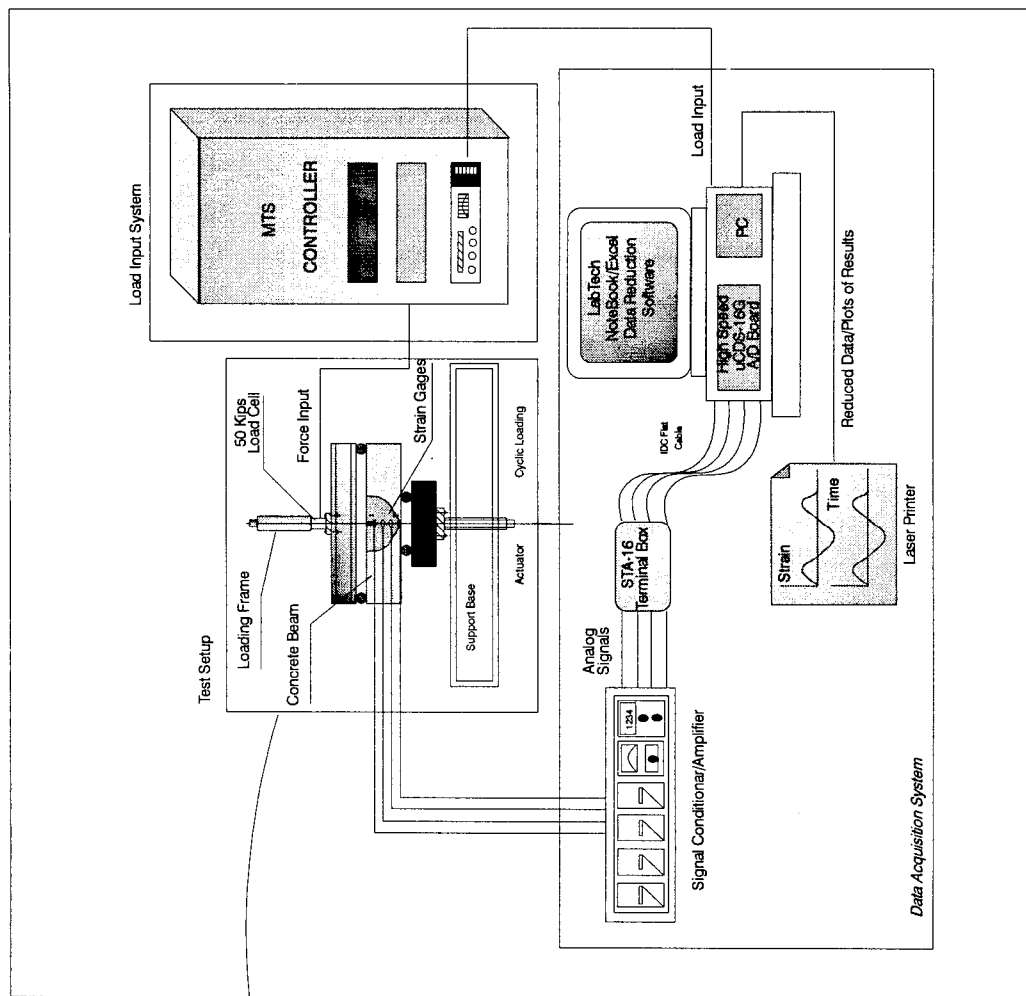


Figure 3.7 Typical Loading Configuration of Beam Sample



**Figure 3.8 Schematic Diagram of Test Set-up**

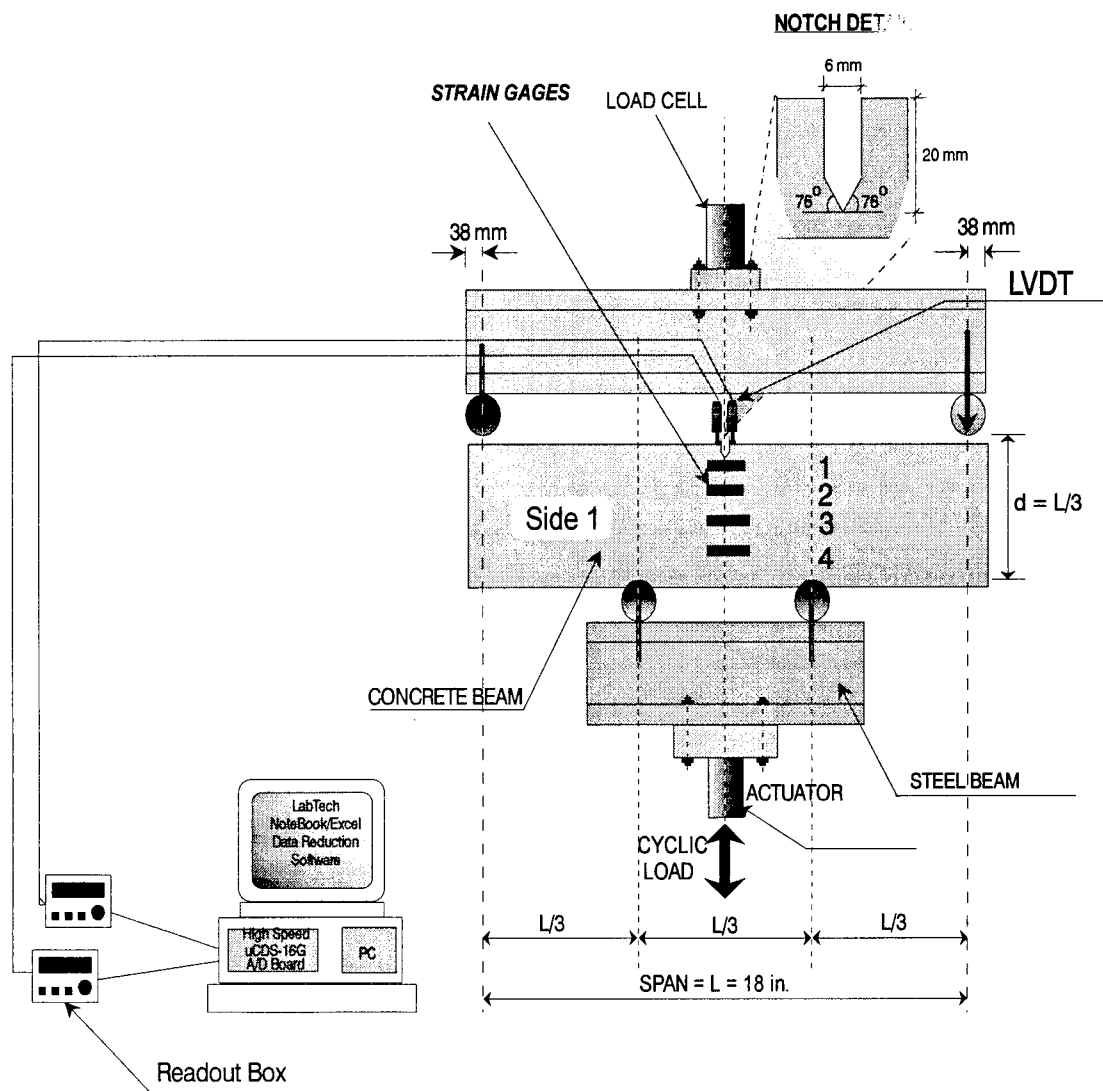
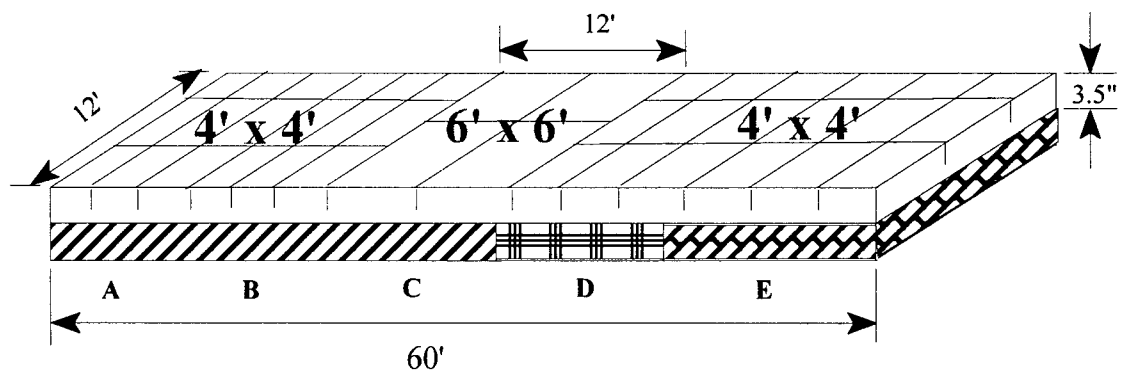



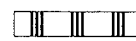
Figure 3.9 Schematic for Deflection Measurements



**A - PCC no fibers**

**B, C, D, E - PCC with fibers**

 Crack Relief Layer

 Existing Surface

 Milled Surface

**A - PCC no fibers**

Figure 3.10 Schematic of Ultra-Thin Concrete Overlay Test Track



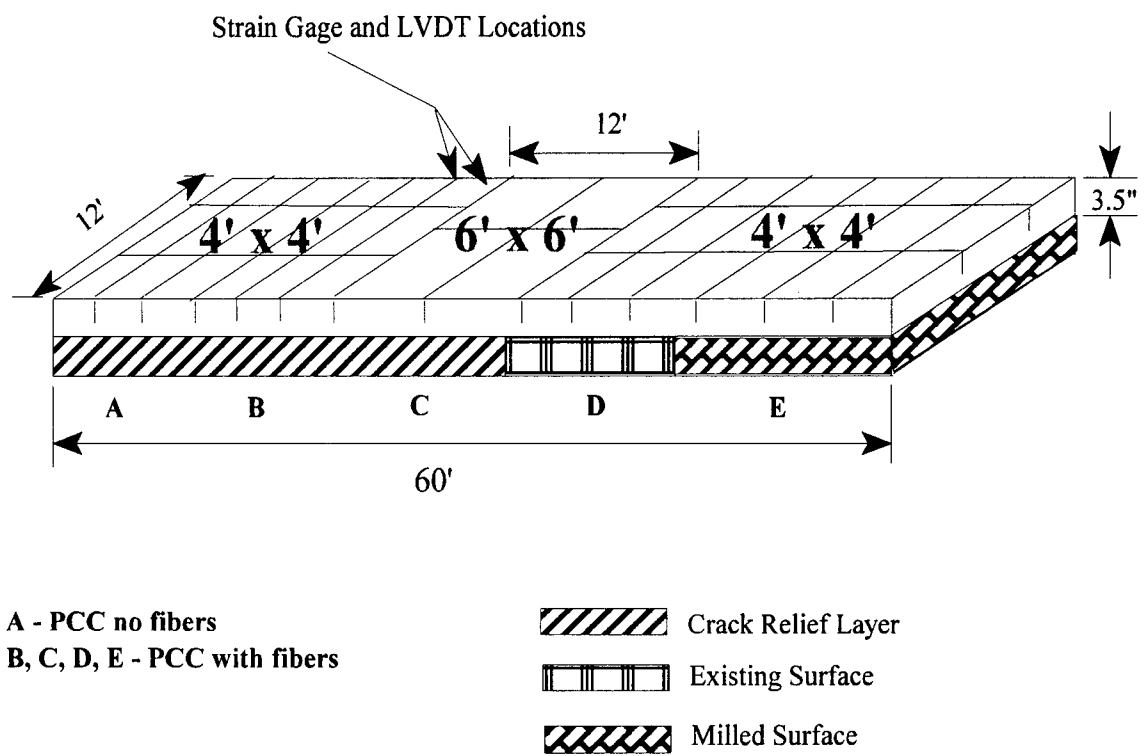


Figure 3.11 Strain Gage Location

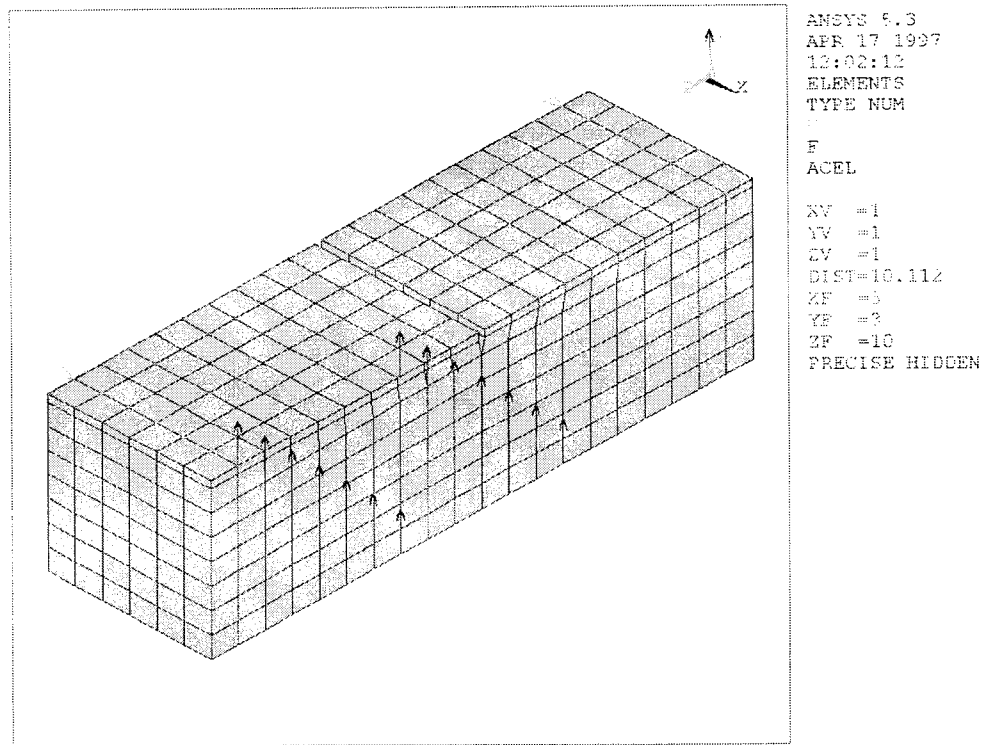


Figure 3.12 Three Dimensional Loading on FEM Beam

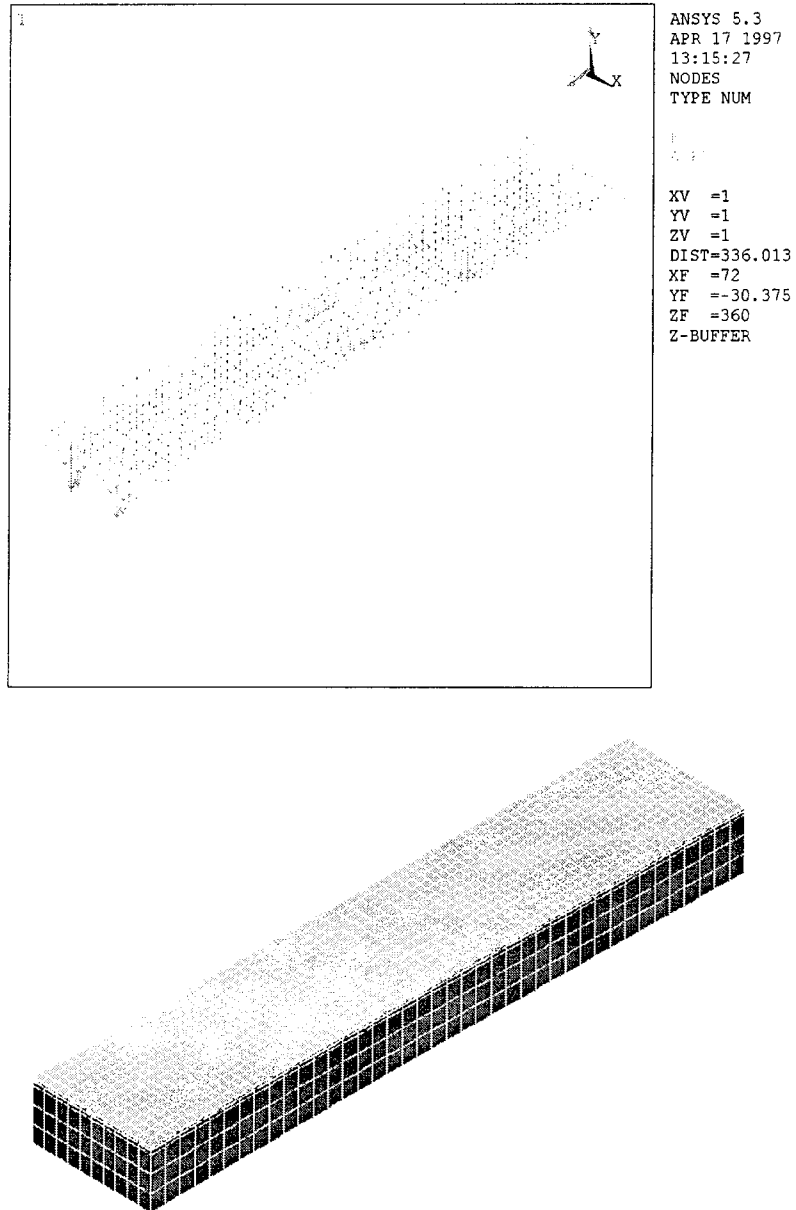


Figure 3.13 Three Dimensional Loading Conditions for FEA Model of The Pavement Overlay



## **CHAPTER IV**

### **RESULTS AND ANALYSIS**

#### **4.1 Introduction**

This chapter presents a discussion of the results obtained during the experimental part of this project. The different testing parameters and fiber reinforced concrete properties are presented for the static and dynamic scenarios. The results are presented in the order that they were obtained during the laboratory testing, followed by the electron scanning microscopy and finite element computer modeling. The chapter is divided into five main areas, namely, fresh properties of FRC, static properties of FRC, dynamic properties of FRC, scanning electron microscopy (SEM), and finite element modeling (FEM).

The first section discusses the fresh properties of concrete. The effect of plastic fiber in the slump, unit weight results, temperature and air content are the core of this section. The analysis of static properties is presented on the second section. It covers the compressive strength (ASTM C39 - 86) of the different mixes, direct tensile strength (ASTM C496 - 90), and flexural strength of FRC beams (ASTM C78 - 84). Following the static properties, is the discussion of the dynamic properties of FRC. This section presents the fatigue test results. Emphasis is given to the hysteretic behavior, strain analysis, stiffness degradation, and maximum stress ratio. Electron Scanning Microscopy is discussed in the fourth section.

Finally, the results obtained from the finite element models are presented on the last section of this chapter.

In order to obtain meaningful comparison among the different fibers used and to facilitate the analysis normalization of data was performed. The normalization of stress and strain has also been used for fatigue behavior of high-performance concrete (Do et al , 1991). The strain was normalized with respect to the maximum strain obtained in a particular test,  $(\epsilon_i / \epsilon_{\max})$ . This procedure was applied also for the number of cycles with respect to the maximum cycles endured,  $(N_i/N_f)$ . The above mentioned parameters are used on the assessment of the damage of concrete.

## **4.2 Fresh Properties of FRC**

The purpose of evaluating concrete mixtures fresh properties is to obtain a product that will perform according to predetermine requirements, such as workability. Workability is defined as the property that determines the ease with which a concrete mixture can be placed, compacted, and finished. Durability is another important property, however this will be evaluated later on this chapter. The concrete mixes were prepared at the FDOT State Materials Office and batched according to the mixing procedures given in the previous chapter. The fresh properties of concrete were measured before placing the concrete in the different beam and cylinder molds. The first objective was to see the mixing behavior of the different ingredients in the mix, specially observing for balling of fibers and segregation of aggregates. The fibers used did not produce balling or segregation when using the standard vertical drum mixer; however, when preparing the FBR3M mix some problems arouse.

There was some balling observed and a high percentage of the fiber did not mix properly. Also, fibers floated on the mix's surface when using the horizontal "pan" mixer. A possible reason for this happening is the lower specific gravity of the fiber versus that of water. Despite of this problem, the strength on the mix were not much different from the others batches prepared as it will be presented on the next sections on this chapter. An extra batch was prepared using the same fibers, but a standard vertical drum mixer was used instead. No problems were observed during mixing and the bundles of fibers broke apart in the time expected. Surface finishing of the FRC did not need extra work when compared to the plain concrete.

The fibers used on the other batches, including the post-consumer recycled plastic fibers were easy to mix, although the aid of superplasticizer was needed in order to produce a more workable mix. The FBR1 and FBRME were the easiest mixes to work with during the different stages. The length (2") of the other fibers, although presented significant improvement on the tensile strength, made it more difficult to work with them at the time of preparing the specimens.

The temperature was taken for each mix prepared after the mixing process was finished. The temperatures for the different mixes are presented on Figure 4.1. The concrete and ambient temperature were recorded during the different batches. There was not a significance change in temperature from the concrete using the different fibers. The change in temperature in concrete was a result of the heat absorbed by the fibers. The range of temperatures ranged from 68 to 85 degrees Fahrenheit. Following the temperature

measurement was the slump measurements (ASTM C143) used to evaluate the workability of the concrete mix. For the different mixes the slump was measured both before and after fiber addition to the concrete. The results indicate that satisfactory workability was obtained even with the larger fibers. This was achieved by adjusting the amount of superplastizicers used. The amount of superplastizer varied from 50 cc for the control to 350 cc for the fiber reinforced concrete. The slump test results are presented on Figure 4.2. The decrease in slump can be observed that has a maximum decrease for longer and stiffer fibers. The decrease in slump did not correlate to a higher strength mix, that is, compressive strength did not increased with a reduction of slump as a result of fiber addition. In addition, the loss in slump did not mean a loss in the workability of the mix. This is an important observation to be considered when design guidelines become available.

The air content was another property measured within the fresh concrete properties. The air content decreased by about 1% for the 3/4" monofilament fibers to 2% for 2" longer and stiffer fibers. The air content test results are presented on Figure 4.3. Finally the unit weight and easiness of finishability were considered. The unit weight of the concrete did not change and slightly varied from 138 to 145 pcf. The unit weight results are presented on Figure 4.4. The finishability was generally good for the mixes except for the monofilament 2" fibers. The reduction in slump lead to believe that finishability would require extra work, however, it was easier to work with it than a collateral mix without fibers.

The fresh properties of concrete varied from the control slightly, however, this change did not affect the hardened properties of concrete. The fiber-reinforced concrete was observed to have less segregation and a significant reduction of the water reaching the



surface, better known as bleeding was observed. A summary of the fresh properties is given in Table 4.1.

### **4.3 Compressive Strength and Tensile Strength of FRC**

The compressive strength ( $f_c$ ), and tensile strength ( $f_t$ ) were evaluated using ASTM standards. All the specimens were prepared, and cured under controlled conditions. Cylinders (6" x 12") were tested for compressive strength (ASTM C 39) at 3, 7, 14 and 28 days, using at least two samples per testing day. The results for compressive strength for the preliminary fiber elimination at the beginning of this research are given in Figures 4.5.a and FIGURE 4.5.b. The compressive strength development is given in Figures 4.6.a to 4.6.c. and Figures 4.6.d to 4.6.f gives the strength development for each separate mix in a bar chart format. The compressive strength was increased in mixes FBR1 and FBR2 (Recycled Plastic) by 7% and 3%, respectively (Figure 4.6.d). A decrease in compressive strength was observed on FBR3M and FBR3MA by 13% and 15% respectively (Figure 4.6.e). The FRBME showed a compressive strength deficit of 4% from the control mix, Figure 4.6.f. The FBRME cylinders were also tested at 8 and 24 hours, achieving more than the required 3,000 psi for 24 hours compressive strength used in fast track construction. The static modulus of elasticity was determined using ASTM method C-469 at 28 days curing. The static modulus test preceded the compressive strength test. The results are presented on Figure 4.7.

The tensile strength ( $f_t$ ), was evaluated using the ASTM C496 - 90 method. Two cylinders (6" x 12") were used for each mix and tested at 28 days. The tensile strength was

increase for all fiber-reinforced mixes particularly the monofilament polyolefin fiber. The fiber did not allow the concrete to have a catastrophic failure such as the failure observed in the control samples. Even though the specimens cracked, the load was transfer directly to the fibers, enabling the fibers to show their tensile and crack arresting capacity. A 8% increased was observed on the FBR1 and FBR2 over the respective control. The FBRME mix presented a increase of 6% in tensile strength over the plain concrete. The specimens reinforced with polyolefin fibers would crack at a strength of about 17% higher than the plain concrete, furthermore, the load carrying capacity did not stop, meaning that the fibers started carrying the applied load not partially but totally until strength of up to 30% increase were observed. This tensile increase represents a significant increase over the plain concrete. The results are presented on Figure 4.8 , 4.9 and 4.10 respectively. This indicates that the length of the fiber is an important factor to be taken into consideration for designing with fibrous concrete. Also, the cross-sectional shape of the home-made post consumer recycled plastic fibers provided an enhancement on the mechanical bonding of the fibers, Figure 1.2.

#### **4.4 Flexural Strength of FRC**

Notched and unnotched beams were prepared to be tested under flexural loading according to ASTM C-78. One specimen from each mix was used to determine the static flexural strength ( $f_r$ ) of each mix and was tested before starting the fatigue testing. This test had a threefold purpose, to obtain the maximum static stress to be used in computing the stress ratio( $f_{max}/f_r$ ) used in the fatigue testing, to obtain the load-deflection data, and establish the stress-strain relationship. The beam was loaded using third point loading

configuration as presented on Figure 3.7. The modulus of rupture ( $f_r$ ) was obtained as explained later on this section. The load-deflection data was obtained by recording the load from the MTS controller display and deflections were obtained from LVDT located on the center of the middle third. For the notched beams two LVDT were used and the average of the results was obtained. A displacement rate of 0.003 in/min was used in all the static testing. The strain was recorded using strain gages as show in Figure 3.8. The load, deflection and strain data where automatically acquired through the DAS. The modulus of rupture,  $f_r$ , was calculated according to ASTM C-78-84 procedure, in which the maximum moment and zero shear are on the middle third of the 18" beam's shear span. The flexural strength,  $f_r$ , for the above configuration and show in Figure 3.7 was calculated as follows:

$$f_r = PL / (bd^2) \quad 4-1$$

where:

- $f_r$  = modulus of rupture in psi
- $P$  = applied load in pounds ( from Eq. 3.1 or 3.2)
- $L$  = shear span length
- $b$  = average width of specimen in inches
- $d$  = average gross depth in inches for un notched beams; for notched specimens  $d_u$  replaced  $d$ , where,  $d_u = d - a$  and  $a = 0.7874$  inches.

The typical load-deflection curves for the virgin plastic and post-consumer plastic fibers are presented on Figures 4.11 to 4.31.. In comparing the fiber-reinforced concrete to the corresponding non-reinforced concrete, it can be observed that there is an increase in the static flexural strength as a result of the inclusion of synthetic fibers. The fibers proved during the flexural test to have the ability to act as crack arrestor. The mix FRB1 ( 1.6 lbs/cy) failed

suddenly when the first flexural crack formed, figure 4.15. This sudden failure was exactly the same for non-reinforced concrete. Plain concrete fails immediately upon cracking without adding any further load carrying capabilities, figure 4.11. The others mixes FBR2 (recycled plastic), FBRME and FBR3M did not have a sudden failure when cracking was visible, however, there was a sudden drop of load but still some load could be carried by the fibers, figures 4.19, 4.29 and 4.30, respectively. The fiber-reinforced concrete deflected on a smooth manner after visible cracks. It was observed that fiber-reinforced beams (FBR2, FBR3M and FBRME) had added ductility and post-crack energy compared to the non-reinforced beams. The addition of fibers changed the failure mode from a sudden brittle failure to a more ductile non-catastrophic mode. The FBR3M produced a residual load carrying capacity from 15% to 35 % of the maximum load which is very significant compared to a non-existent post-failure load carrying capacity of the plain concrete.

The use of a notch as a pre-existing crack, had an effect on the flexural stress concentration under the tip of the notch, thus, flexural strength values need to take into account this stress intensity being produced. Evaluation of the critical effective stress was obtained using equation 2.2 (Jeng and Shah, 1985) and the relationship of the critical stress intensity factor was evaluated using equation 2.1 as suggested by Naus and Lott (1969). Using the aforementioned equations the critical intensity factor was found to be 0.1364 of the corresponding load being applied, leading to an increase in stress of 35% on the location of strain gage number one, which is located on tension fiber of the beam. The stresses below the notch at gage no. 1 were determined from the following equation (Maalej and Li, 1994):

$$\sigma_2(x) = 1/(d-a)[T_c (d-x) - C (x-a)]$$

4-2

where:

- $\sigma_2(x)$  = stress distribution outside fracture process zone
- $d$  = beam depth
- $a$  = length of notch (pre-crack)
- $C$  = compressive stress at beam-compression face
- $T_c$  = composite tensile strength
- $x$  = distance from the beam tension face

The stresses for the rest of the gages was not changed, therefore the elastic analysis of the modulus of rupture could be based on equation 4-1, using the ligament depth ( $d_u$ ) for the notched and using the gross depth ( $d$ ) for the unnotched beams (Espiritu, 1994 and Gopalaratnam et al 1991). The comparison of the stress development of non-reinforced and fiber-reinforced concrete specimens at loads near failure both groups exhibit same strain development. However, fiber-reinforced failed at higher load, 5250 lbs, than non-reinforced concrete, 4770 lbs. The 10% increase in flexural strength was observed on the different fibers used. The strain values were compared at 500 psi applied stress and was found that there was more strain in non-reinforced concrete versus the fiber-reinforced Figure 4.32. This could be as a result of the added ductility given by the fibers. This comparison was also shown in the finite element method as presented in Fig. 4.32.a and Fig. 4.32.b. This results quantify the delay period in strain development and shows the fiber capacity to act as crack arrester.

The stress-strain relationship for the different mixes is shown in Fig. 4.32. This graphs shows that fiber-reinforced concrete had a lower strain rate compared to non-reinforced and the ability to sustain loads longer past beyond the failure point for plain concrete. The crack would travel in some of the specimen through all the gages, from which the velocity of

cracking was obtained. The speed of cracking was decreased by 35% in comparison to the speed obtained on previous research (Espiritu, 1994).

The strain development showed three distinctive stages which are presented on Figure 4.33. The crack initiation stage, **Stage I**, runs from 0 to about 40%, the second stage, **Stage II**, or crack propagation ranges from 40% to 90% and the final stage, **Stage III**, the rapid propagation stage developed from 90% to failure. The first stage shows a decrease of 20% rate of strain compared to plain concrete. During this stage no macro cracks were noticed under the tip of the notch. The fibers helped to delay the crack initiation as is seen on Figure 4.34. It is believed that some micro cracks are formed and propagated through the inherent discontinuities of the concrete, but they are arrested by the presence of the fiber, which creates a need for an increase in energy for the crack to travel around the fiber after traveling through the discontinuities and mortar interfaces. The second, stage presented a more linear behavior and the crack propagation rate was considerably slowed. The rate was extended between 90 and 95 % of the strength. This stage represents the border-line between the appearance of micro-crack and macro-cracks as load increased. The last stage, is high rate increase of strain and rapid crack propagation was seen until failure. The fiber-reinforced concrete showed the load-carrying capability after macro-cracks were observed, compared to the non-load-carrying capability of non-reinforced concrete.

## **4.5 Fatigue Strength of FRC**

The variety of fiber-reinforced concrete samples tested in this study, produced different fatigue fracture behavior. Using the same stress ratio and concrete strength, non-reinforced concrete showed different fatigue life in comparison to fiber-reinforced specimens. Also, it was noticed that even the non-reinforced concrete resulted in different number of cycles. Because of this variation in the fatigue life, the number of cycles,  $N_i$ , for the beams subjected to fatigue loading, was divide by the maximum number of cycles,  $N_f$ , that a specimen would sustained. This value , know as normalization, gave the percentage fatigue life of the specimen, facilitating the comparison among the other mixes.

The fatigue test were carried out according to the method described on chapter three. The main parameters used were the stress ratio and the compressive strength,  $f'_c$ , obtained from each mix. The fatigue testing was performed on three mixes, namely, FBR1, FBR3M and FBRME using 5 to 7 samples per mix. The applied maximum and minimum stress levels were given as a ratio of the flexural strength,  $f_r$ , and ranged from 50 to 90%. Continuous acquisition of data was obtained from the strain foil gages and MTS controller at different intervals of time. The entire setup is shown in Figure 3.8.

### **4.5.1 Hysteresis Behavior of FRC**

The stress-strain diagrams also know as hysteresis loops for strain gage #1 in the different samples are show in Figure 4.35 to 4.44. The hysteresis loops are presented for the notched samples only, unnotched samples were not presented due to the scatter of the data obtained. Strain irregularities were observed sometimes, the values would decrease as the number of cycles would increase. The data recorded was normalized in order to obtain valid

comparisons between the different samples tested.

The magnitude of the strain from the gages was divided between the permanent strain and recovered strain. The permanent or plastic strain is what remained after unloading. The recovered or elastic strain is the difference between the permanent strain and the total strain. The permanent strain is not always equal to the remaining strain because there could be a recovery period or pause period. The testing was conducted without rest periods. The equation that expresses the relationship among the different terms explain above is as follows:

$$\epsilon_t = \epsilon_r + \epsilon_p \quad 4-3$$

where:

$\epsilon_t$  = total strain in micro in/in

$\epsilon_r$  = recovered (elastic) strain in micro in/in

$\epsilon_p$  = permanent (plastic) strain in micro in/in

It was observed that the loops at the beginning of the cycles the slope is higher indicating a more plastic behavior for the plain concrete, however, it was less severe for the fiber reinforced concrete. The slope of the loop decreased as the sample started to approach failure. This behavior lasted longer for the fiber-reinforced concrete than the plain concrete. This behavior is typical of materials such as concrete, that is elasto-plastic materials. The permanent strain range from 100 to 4500 $\mu$  strains. In general, it was observed that the rate of strain increased a lot faster for the plain concrete than fiber-reinforced concrete.



#### **4.5.2 Strain Analysis and Stiffness Degradation**

The chord modulus is the slope of the line between maximum load,  $S_{max}$ , and the minimum load,  $S_{min}$ , of each cycle load. During this study the chord modulus versus number of cycle ratio, was study throughout the fatigue life of the specimen. Table 4.2 summarizes the stress ratios used and the number of cycles sustained from each specimen. The strain obtained, the number of cycles and the chord modulus are included also. The chord modulus of elasticity was determined as follows:

$$E_c = (S_{max} - S_{min}) / \epsilon_r \quad 4-4$$

$E_c$  = chord modulus of elasticity in millions psi.  
 $S_{max}$  = maximum stress ratio in psi  
 $S_{min}$  = minimum stress ratio in psi  
 $\epsilon_r$  = recovered strain

The results from the gage number one, revealed that the development and propagation of microcracking in plain and fiber-reinforced concrete have almost the same pattern with different rates of propagation. This patter was distinguished by three clearly marked stages during the total fatigue life of the concrete beams. The first stage, Stage I, which represented the crack initiation where the strain increased up to a certain level. At this stage cracks started to appear on the surface of the specimen. The strain rate of plain concrete during this stage was higher than the fiber -reinforced concrete. This stage would represent 5% of the cycles in plain concrete; however the fiber reinforced concrete would be extended up to 15 to 20% of the total cycles to failure. The strain rate development was of about 527 micro strain per 1% cycle ratio, and 750 micro strain per cycle ratio for the fiber reinforced concrete.

The second stage was well steady and almost linear for the plain concrete. This stage represents the crack propagation phase where the micro-cracks have evolved into macro-

cracks. In the plain concrete the second stage represented about 75 to 80 % of the cycles, being it the longest period in the cracking process. The fiber reinforced concrete, presented longer duration during this period, extending up to 90% of the cycles to failure. This increase of 10% is significant compared to plain concrete. At this interval, the crack path continued to advance forward toward the compression zone. This advancement was very noticeable in the fiber reinforced concrete beam but did not imply a sudden failure of the concrete. This same situation was observed in plain concrete, however the appearance of cracks implied failure at any moment. As the load ratios reduced, the second stage stabilized and the third stage was more controllable when the fibers were present.

The last stage, Stage III, depicts the rapid crack propagation, massive crack development and failure. This stage was very unstable and cracking was uncontrollable up to failure when fibers were not present; however, as mentioned above the fiber were acting as crack arrester holding the two concrete crack walls together, producing a more stable phase. The rate of strain increased significantly during this period in the plain concrete. The range measurement was from about 5500  $\mu$  strains to failure. This stage constituted between 20 to 25 % of the plain concrete total duration of the fatigue testing. The fiber-reinforced concrete represented only 5 to 8% of the fatigue life of the concrete during this stage. The presence of macro-cracks was unavoidable, however the catastrophic failure seen in the plain concrete was not present in the fiber reinforced concrete. The strain development is show in Figures 4.45 to 4.54.

It was expected the speed of propagation was faster for the higher stress ratios in plain concrete and an average speed of 152.36 inches/second was obtained. The fibers

helped reduced the speed of cracking. The percentage reduction of 35% for the higher ratios was found. This demonstrates again the added ductility and post-crack load carrying capacity given to the concrete when the fiber are added. In general, it was found that the addition of fibers to the concrete delayed the first stage and second stage. The strain gage number four was also analyzed. The location of this gage was within the compression fiber of the beam. The values were very much smaller than the strains obtained for the strains in the tension fiber of the beam. This was true for the fiber-reinforced concrete as well as the plain concrete.

The damage of concrete has been assessed by some researchers by using the stiffness degradation of the concrete matrix. Holmes (1982), indicated that a decrease in concrete stiffness is an indicator of the degree of damage experienced by concrete. Also, the durability of the concrete has been related to the stiffness degradation of concrete through the process of disruption caused by concrete fracture. The chord moduli ( $E_c$ ) versus cycle ratio ( $N_i/N_f$ ) are presented on Figures 4.55 to 4.64. The values obtained were produced from the maximum and minimum values of each loading curve per cycle applied. The plain concrete presented a nonlinear relationship when plot in a chord modulus ( $E_c$ ) versus number of cycles. This behavior was also present in the fiber-reinforced concrete and as before three stages were clearly defined. The stiffness degradation was found to be lower for samples subjected to higher stress ratios. From the fatigue results, a plain concrete sample subjected to a stress ratio of 63% ( $S=63\%$ ), the chord modulus decreased by about  $1.1 \times 10^6$  psi per cycle ratio ( $N_i/N_f$ ), and it was about  $0.657 \times 10^6$  psi per cycle ratio for fiber reinforce concrete beams of FBR3M mix. As mentioned earlier, the addition of fiber was found to delay the STAGE I and STAGE II extending the life of the concrete.

The addition of fiber to the concrete helped to extend the percentage of the second stage by as much as 40%. The ability of the fiber-reinforced concrete to resist the cyclic loading beyond the one million cycles, was due to the bridging provided by the fiber by not allowing the concrete to shatter, and carrying the stress concentration instead of the concrete. In general the best behavior was observed by the combination of lower strength concrete and plastic fiber addition. Lower strength concrete exhibits larger strain capacity, which is significantly enhanced by the incorporation of fibers. The fiber addition to the concrete prolonged the fatigue life and a 15 to 18% improvement on the fatigue endurance was observed by the reinforcement of concrete with fibers.

#### **4.5.3 Maximum Stress Ratio and Cycles Endured**

The stress ratio range used on this research was from 50% to 90% of the flexural strength,  $f_r$ . The results are summarized on Table 4.2. The main parameters studied were the maximum stress ratio,  $S$ , the number of cycles sustained,  $N$ , the compressive strength,  $f'_c$ , and the type of fiber used. The results obtained were plotted in typical two-dimensional graph where the ordinate represents the stress ratio of the maximum flexural stress,  $S_{max}$ , to the ultimate static strength,  $f_r$ , given in percentage and the abscissa is used for the number of cycles ( $N$ ) sustained to failure in logarithmic scale. This plot is better known as Wohler's diagram.

Concrete testing results are known to be inconsistent, therefore, the data obtained was treated statistically before it was plotted in the S-N diagrams. The scatterness of the data, that is the inconsistency of the concrete strength and applied ratios as well as the fact of the fiber random orientation suggested that data obtained must be treated using regression

analysis. In calculating N, the number of cycles was used as the independent variable and the stress ratio, S, was used as the predictor. The process of statistically evaluating this models consisted of checking its adequacy by plotting the different variables, testing for lack of fit, detecting outlier, and other regression analysis techniques used for model adequacy.

The number of cycles or independent variable was transformed into its logarithmic form, resulting in a more normal distribution. The comparison of the different mixes was done using the S-N curves, and presented in Figure 4.65. The equation used was:

$$S = \beta_0 + \beta_1 \text{Log} (N) \quad 4-5$$

Where:

- S = Smax / fr ; maximum stress ratio in %
- N = Number of cycles to failure
- $\beta_0$  = Numerical coefficient
- $\beta_1$  = Numerical coefficient

The first numerical constant,  $\beta_0$ , represents the intercept of the least squares line while  $\beta_1$  stands for the change in stress ratio, S, per unit change in the cycle number, N. The graph presented in Figure 4.65, shows that the different mixes were parallel, implying that fiber reinforced concrete is sensitive to small changes on the Smax.

The linear regression analysis performed on the different mixes used on this research the following equations would best represent the best fit line that would give the stress ratio given the number of cycles applied. Equation 4-6, 4-7 and 4-8, represent the best fit line for FBR1, FBR3M and FBRME, respectively.

$$S = 100 - 5.411 \log (N) \quad 4-6$$

$$S = 98 - 6.44 \log (N) \quad 4-7$$

$$S = 115 - 7 \log (N) \quad 4-8$$

where:

S = Stress Ratio

N = Number of applied cycles

#### **4.6 Scanning Electron Microscopy**

Since the 1960s, there has been extensive research performed on fiber-reinforced concrete related to the mechanical bonding performance of the fibers, and is these research that pioneer on the standard of synthetic fiber. The interfacial bond strength was not the main objective in this research, however, it was thought of being an important factor in the overall behavior of the concrete.

The efficiency of the fiber depends heavily on the interfacial bond strength between the fiber and the cement matrix. Naamn et al (1986) cited the characteristics of polypropylene fiber as chemically inert and very stable because of the hydrophobic nature of its surfaces. They enumerated some of the shortcoming of using this fibers as well as the poor bonding with cementitious materials. The ACI committee 544 (1985) reported that sulfur impregnated and polymer impregnated fiber reinforced concretes did exhibit better fibers bonding as well as improvements in the overall strength of the concrete composite.

In this study various samples from the different mixes were obtained randomly from failed specimens for Scanning Electron Microscopy (SEM), a technique that allows to study the interfacial bonding of the concrete and the fiber at microscopic level. The samples

obtained were prepared using a gold coat prior to the inspection under the microscope. The samples used were from the FBR1 and FBRME mixes, and are illustrated in FIG 4.66 to 4.71.

The fibers presented on its morphology, small crystals with a low density of some kind of precipitates all around its surface, Figure 4.66. Lovata et al (1987) reported similar findings in chemically untreated fibers used for concrete reinforcement. The fibers taken from the tensile test specimens presented some tear at the end of the fibers, Figure 4.67, resembling a shear fiber failure rather than a pullout fiber failure. In the other hand, failure in tension was found on some of the fibers by seeing the abruption at the end of the fiber, Figure 4.69 and 4.70, explaining the fiber capacity of having an excellent efficiency and load transfer from the failed concrete matrix to the fiber.

The finding presented above help explained why some of the compressive test specimens were no longer able to support any more load after failure even though their surface did not show any major visible cracking, that is in other words, the specimen obviously failed because of a network of micro cracks while the fibers resisted the propagation of major macro cracks to the surface of the specimen. Similar situation were observed during the flexural test of beams, where at peak loadings or failure loadings were sustained for several seconds before the load would drop. This again, is an evidence of the high efficiency that fibers have in load transferring, particularly at peak loads.

In this research there was not chemical treatment of the fibers, however according to Lovata et al (1987) chemical treatment of the fibers using a basic solution of linear alcohol alkoxylates would improve the mechanical bonding of the fibers to the matrix, and improve the overall performance of the concrete. It was also cited in this research that fibers that

were chemically treated started to fail rather than pull out of the matrix under loading.

In short, the plastic fibers used on this research would improve the durability of the concrete in the long term, since is shown from the SEM that alkaline environment, such as concrete do not disintegrate the fiber, therefore maintaining its crack arresting capabilities intact and not having a negative effect on its surfaces.

#### **4.7 Finite Element Analysis**

The purpose of using Finite Element Analysis in this project was to visualize the distribution path of strains and nucleation of growth of fatigue cracking inside the concrete beams. The laboratory testing along with the FEA help to better comprehend the effects of material properties, boundary conditions, and geometrical characteristics on the fatigue behavior of structures such as pavement overlays also know as white toppings. The use of FEA helped to better understand the effect of fiber orientation, the aspect ratio of the fiber, and the ratio of volume of fiber used.

Two three-dimensional models were built in this project, Figure 1.7 and 1.8. The main finite element program used was ANSYS 5.2 which allows the use of concrete elements. The first model was a notched concrete beam using the same dimensions as the beams used during the flexure testing. This dimensions are given in Figure 3.3. The second and more complicated model was a pavement overlay, which is scaled to the full-size test track built on the FDOT test yard. The dimensions for this model are given in Figure 3.10.

The proper calibration of these numerical models were based on the results obtained from the laboratory testing such as static and fatigue testing. The parametric analysis was



easily done once the different parameters were verified. A more detailed description of the FE models follows.

#### **4.7.1 Three-Dimensional Notched Beam FE Model**

A three-dimensional model was developed for the non-linear study of this fiber-cement composite. The shape and size of the model followed ASTM-1018 standards, which is used for flexural testing of fiber reinforced concrete. The boundary conditions were set in such a way that the model could respond to typical loads applied on flexure, such as third point loading conditions. The reinforcement was oriented in the three main global axis, namely X, Y and Z, and runs were performed for each orientation.

The model was built having in mind the flexibility of use for other types of concretes. The model can be used for concrete matrix with different Young's modulus, tensile strength properties, compressive properties and Poisson's ratio. The model helped to find the flexural strength of the given parameters, identify areas of high stress and strain, deflection and crack formation through the test process which is very difficult to obtain under laboratory conditions. Furthermore, the model can be reinforced, if desired, with steel in any direction by using the smearing process and the a volume ratio of reinforcing material to the concrete volume. Additionally, the model was built to be temperature sensitive if desired, that is, temperature can be one of the variables to be included in the analysis process.

The single notch was used in this beam in accordance to fracture mechanics of concrete with the idea of obtaining high stresses at the middle section and obtaining cracking in the middle third shear span of the beam. The element used in this model was SOLID-65 with one inch by side elements except for the one-quarter inch elements on the middle section

below the tip of the notch. The element selected is used for three-dimensional modeling, and is defined by eight nodes having three degrees of freedom at each node: translations in the nodal, y, and z directions. Furthermore, the cracking in tension and crushing in compression capabilities are built into this model in addition to the plastic deformation and creep capabilities. A total of about one thousand elements were used on this model.

This program was executed different times for debugging purposes. Before each run all output parameters were set. This computer software is based on a linear solver, therefore a high number of iterations are need in order to obtain converged results. The load was applied using substeps, that is, a percentage of the total load. The program would run at ten percent of the total load and obtain the pertinent result, then a ten percent increment would be applied until the maximum load that can be carried was obtained. The output result consist of plane stress, plane strain, principle stress and strain, strain and stress in all directions (x, y, z), and deflections in all axis. The main output to be looked at in this project were stress in Z-axis or parallel to the axis of bending, strain and deflection in the Y-axis or axis of perpendicular to the axis of bending.

The results are presented on Figures 4.72 to 4.78. The figures show clearly the effect of fiber orientation in all cementitious matrix. The preferred orientation is parallel to the axis of bending when using the same 1.6% of fiber by volume. The 90 degrees and 45 degrees followed as the second and third angle of preferred orientations. The stress deflection curve shows that having reinforcement on the bending axis gives high flexural strength and low deflection. The stress development from this model are presented on Figures 4.79 to 4.82. The maximum stress on the zero-degree reinforcement is 579 psi and a maximum deflection

of eight thousands of an inch (0.008"). Also, there is a residual strength of 80 psi after the formation and propagation of cracks. The results show in the stress vs. deflection of each axis shows that the z-axis does not suffer a complete failure as opposed to the other two angle of reinforcement. The first cracks are seen at 76% of the load and this are closed cracks. The total length for this particular load is about five inches for the Z-axis reinforcement, however, there is catastrophic failure for the other two angle of reinforcement.

The second best results are obtained using reinforcement on the he 45 degree angle. The maximum deflection was 40 thousands of an inch (0.040"). There is a phenomenon that is also seen in laboratory work when performing flexure tests. There is a sudden and catastrophic failure without leaving any residual strength. The programs that were ran using 45 degree reinforcement failed at a stress of 579.4 psi and immediately decreased to a 2.4 psi stress before totally failing.

The ninety degree reinforcement showed as expected the highest deflection of 200 thousands of an in (0.200'). In contrast to the gentle failure of the z-axis reinforcement, the 90 degree reinforcement showed a sudden failure. Although, this orientation shows what seems to be residual strength, in actually it will be not, because there is not an increase of strength after a high drop of strength after cracking.

#### **4.7.2 Ultra-Thin Pavement Overlay FE Model**

This model was developed with the objective of investigating the mechanic which initiated debonding of pavement overlays, effect of joint spacing and slab size. The model was used to compare results from deformations obtained from the full scale test tracks built in the FDOT test yard. The dimensions of the model and the full scale track is show in Figure

3.10. Three sizes were used for the fiber reinforced concrete slabs used in this projects. The thickness of the overlay was from 2 to 4 inches and different surface preparations were used to observe the effect of bonding in milled surface and non-milled surfaces.

Overlay is a paving process in which a two to four inches layer of fiber-reinforced concrete is placed over a prepared surface of distress asphalt. The resulting composite pavement delivers longer life and more durable characteristics of rigid pavements. A similar approach was used when building the model. The four inches concrete elements were placed over the asphalt elements , which were differentiated by the material characteristics such as young modulus, Poisson's's ratio and tensile and compressive strength of the material. The different milled surfaces were simulated by using different coefficients of frictions between the two surfaces. The same SOLID-65 was used as in the previous model and reinforced in only one direction. The joint spacing was of 1/30 of an inch by 1 ½ inch deep. The results obtained are presented on Figure 4.83 to 4.88.

The various reports on research done on pavement overlays identified thermal stresses and adverse curing conditions as initiators of debonding. This numerical model has the capability to analyze stress near a crack or joints and thermal and early shrinkage stresses. The finite element model presented is an appropriate modeling technique because is able to address the following issues in overlay pavement system: continuous support of the original pavement, cracks in the original pavement, cracks in the overlay, development of interfacial shear stress as a result of differential material characteristics, reinforcement of any kind and in any angle, and use of complex temperature distributions in the pavement. It is the best technique because there is no other method to address all of the aforementioned issues

simultaneously. The material properties for the different materials used are presented on Table 4.3. The system consisted of soil sub-base, asphalt and concrete reinforced with fibers. There were four important material properties used, compressive strength, young's modulus, tensile strength and concrete temperature. The temperature was used uniformly and without variation through the test.

The results show that debonding is of higher proportion on the corners of the overlay, that is pavement loading is transferred into an uplift force at the critical sections of the slab. The use of this model for stress analysis is appropriate. The stresses were transferred from the different layers in the system.

#### **4.8 Ultra-Thin Pavement Overlay (Test Track #1)**

Pavement overlays are thin fiber reinforced concrete layers that rest on asphalt concrete. The overlay have a thickness of 2" to 4" and different slab sizes. The project engineer from FDOT needed to see the performance of the fibers under field conditions. The layout of the test track is presented in Figure 3.10. The first step in the execution of this project was to prepare the pavement surface where the overlay was placed. There were three types of surface studied, namely, crack relief layer, milled surface, and plain asphalt. The second step was to install the form work where the the concrete was going to be placed. The next step was to placed the concrete and do the corresponding sampling to be tested at the lab. The process continue by placing the fiber reinforced concrete and instrumenting the slabs. Finally the joint cutting was done using a soft cut machine, Figure 4.104. The whole construction process is summarized in Figures 4.98 to 4.108.

The concrete was placed and vibrated using a screed, Figure 4.101, and later the

surface was finished using manual trowels, figure 4.103. The overlay was loaded after 24 hours of curing. The slabs have been loaded every day, two times a day, once in the morning and once in the afternoon using a 20-kip/axle loading truck. The results obtained from the strain gages and deflectometers (LVDT) are presented in Figure 4.89 to Figure 4.97.

The reduction of the slab thickness and the enhancement of the bond using the milling process was found to be satisfactory. The bond helped reduce stresses by making the overlay act as one layer with the distress asphalt. Furthermore, reduction of stresses was observed by the reconfiguring the joint spacing. The three slab sizes used were, 6'x6', 4'x4' and 12'x12'. The cracking observed was as expected, only cracks that developed from the joints. There were only two transversal cracks in the 6'x6' slab and one longitudinal crack in the 12'x12' slab. The fibers performed well and no problems were observed during the construction. This new technique would help in reducing the thickness of the pavements, would allow the use of fast track methods making it competitive to asphalt concrete because traffic can be open 24 hours after construction.

**Table 4.1 Mechanical Properties of Fiber Reinforced Concrete.**

Mix Type	Temperature* Deg. F	Slump** In.	Air Content (%)	Unit Weigth Lbs/cf
FBRC	68 / 69	6.5	5	138.3
FBR1	67 / 69	6.5 / 3.5	4	141.0
FBR2	74 / 80	6 / 4	3.8	141.0
FBRCNT	83 / 87	6	3.2	139.8
FBR3M	83 / 87	6 / 3.5	2.4	141.2
FBR3MA	83 / 89	9 / 3.5	2.2	140.5
FBRMEC	85 / 90	2.5	2.5	145.3
FBRME	83 / 90	2.5	1.5	142.3

\* Concrete temp. / Ambient temperature

\*\* Before adding fibers / After adding fibers.

**Mix desig Labels:**

- FBRC - Control mix for FBR1 & FBR2
- FBR1 - 3/4" Virgin, Monofilament, Polypropylene fiber.
- FBR2 - Postconsumer Recycled Plastic (PET).
- FBRCNT - Control mix for FBR3M & FBR3MA
- FBR3M - 3M Polyolefin fiber using horizontal (PAN) mixer.
- FBR3MA - 3M Polyolefin fiber using vertical (standar) mixer.
- FBRMEC - Control mix for FBRME.
- FBRME - Virgin 2" Collated Fibrillated Polypropylene Fiber.

**Table 4-2 Stress Ratio, Number of Cycles Endured and Speed of Cracking**

<b>BEAM Id</b>	<b>Stress Ratio S</b>	<b>Number of Cycles N</b>
FBR1-1	84	3100
FBR1-2	74	105362
FBR1-3	71	225682
FBR1-4	67	314216

**Average speed of cracking = 123 ft/sec**

<b>BEAM Id</b>	<b>Stress Ratio S</b>	<b>Number of Cycles N</b>
FBR3M-1	82	800
FBR3M-2	73	29480
FBR3M-3	64	239372
FBR3M-4	60	374416

**Average speed of cracking = 98 ft/sec**

<b>BEAM Id</b>	<b>Stress Ratio S</b>	<b>Number of Cycles N</b>
FBRME-1	93	1250
FBRME-2	84	8500
FBRME-3	80	500000
FBRME-4	75	1.41E+06

**Average speed of cracking = 112 ft/sec**

<b>BEAM Id</b>	<b>Stress Ratio S</b>	<b>Number of Cycles N</b>
FBRC-1	72	100
FBRC-2	70	1000
FBRC-3	62	10000
FBRC-4	51	100000

**Average speed of cracking = 152 ft/sec**



Table 4.3 Material Properties Used in FEA Model

Material Property & Element Type	Value
Poisson's Ratio	0.18
Uniaxial Tensile Strength (psi)	530
Compressive Strength (psi)	4,500
Flexural Strength (psi)	493
Element Type:	<i>Solid 65</i>

## Concrete and Ambient Temperatures

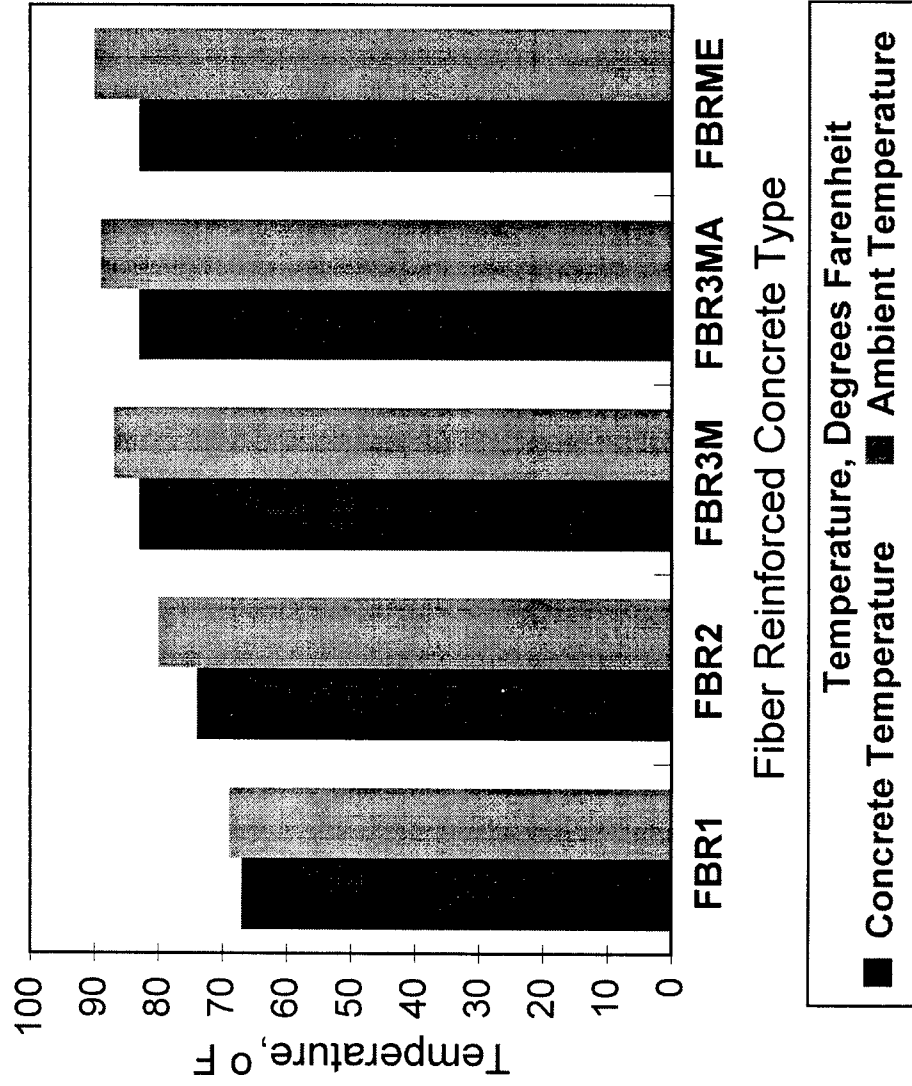
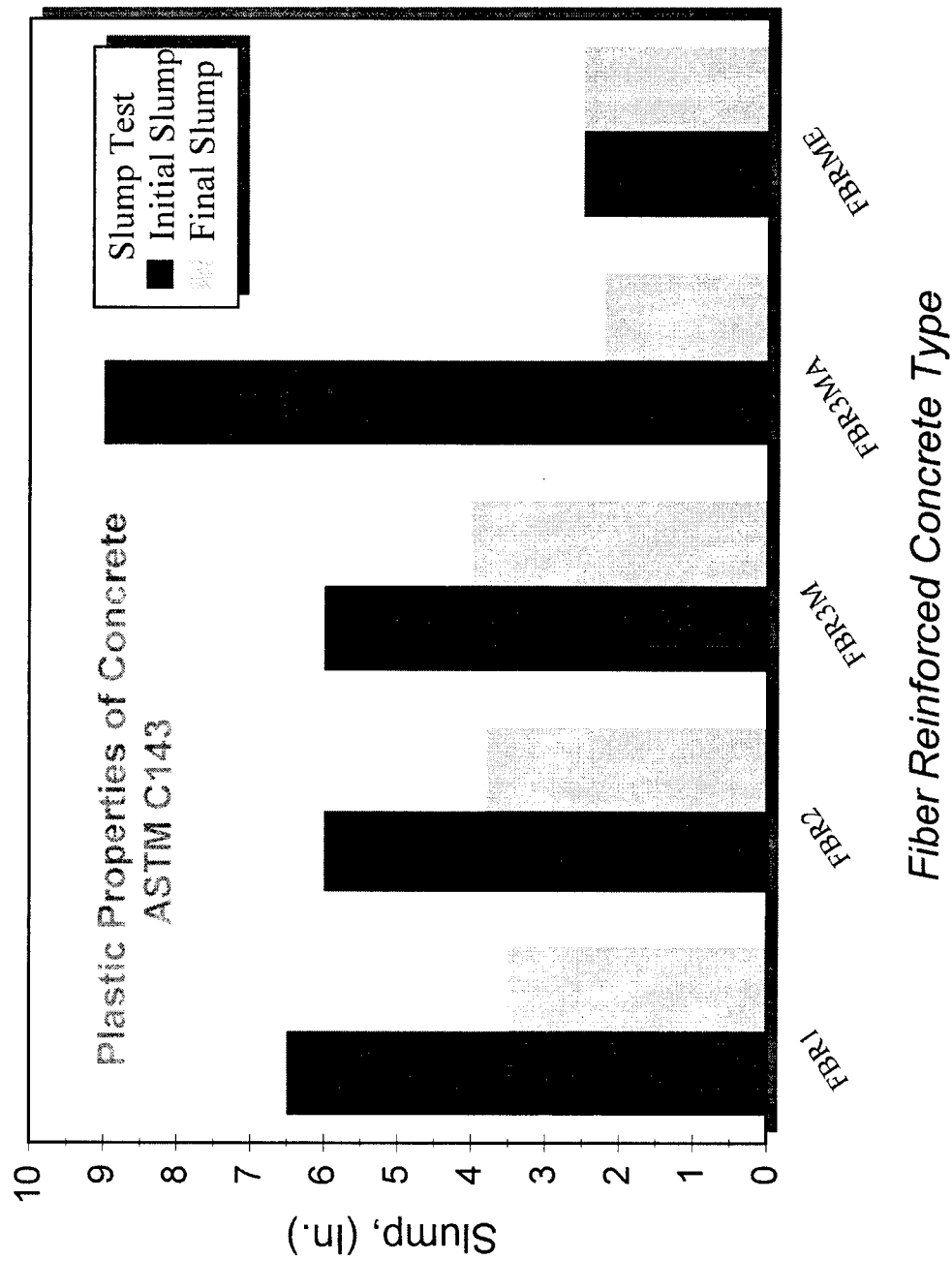


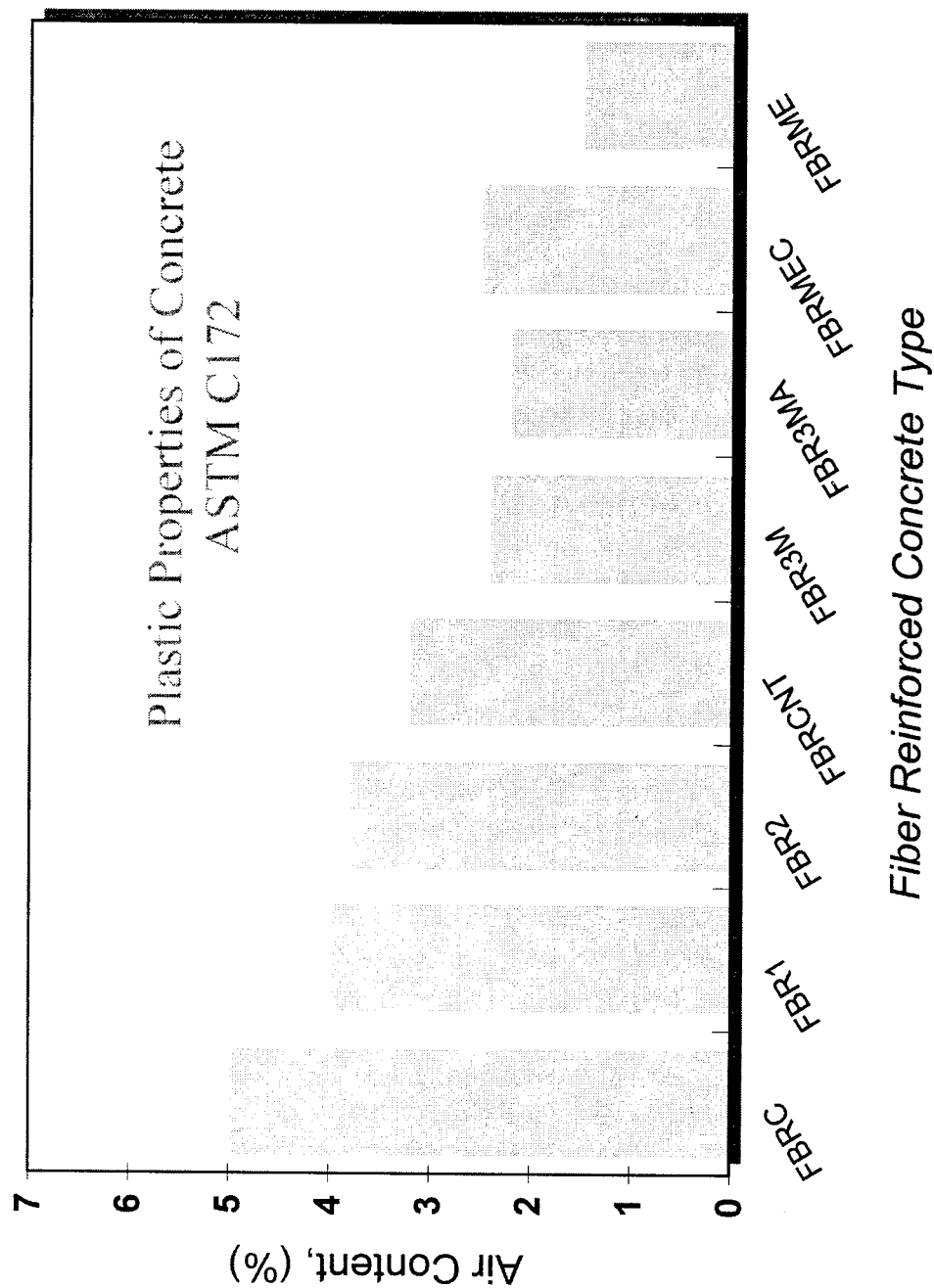
Figure 4.1 Concrete Temperature Results

## Slump vs. FBRC Type



**Figure 4.2 Slump of Concrete Test Results**

## Air Content vs. FBRC Type



**Figure 4.3 Air Content of Concrete Test Results**

# Unit Weight vs. Type of Concrete ASTM C138

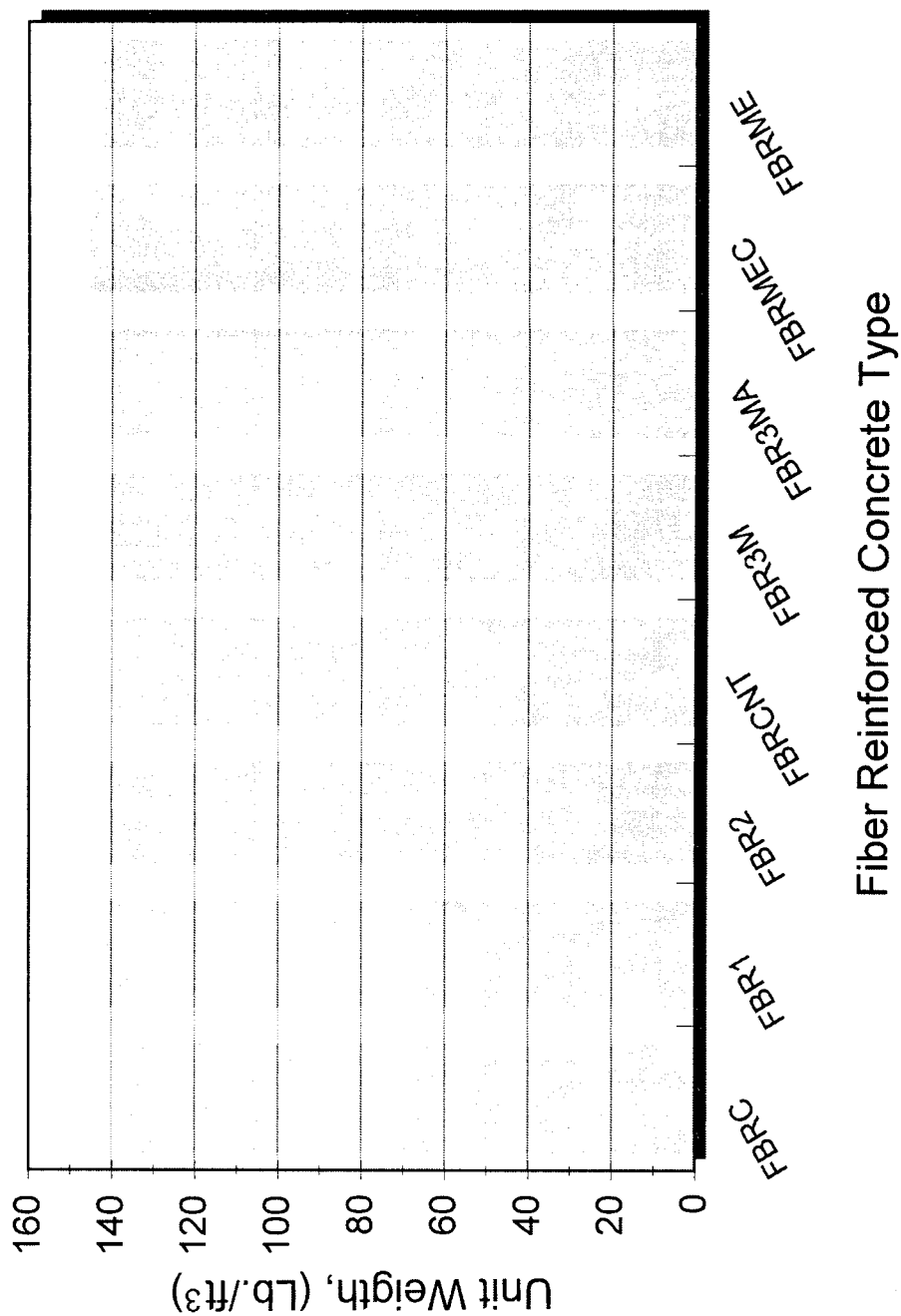


Figure 4.4 Unit Weight of Concrete

Figure 4.5.a Preliminary Compressive Strength Results

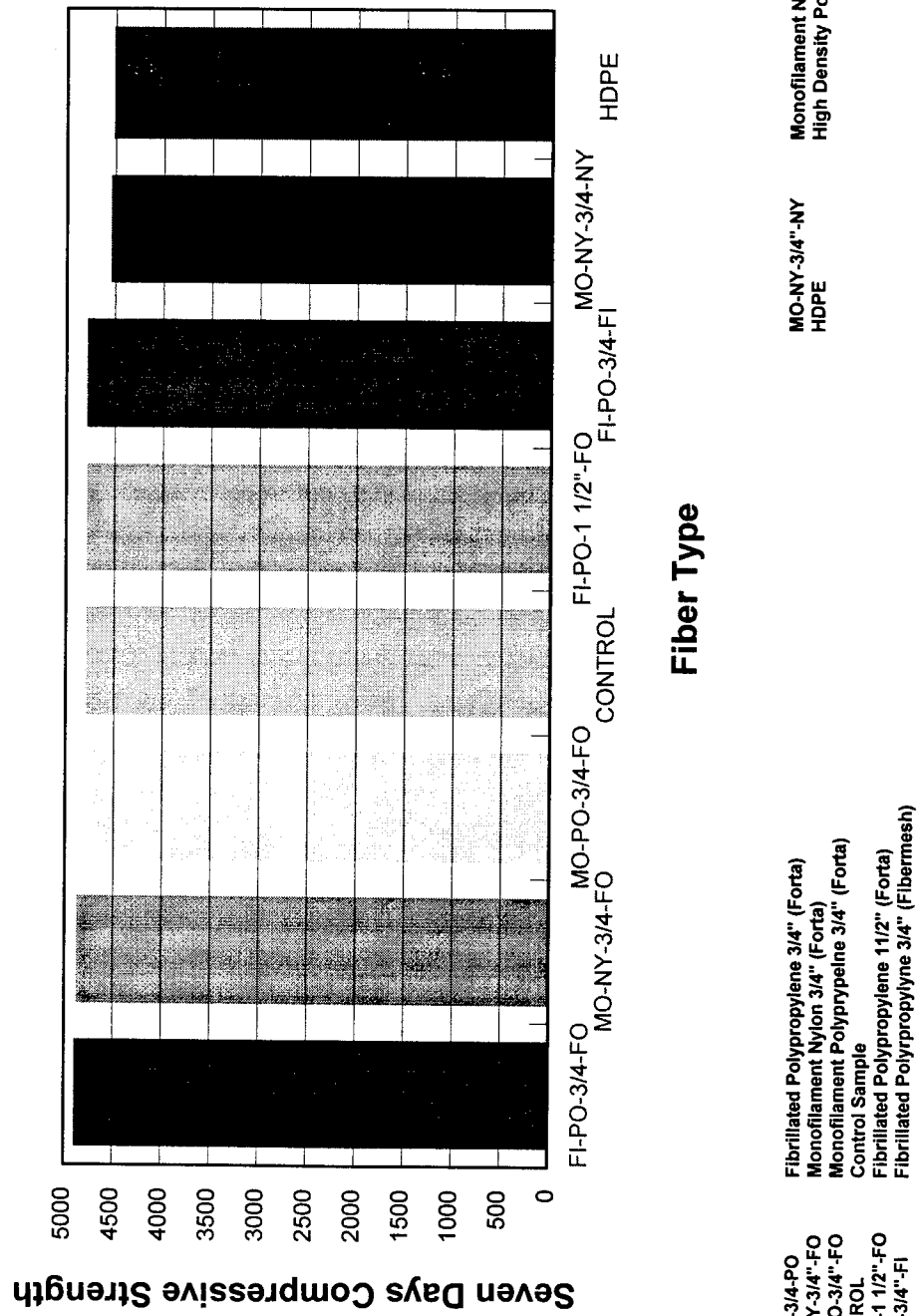
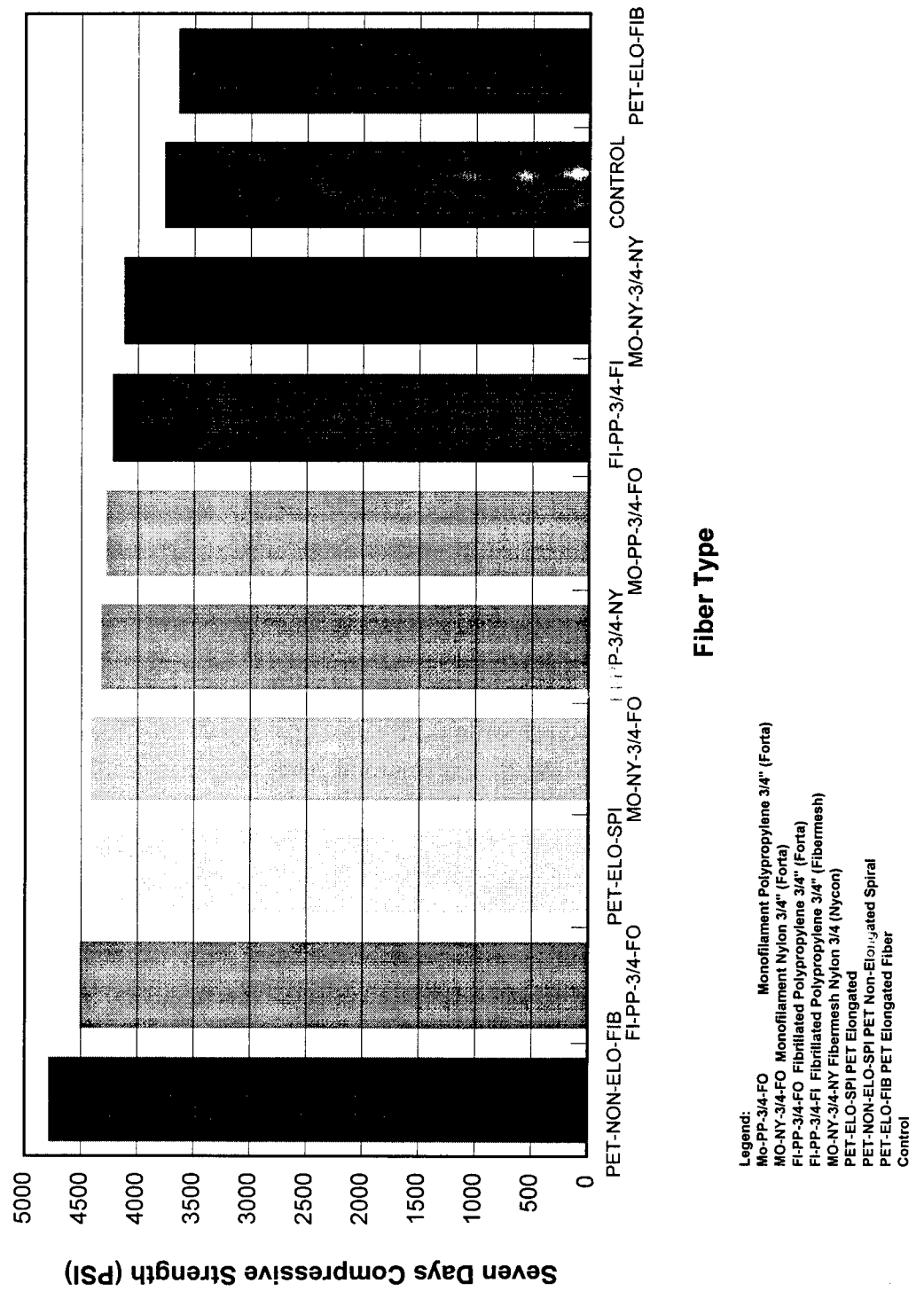


Figure 4.5.b Preliminary Compressive Strength



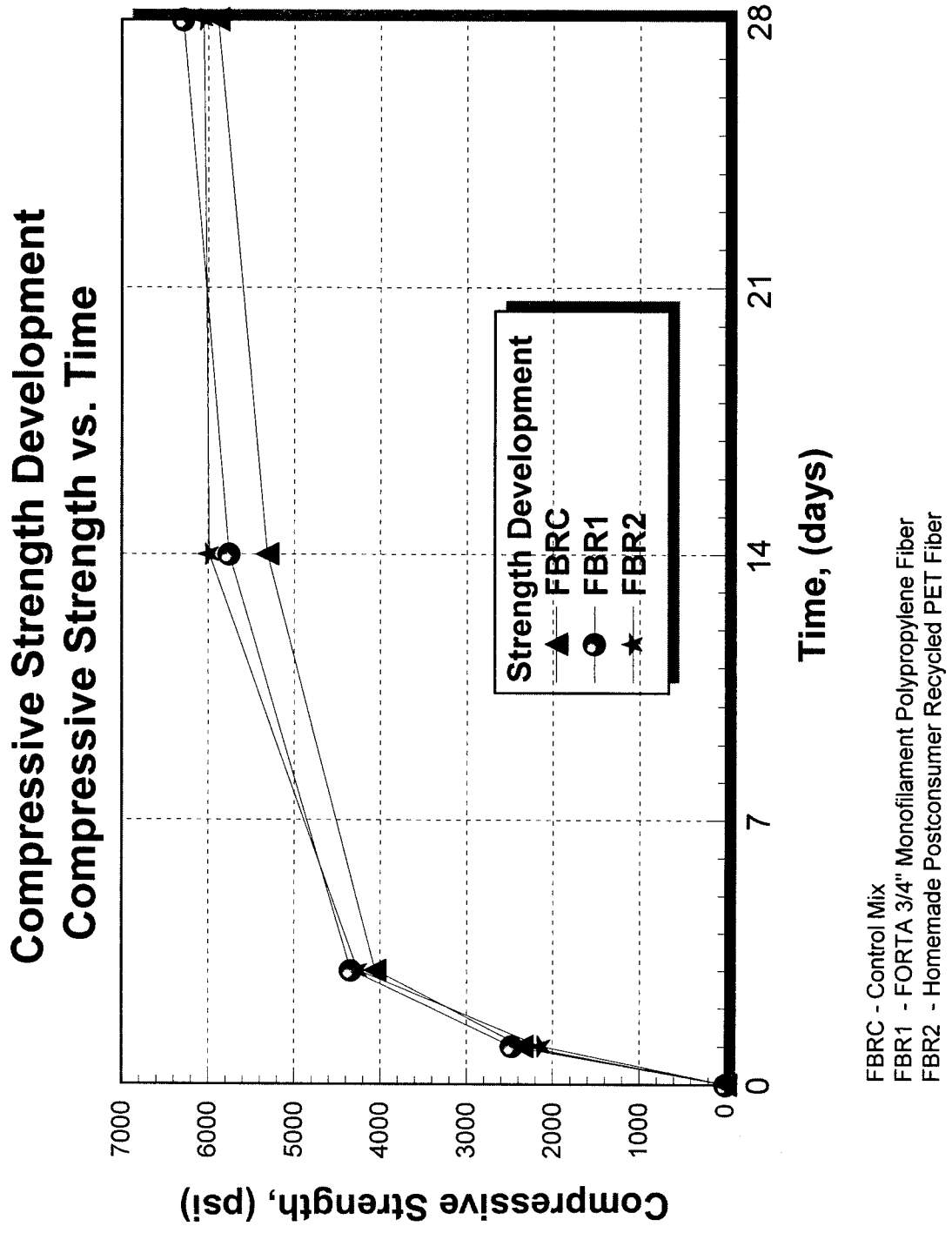
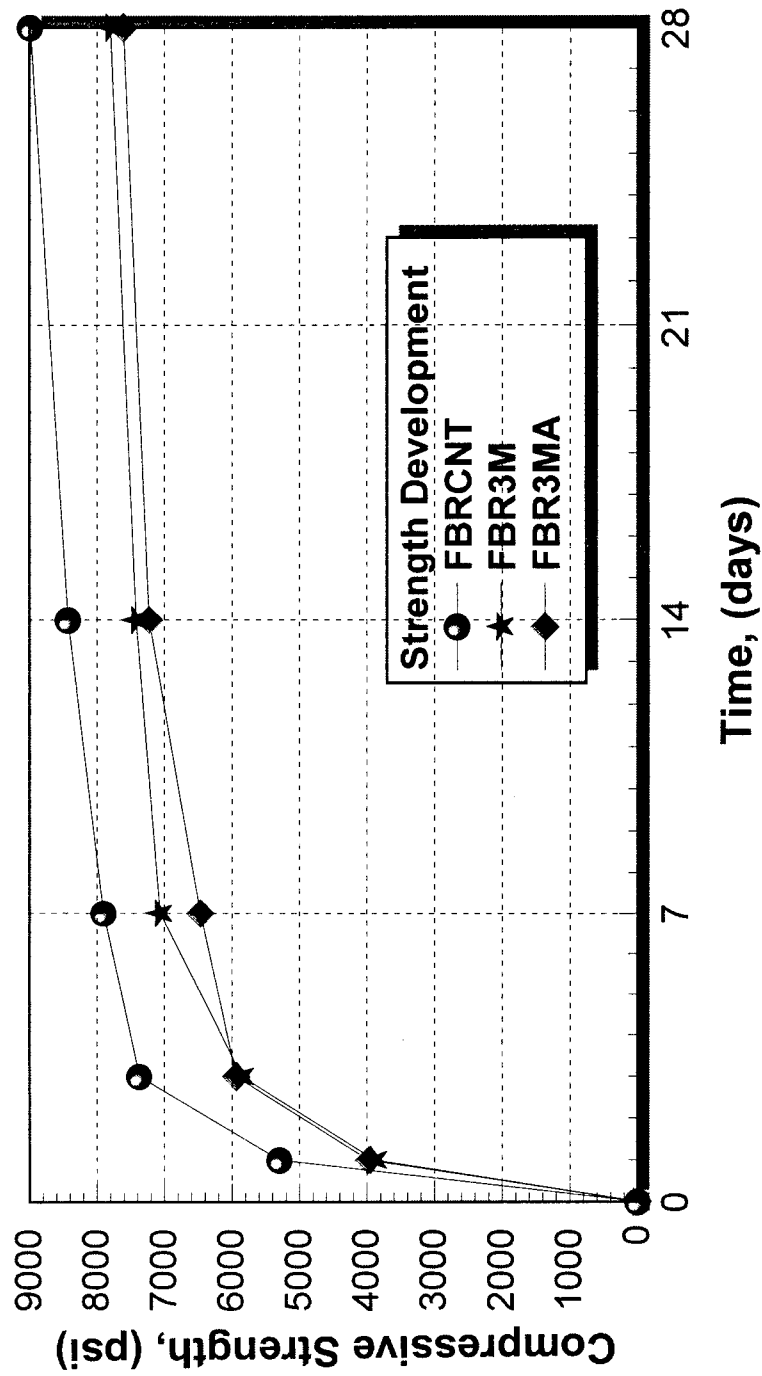


Figure 4.6.a Compressive Strength Development of Concrete



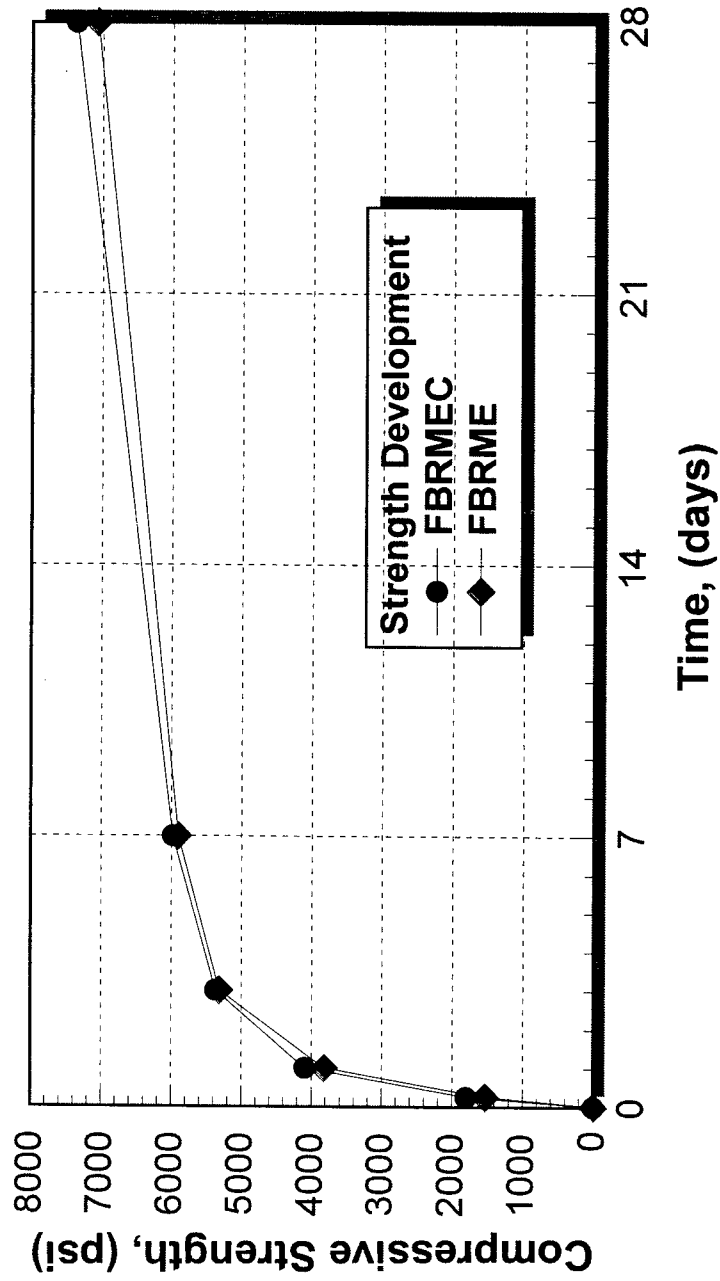
## Compressive Strength Development Compressive Strength vs. Time



FBRCNT - Control Mix  
 FBR3M - 3M Monofilament Polyolefin Fiber Using Horizontal Mixer  
 FBR3MA - 3M Monofilament Polyolefin Fiber Using Vertical Mixer

**Figure 4.6.b Compressive Strength Development of Concrete**

## Compressive Strength Development Compressive Strength vs. Time

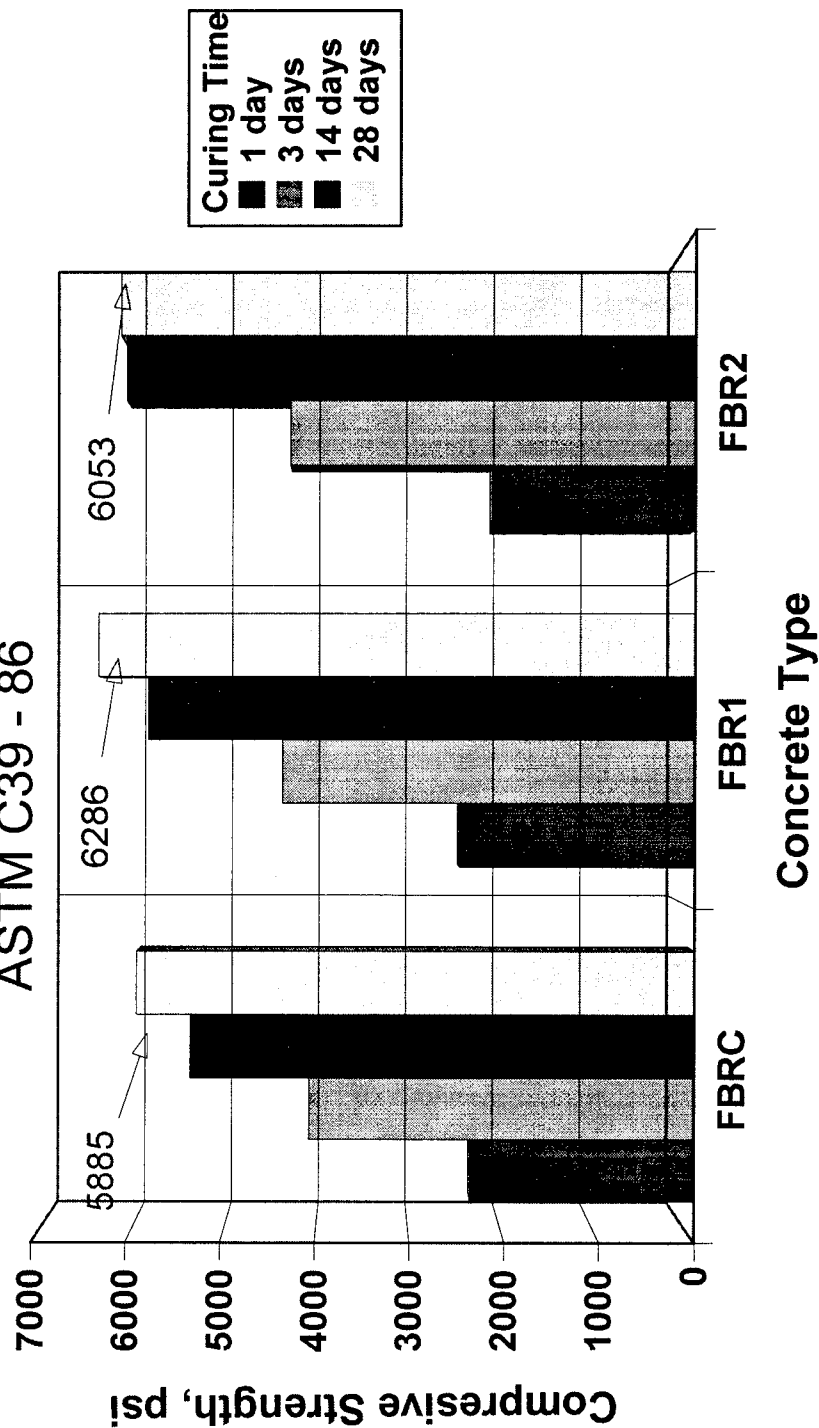


FBRMEC - Control Mix

FBRME - FIBERMESH 2" Collated Fibrillated Polypropylene Fiber

**Figure 4.6.c Compressive Strength Development of Concrete**

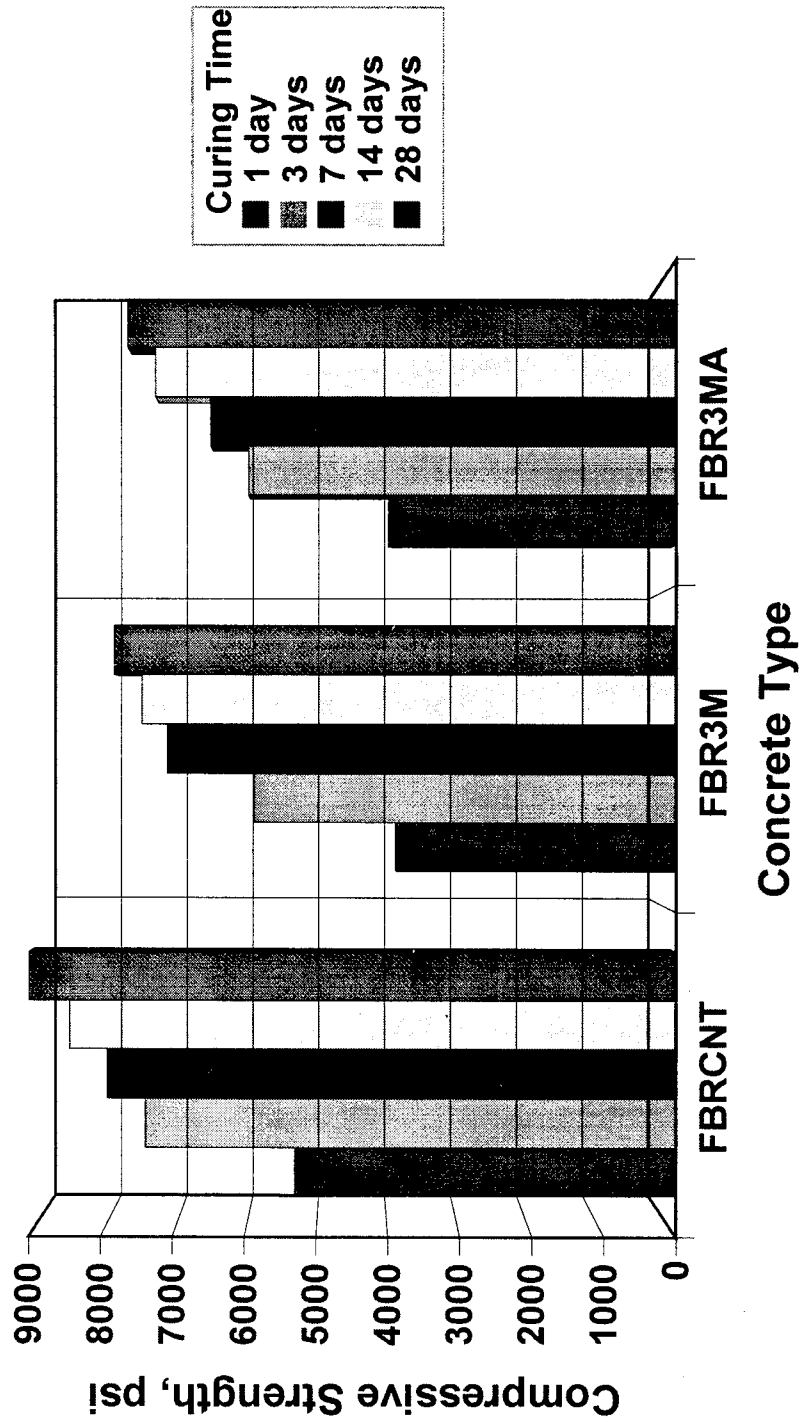
# Hardened Properties of Concrete Compressive Strength ASTM C39 - 86



FBRC - Control  
FBR1 - FORTA 3/4" Monofilament Polypropylene Fiber  
FBR2 - Home made Postconsumer Recycled PET Fiber

Figure 4.6.d Compression Strength Results of Concrete

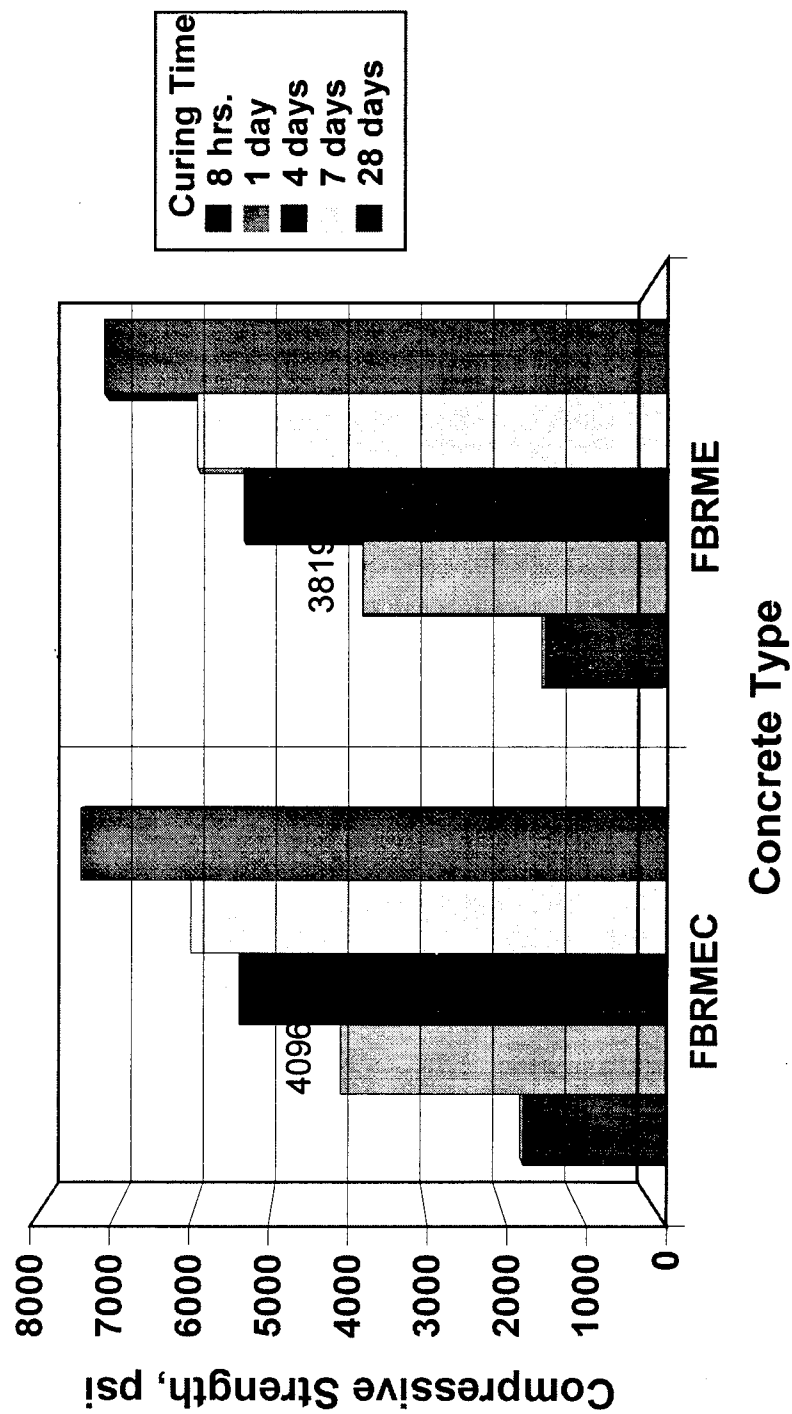
# Hardened Properties of Concrete Compressive Strength ASTM C39 - 86



FBR3NT - Control  
FBR3M - Monofilament Polyolefin Fiber using Horizontal Mixer  
FBR3MA - Monofilament Polyolefin Fiber using Vertical Mixer

**Figure 4.6.e Compression Strength Results of Concrete**

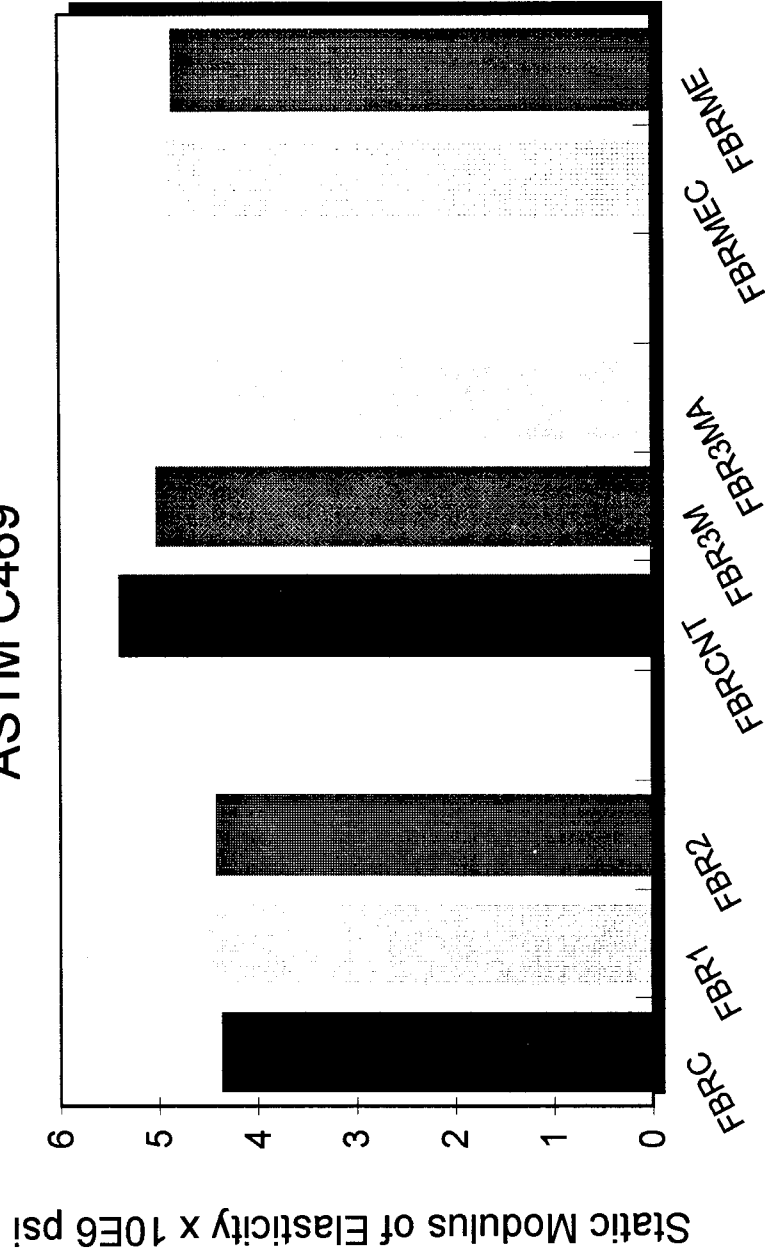
# Hardened Properties of Concrete Compressive Strength ASTM C39 - 86



FBRMEC - Control  
FBRME - Fibermesh 2" Collated Fibrillated Polypropylene Fiber

**Figure 4.6.f Compression Strength Results of Concrete**

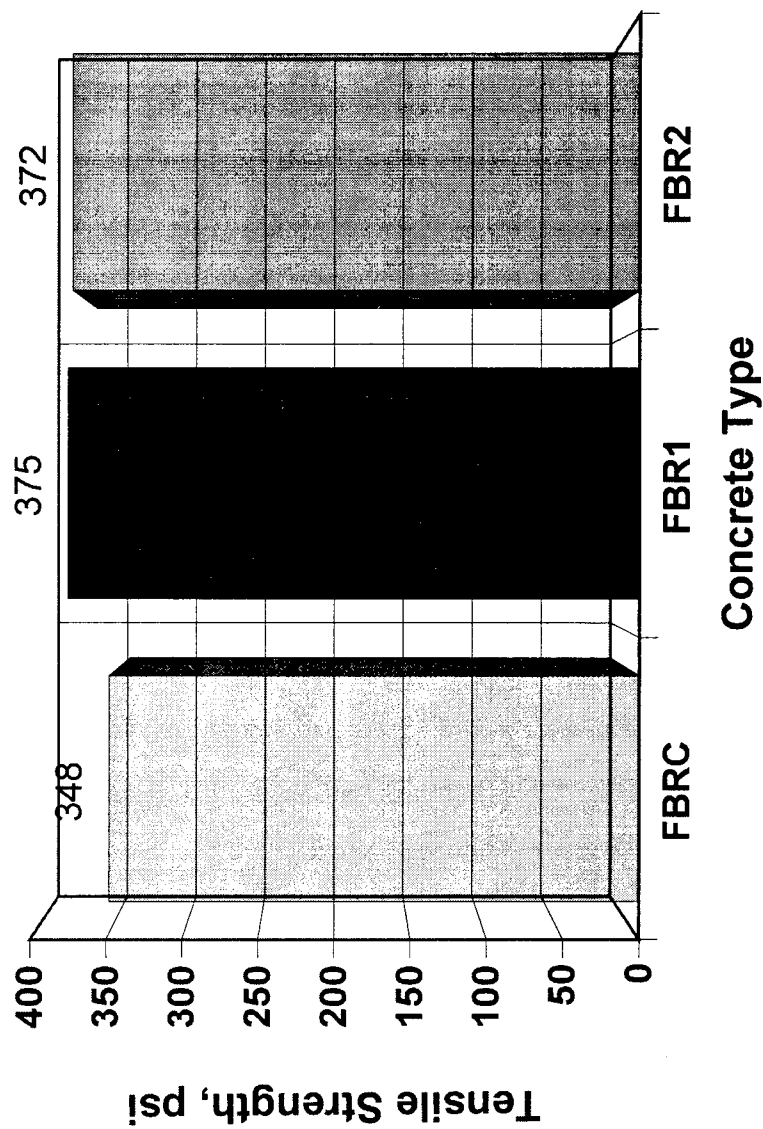
# Hardened Properties of Concrete Static Modulus vs. FBRC Type ASTM C469



Fiber Reinforced Concrete Type

Figure 4.7 Static Modulus of Elasticity

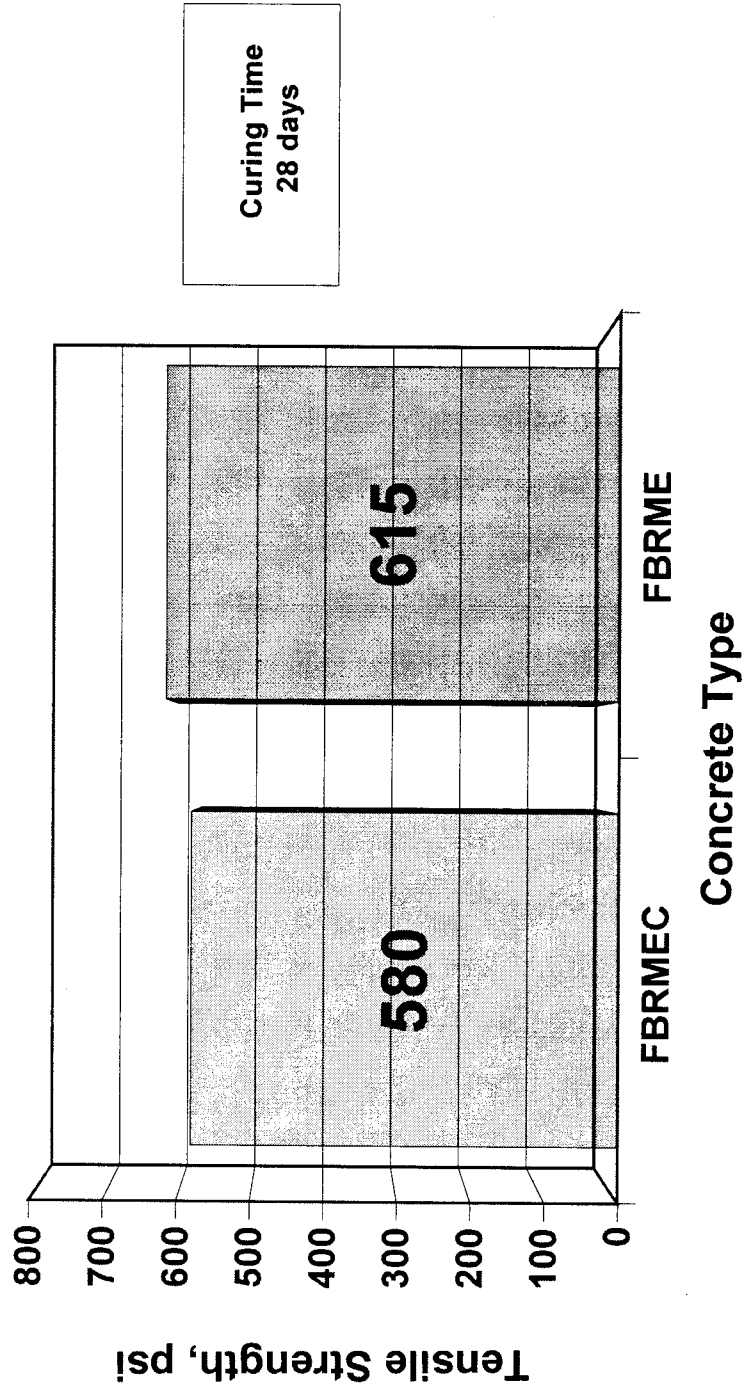
# Hardened Properties of Concrete Tensile Strength ASTM C496 - 90



FBRC - Control  
FBR1 - FORTA 3/4" Monofilament Polypropylene Fiber  
FBR2 - Home made Postconsumer Recycled PET Fiber

Figure 4.8 Tensile Strength for FBR1 and FBR2

Hardened Properties of Concrete  
Tensile Strength  
ASTM C496 - 90



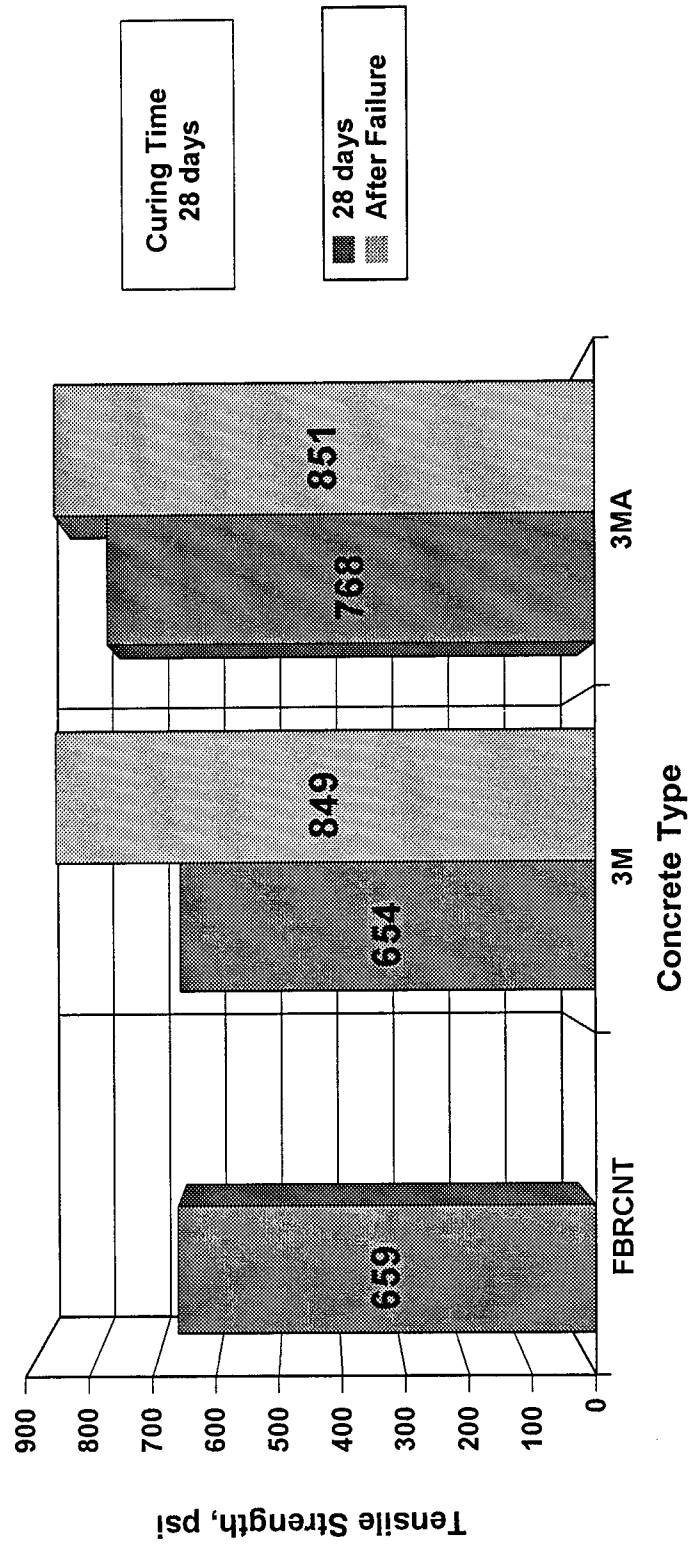
FBRC - Control

FBRME - Fibermesh 2" Collated Fibrillated Polypropylene Fiber

**Figure 4.9 Tensile Strength Results for FBRME**



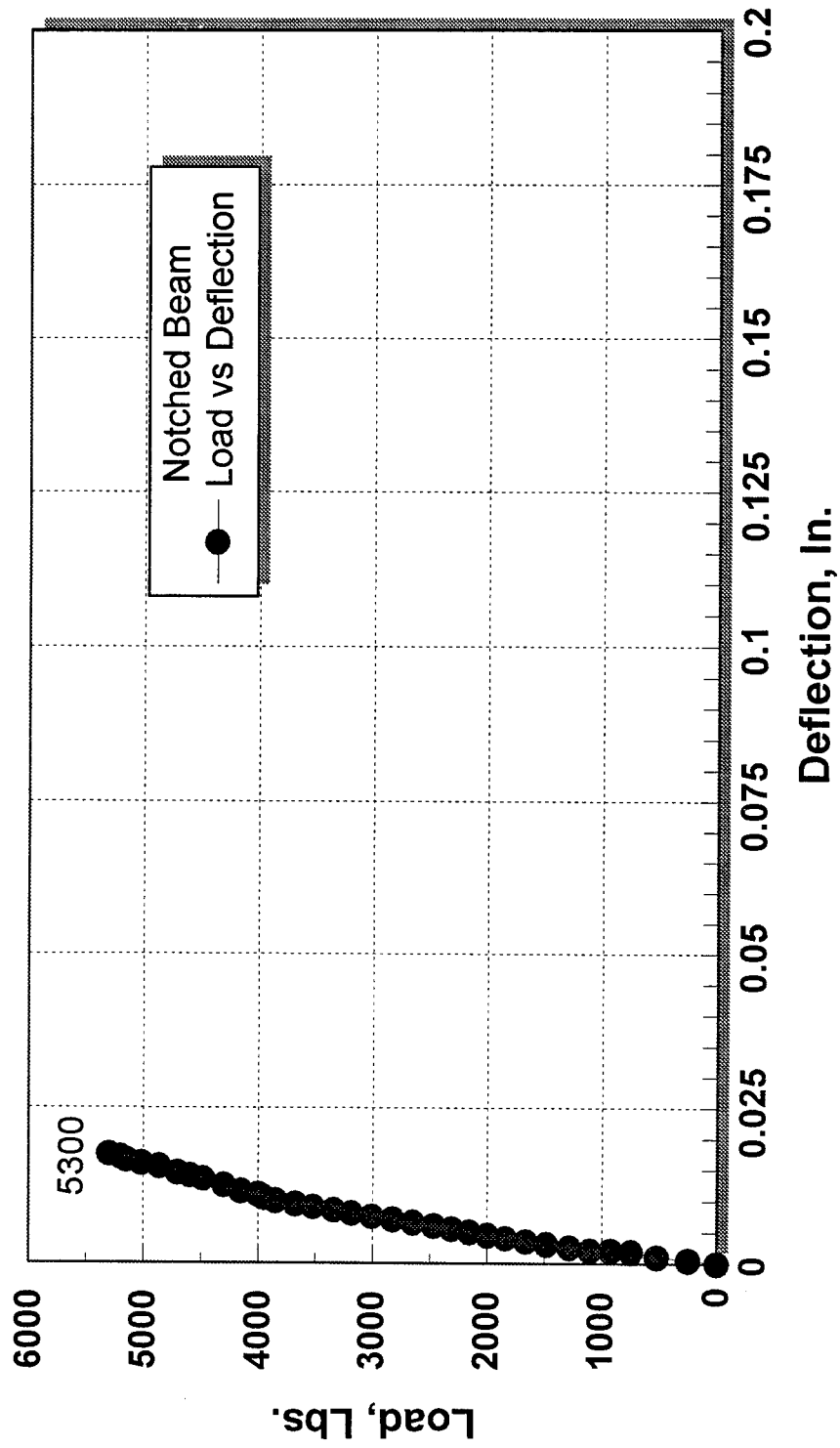
# Hardened Properties of Concrete Tensile Strength ASTM C496 - 90



FBRCNT - Control  
FBR3M - Monofilament Polyolefin Fiber using Horizontal Mixer  
FBR3MA - Monofilament Polyolefin Fiber using Vertical Mixer

Figure 4.10 Tensile Strength Results

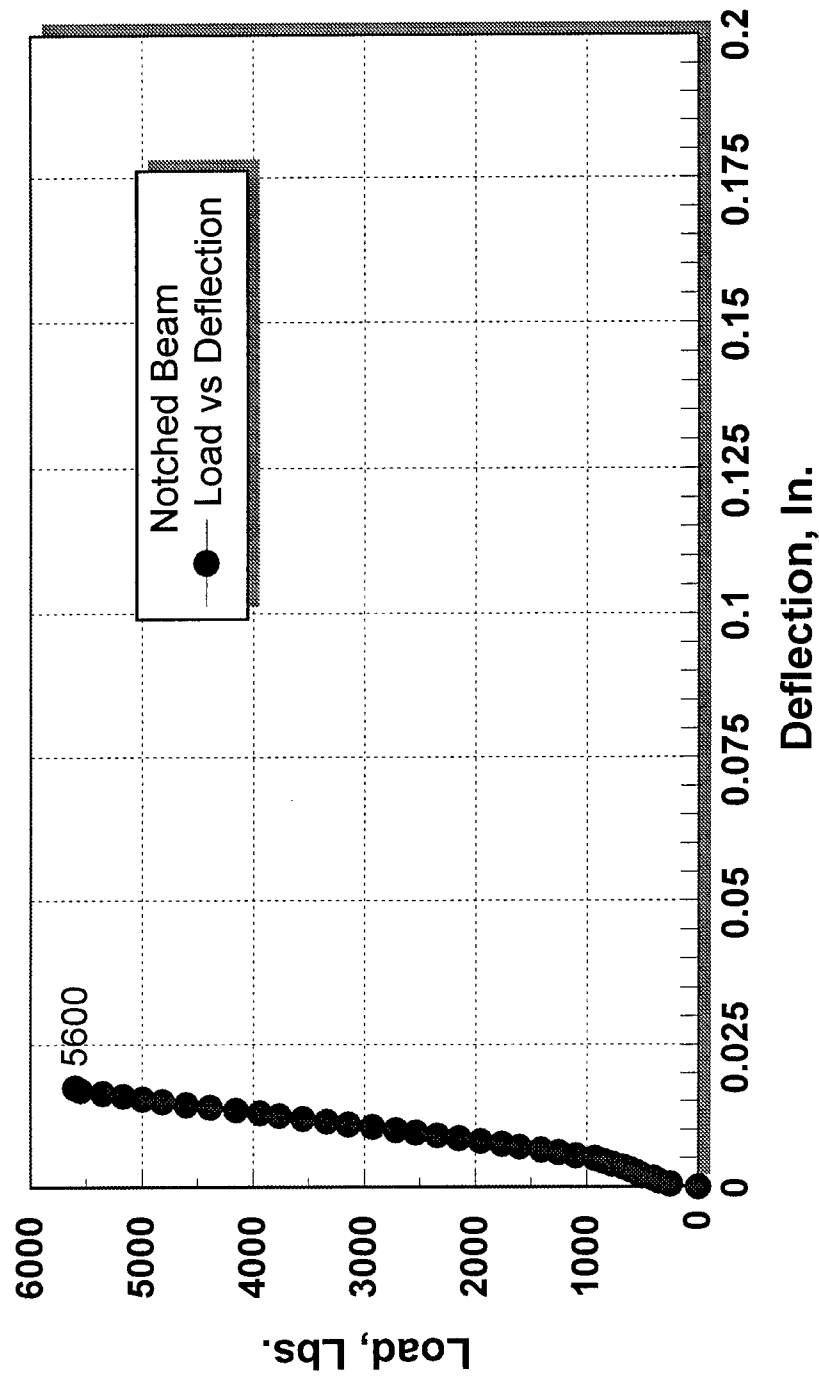
# Load vs. Deflection Curve ASTM C78 - 84



FBRC - Control mix for FBR1 & FBR2 reinforced mixes

Figure 4.11 Flexural Strength of Concrete

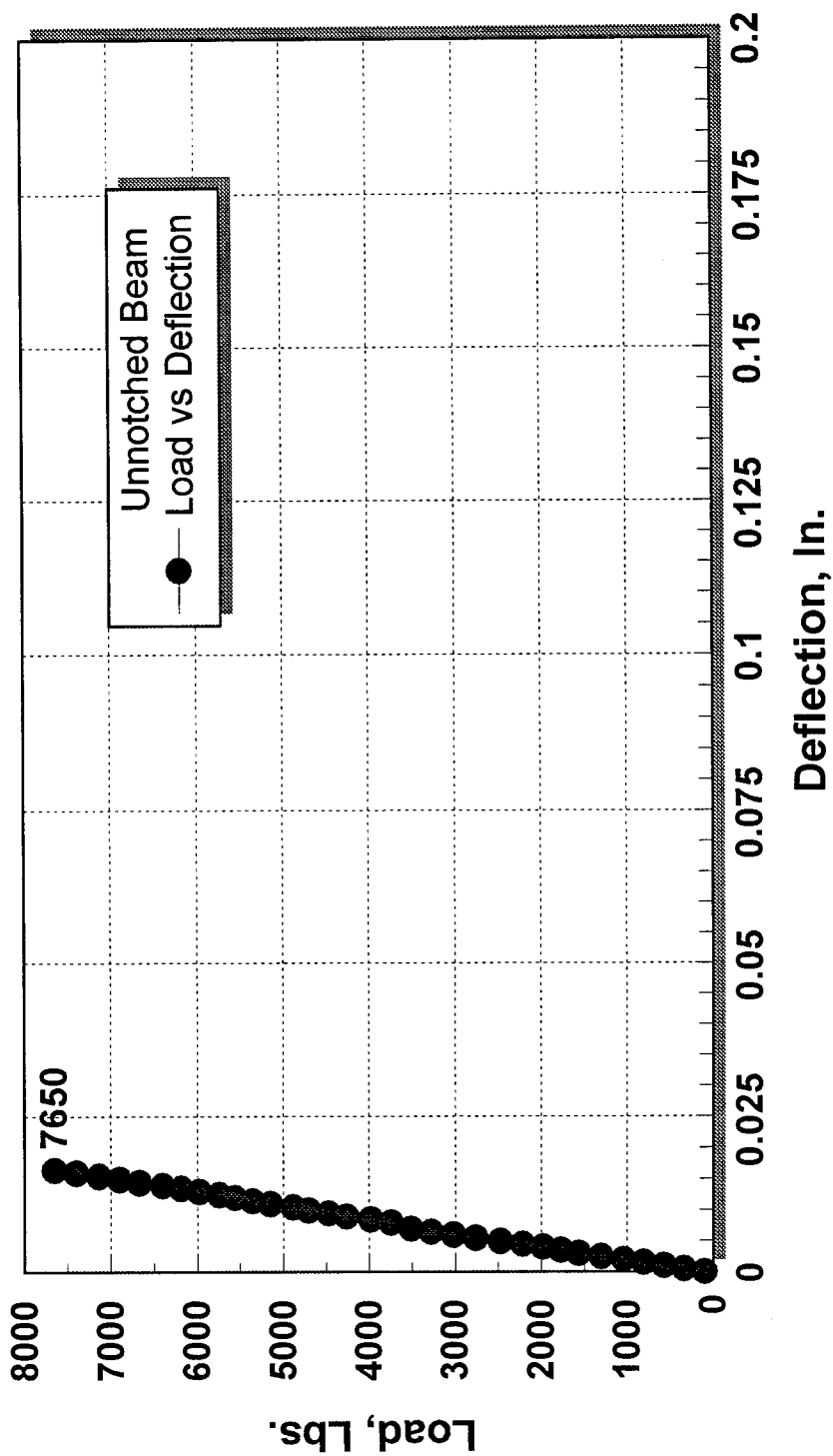
Load vs. Deflection Curve  
ASTM C78 - 84



FBRC - Control mix for FBR1 & FBR2 reinforced mixes

Figure 4.12 Flexural Strength of Concrete

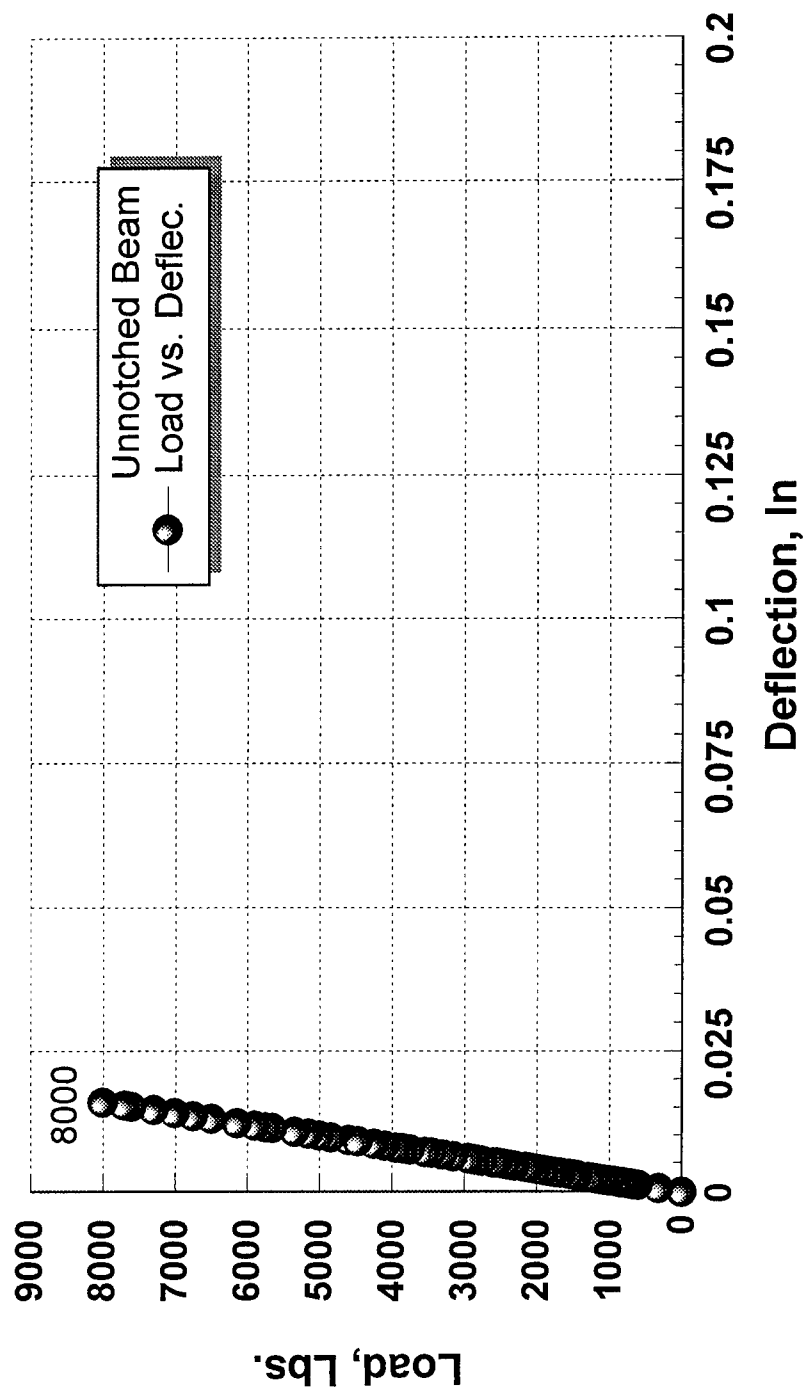
# Load vs. Deflection Curve ASTM C78 - 84



FBRC - Control mix for FBR1 & FBR2 reinforced mixes

Figure 4.13 Flexural Strength of Concrete

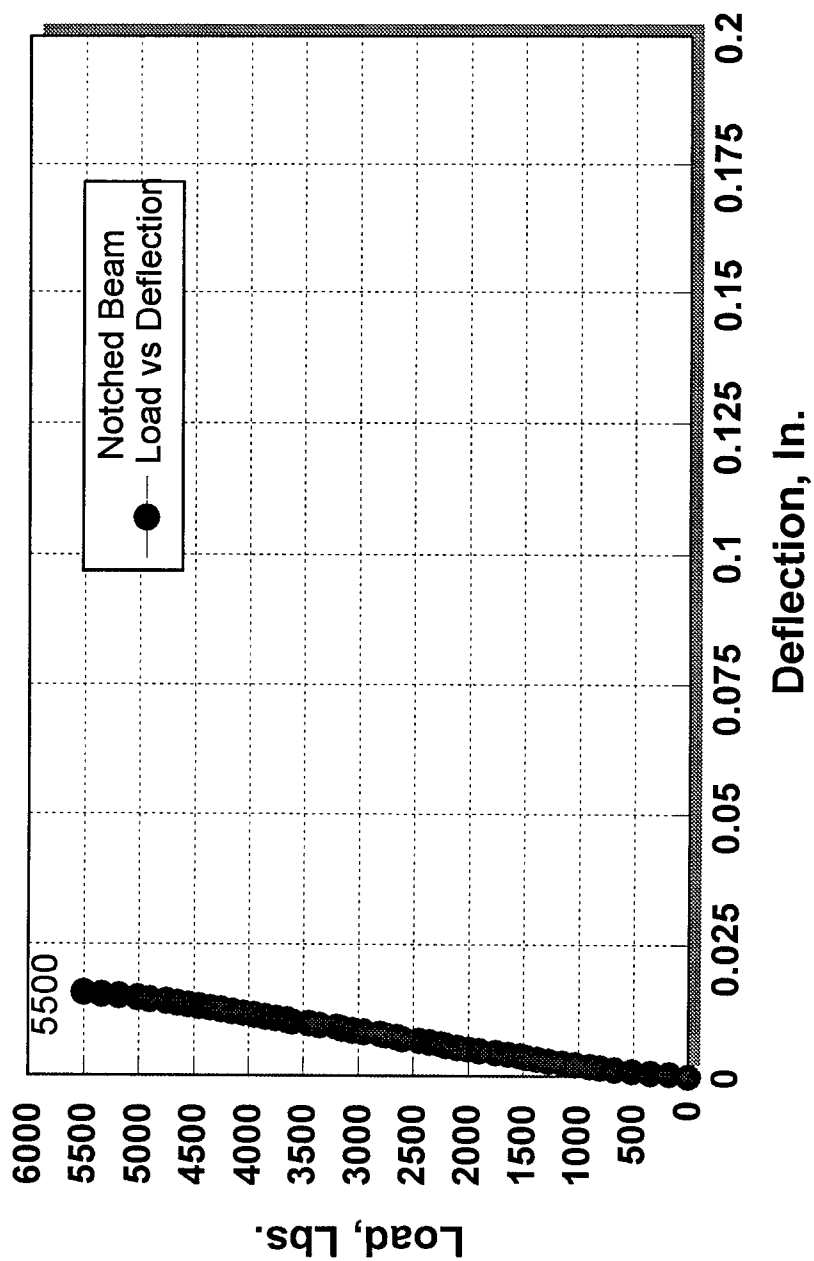
# Load vs. Deflection Curve ASTM C78 - 84



FBRC - Control mix for FBR1 & FBR2 reinforced mixes

**Figure 4.14 Flexural Strength of Concrete**

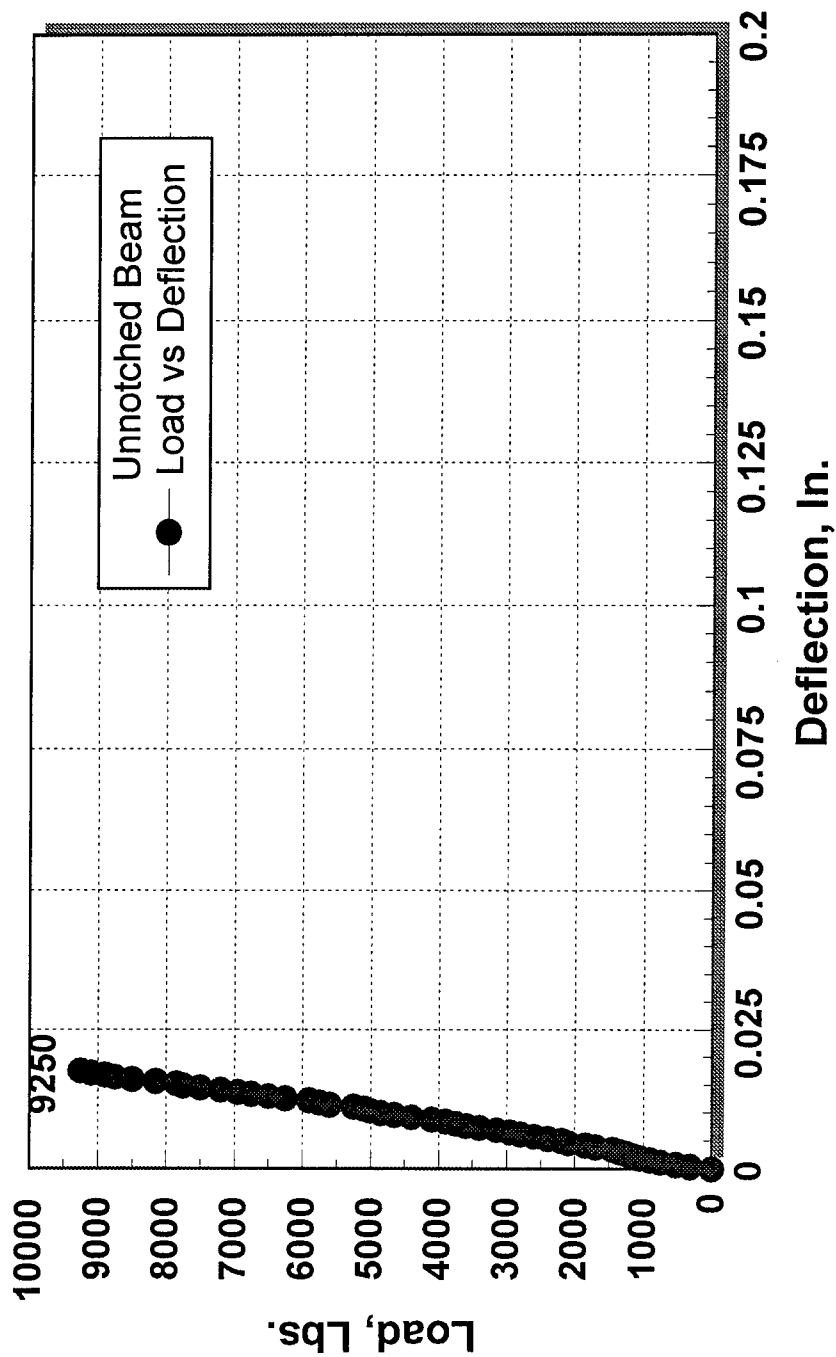
Load vs. Deflection Curve  
ASTM C78 - 84



FBR1 - FORTA 3/4" Monofilament Polypropylene Fiber

Figure 4.15 Flexural Strength of Concrete

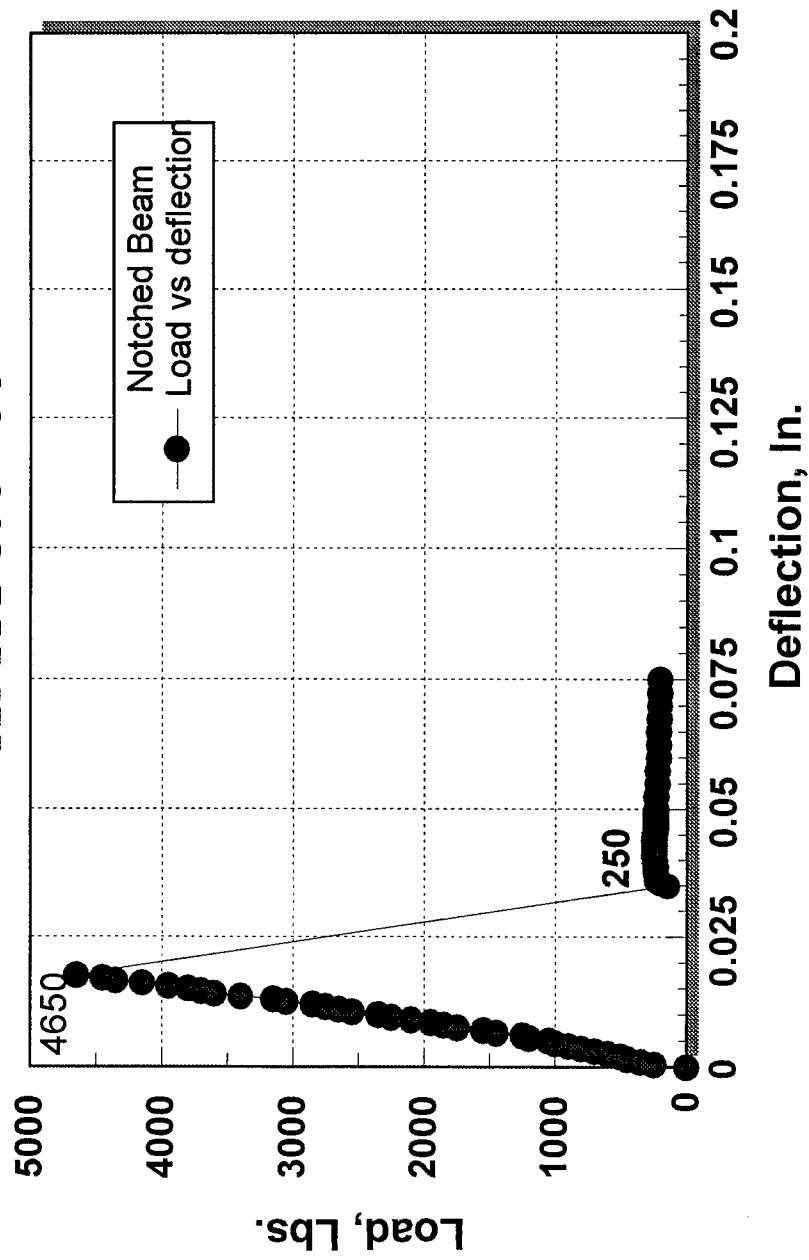
# Load vs. Deflection Curve ASTM C78 - 84



FBR1 - FORTA 3/4" Monofilament Polypropylene Fiber

**Figure 4.16 Flexural Strength of Concrete**

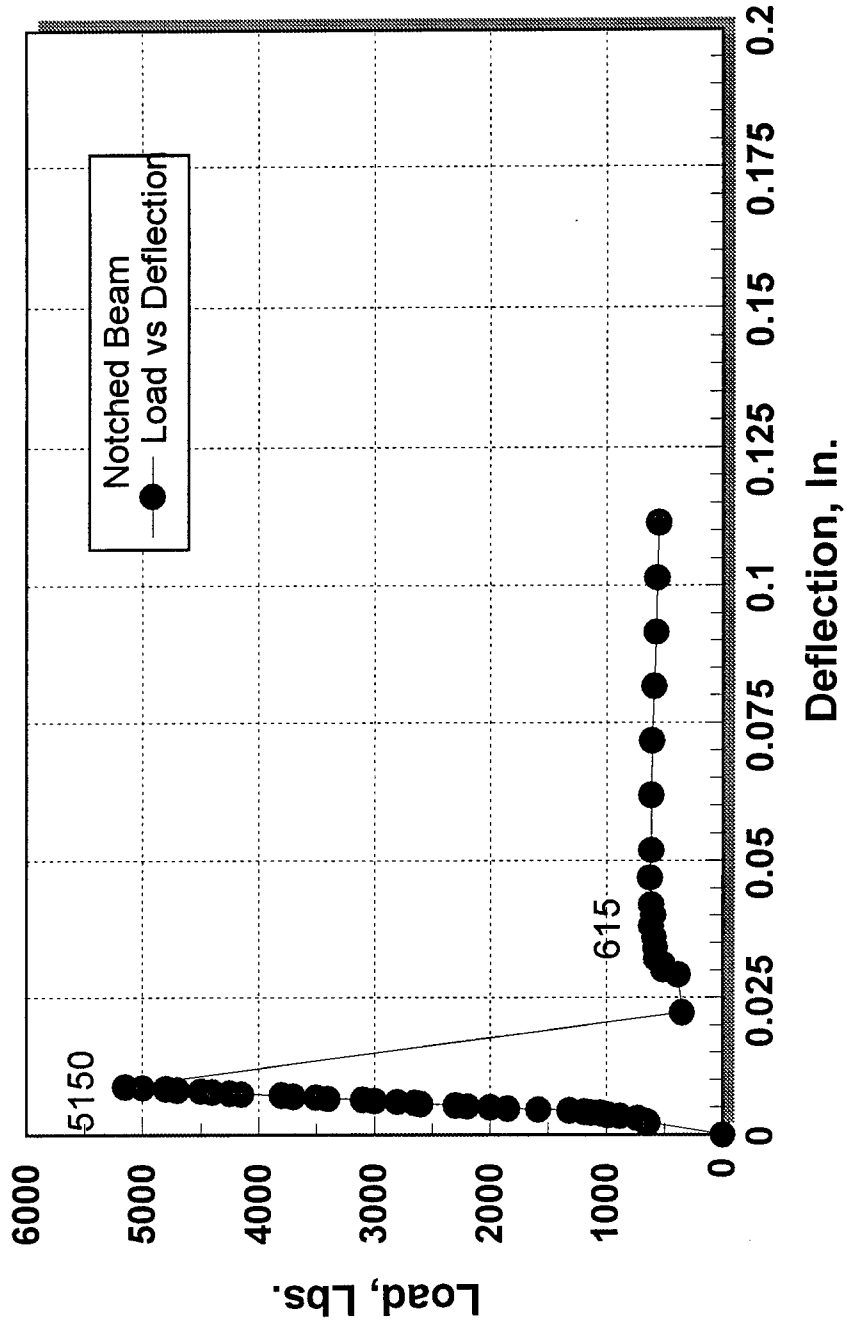
# Load vs. Deflection Curve ASTM C78 - 84



FBR2 - Recycled Polyethalene Theraphtelate Fiber (PET)  
Figure 4.17 Flexural Strength of Concrete



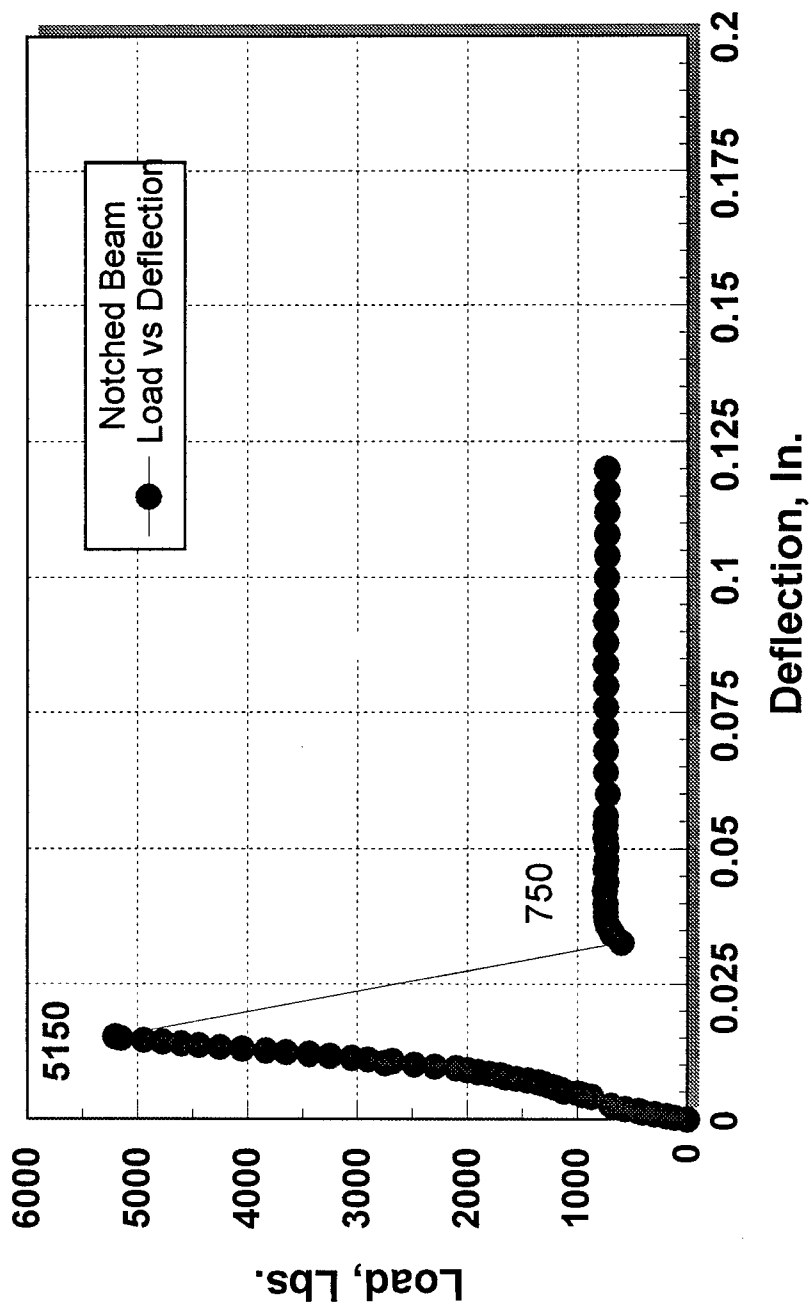
# Load vs. Deflection Curve ASTM C78 - 84



FBR2 - Recycled Polyethalene Theraphtelate Fiber (PET)

Figure 4.18 Flexural Strength of Concrete

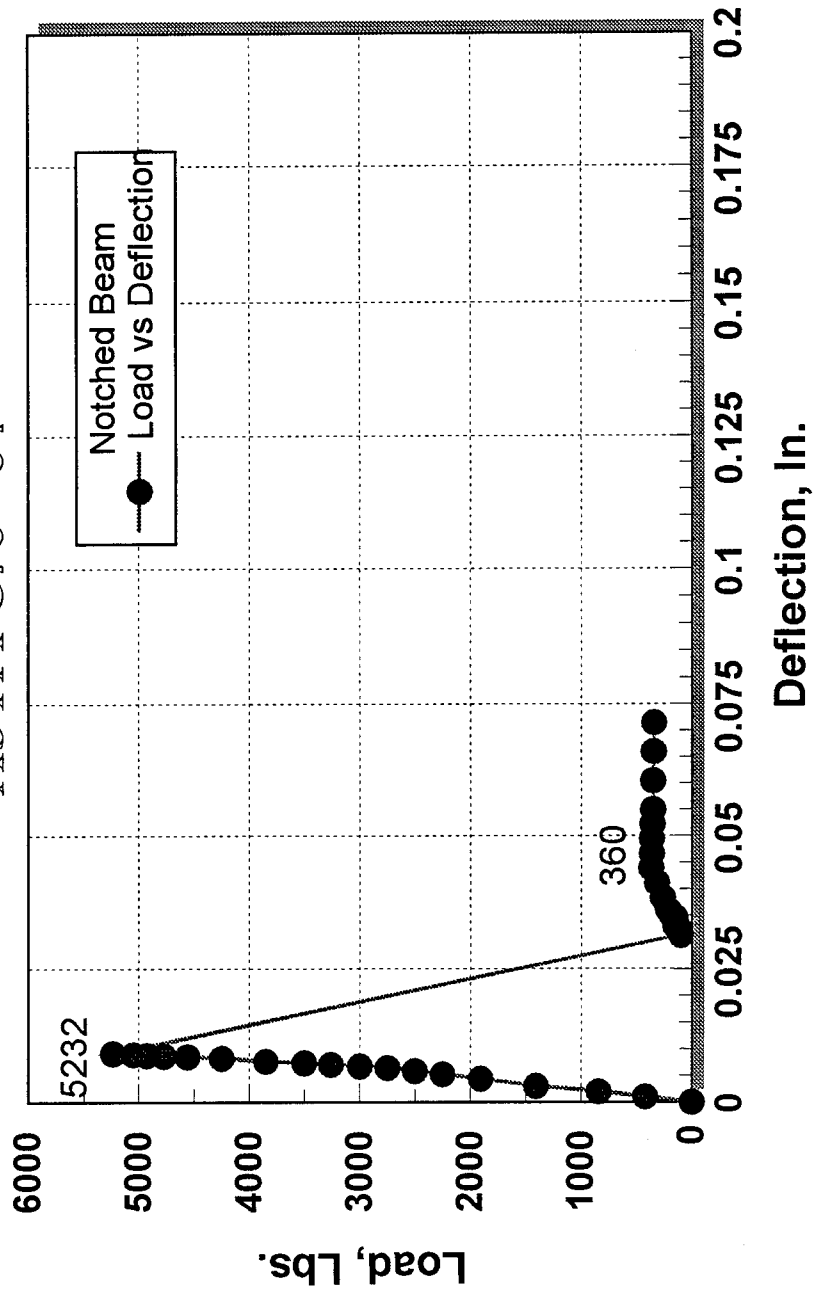
Load vs. Deflection Curve  
ASTM C78 - 84



FBR2 - Recycled Polyethalene Theraphtelate Fiber (PET)

Figure 4.19 Flexural Strength of Concrete

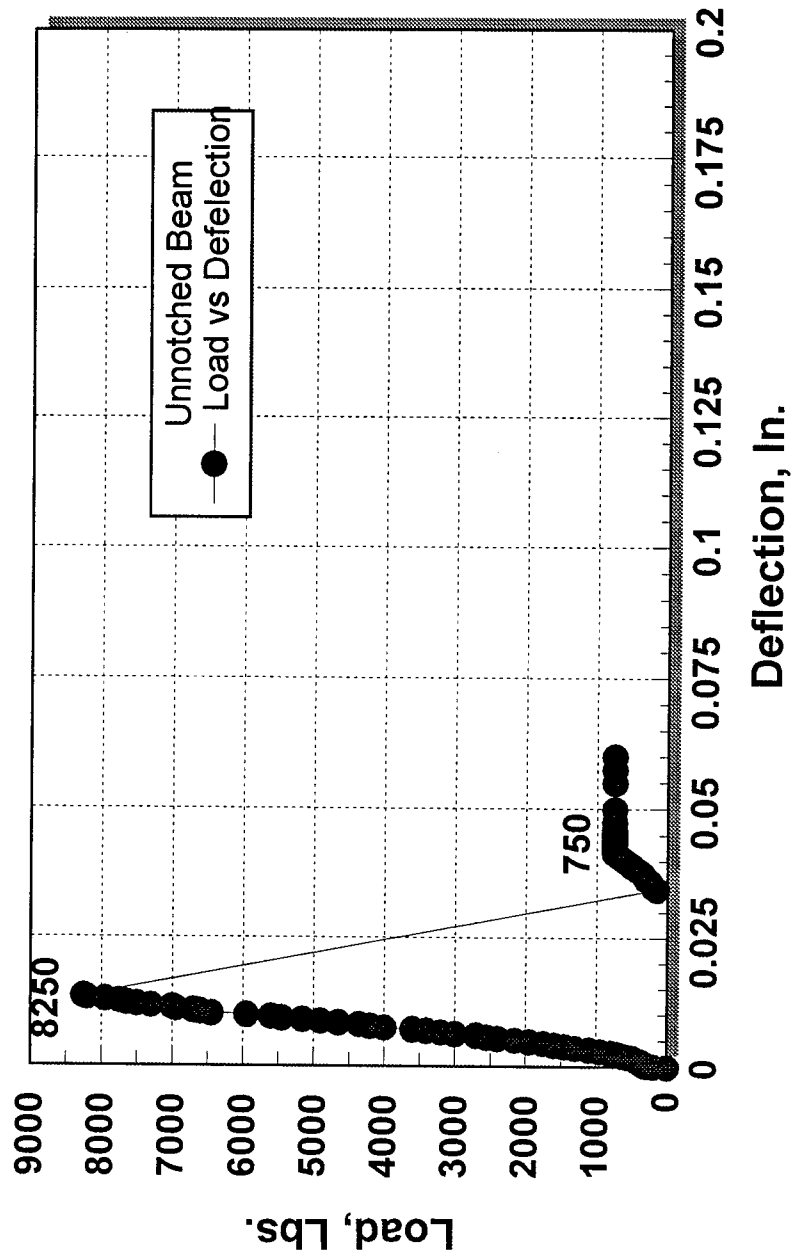
# Load vs. Deflection Curve ASTM C78 - 84



FBR2 - Recycled Polyethalene Theraphtelate Fiber (PET)

Figure 4.20 Flexural Strength of Concrete

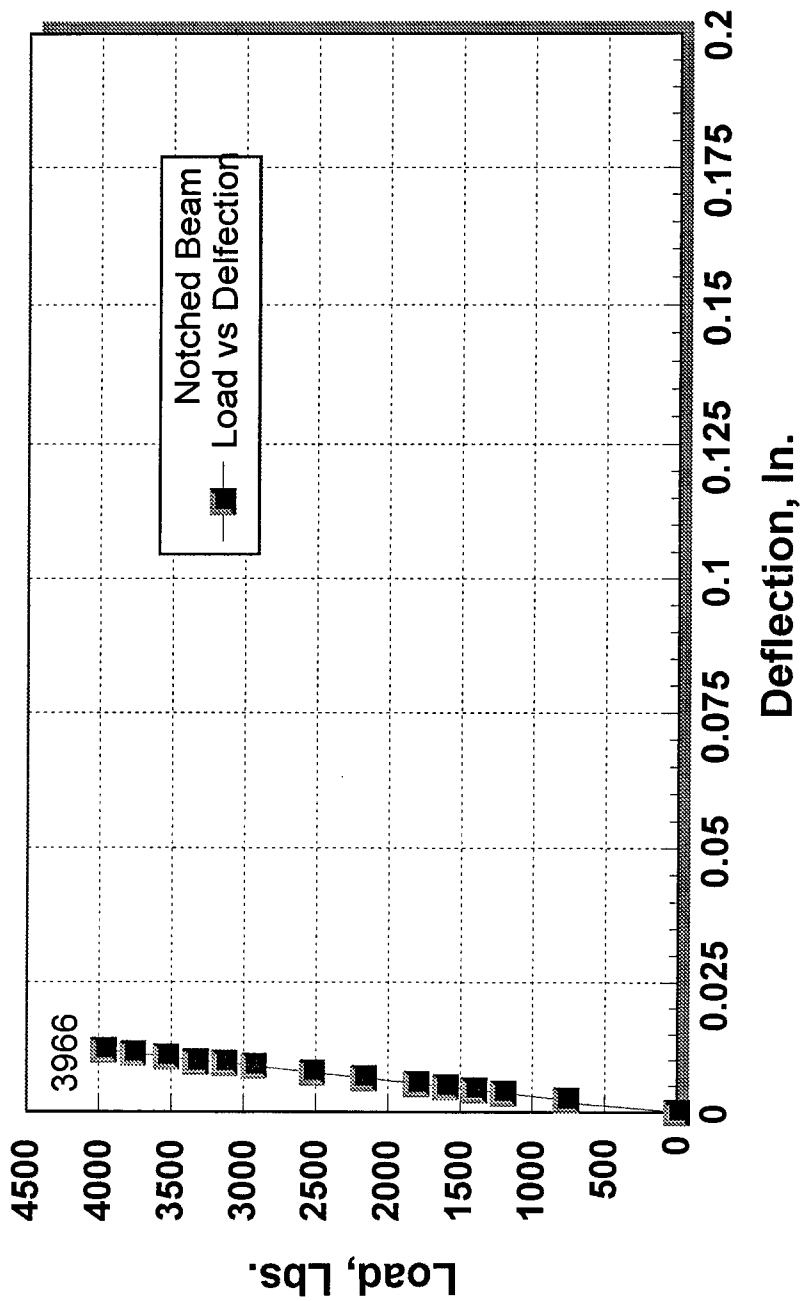
# Load vs. Deflection Curve ASTM C78 - 84



FBR2 - Recycled Polyethylene Theraphtelate Fiber (PET)

Figure 4.21 Flexural Strength of Concrete

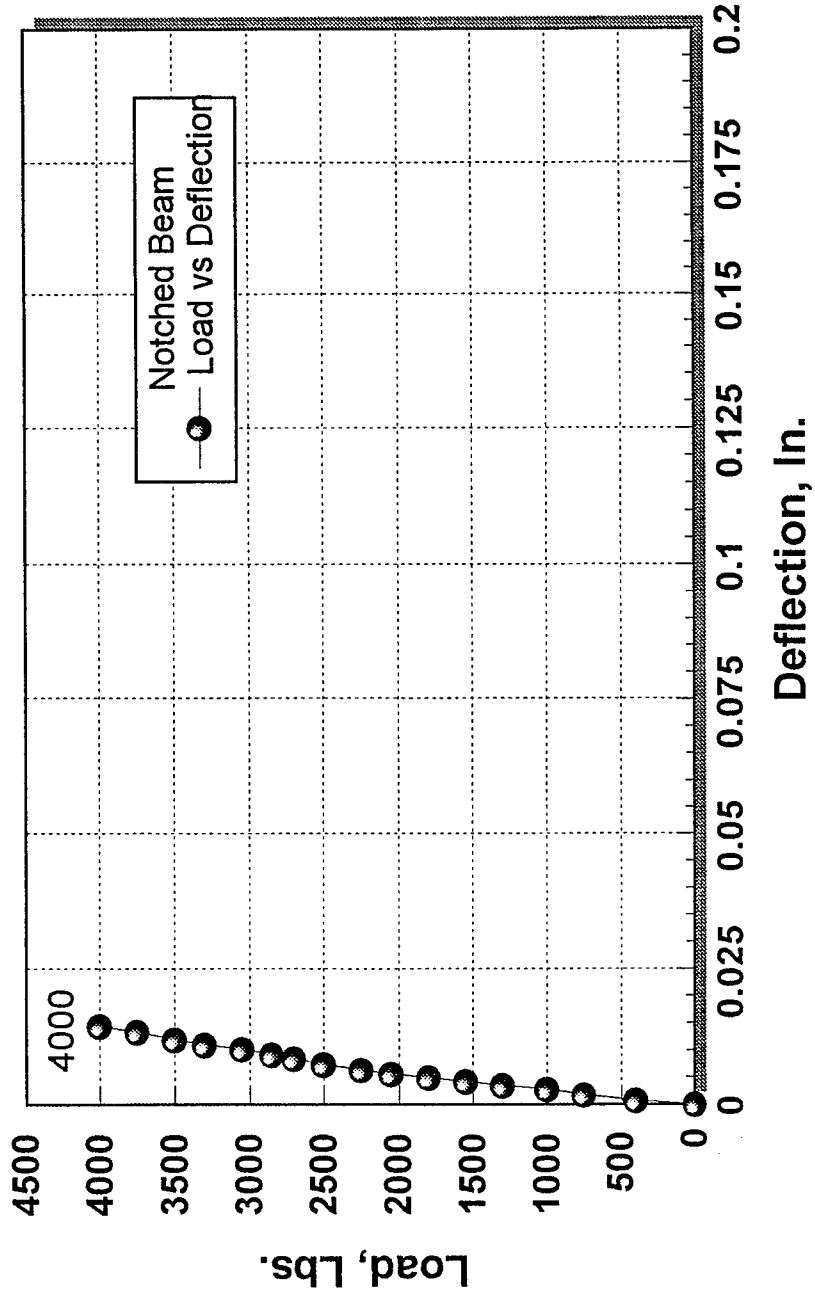
# Load vs. Deflection Curve ASTM C78 - 84



FBR3M - Control mix for FBR3M & FBR3MA

Figure 4.22 Flexural Strength of Concrete

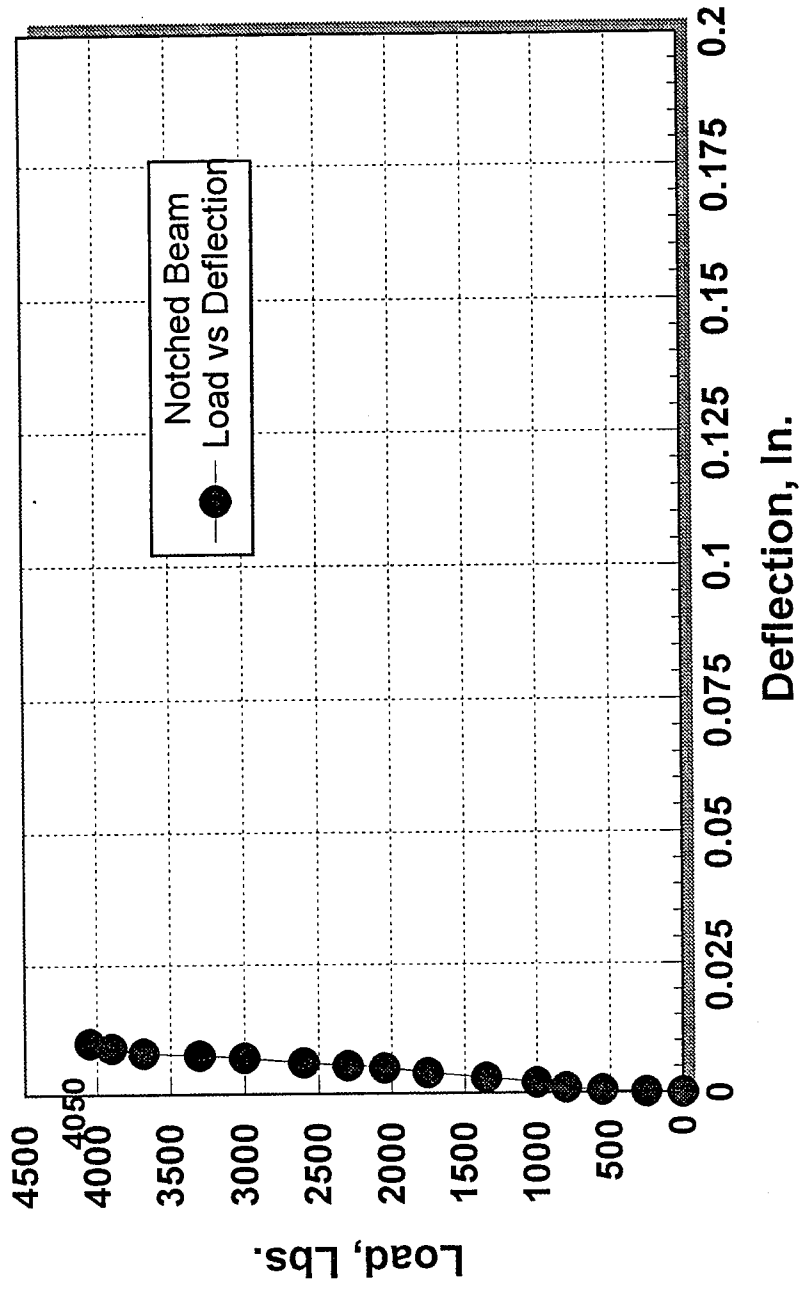
# Load vs. Deflection Curve ASTM C78 - 84



FBRCNT - Control mix for FBR3M & FBR3MA

Figure 4.23 Flexural Strength of Concrete

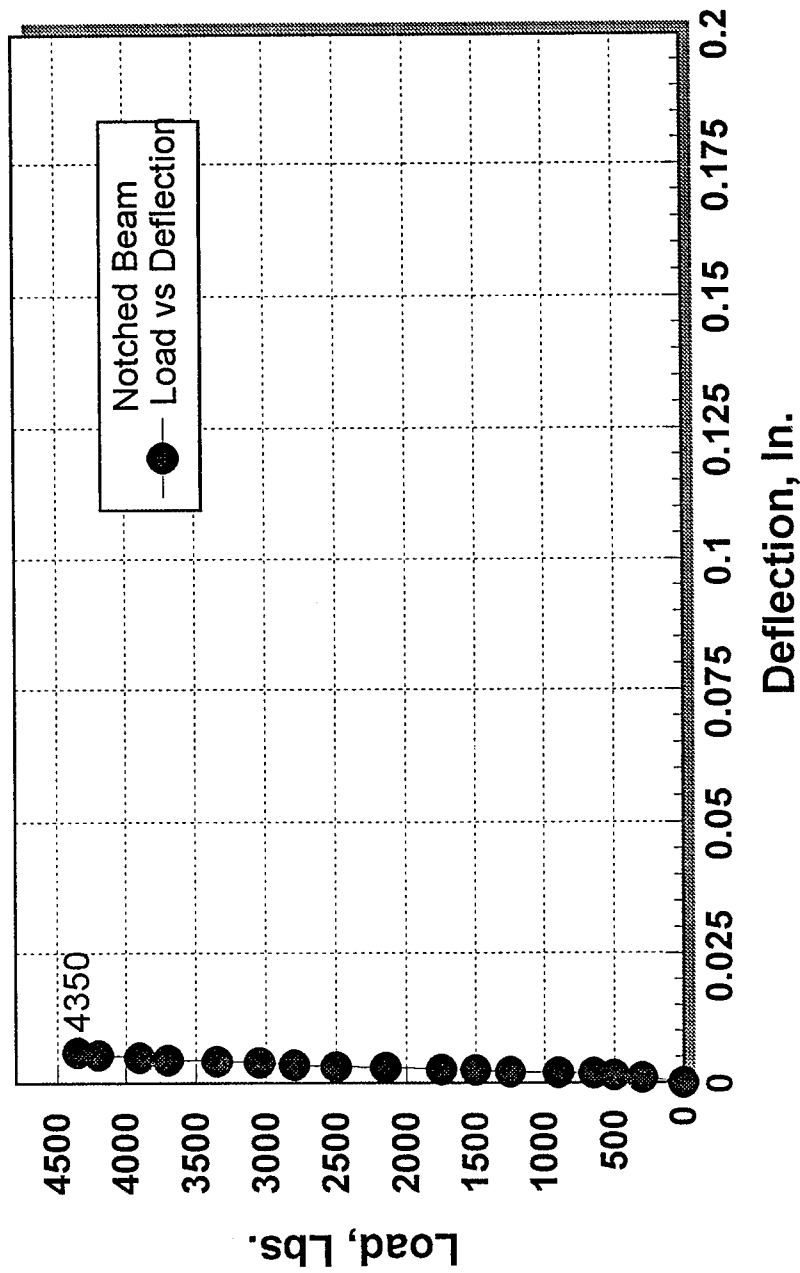
Load vs. Deflection Curve  
ASTM C78 - 84



FBR3M - Control mix for FBR3M & FBR3MA

Figure 4.24 Flexural Strength of Concrete

# Load vs. Deflection Curve ASTM C78 - 84

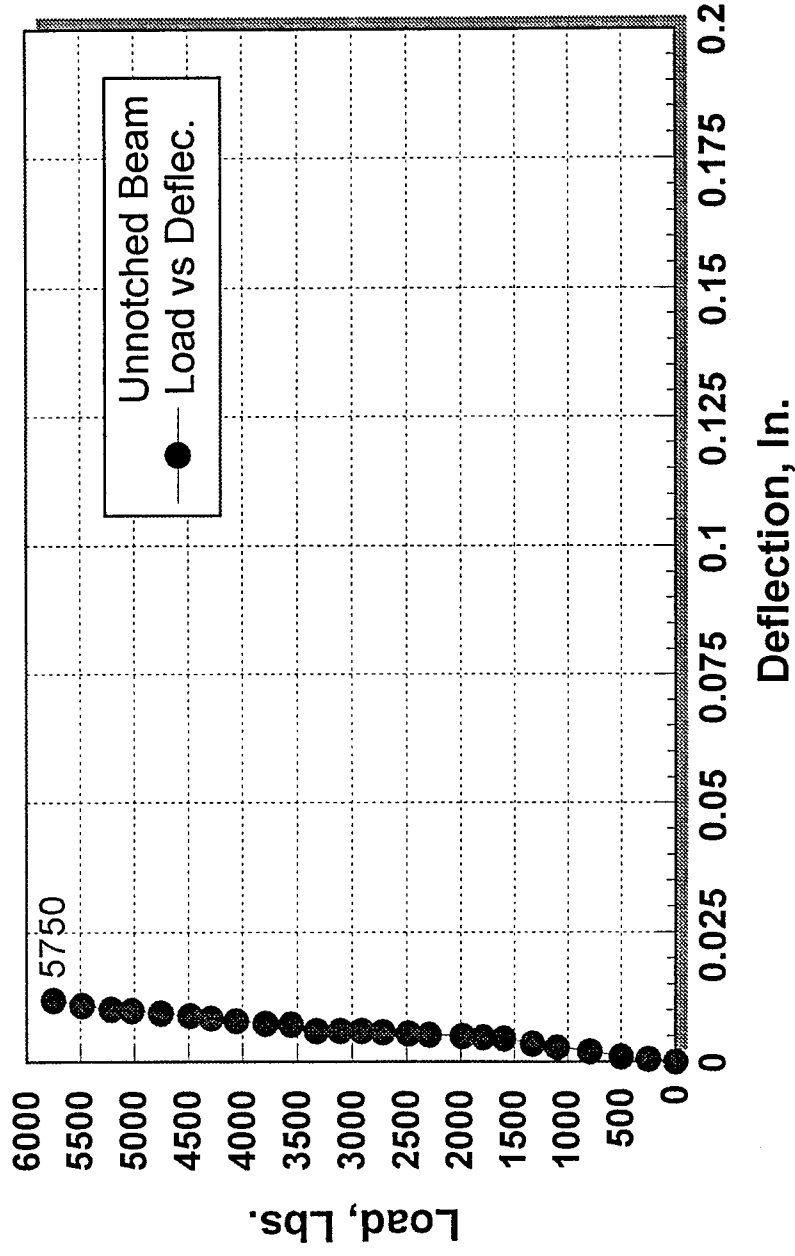


FBR3M - Control mix for FBR3M & FBR3MA

Figure 4.25 Flexural Strength of Concrete



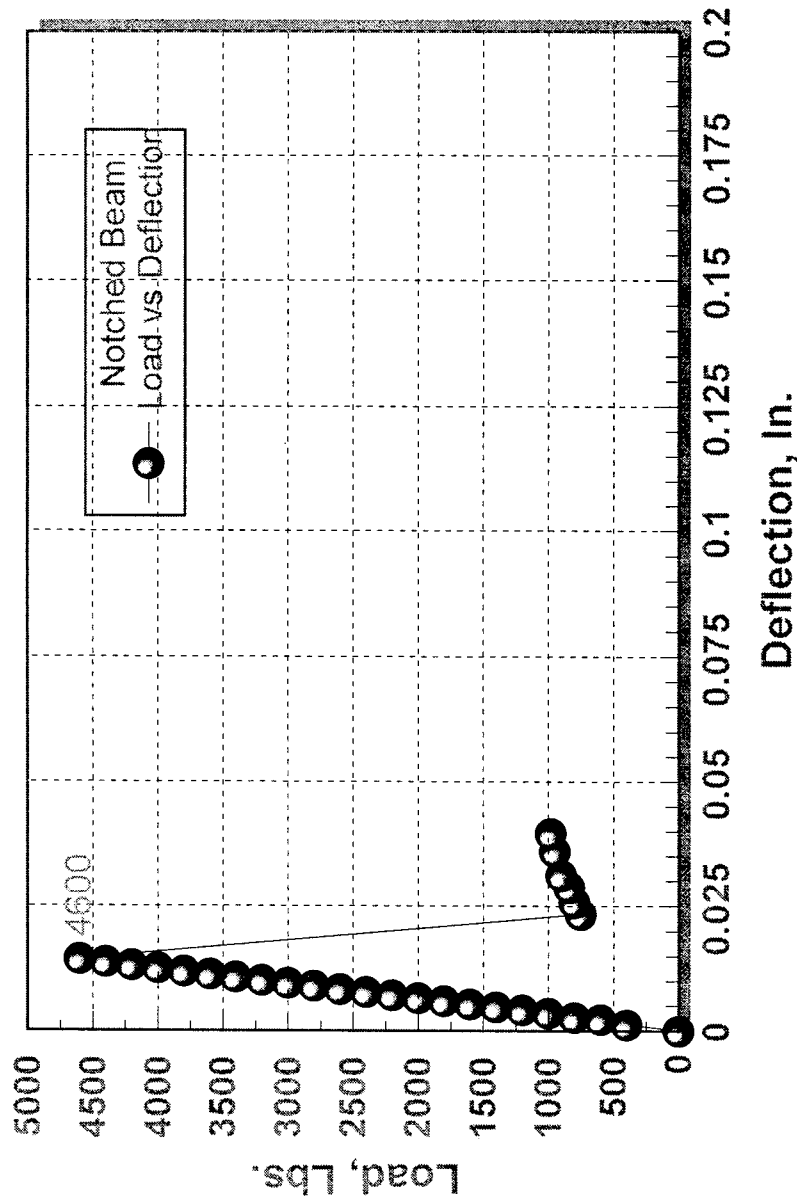
# Load vs. Deflection Curve ASTM C78 - 84



FBRCNT - Control mix for FBR3M & FBR3MA

Figure 4.26 Flexural Strength of Concrete

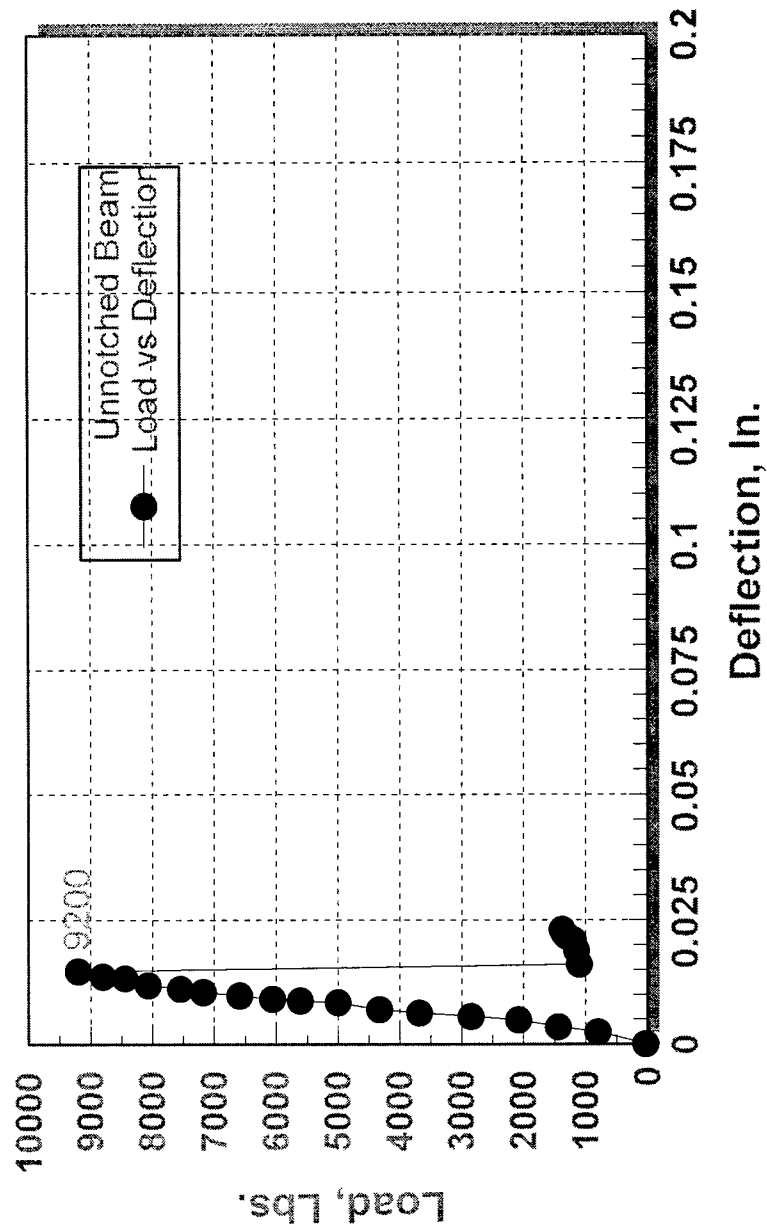
# Load vs. Deflection Curve ASTM C78 - 84



FBRME - FIBERMESH 2" Fibrillated Polypropylene Fiber

Figure 4.27 Flexural Strength of Concrete

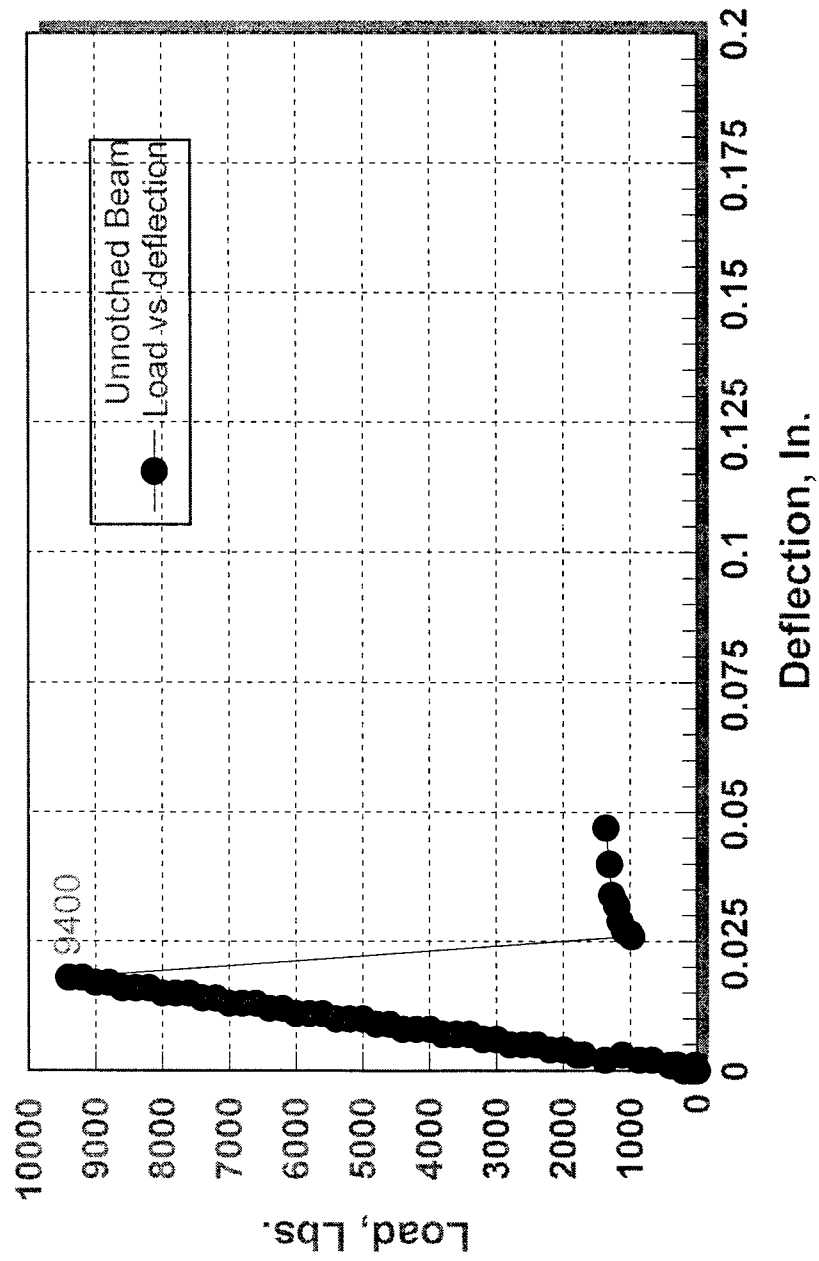
# Load vs. Deflection Curve ASTM C78 - 84



FBRME - FIBERMESH 2" Fibrillated Polypropylene Fiber

Figure 4.28 Flexural Strength of Concrete

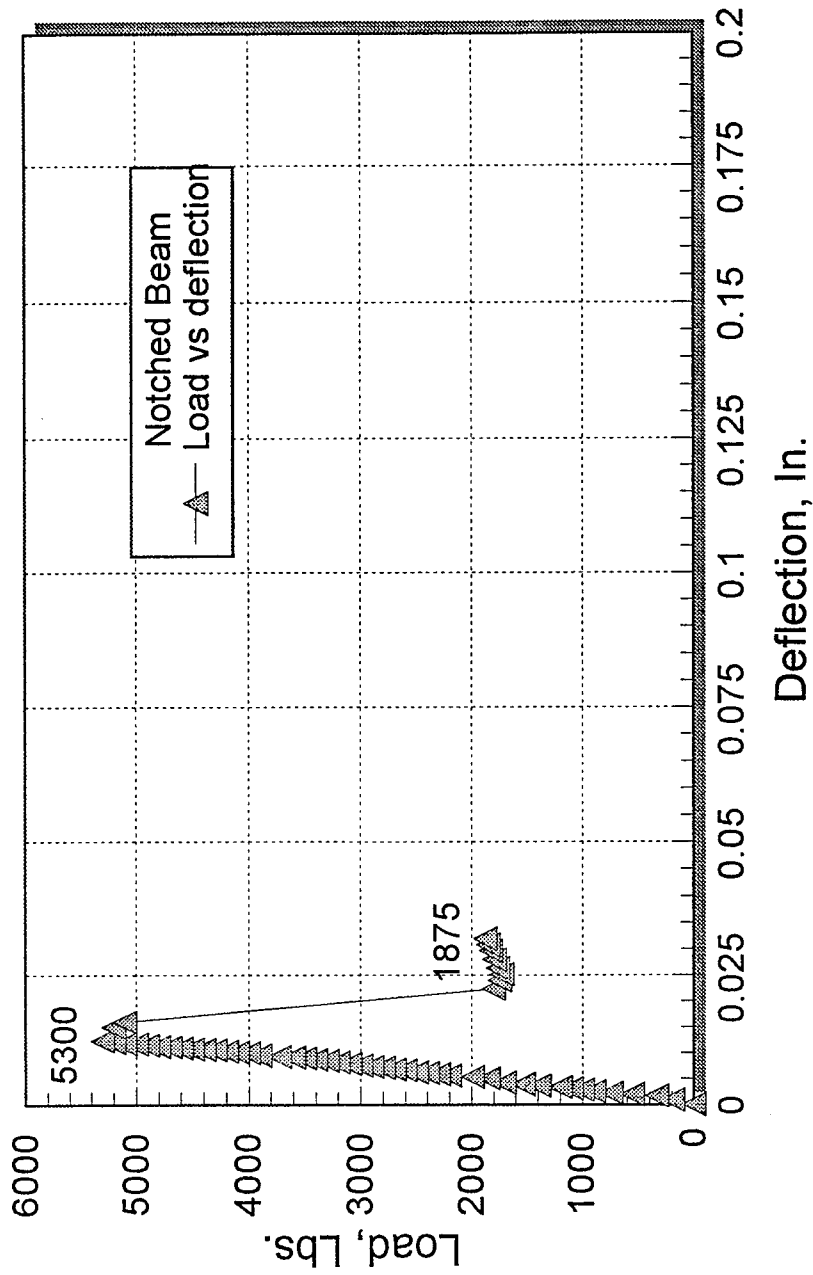
# Load vs. Deflection Curve ASTM C78 - 84



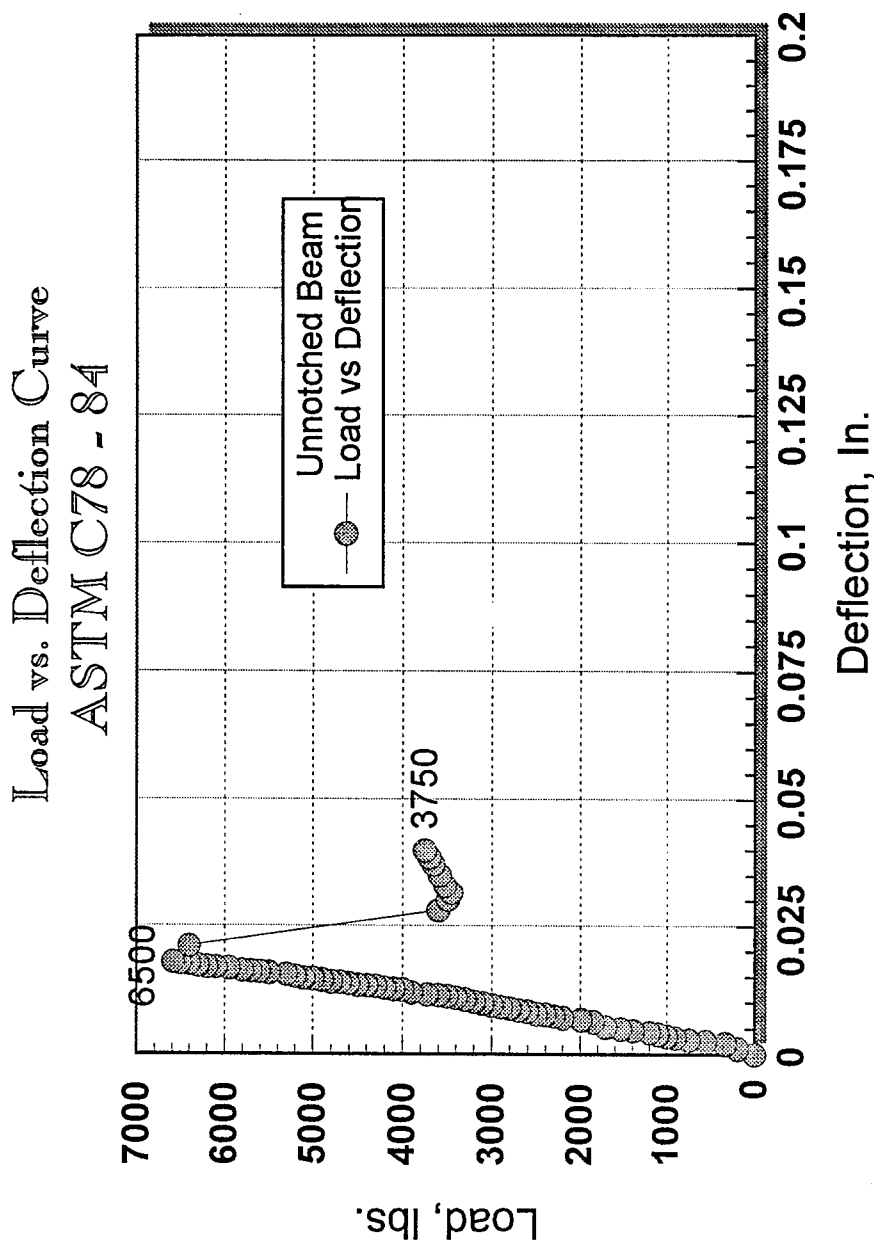
FBRME - FIBERMESH 2" Fibrillated Polypropylene Fiber

Figure 4.29 Flexural Strength of Concrete

# Load vs. Deflection Curve ASTM C78 - 84



FBR3M - 3M Monofilament Polyolefin Fiber  
Figure 4.30 Flexural Strength of Concrete



FBR3M - 3M Monofilament Polyolefin Fiber  
Figure 4.31 Flexural Strength of Concrete

# Stress vs Strain Curve ASTM C469 - 87a

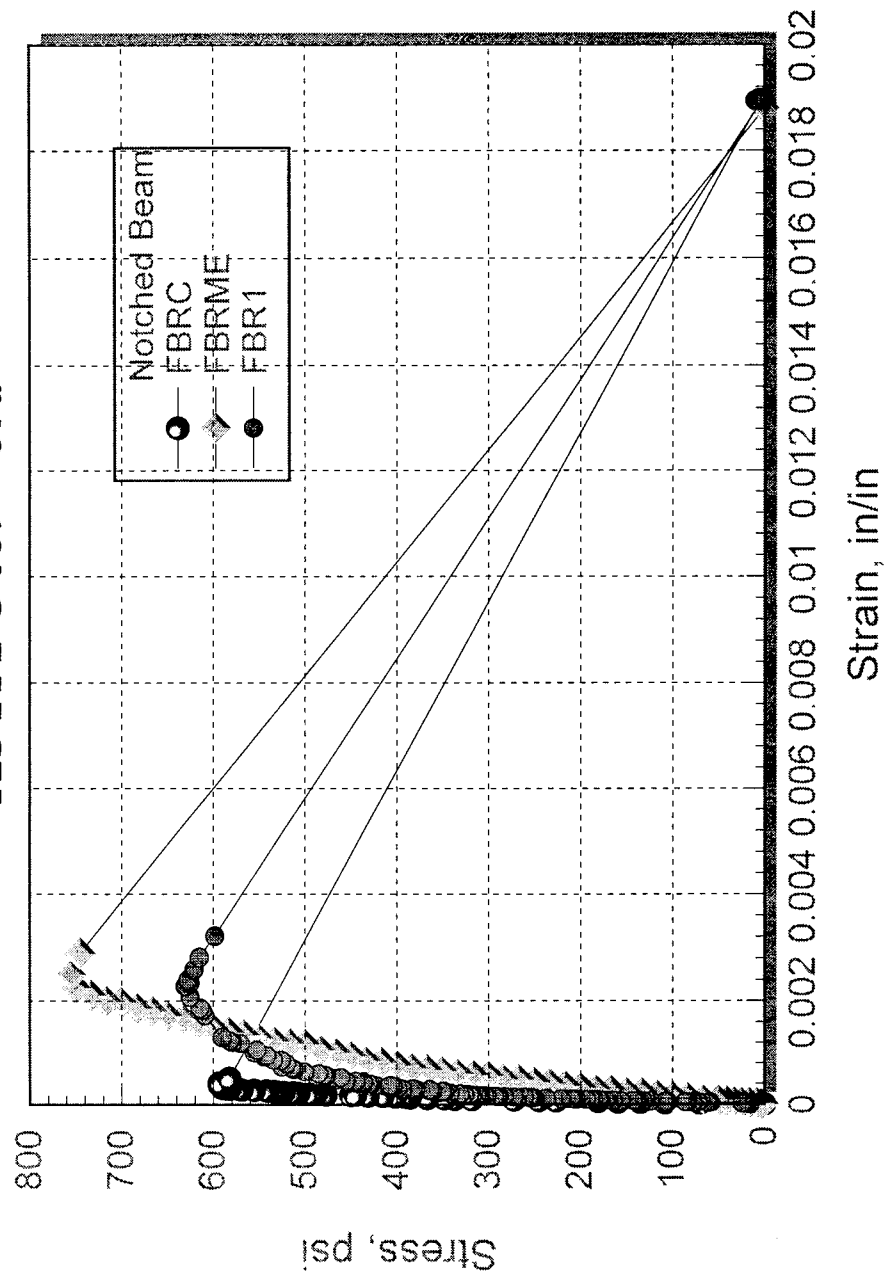


Figure 4.32 Stress-Strain Relationship

ANSYS 5.2  
 JUL 28 1996  
 07:52:20  
 NODAL SOLUTION  
 TIME=8.55  
 EPTOZ (AVG)  
 RSYS=0  
 DMX =.006486  
 SMN =-.176E-03  
 SMX =.003405

XV =1.478  
 YV =.866025  
 ZV =.253653  
 \*DIST=11.247  
 \*XF =3.304  
 \*YF =2.728  
 \*ZF =9.88  
 A-ZS=19.471  
 PRECISE HIDDEN  
 -.176E-03  
 .266E-05  
 .182E-03  
 .361E-03  
 .540E-03  
 .719E-03  
 .898E-03  
 .001077  
 .001256  
 .002331  
 .00251  
 .002689  
 .002868  
 .003047  
 .003226  
 .003405

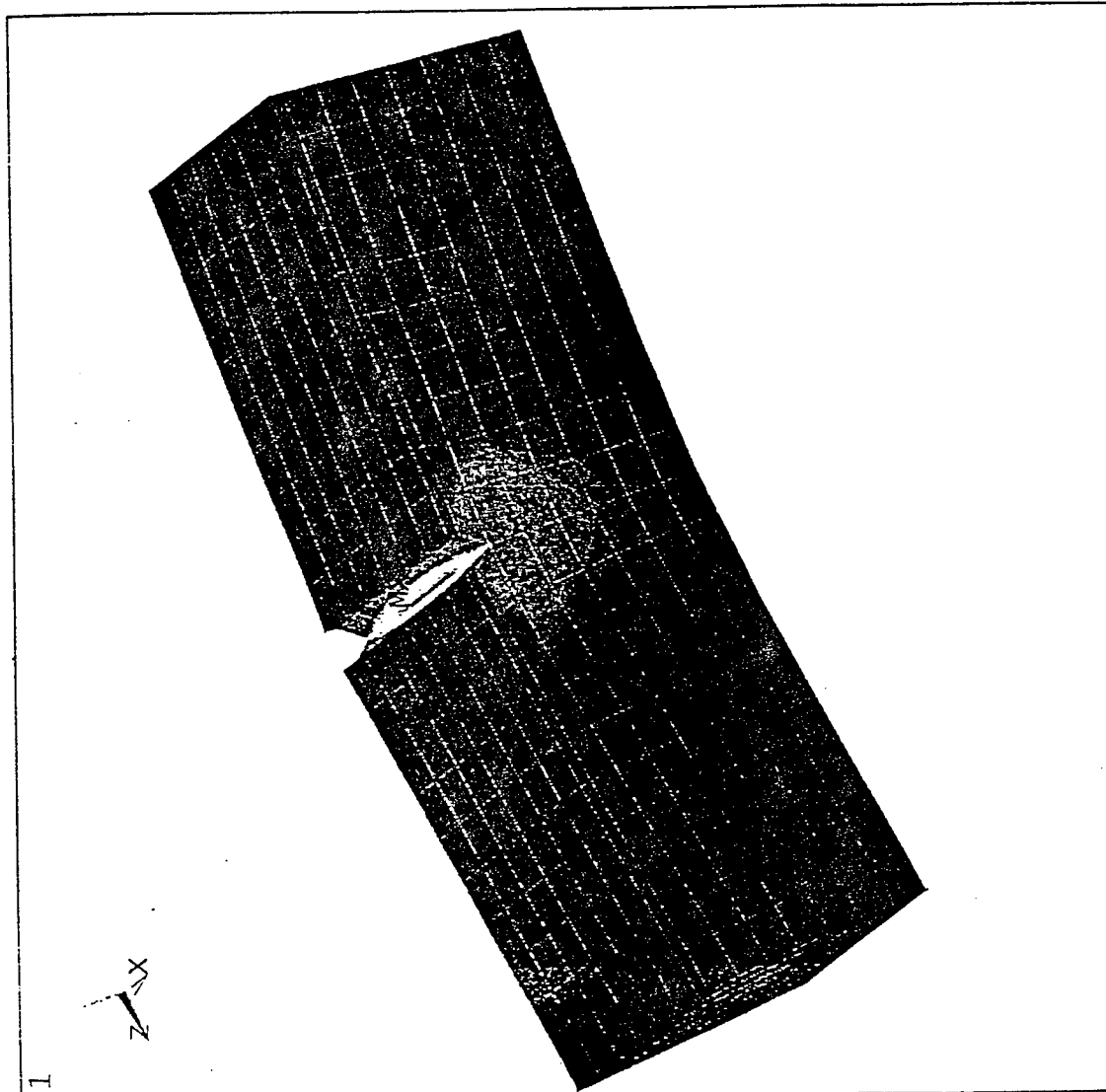


Figure 4.32.a Strain Distribution in the Z direction of Plain Concrete  
 at Flexural Load = 4770 lb



ANSYS 5.2  
 JUL 28 1996  
 07:58:10  
 NODAL SOLUTION  
 TIME=8.55  
 EPTOZ (AVG)  
 RSYS=0  
 DMX =.001542  
 SMN =-.896E-04  
 SMX =.924E-04  
 XV =1.475  
 YV =.873475  
 ZV =.249919  
 \*DIST=11.452  
 \*XF =3.385  
 \*YF =2.599  
 \*ZF =10.27  
 A-ZS=16.127  
 PRECISE HIDDEN  
 -.896E-04  
 -.805E-04  
 -.714E-04  
 -.623E-04  
 -.532E-04  
 -.441E-04  
 -.350E-04  
 -.259E-04  
 -.168E-04  
 .378E-04  
 .469E-04  
 .560E-04  
 .651E-04  
 .742E-04  
 .833E-04  
 .924E-04

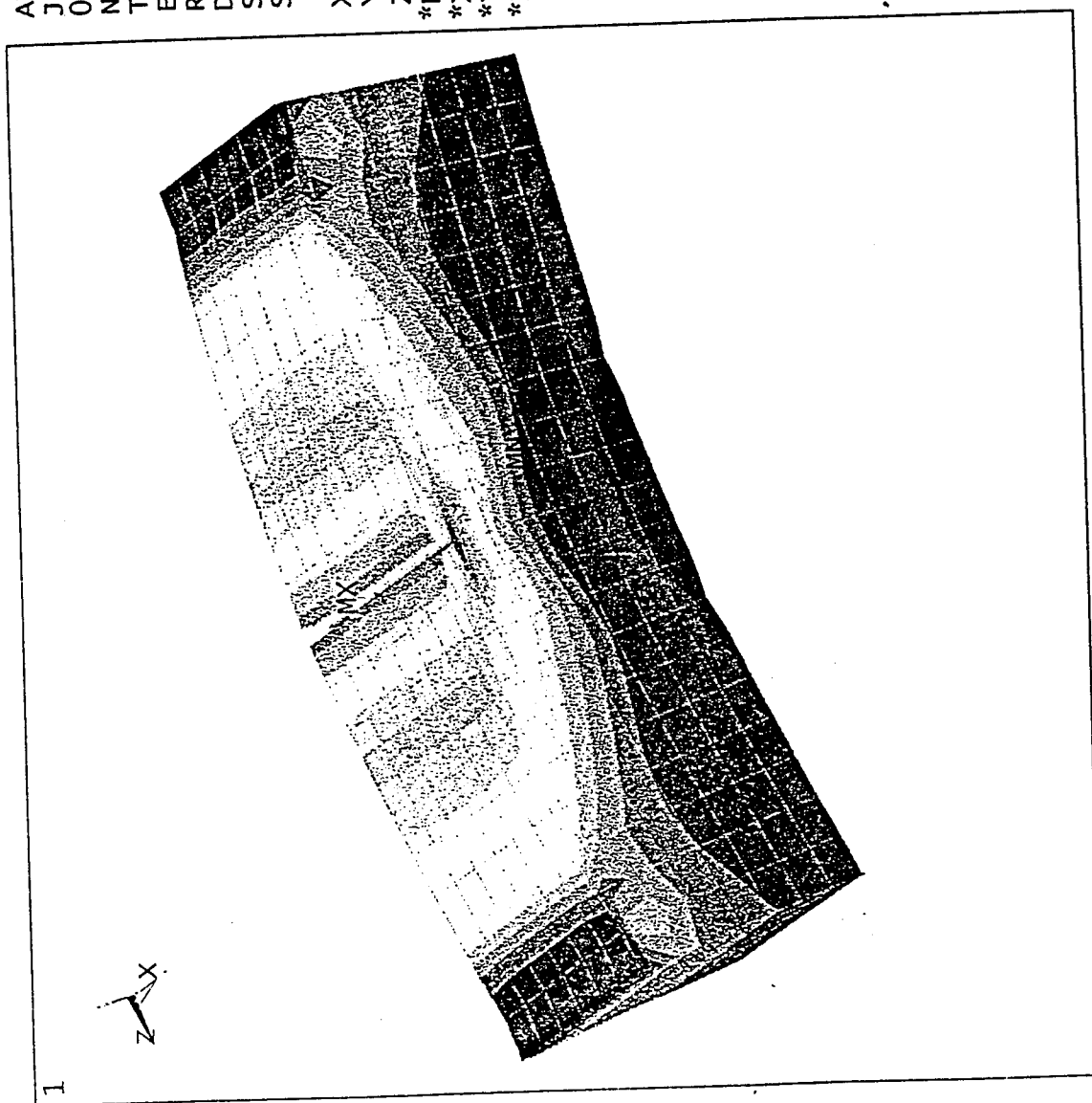


Figure 4.32.b Strain Distribution in the Z direction of Fiber Reinforced Concrete  
 at Flexural Load = 4770 lb

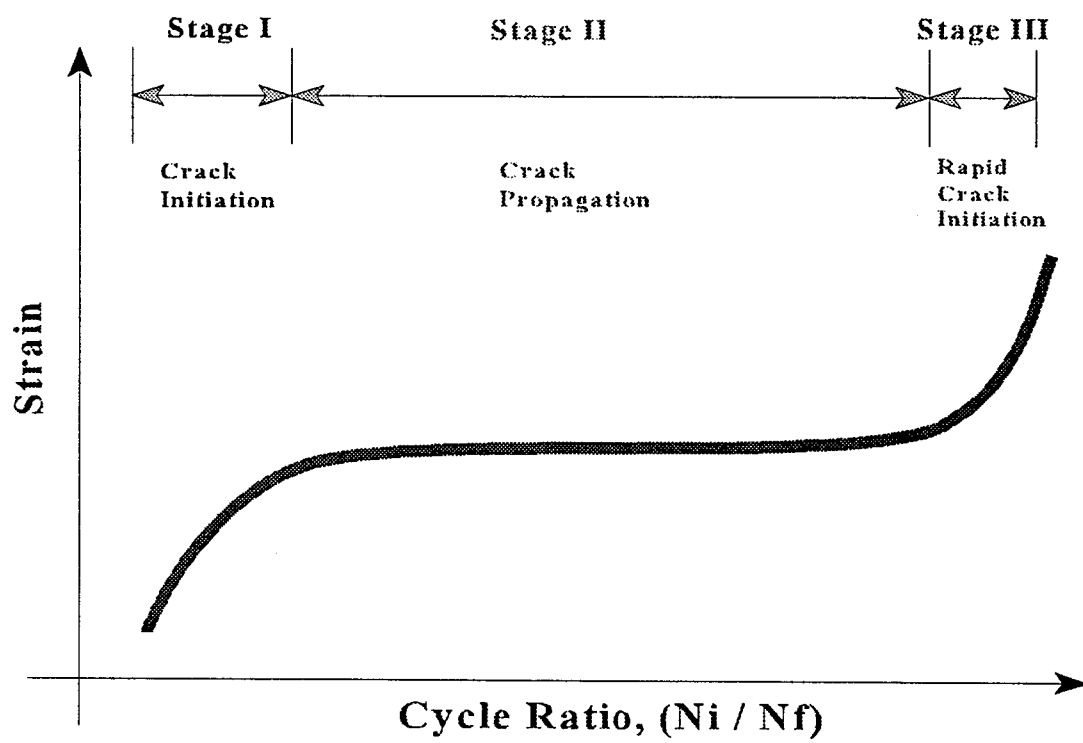


Figure 4.33 Crack Development Stages

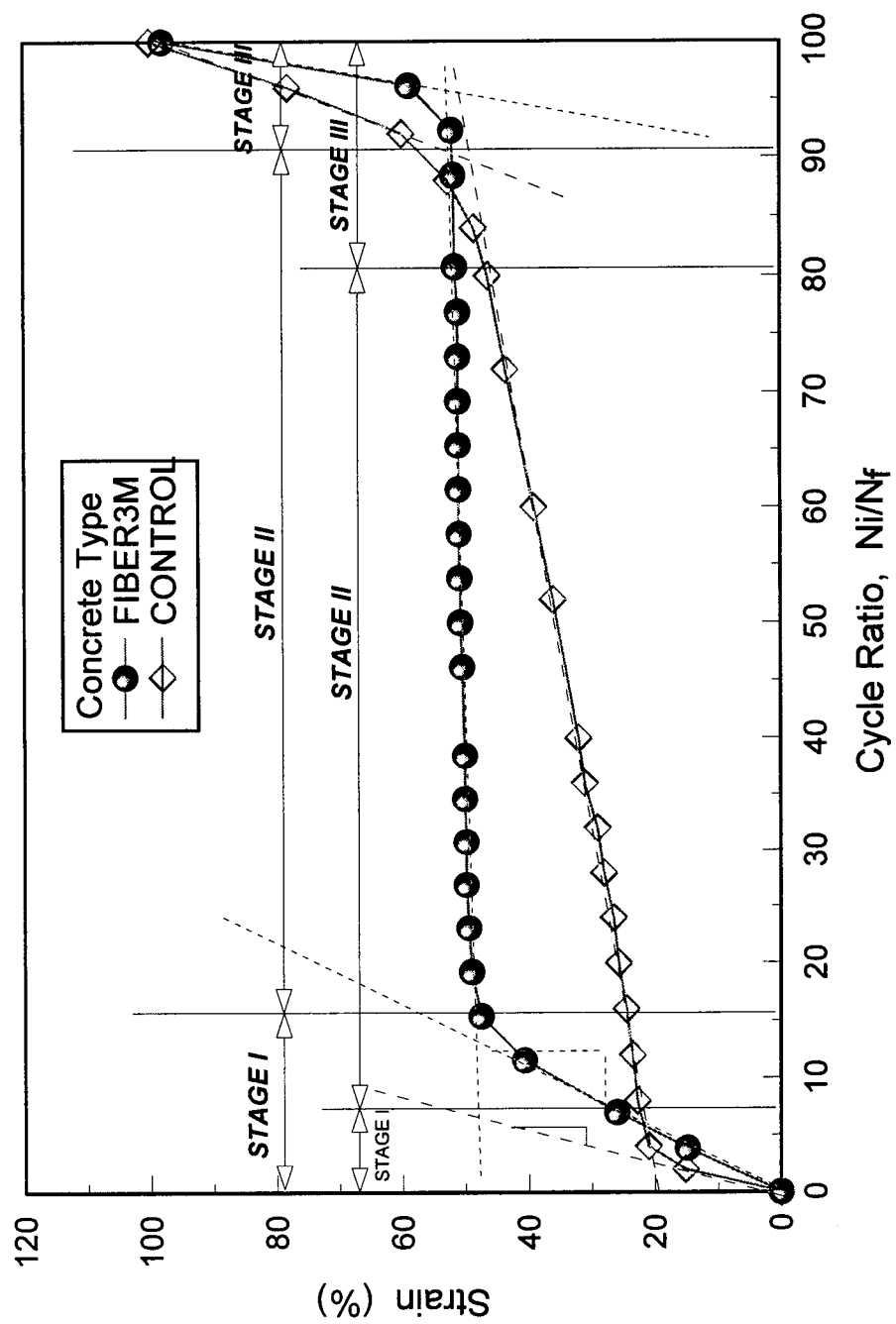


Figure 4.34. Crack Initiation Delay at Stage I.

# Hysteresis Loops Strain Gage #1

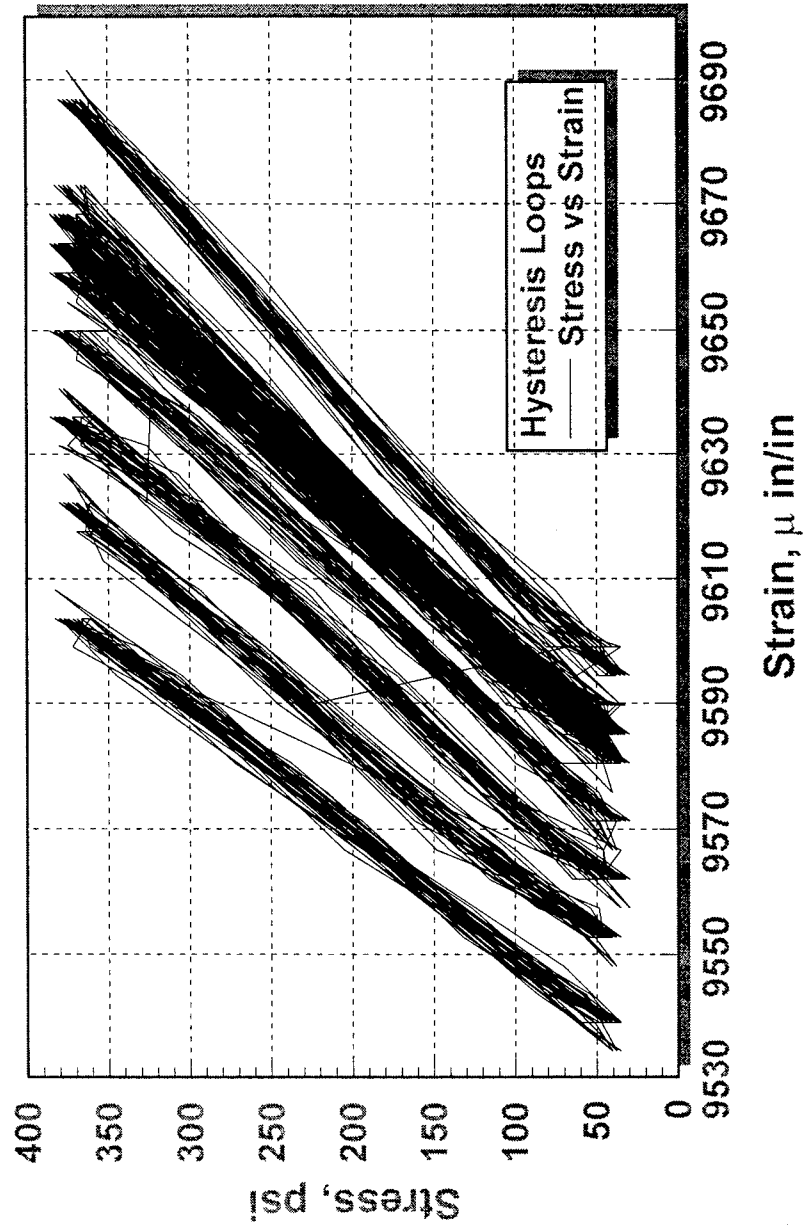


Figure 4.35 Hysteresis Loops for FBR3M (S = 60%)

# Hysteresis Loops Strain Gage #1

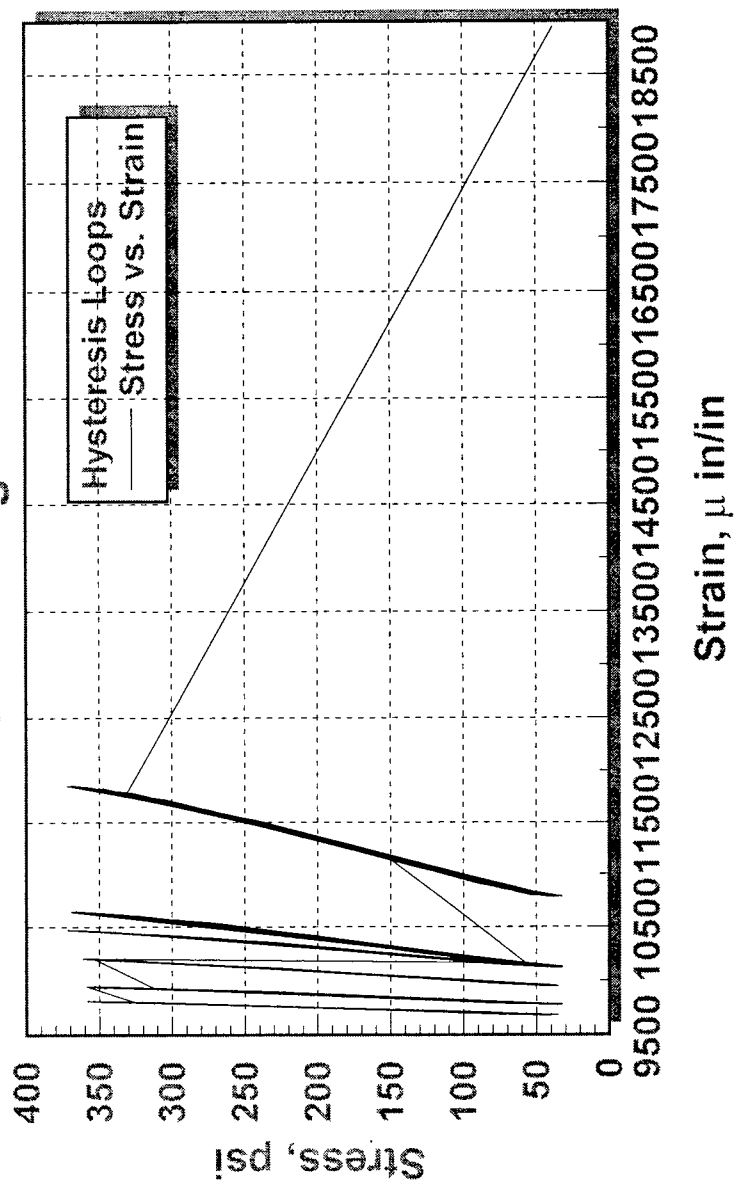


Figure 4.36 Hysteresis Loops for FBR3M (S = 73%)

# Hysteresis Loops Strain Gage #1

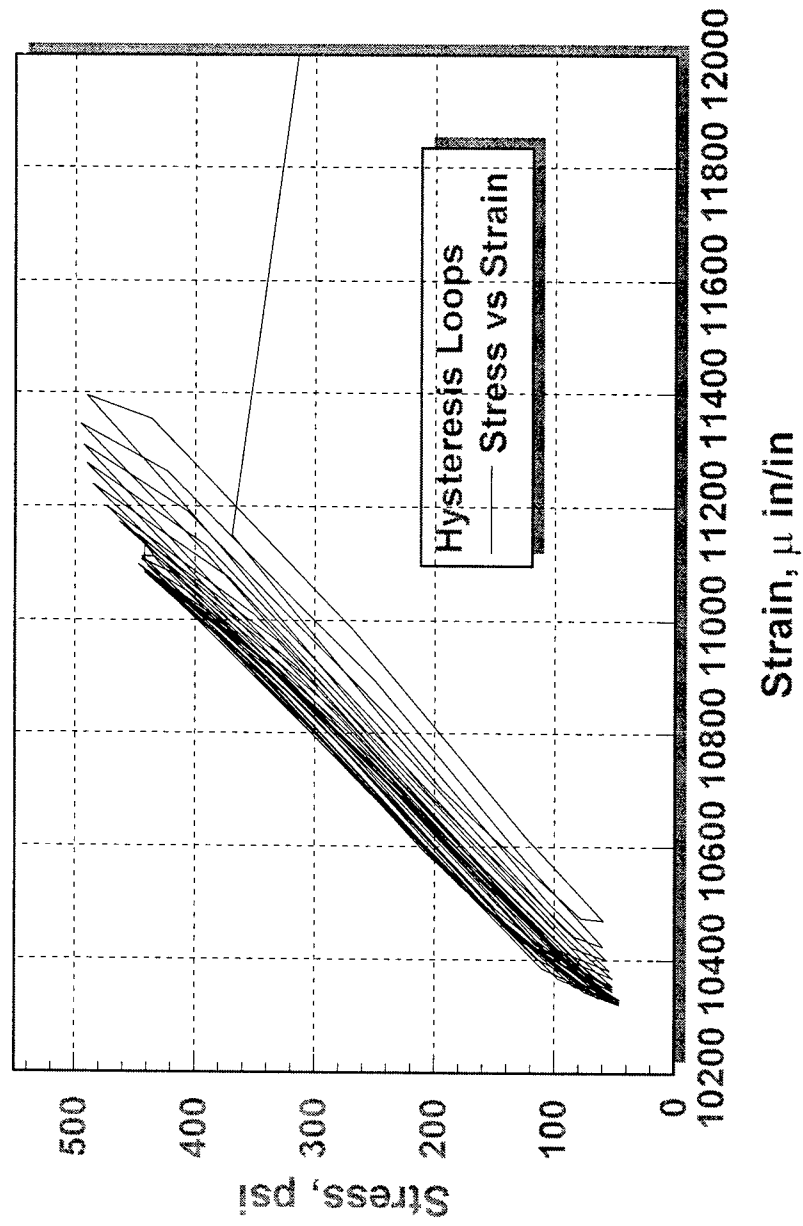


Figure 4.37 Hysteresis Loops for FBR3M (S = 82%)

# Hysteresis Loops Strain Gage #1

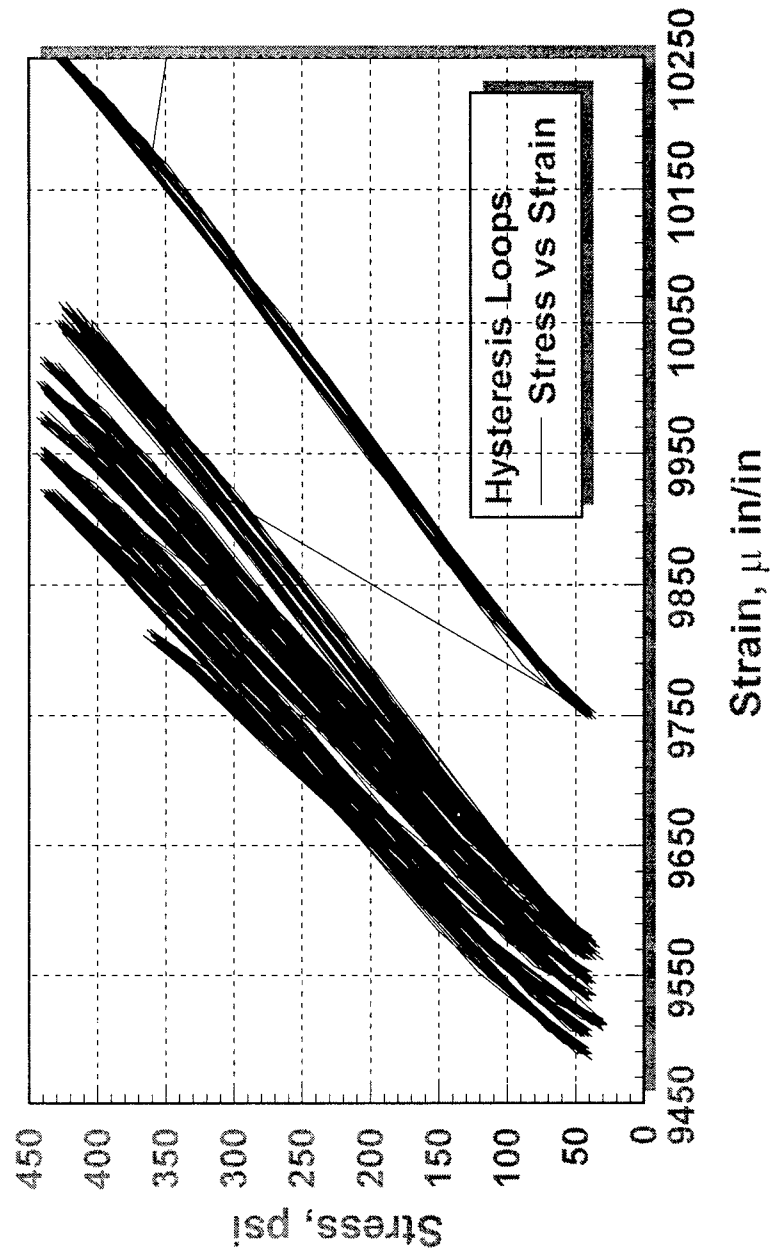


Figure 4.38 Hysteresis Loops for FBR1 (S = 67%)

### Hysteresis Loops Strain Gage #1

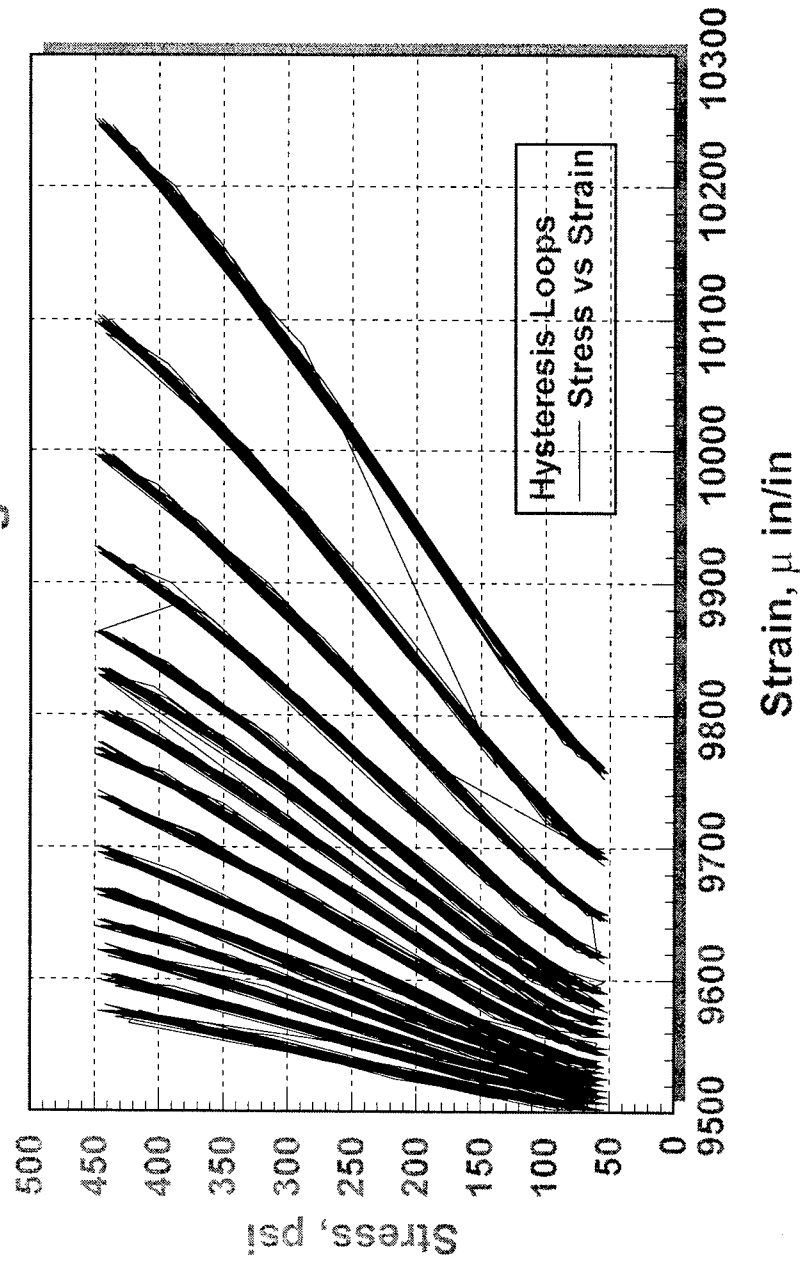


Figure 4.39 Hysteresis Loops for FBR1 (S = 71%)



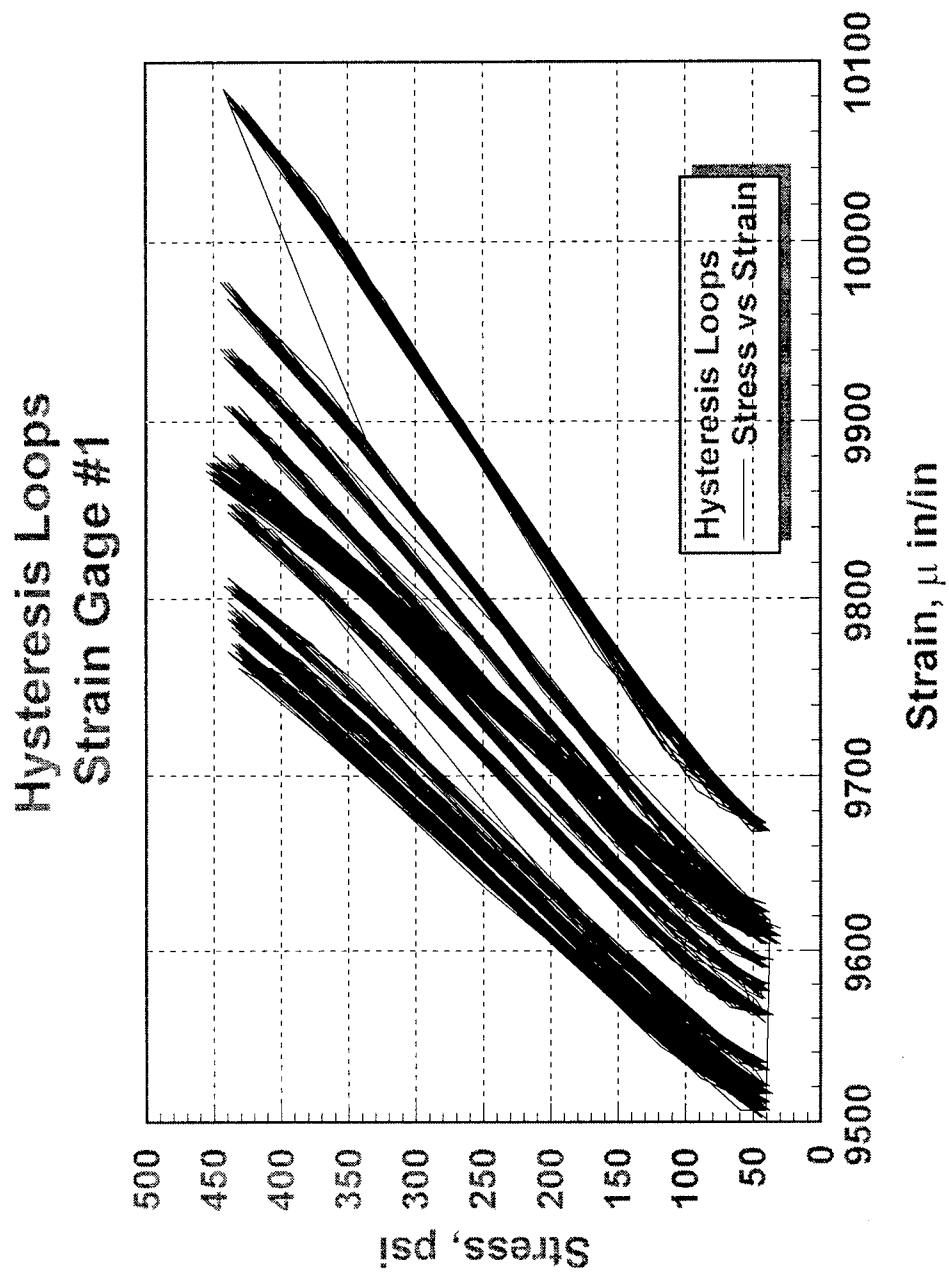


Figure 4.40 Hysteresis Loops for FBR1 (S = 74%)

## Hysteresis Loops Strain Gage #1

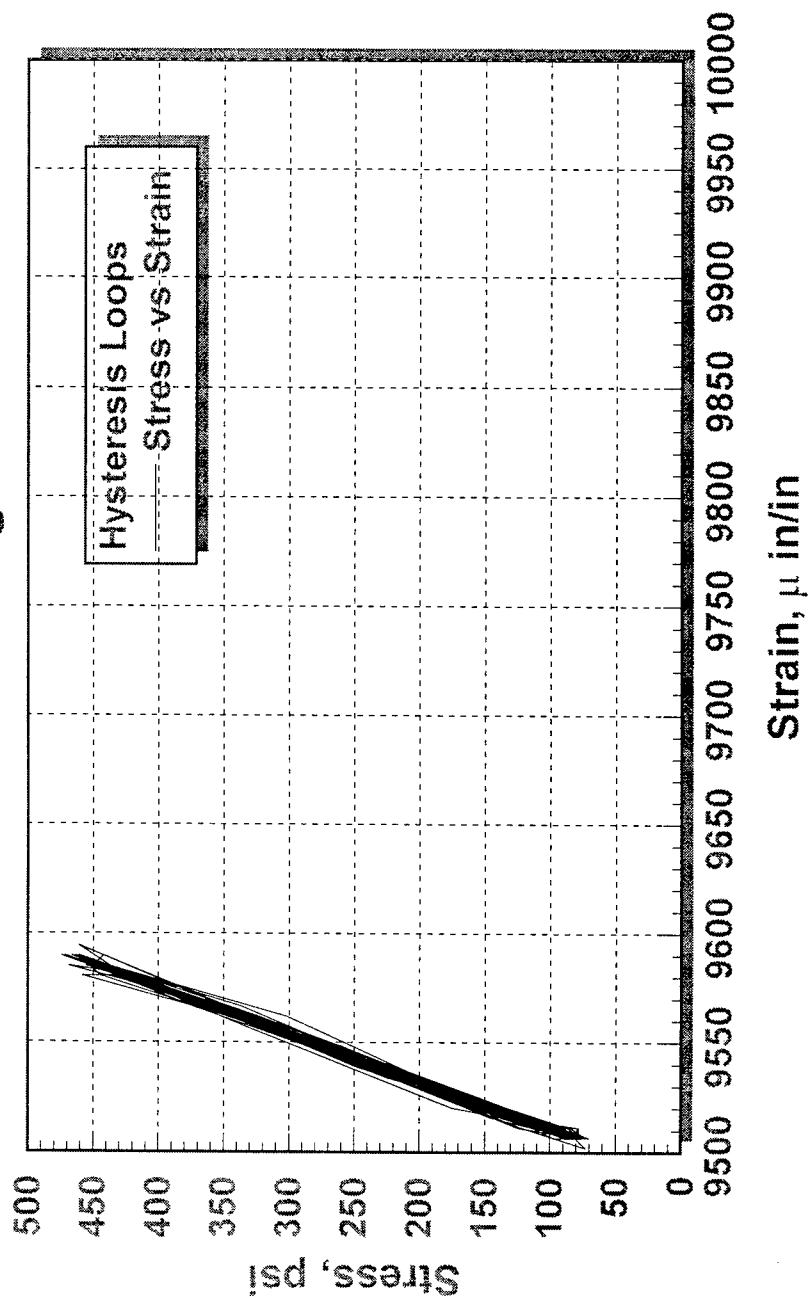


Figure 4.41 Hysteresis Loops for FBR1 (S = 84%)

## Hysteresis Loops Strain Gage #1

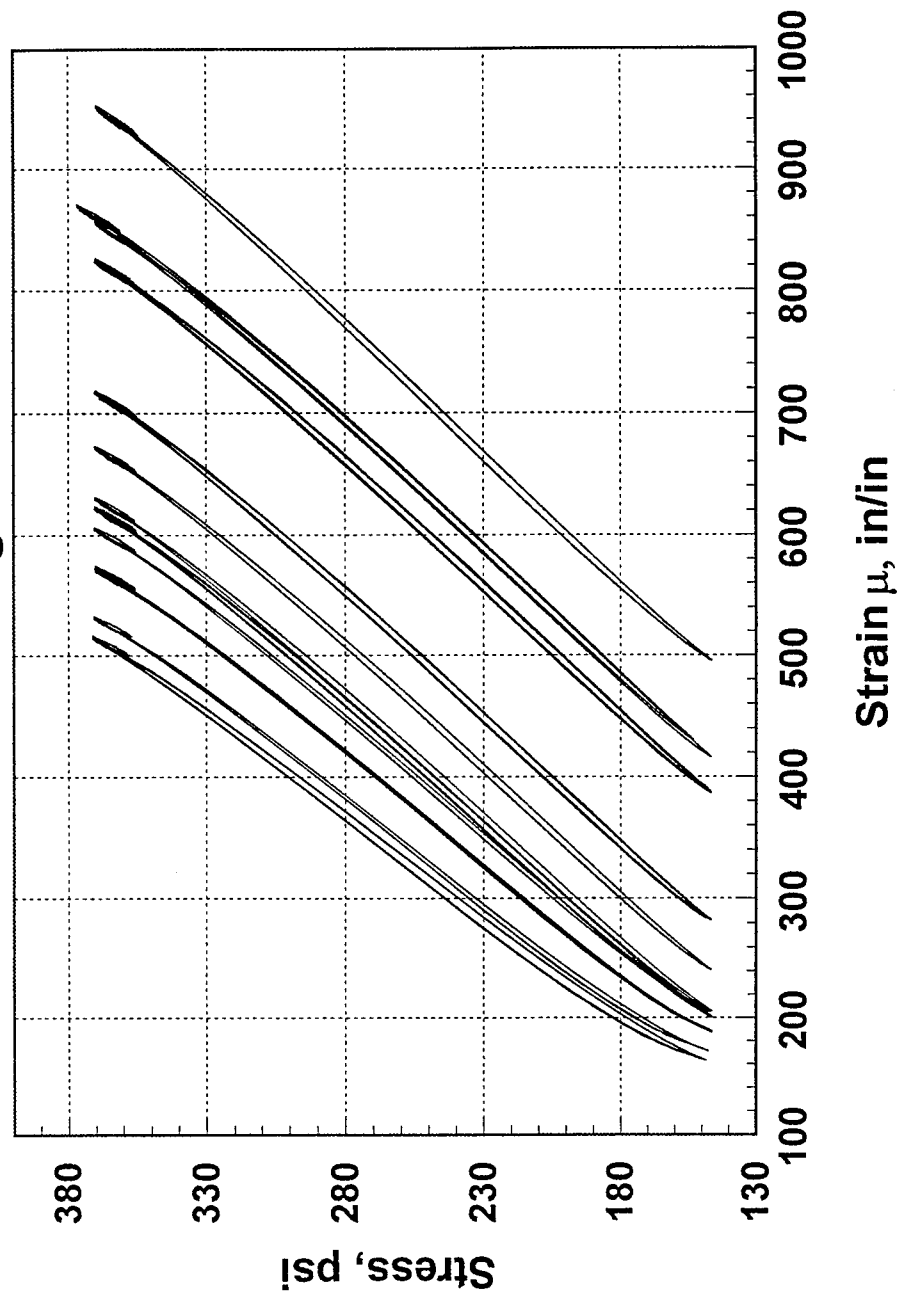


Figure 4.42 Hysteresis Loops for FBRME (S =75 %)

# Hysteresis Loops Strain Gage #1

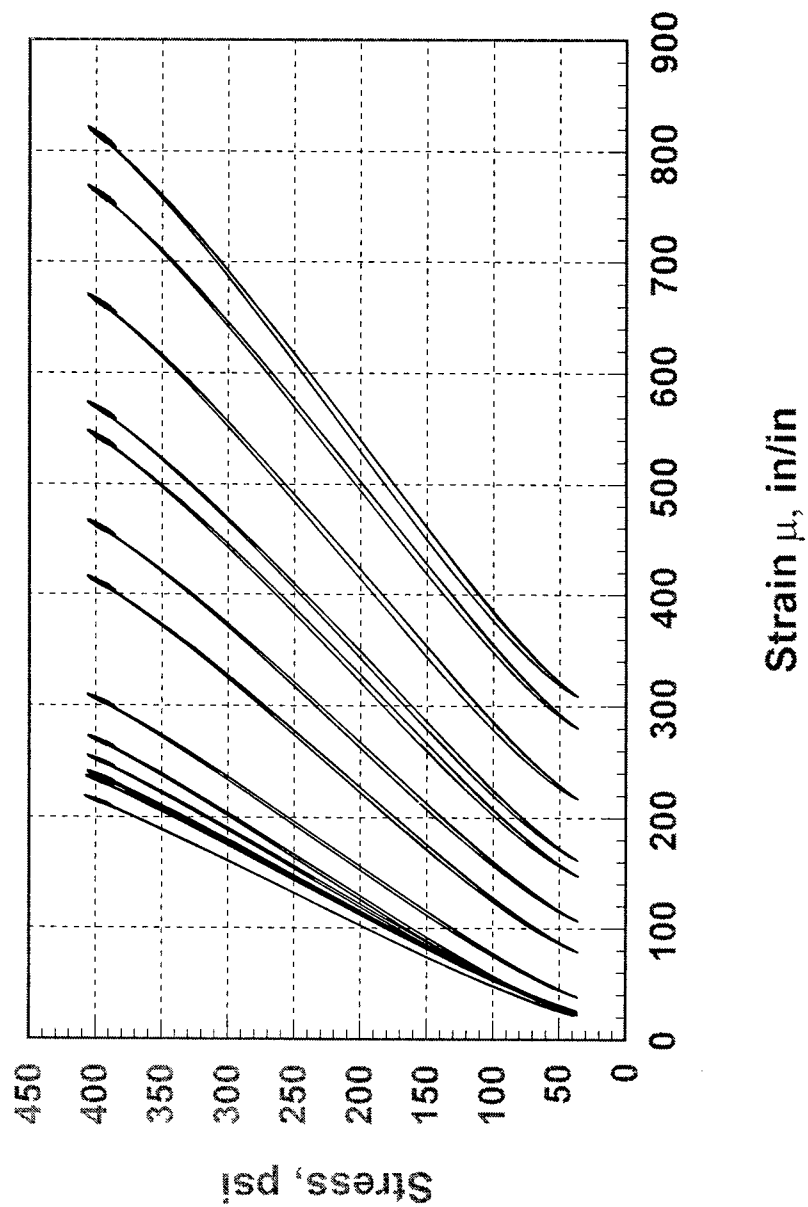


Figure 4.43 Hysteresis Loops for FBRME (S = 84%)

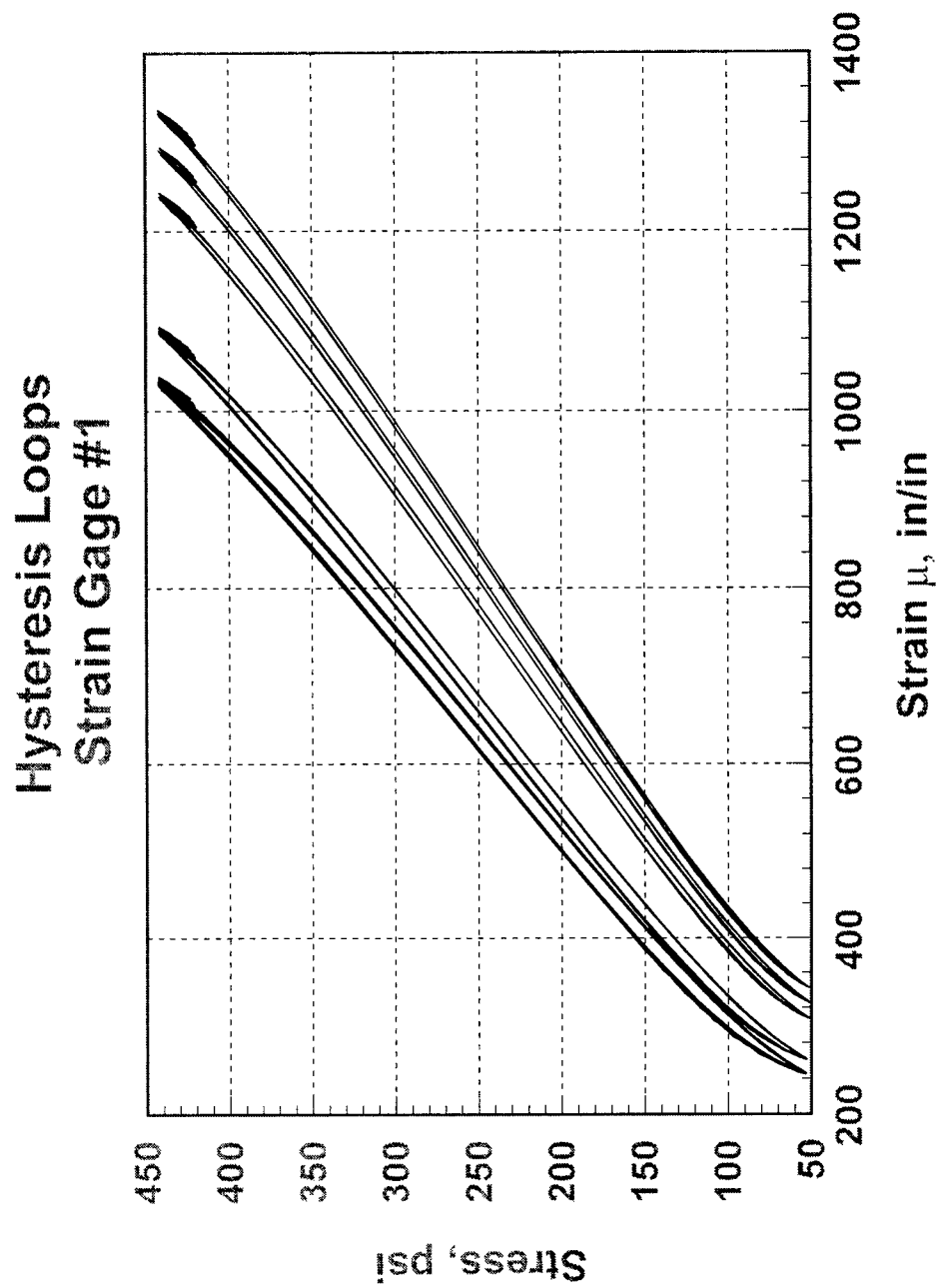


Figure 4.44 Hysteresis Loops for FBRME (S = 93 %)

# Strain vs. Cycle Ratio Strain Gage #1

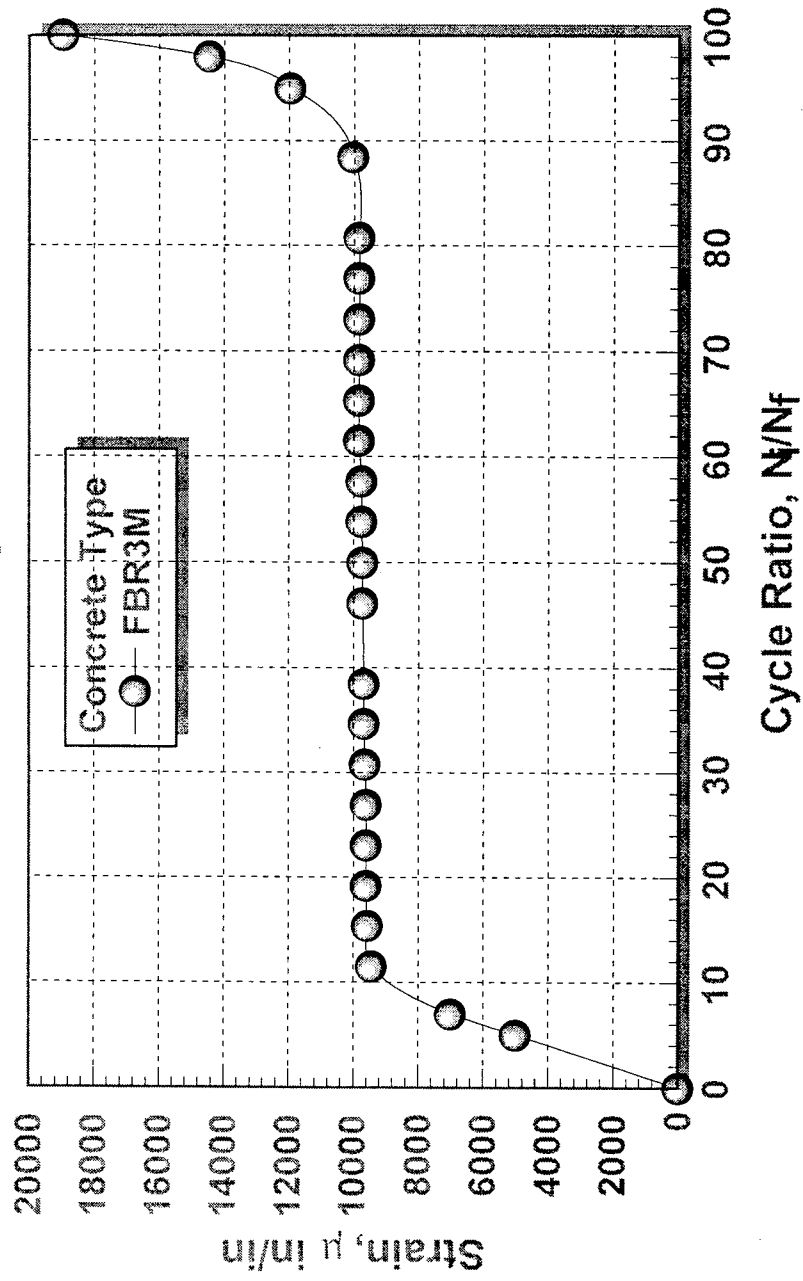


Figure 4.45 Strain Development for FBR3M (S = 60%)

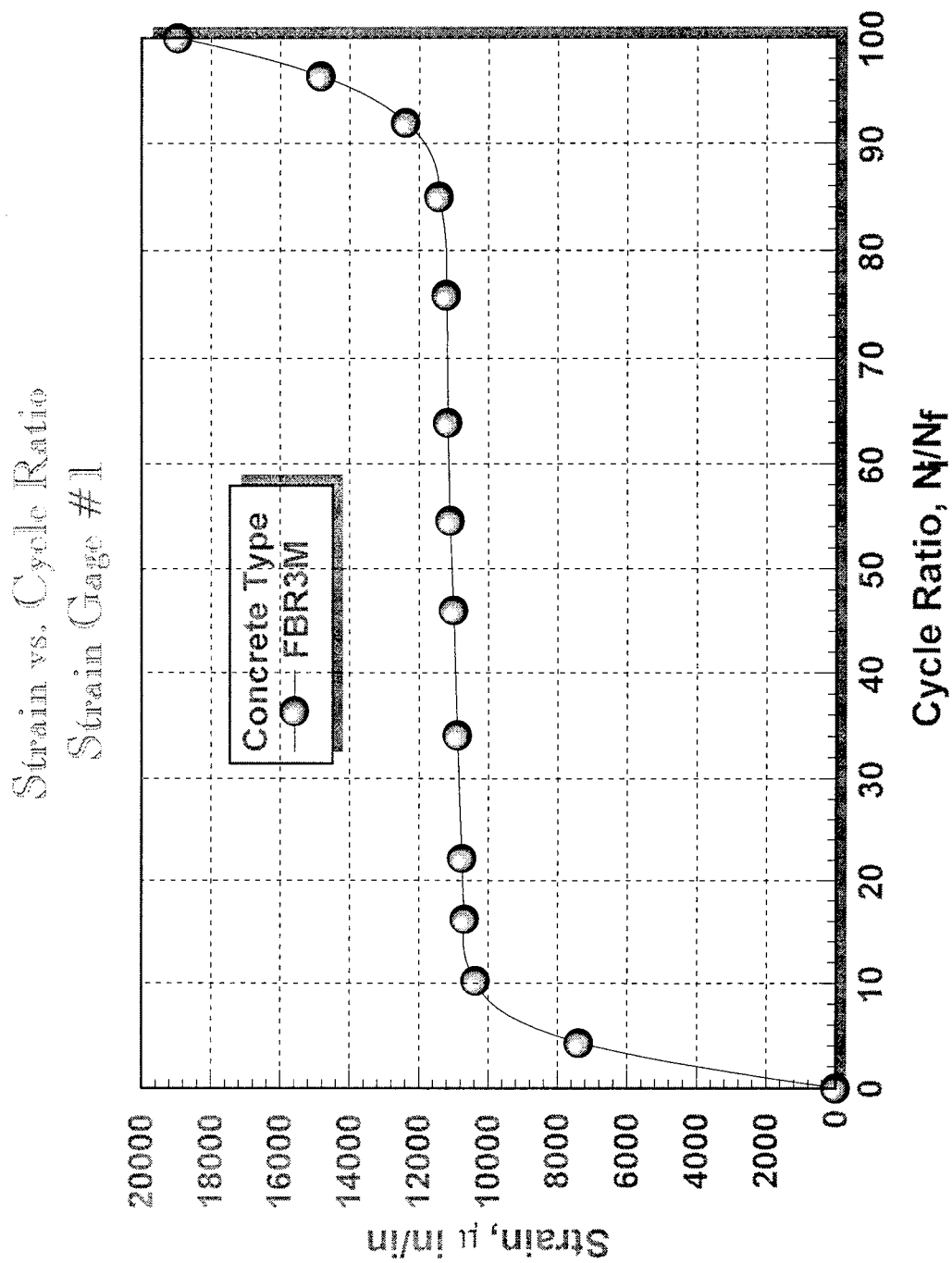


Figure 4.46 Strain Development for FBR3M ( $S = 73\%$ )

# Strain vs. Cycle Ratio Strain Cage #1

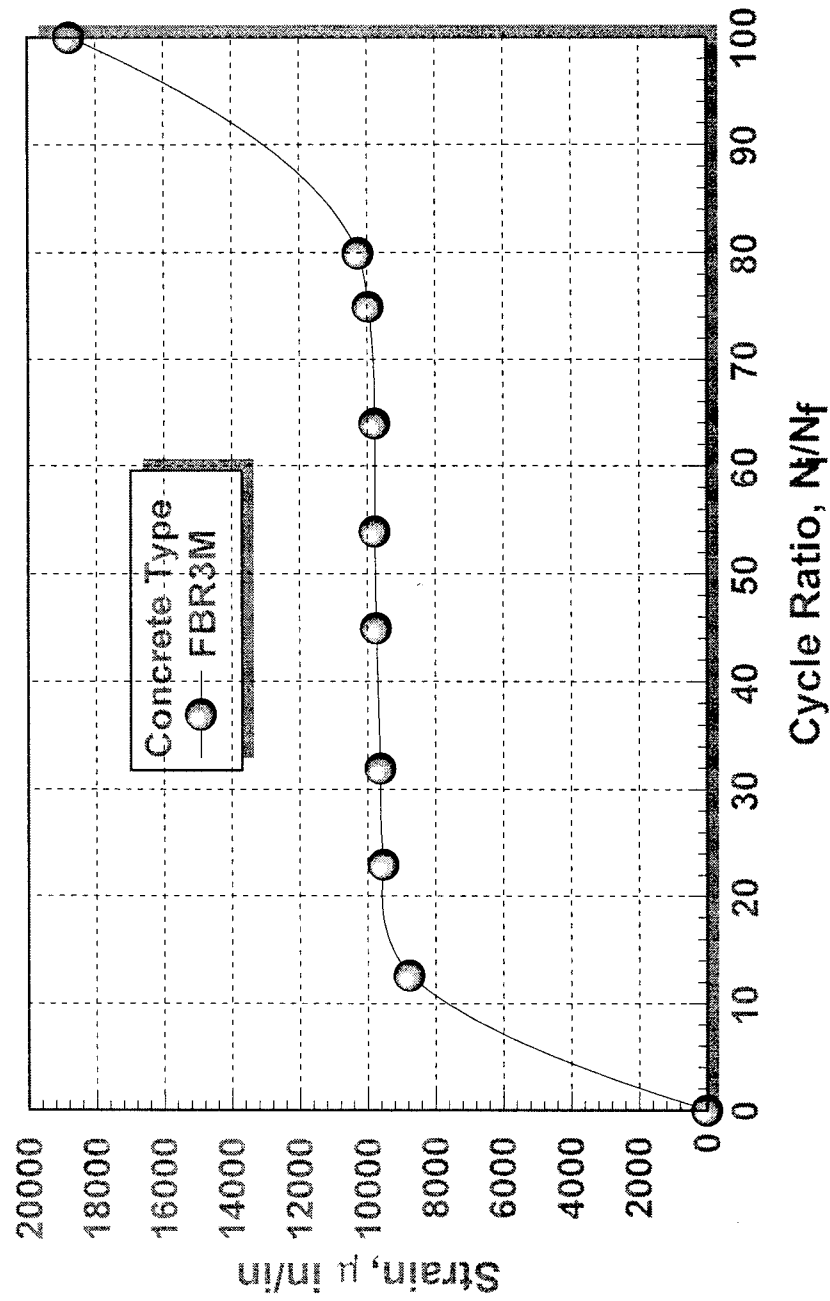


Figure 4.47 Strain Development for FBR3M (S = 82%)



# Strain vs. Cycle Ratio Strain Gage #1

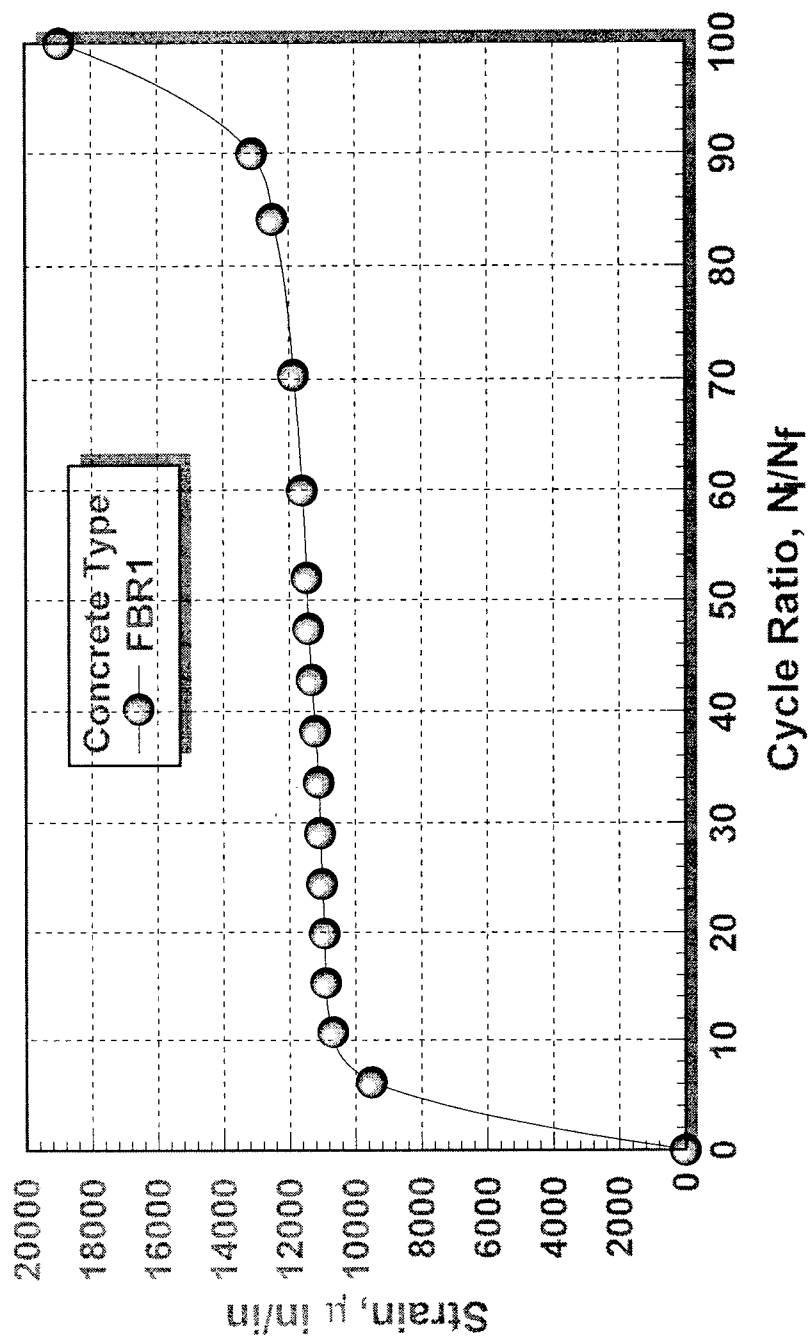


Figure 4.48 Strain Development for FBR1 (S = 67%)

# Strain vs. Cycle Ratio Strain Gage #1

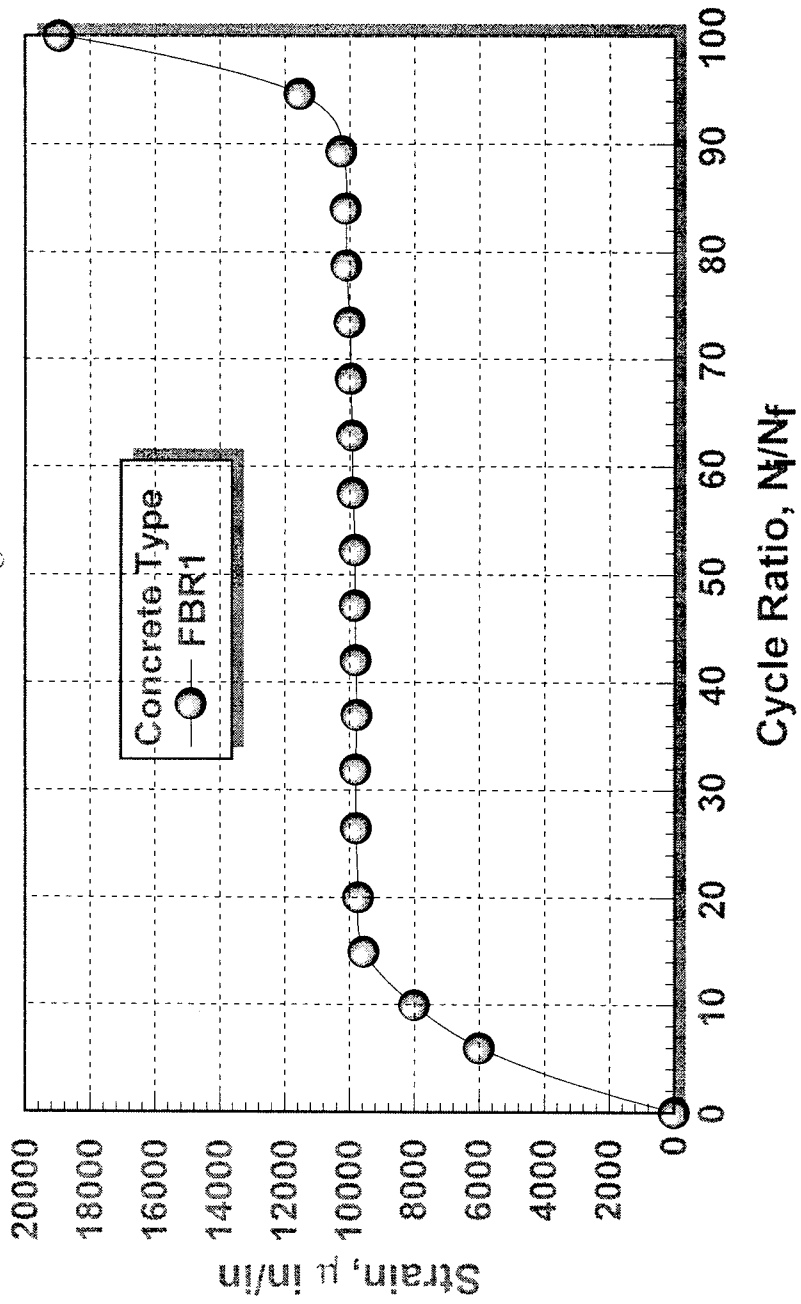


Figure 4.49 Strain Development for FBR1 (S = 71%)

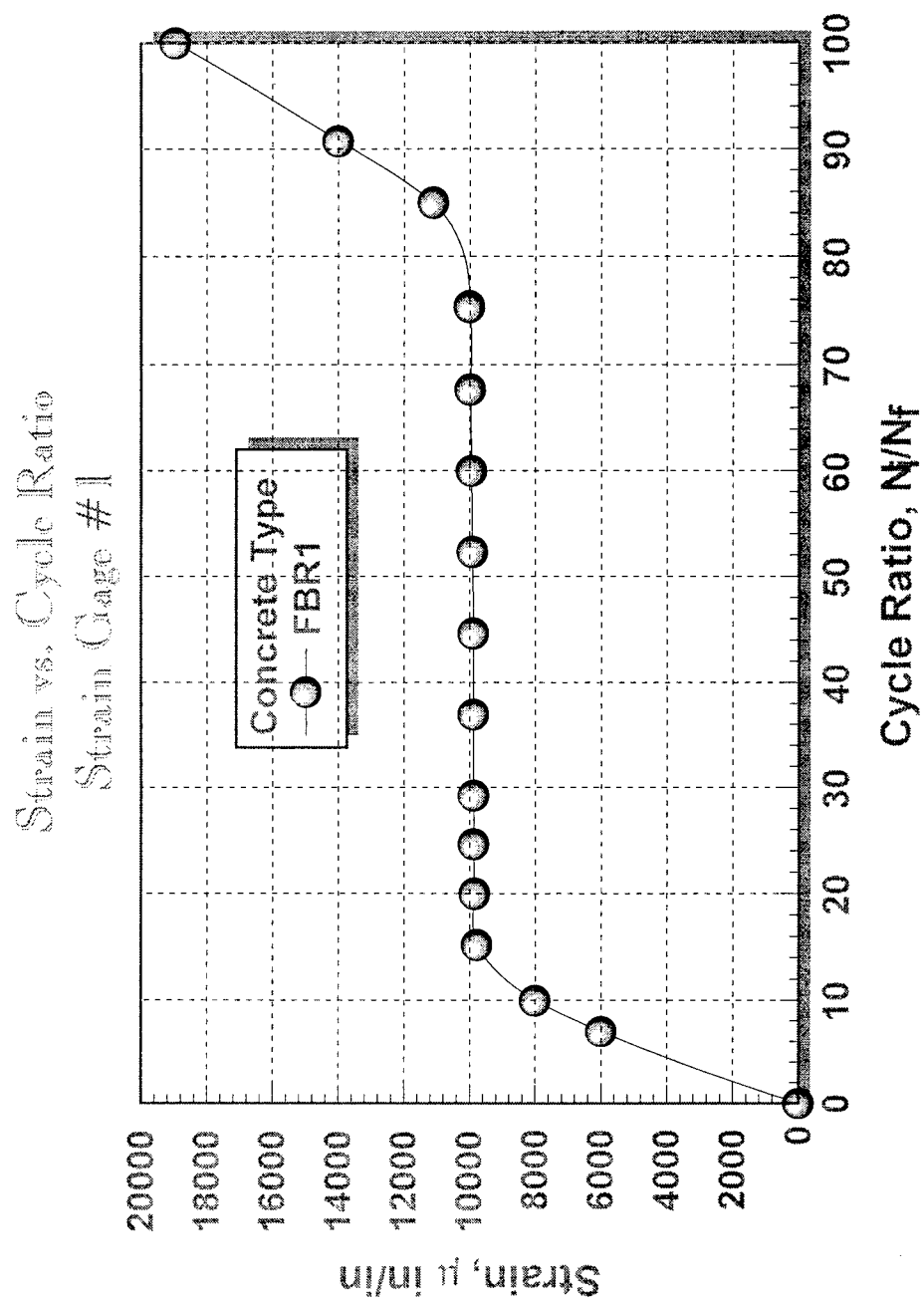


Figure 4.50 Strain Development for FBR1 (S = 74%)

# Strain vs. Cycle Ratio Strain Gage #1

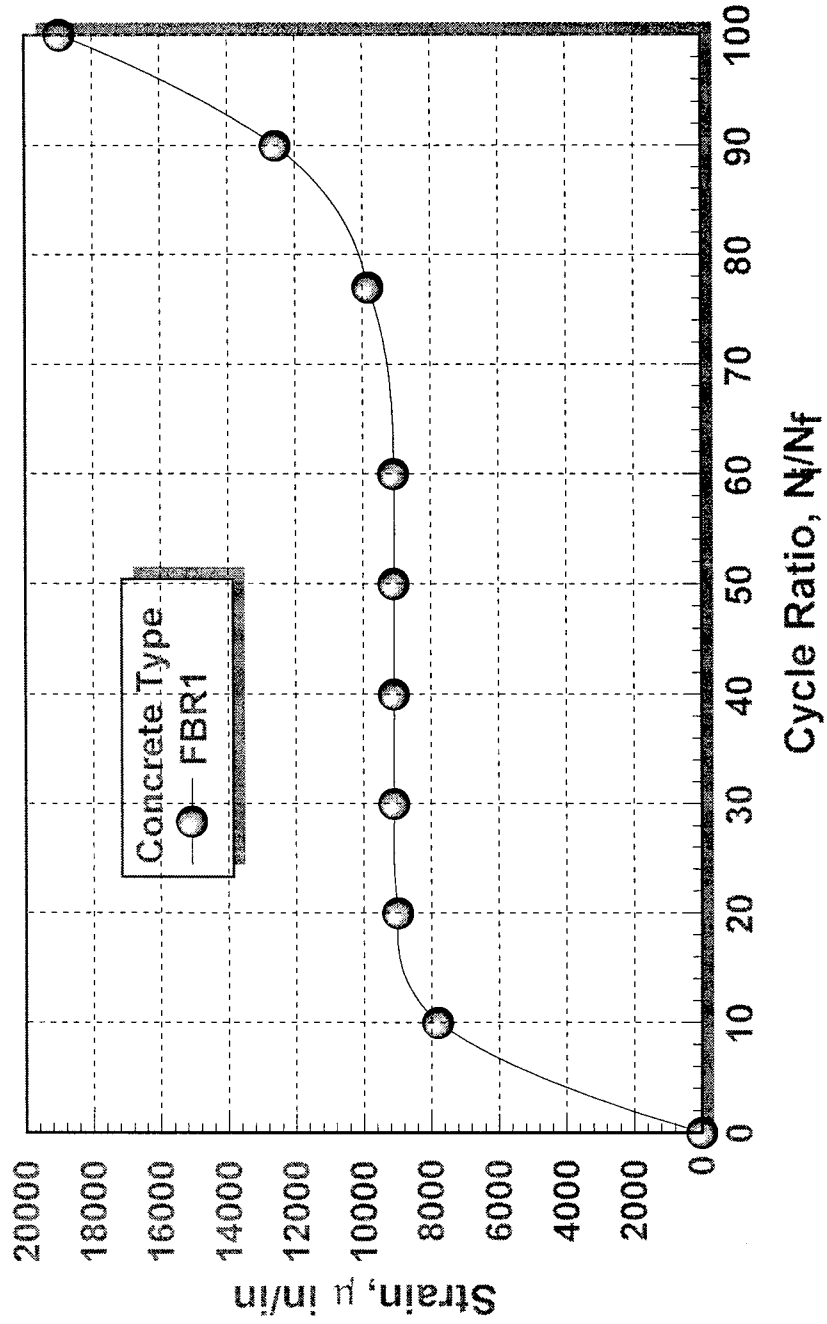


Figure 4.51 Strain Development for FBR1 (S = 84%)

# Strain Vs. Cycle Ratio Strain Gage#1

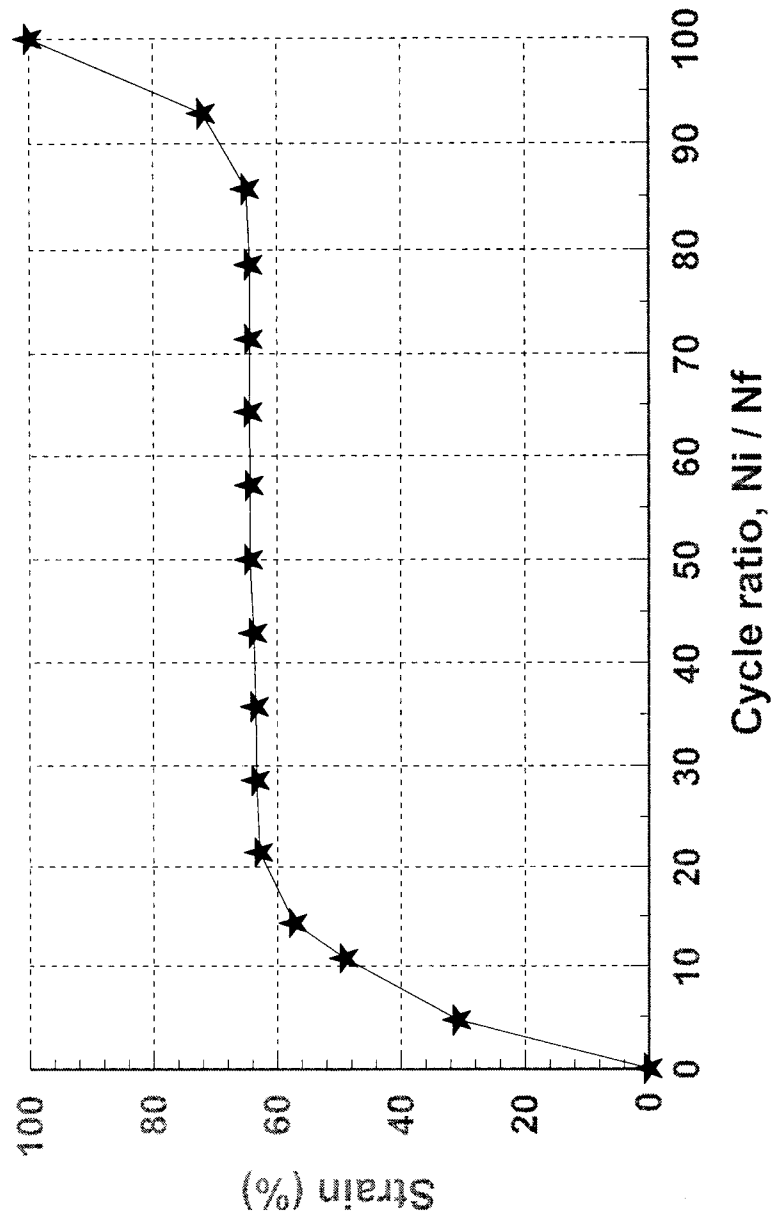


Figure 4.52 Strain Development for FBRME (S = 75%)

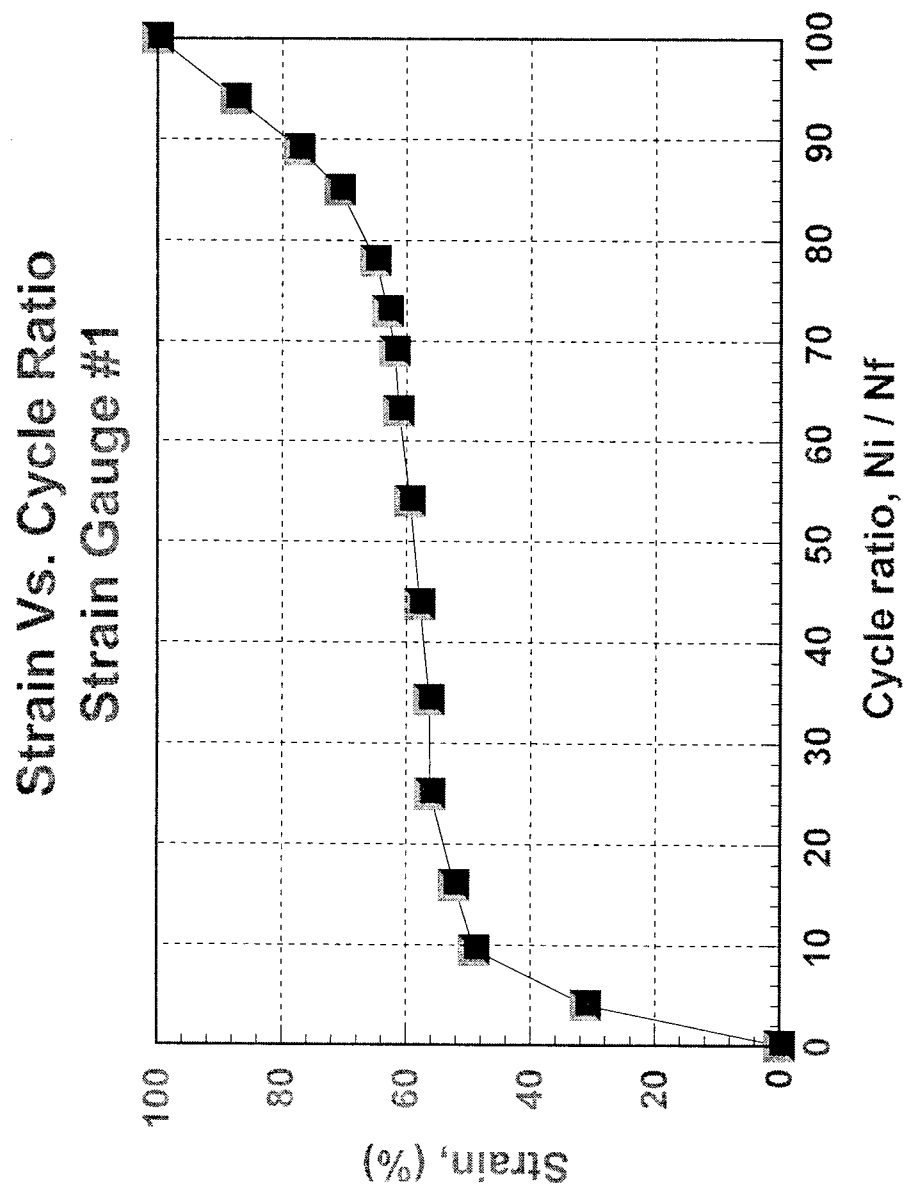


Figure 4.53 Strain Development for FBRME (S =84%)

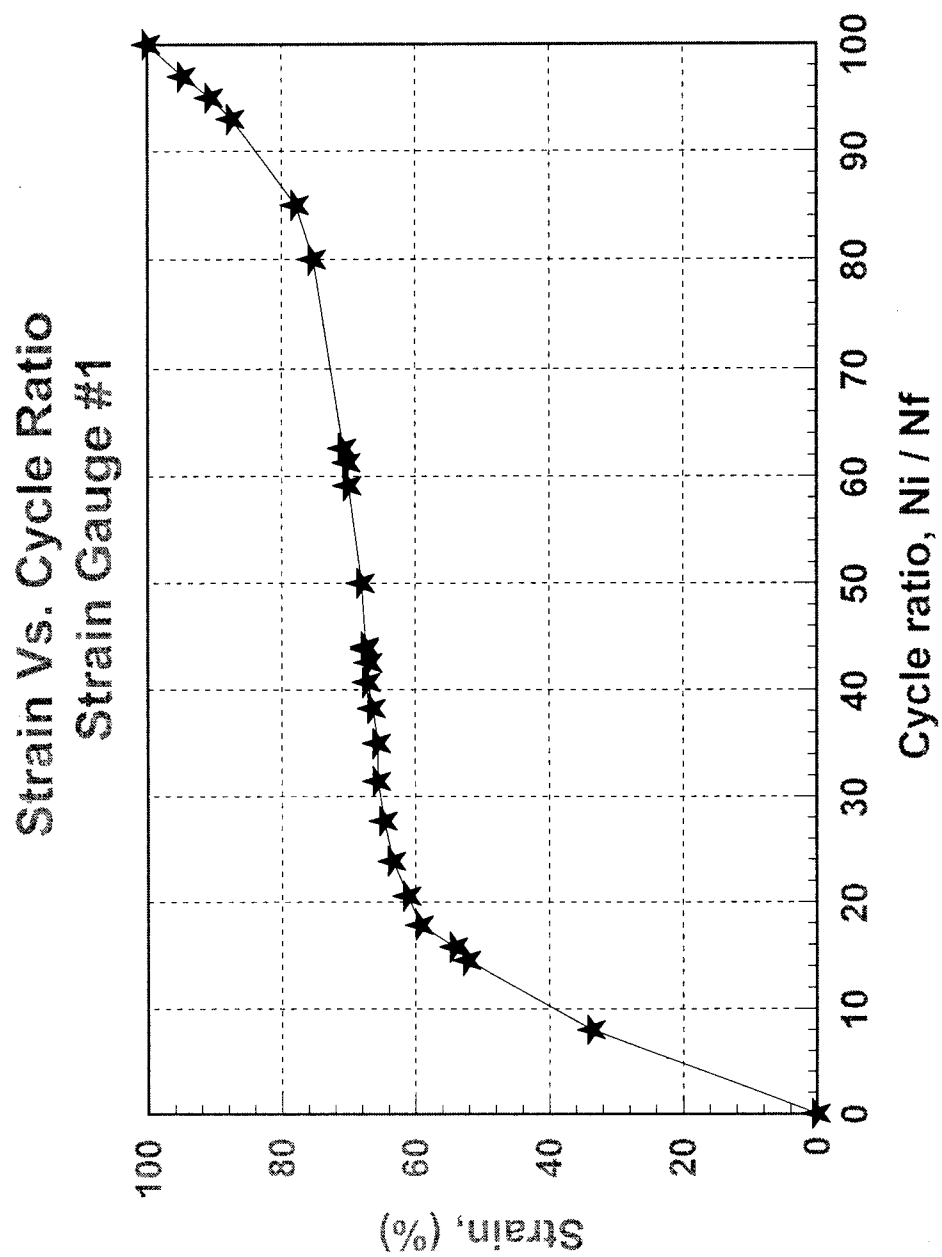


Figure 4.54 Strain Development of FBRME (S = 93%)

# Chord Modulus vs. Cycle Ratio Strain Gage #1

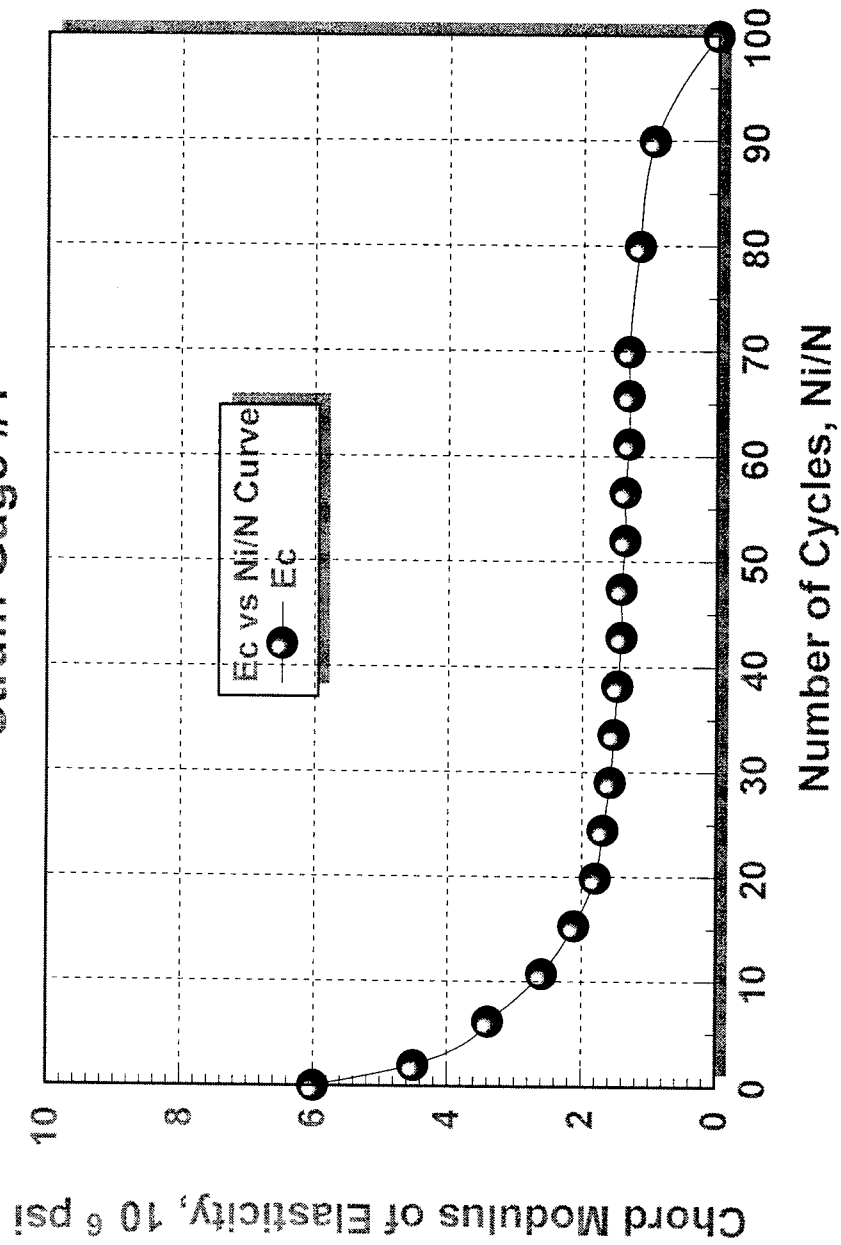


Figure 4.55 Stiffness Degradation for FBR1 ( $S = 67\%$ )



# Chord Modulus vs. Cycle Ratio Strain Gage #1

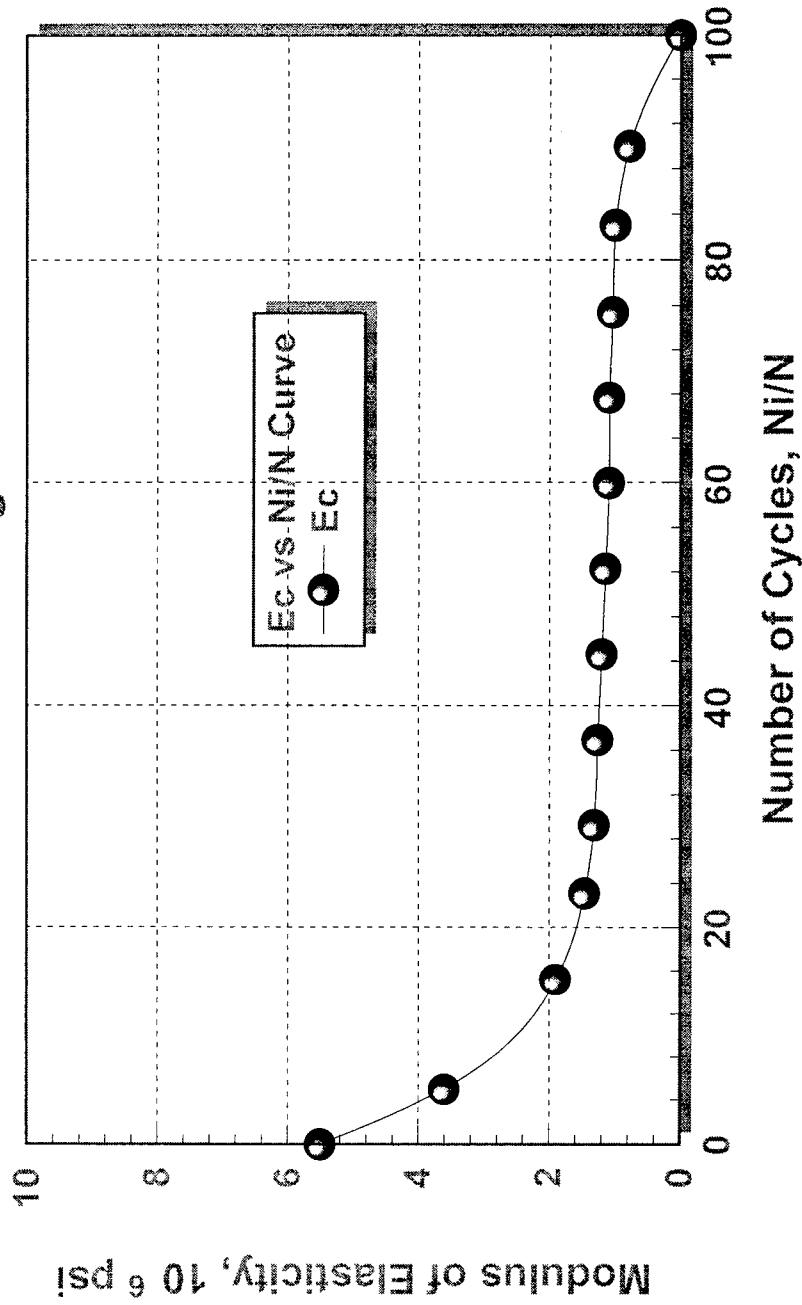


Figure 4.56 Stiffness Degradation for FBR1 (S = 71%)

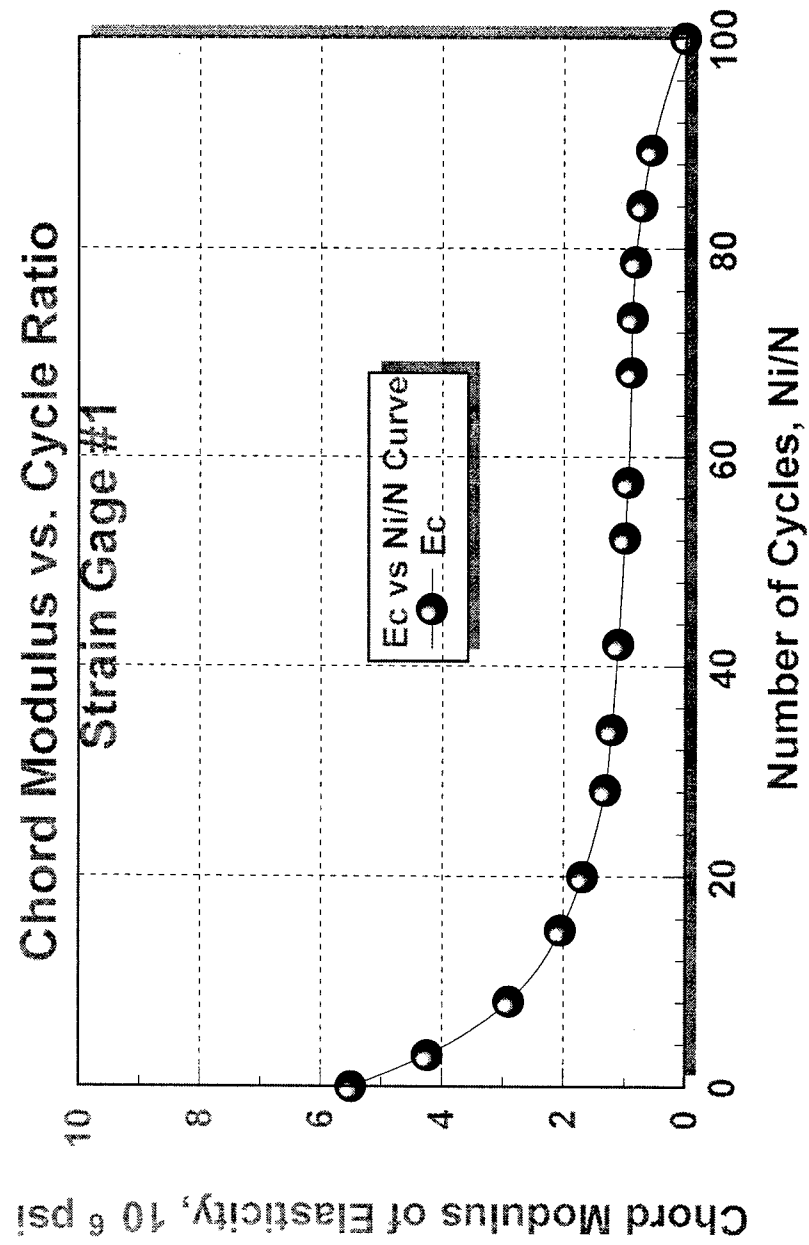


Figure 4.57 Stiffness Degradation for FBR1 ( $S = 74\%$ )

# Chord Modulus vs. Cycle Ratio Strain Gage #1

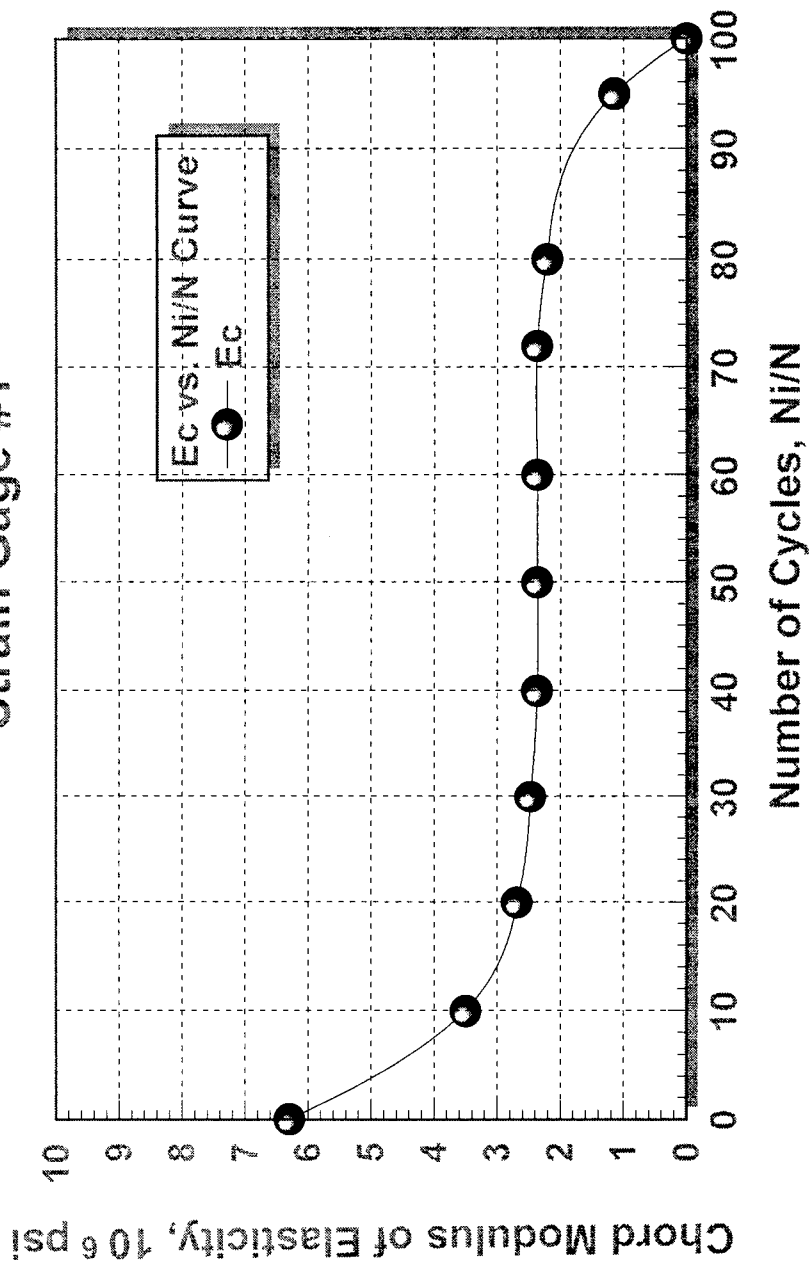


Figure 4.58 Stiffness Degradation for FBR1 (S = 84%)

# Chord Modulus vs. Cycle Ratio Strain Gage #1

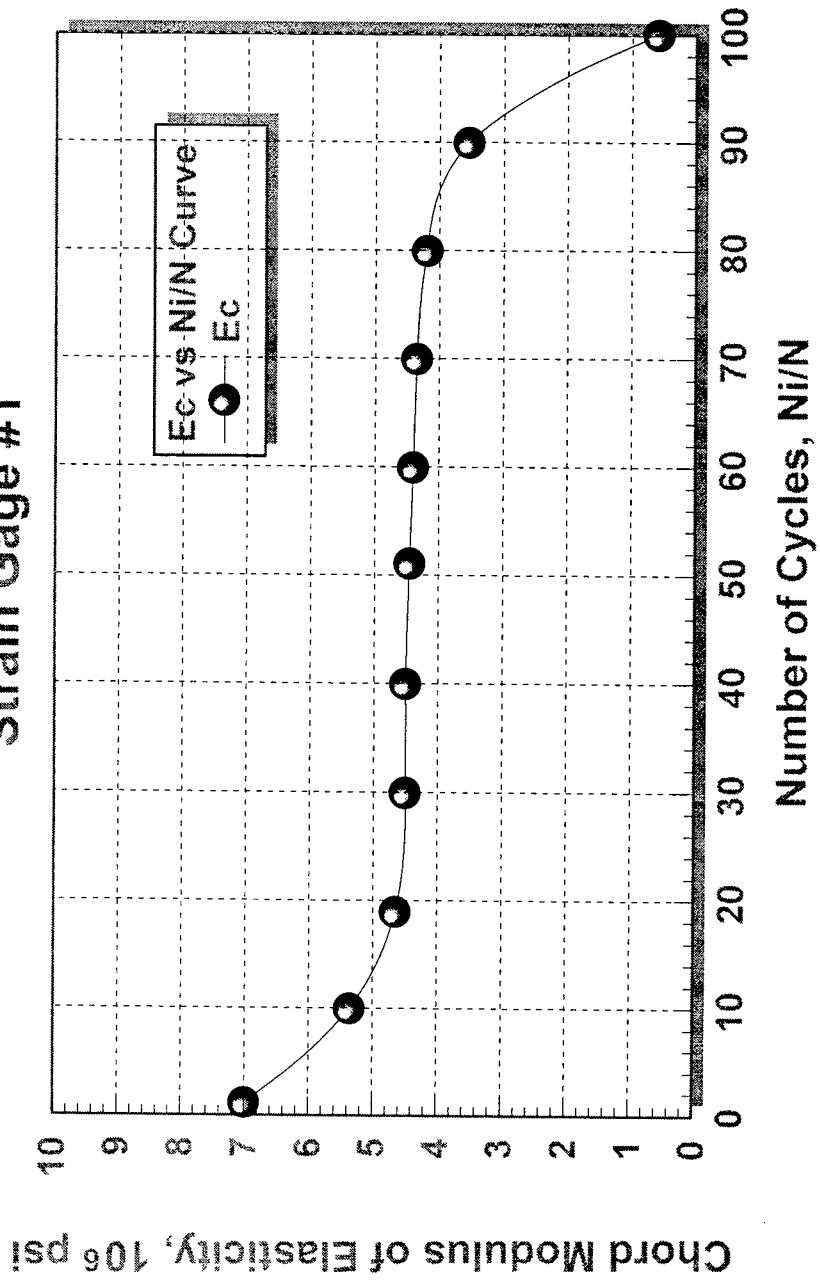


Figure 4.59 Stiffness Degradation for FBR3M (S = 60%)

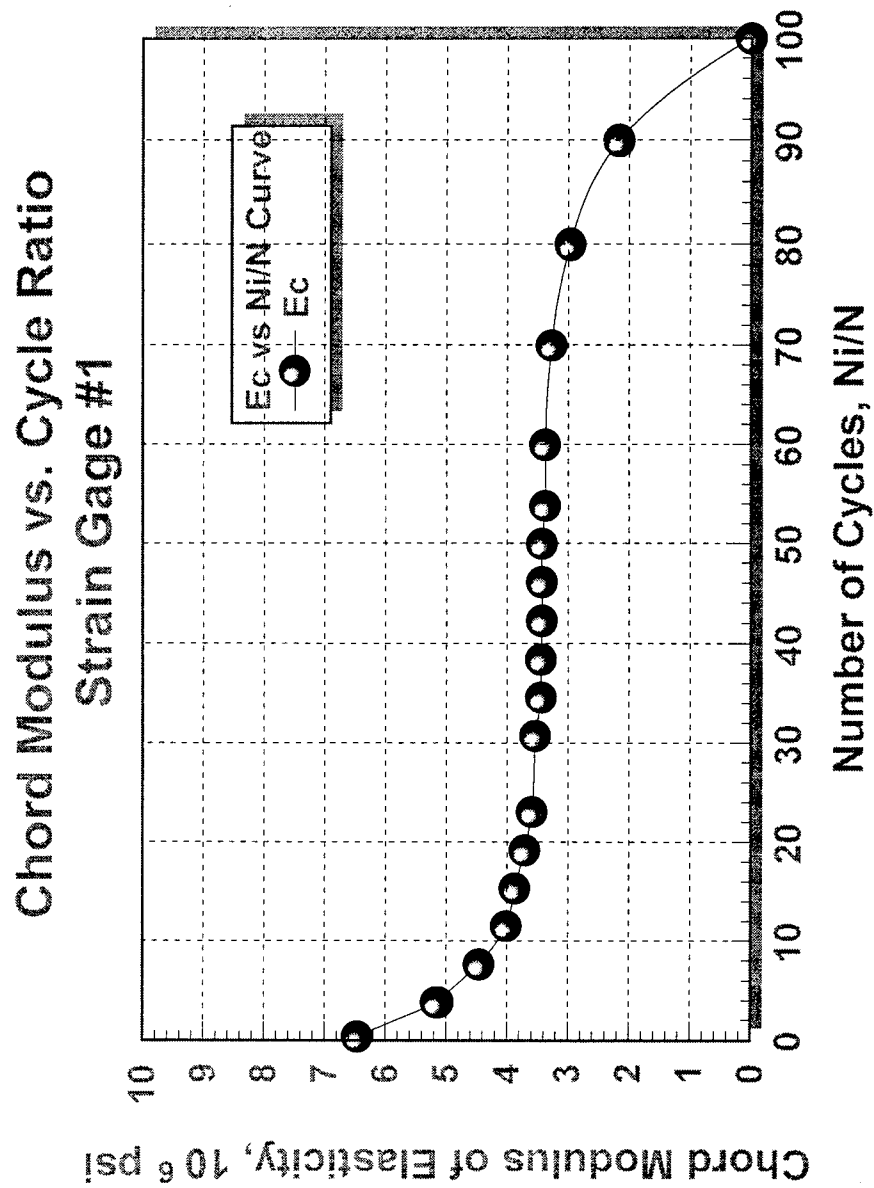


Figure 4.60 Stiffness Degradation for FBR3M ( $S = 73\%$ )

# Chord Modulus vs. Cycle Ratio Strain Gage #1

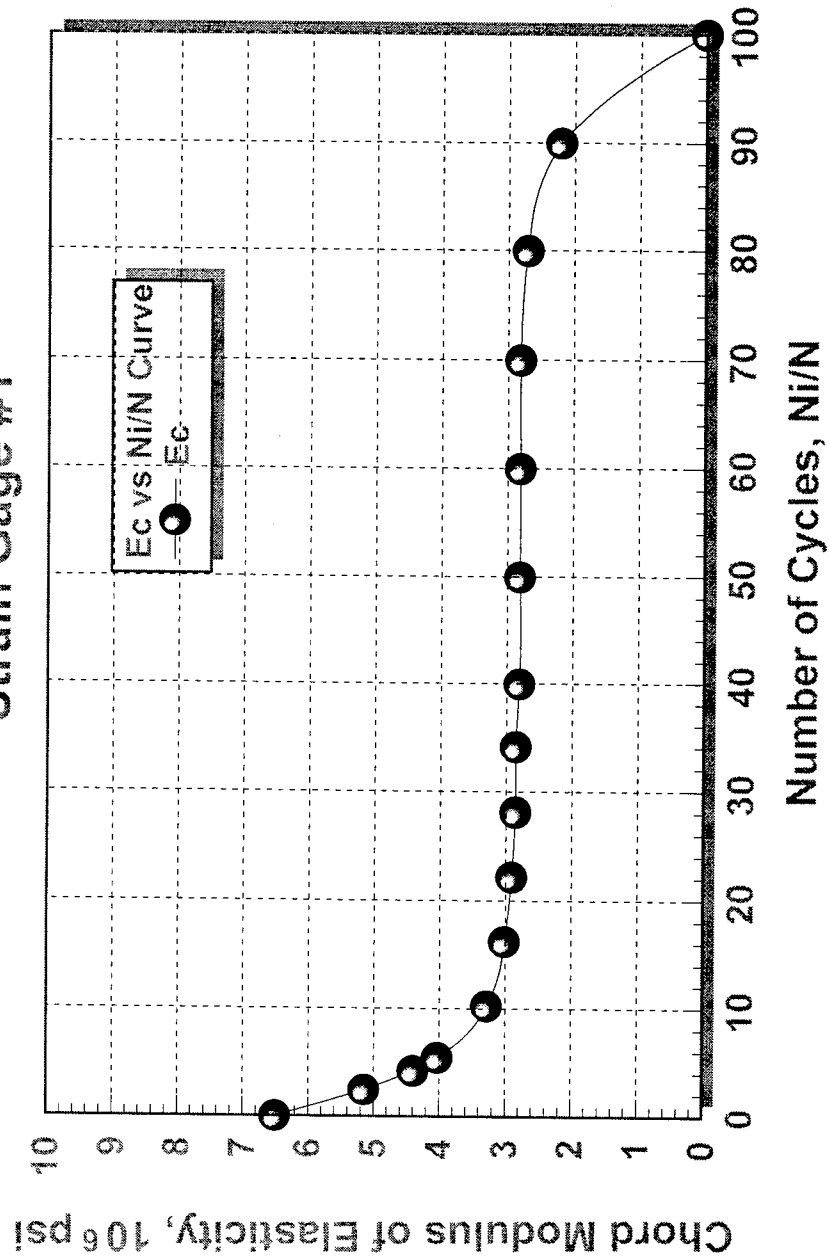


Figure 4.61 Stiffness Degradation for FBR3M (S = 82%)

# Chord Modulus Vrs. Cycle Ratio Strain Gauge #1

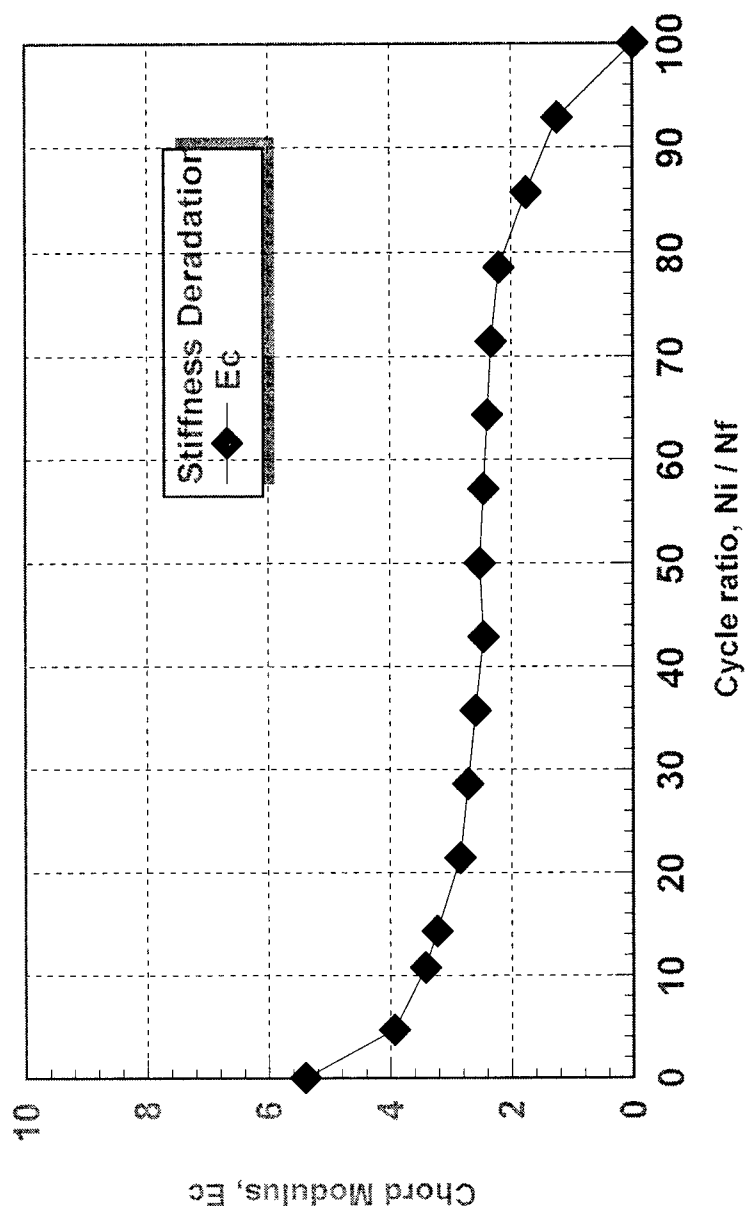
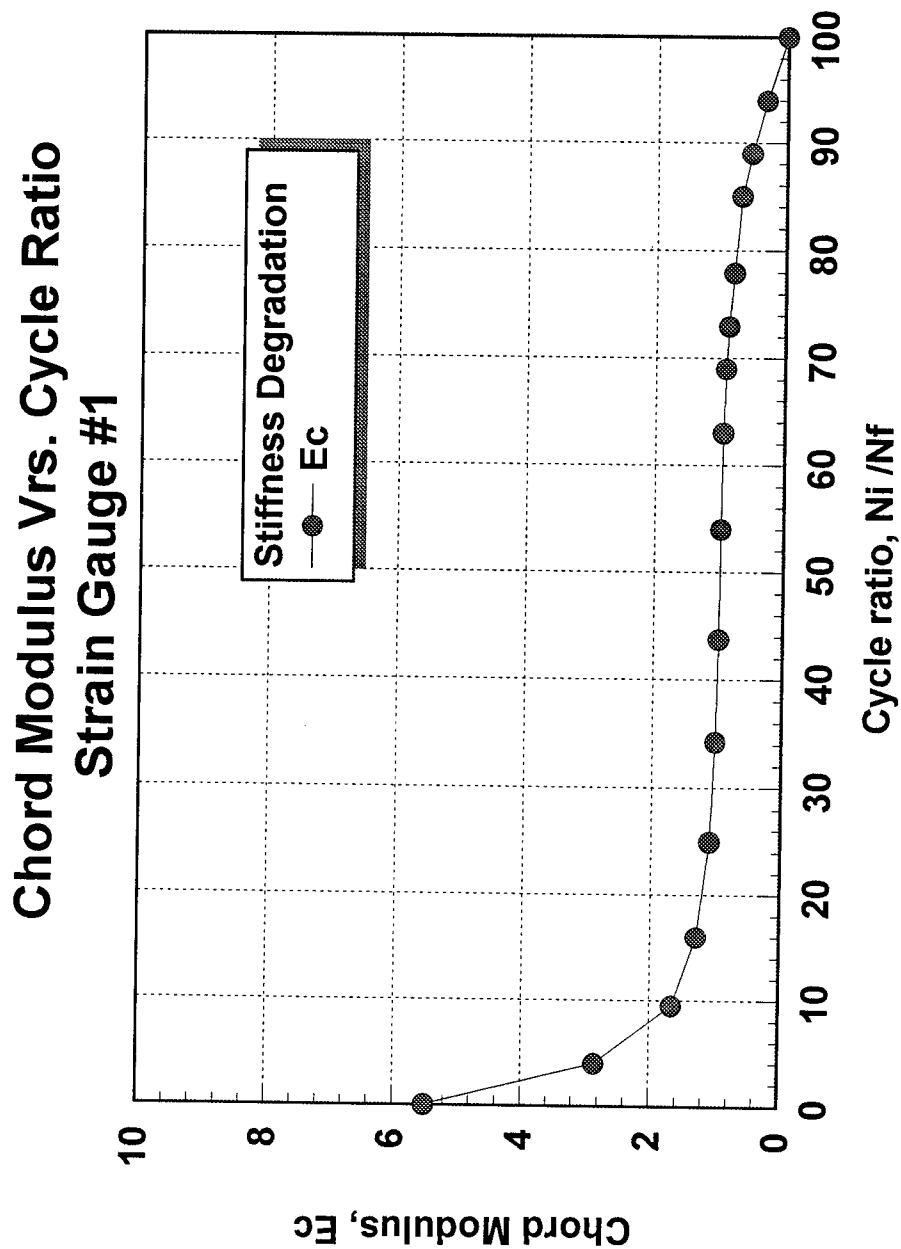
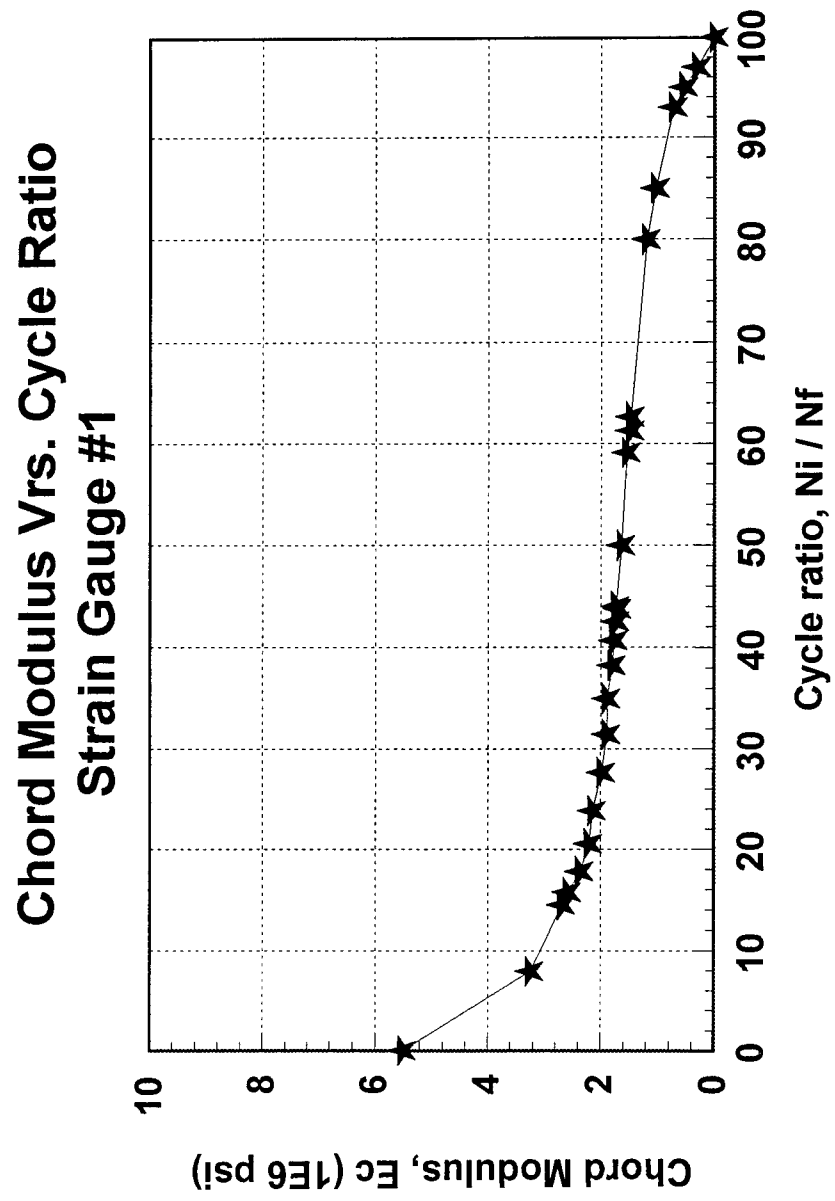


Figure 4.62 Stiffness Degradation for FBRME (S = 75%)



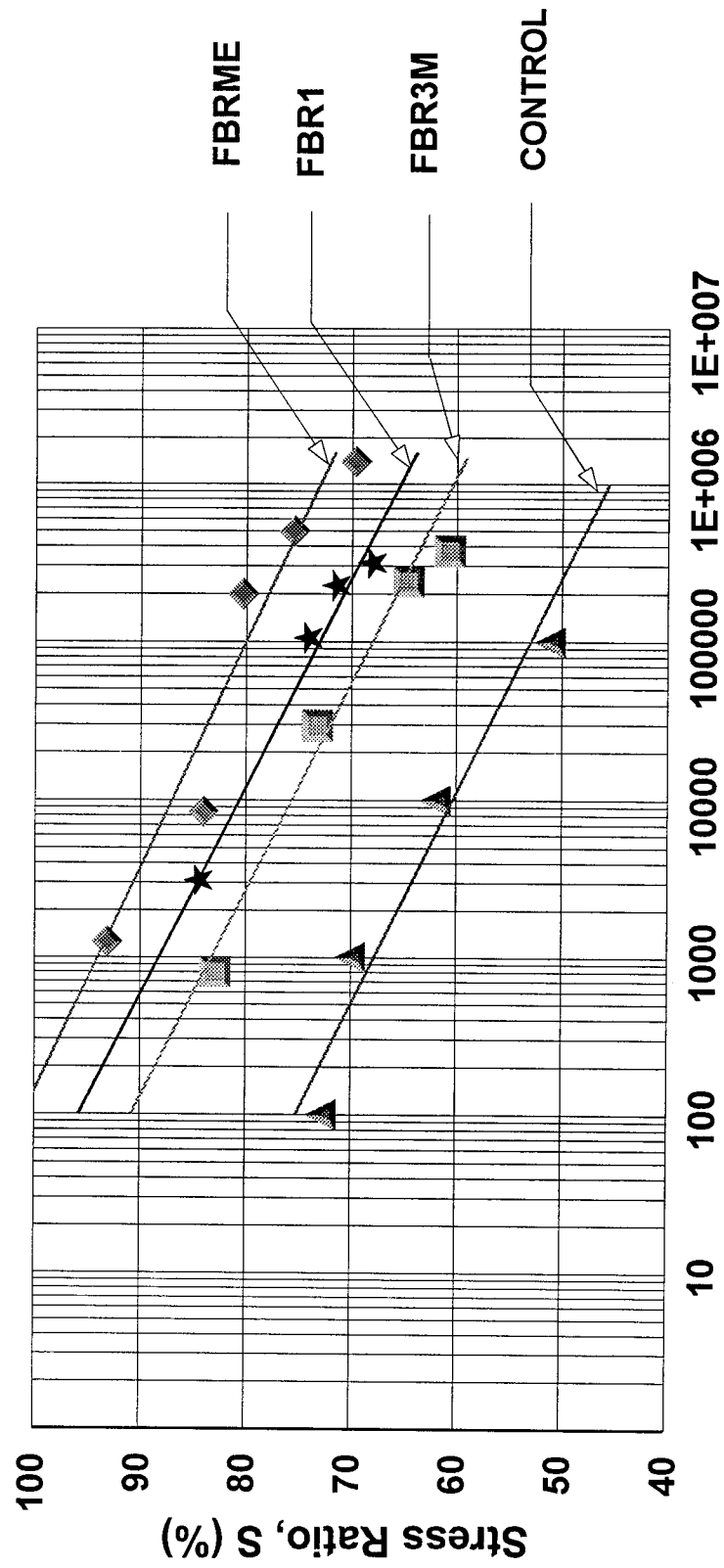
**Figure 4.63 Stiffness Degradation of FBRME (S = 84%)**



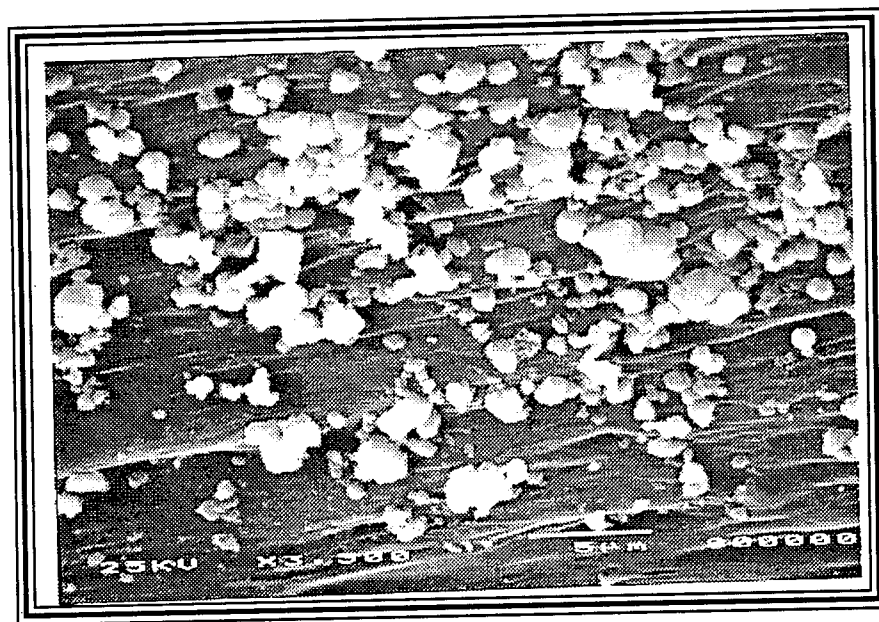


**Figure 4.64 Stiffness Degradation for FBRME (S = 93%)**

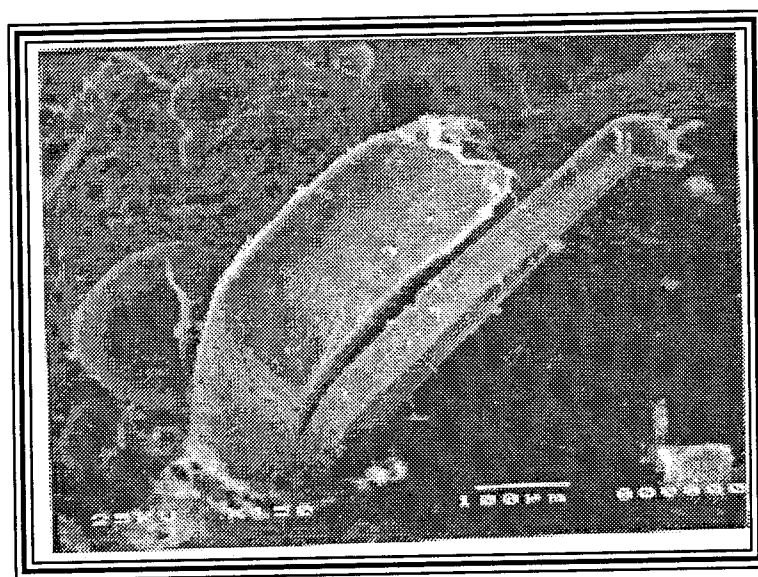
## S - N Diagrams



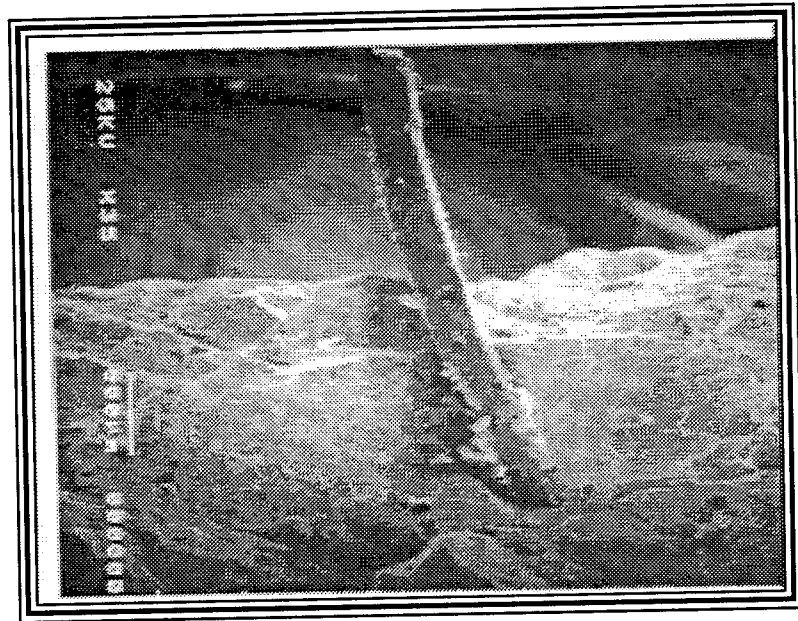
Number of Cycles, N  
Figure 4.65 Wholer Diagrams



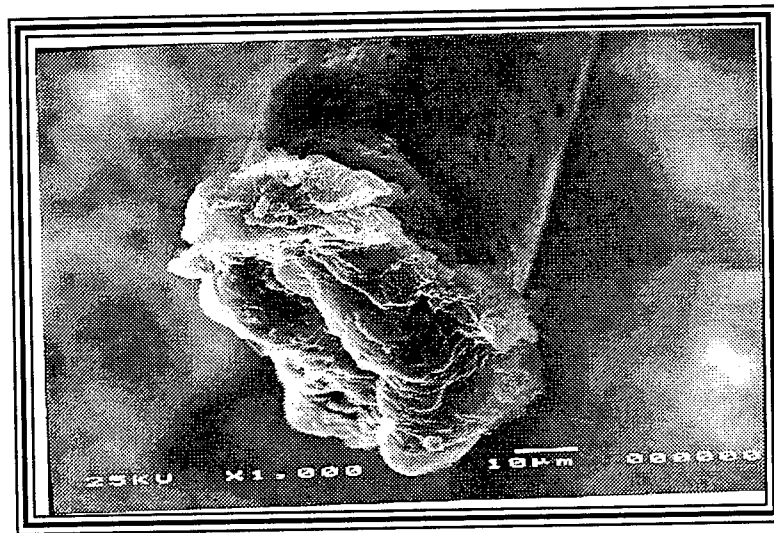
**Figure 4.66 Calcium Formation on Fibrillated Fibers' Surface**



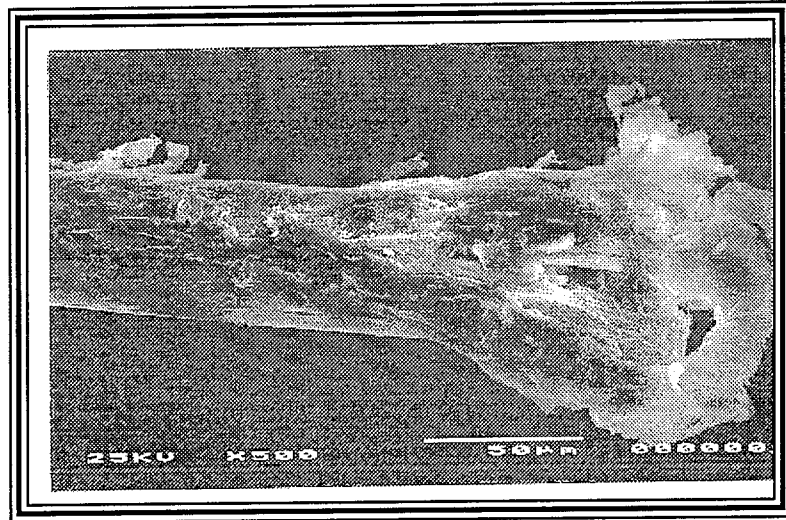
**Figure 4.67 Fibrillated Fiber After Failure**



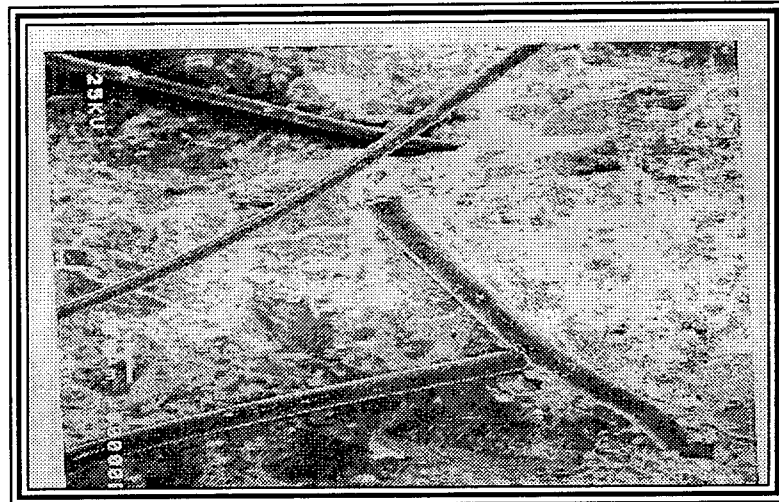
**Figure 4.68 Monofilament Fiber Bonded to Concrete**



**Figure 4.69 Monofilament Fiber Failed in Tension**



**Figure 4.70 Monofilament Fiber After Failure**



**Figure 4. 71 Random Orientation of Fibers**

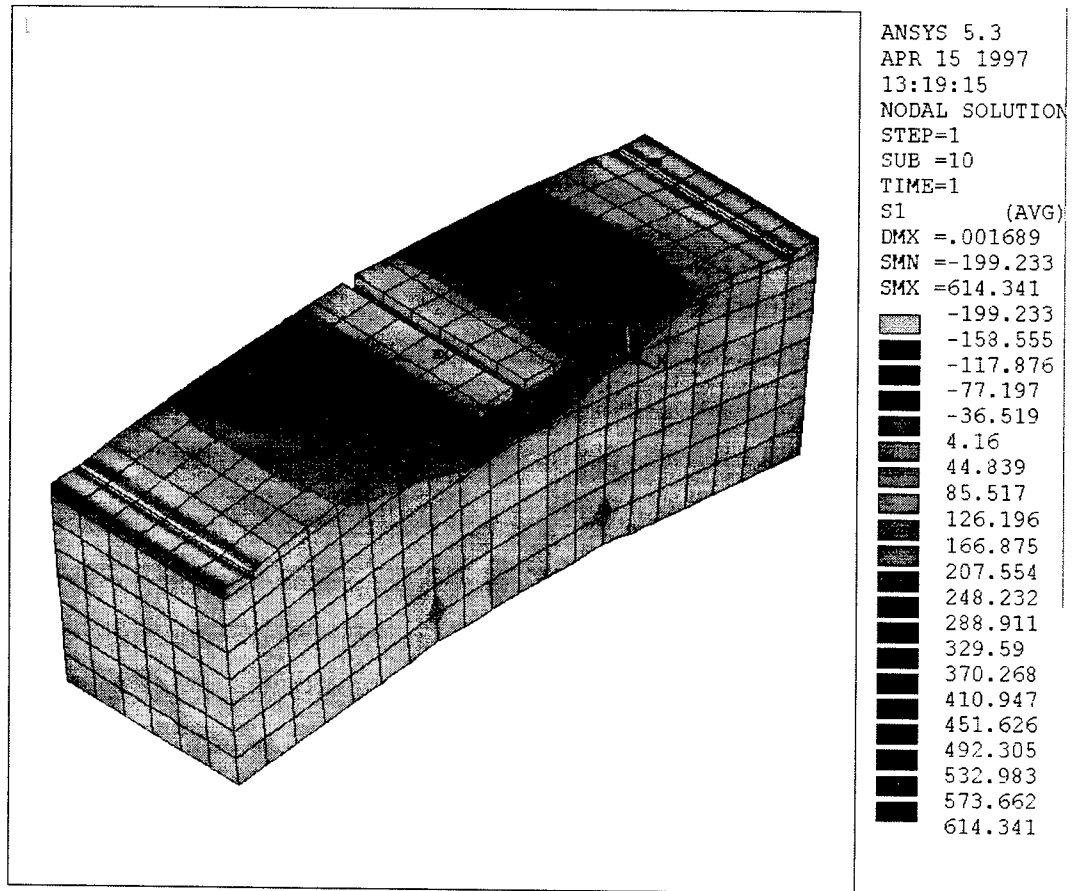


Figure 4.72 Major Principal Stresses ( $\sigma_1$ ) in a Plain Concrete Notched Beam

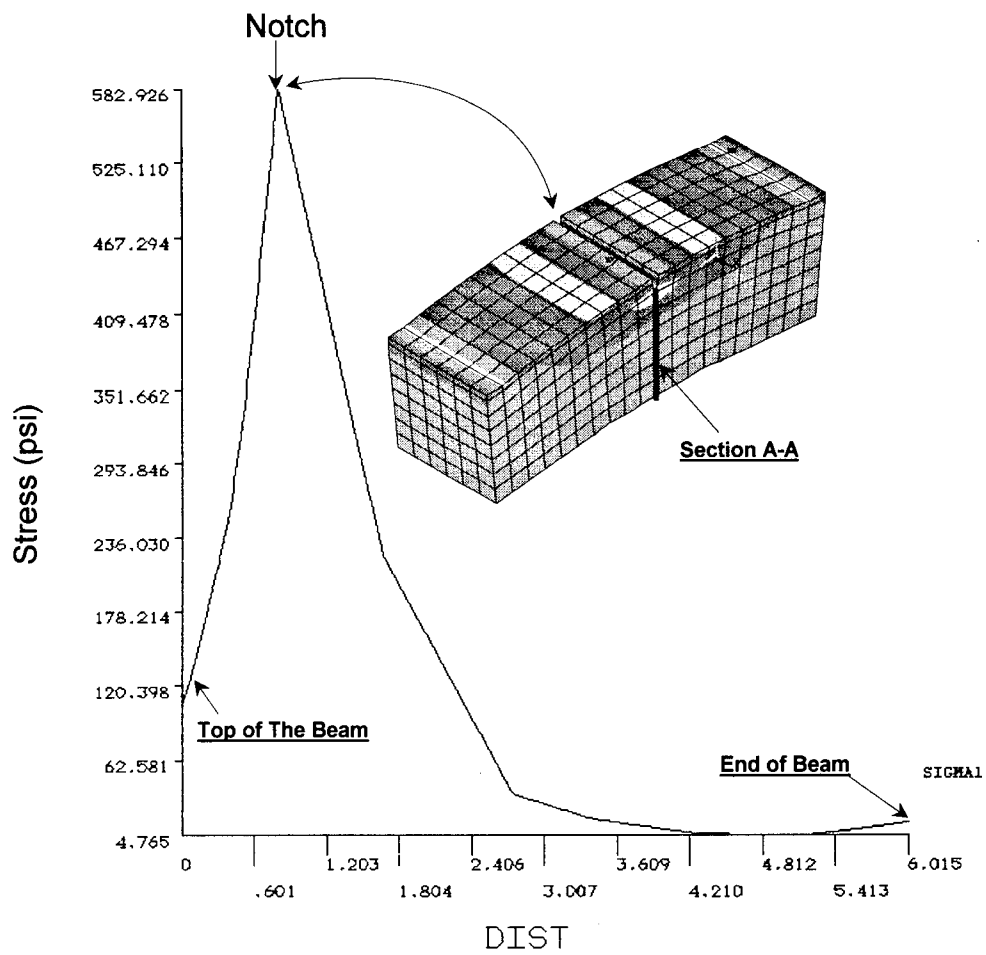


Figure 4.73 Major Principal Stress ( $\sigma_1$ ) Along The Notch Section A-A.

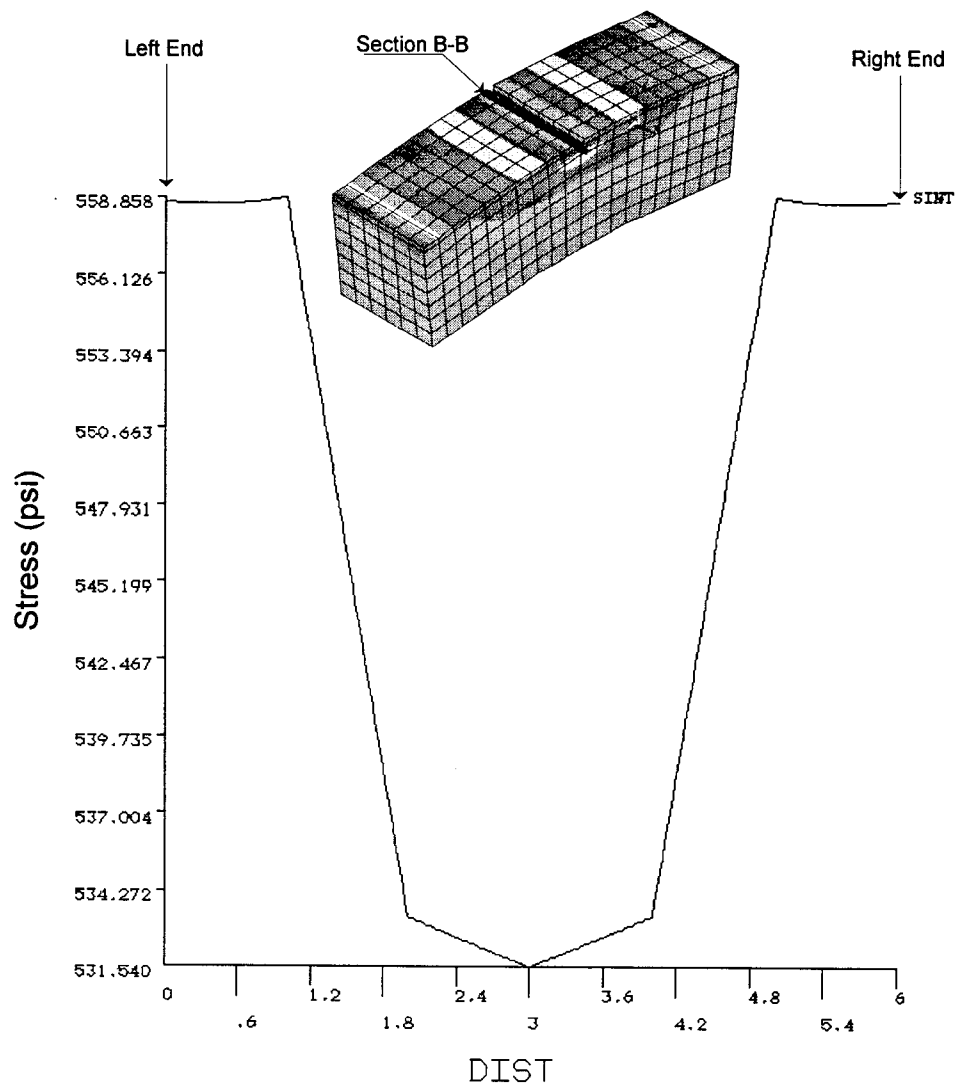


Figure 4.74 Stress Distribution Across The Notch Section B-B



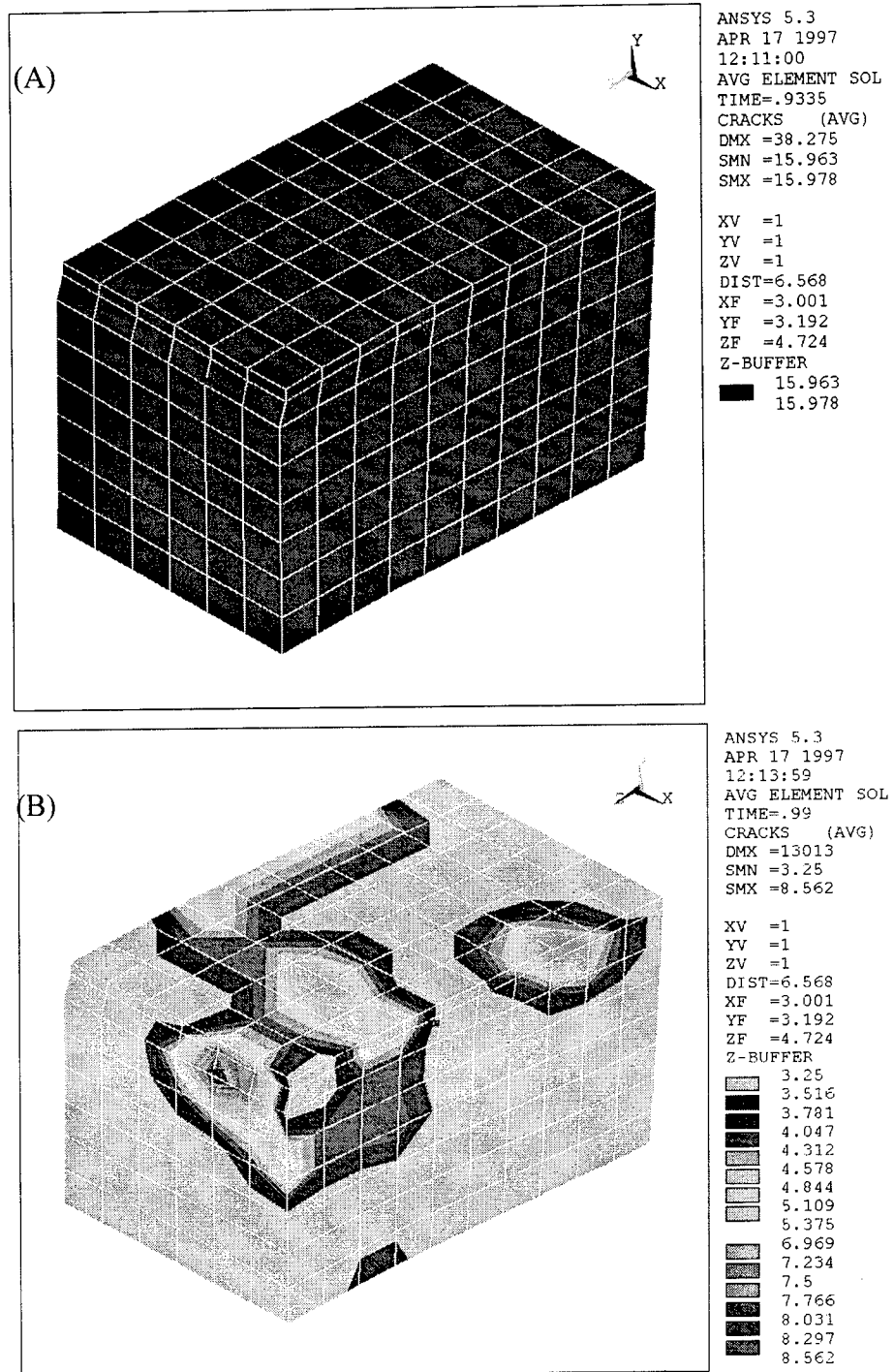


Figure 4.75 Crack Distribution in a FRC Beam at 45 deg. Fiber Orientation  
(a) At load 5227.6 lb, (B) At Load 5544.0 lb.

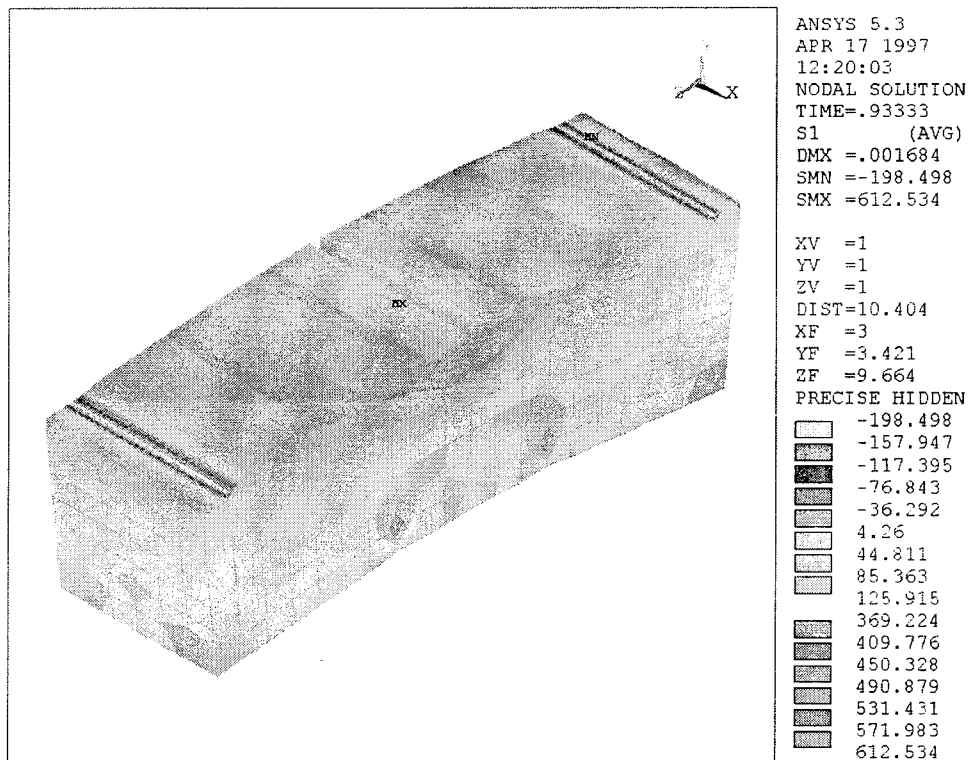


Figure 4.76 Stress Distribution in a FRC Beam at 45 deg. Fiber Orientation  
 At load 5227.6 lb

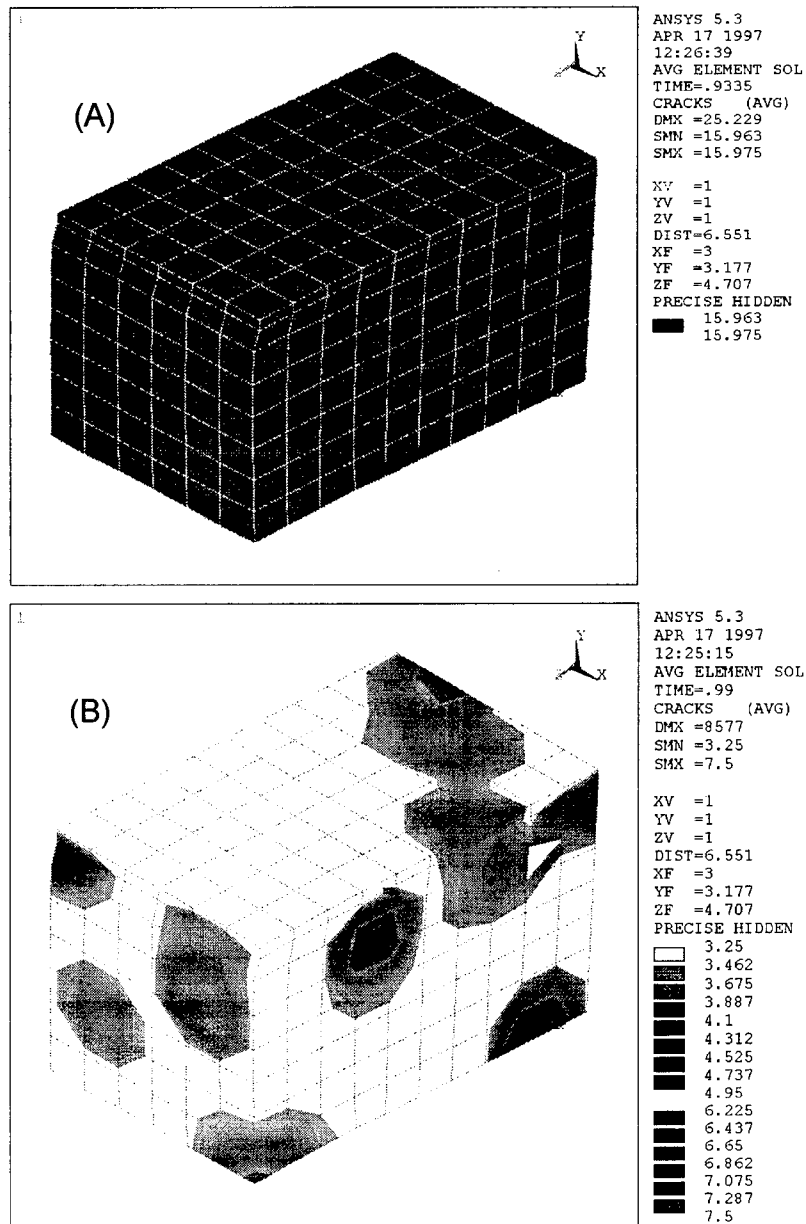


Figure 4.77 Crack Distribution in a FRC Beam at 90 deg. Fiber Orientation  
(a) At load 5227.6 lb, (B) At Load 5544.0 lb.

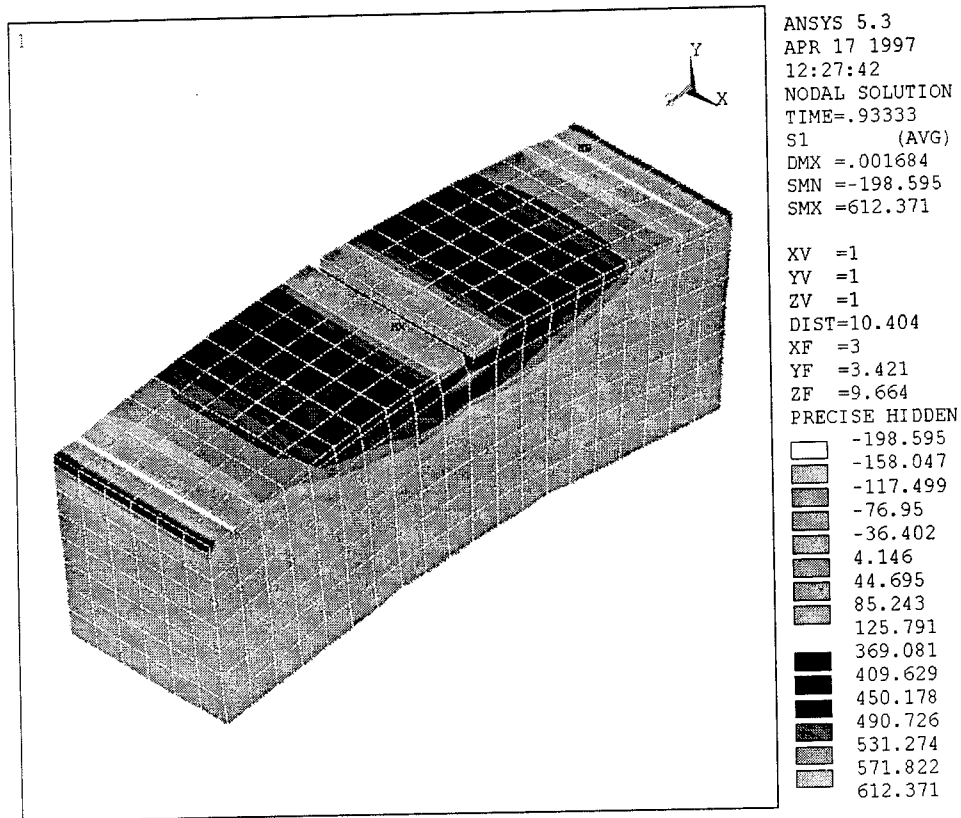


Figure 4.78 Stress Distribution in a FRC Beam at 90 deg. Fiber Orientation  
 At load 5227.6 lb

# Stress vs. Deflection of Fiber Reinforced Concrete Beam with Fiber Orientation = 0 °

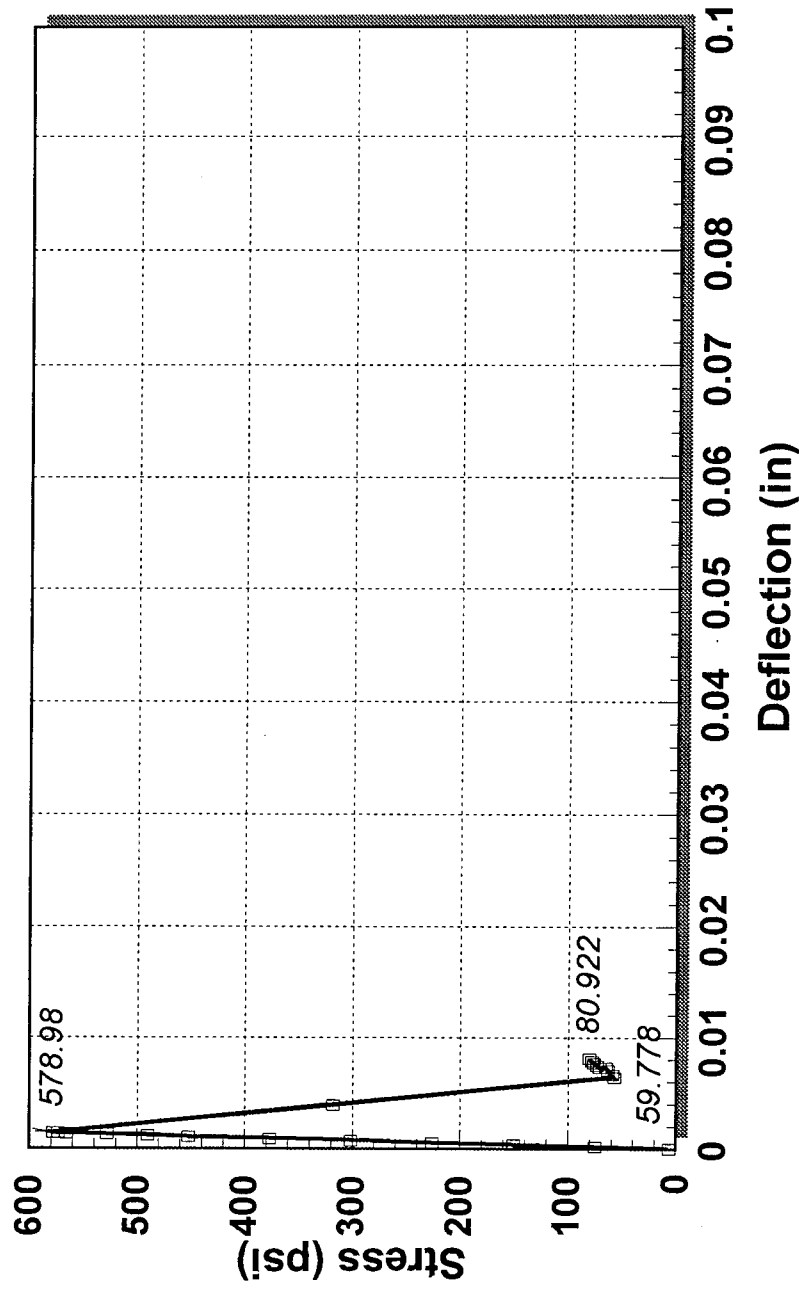


Figure 4.79 Stress-Deflection Results from FEM Model

# Stress vs. Deflection of Fiber Reinforced Concrete Beam with Fiber Orientation = 0°

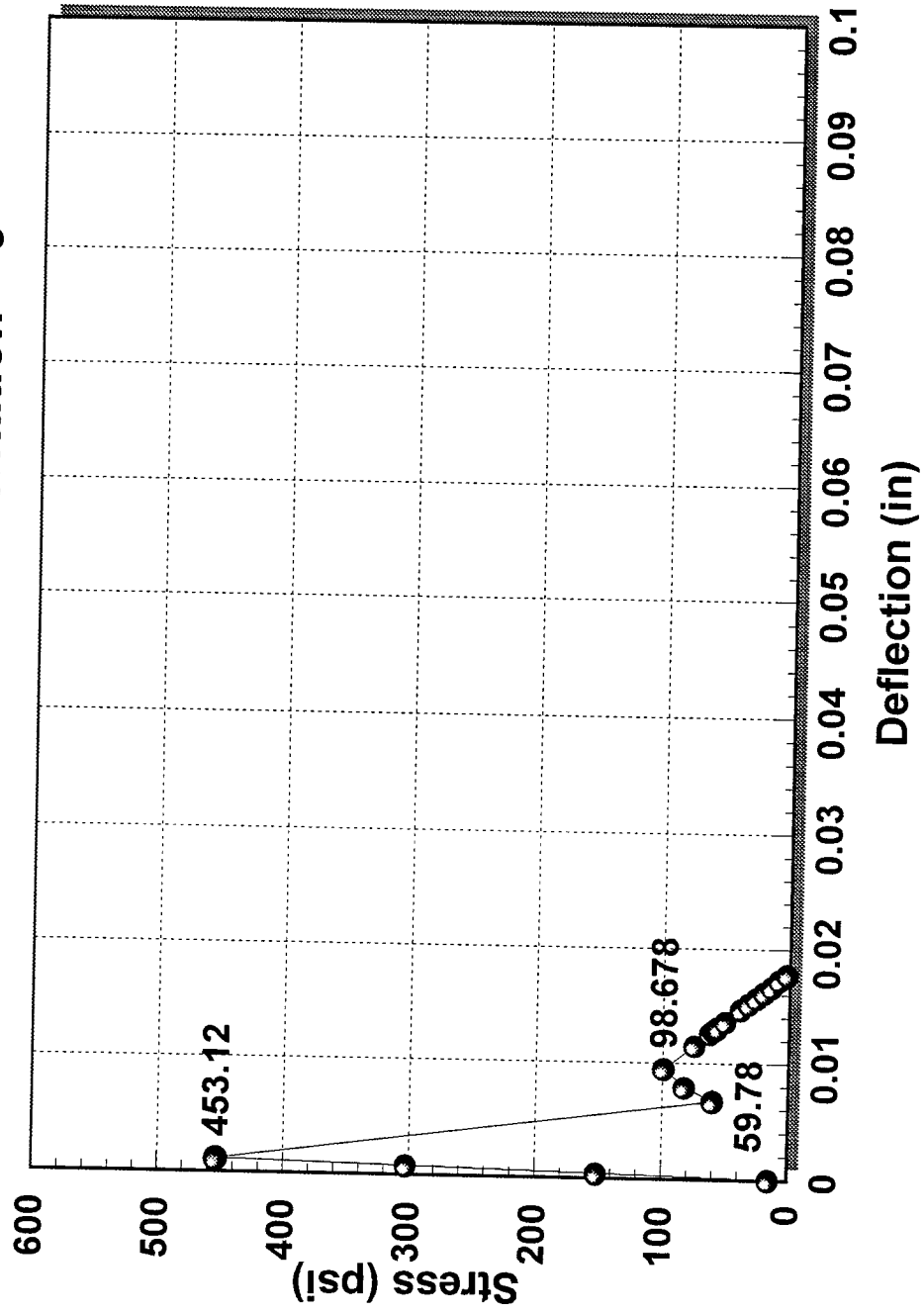


Figure 4.80 Stress-Deflection Results from FEM Model

# Stress-Deflection for Fiber Reinforced Concrete Beam with Fiber Orientation = 45°

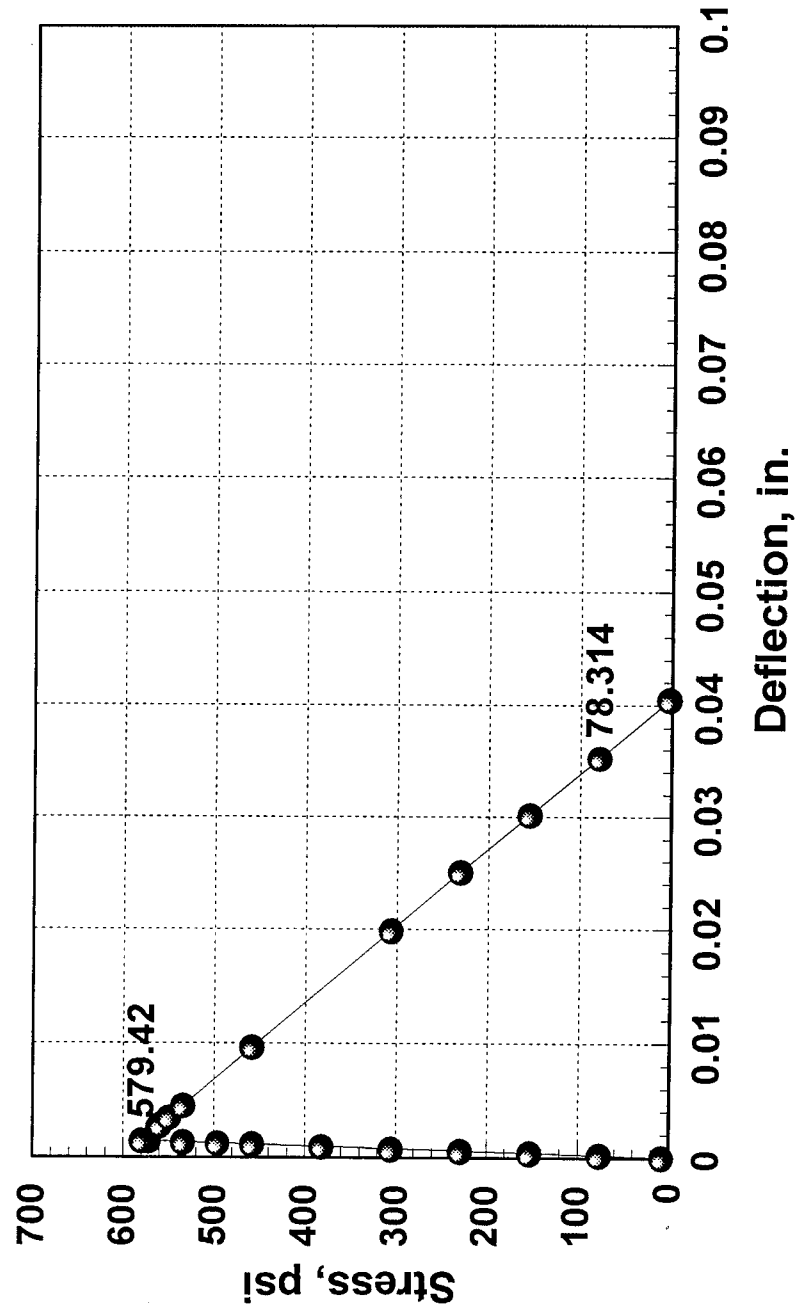


Figure 4. 81 Stress-Deflection Results from FEM Model

# Stress vs. Deflection of Fiber Reinforced Concrete Beam with Fiber Orientation = 90 °

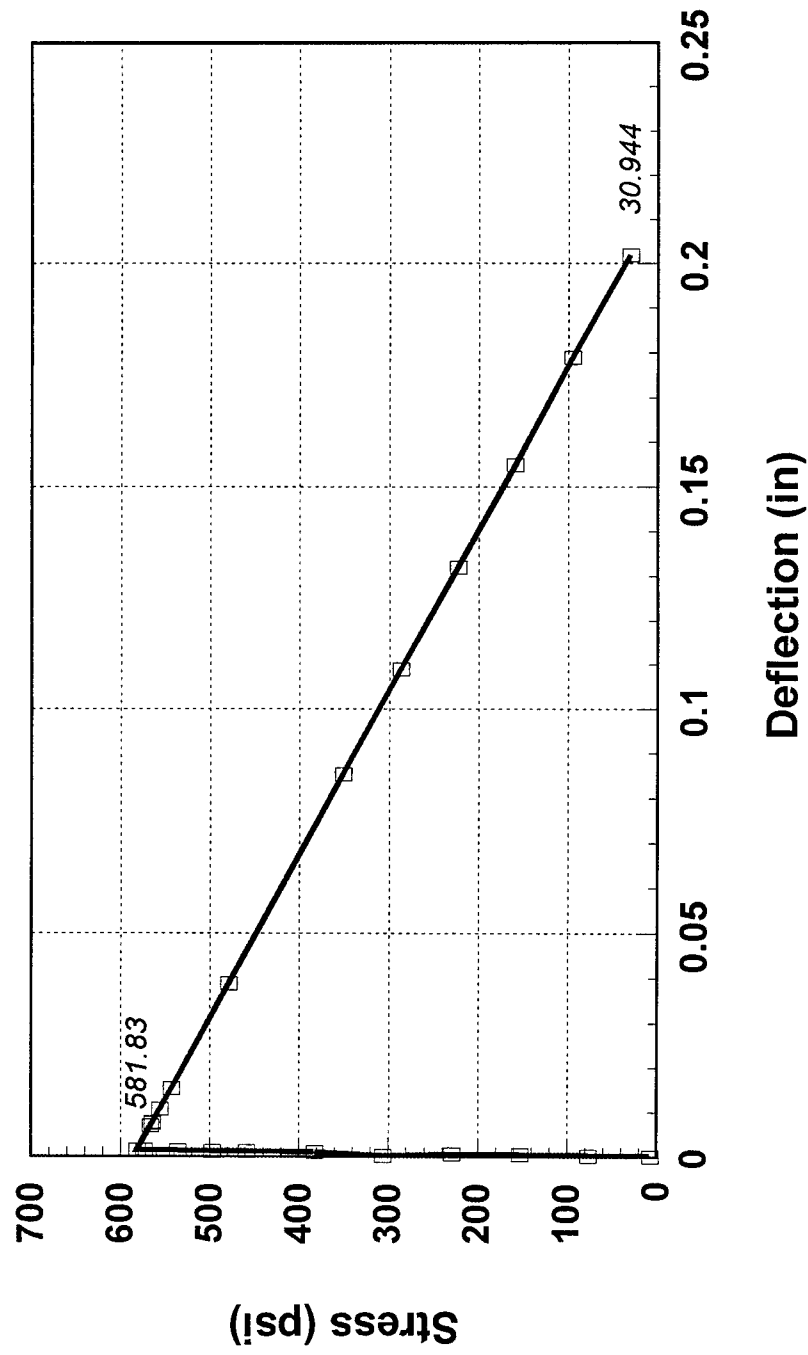


Figure 4. 82 Stress-Deflection Results from FEM Model



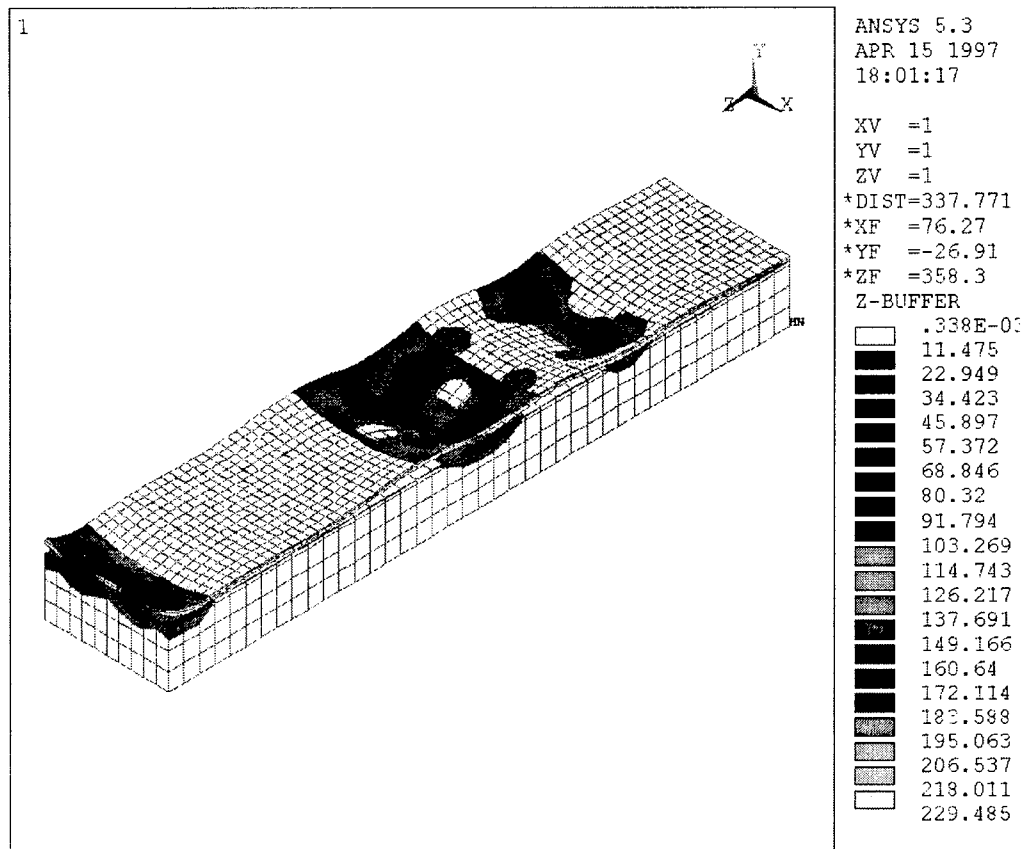


Figure 4.83 Stress Distribution in the Concrete Pavement Overlay

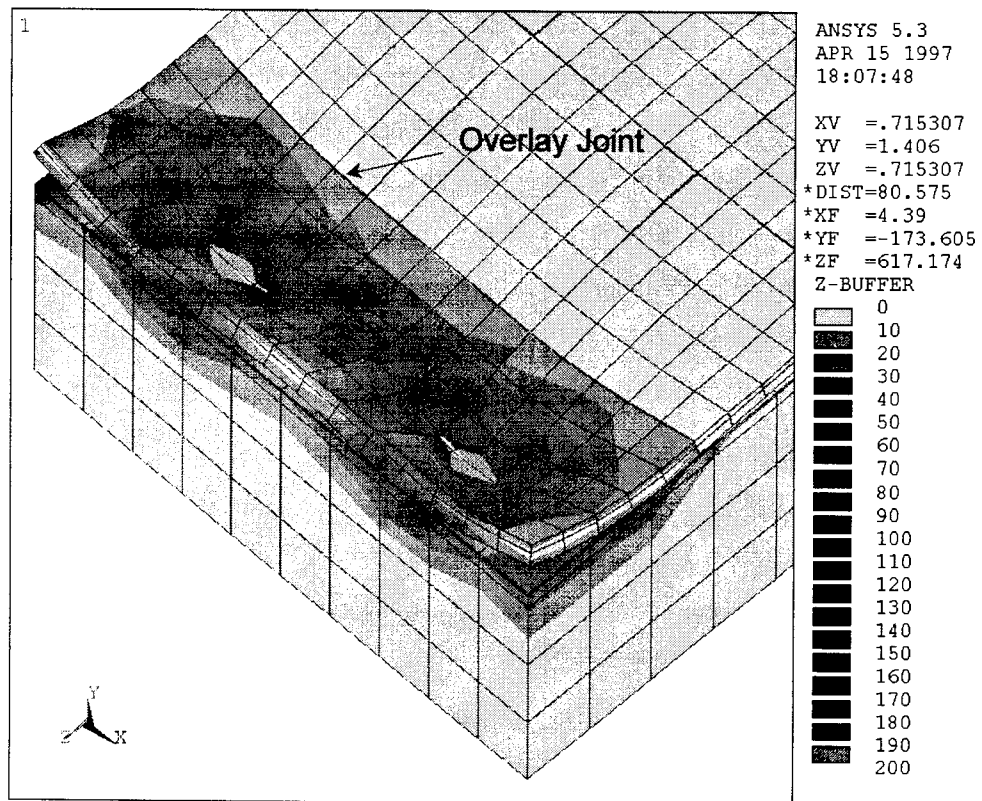


Figure 4.84 Stress Distribution At the Overlay Edge

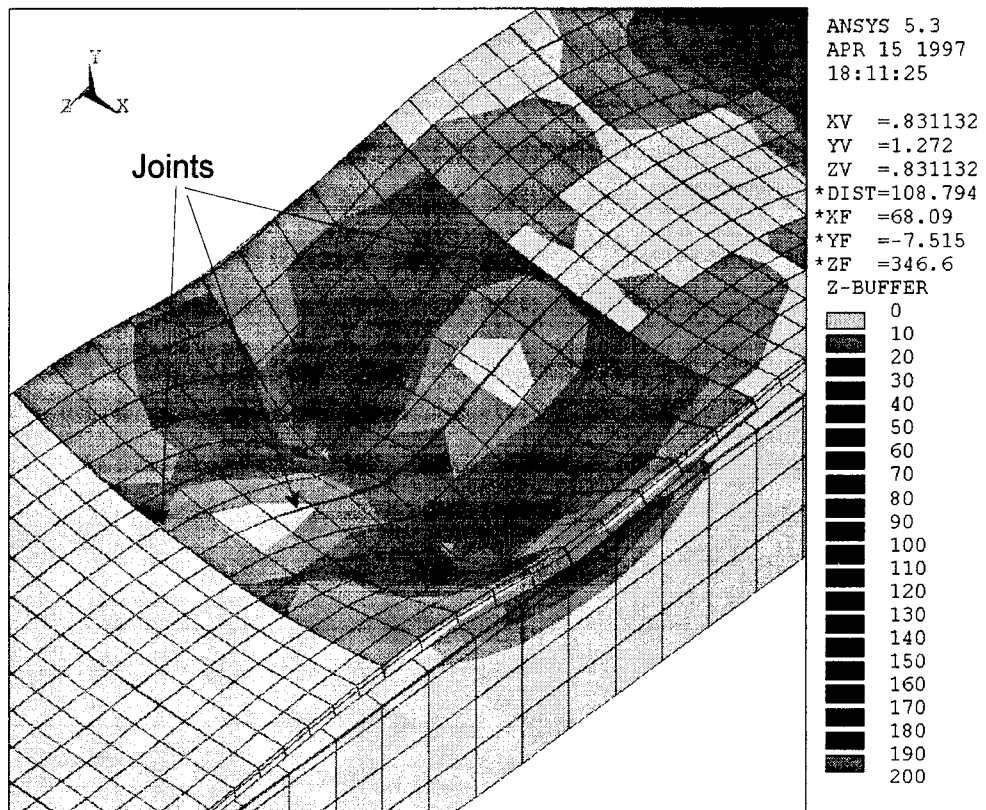


Figure 4.85 Stress Distribution At the Middle Section.

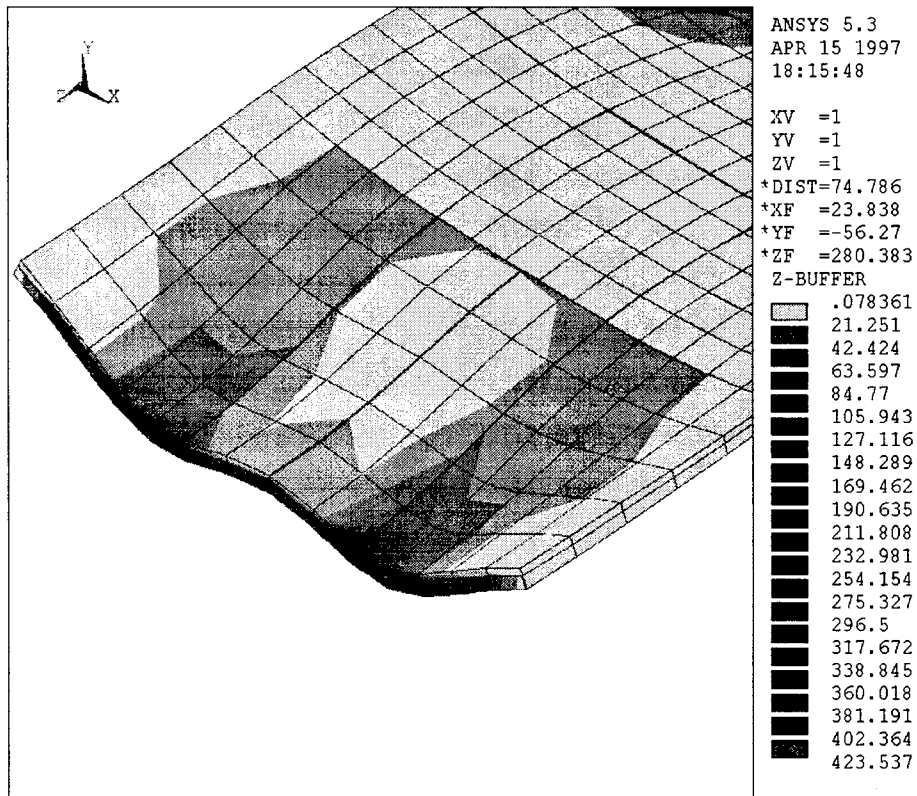


Figure 4.86 Stress Distribution in The Concrete Overlay at The Middle Section

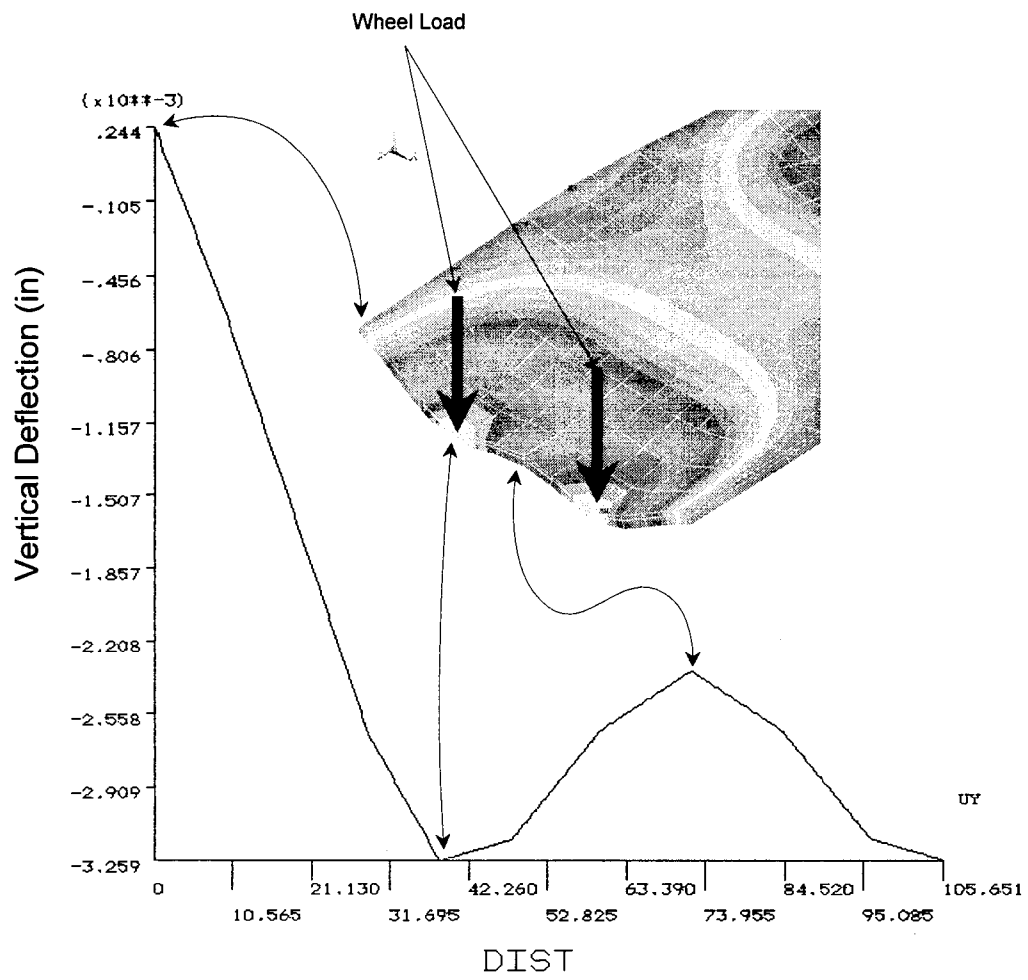


Figure 4.87 Vertical Deflection at The Middle Section Underneath The Middle Tandem

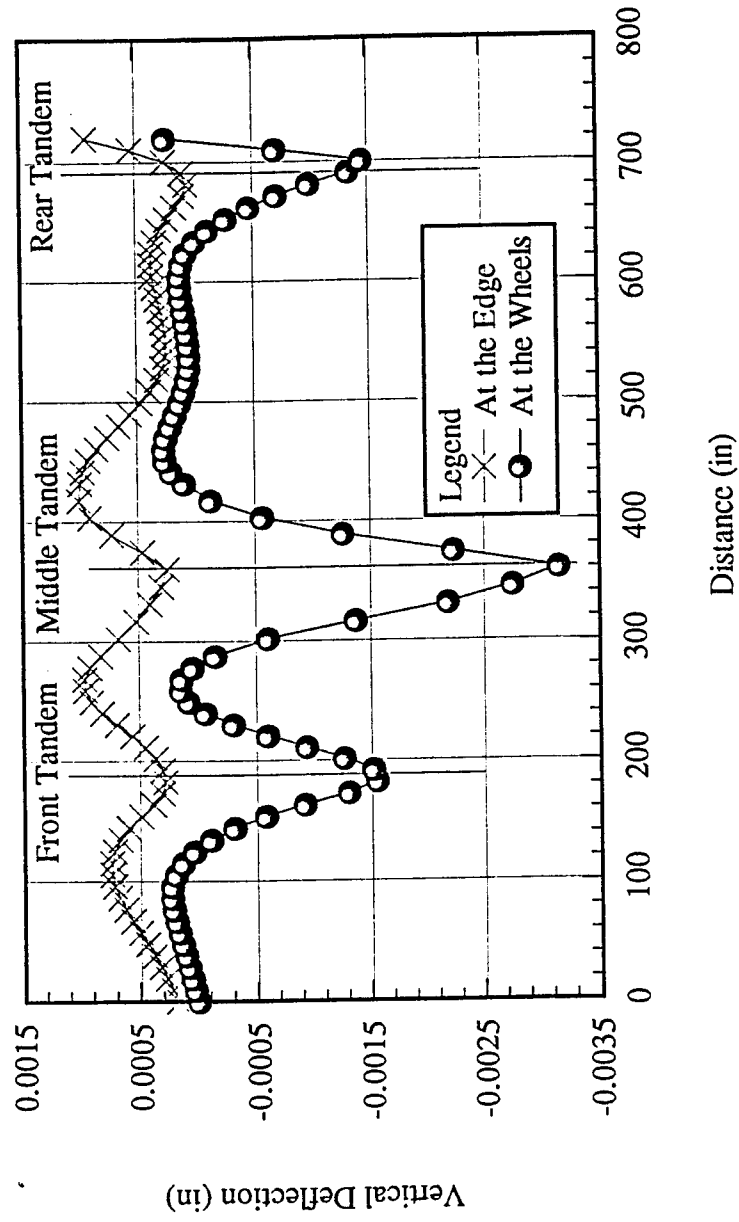
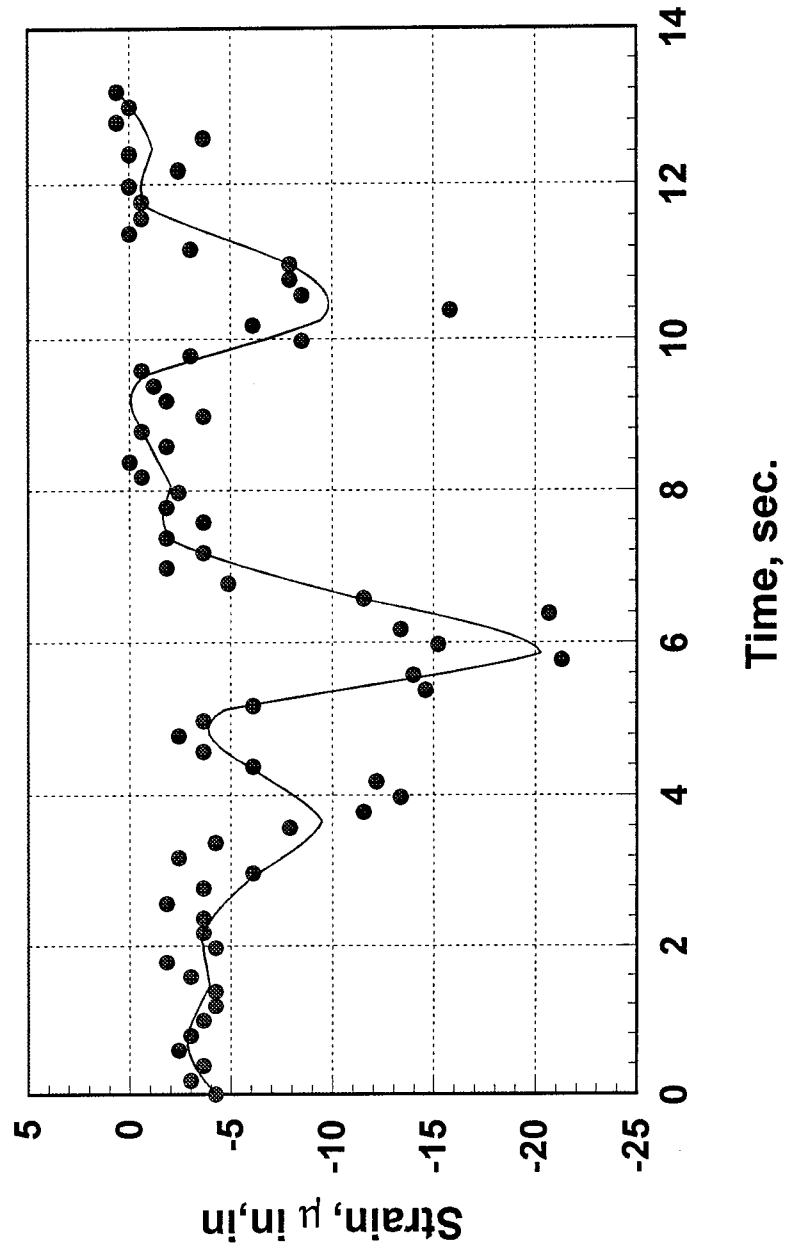


Figure 4.88 Vertical Deflection Along the Pavement From Finite Element Analysis

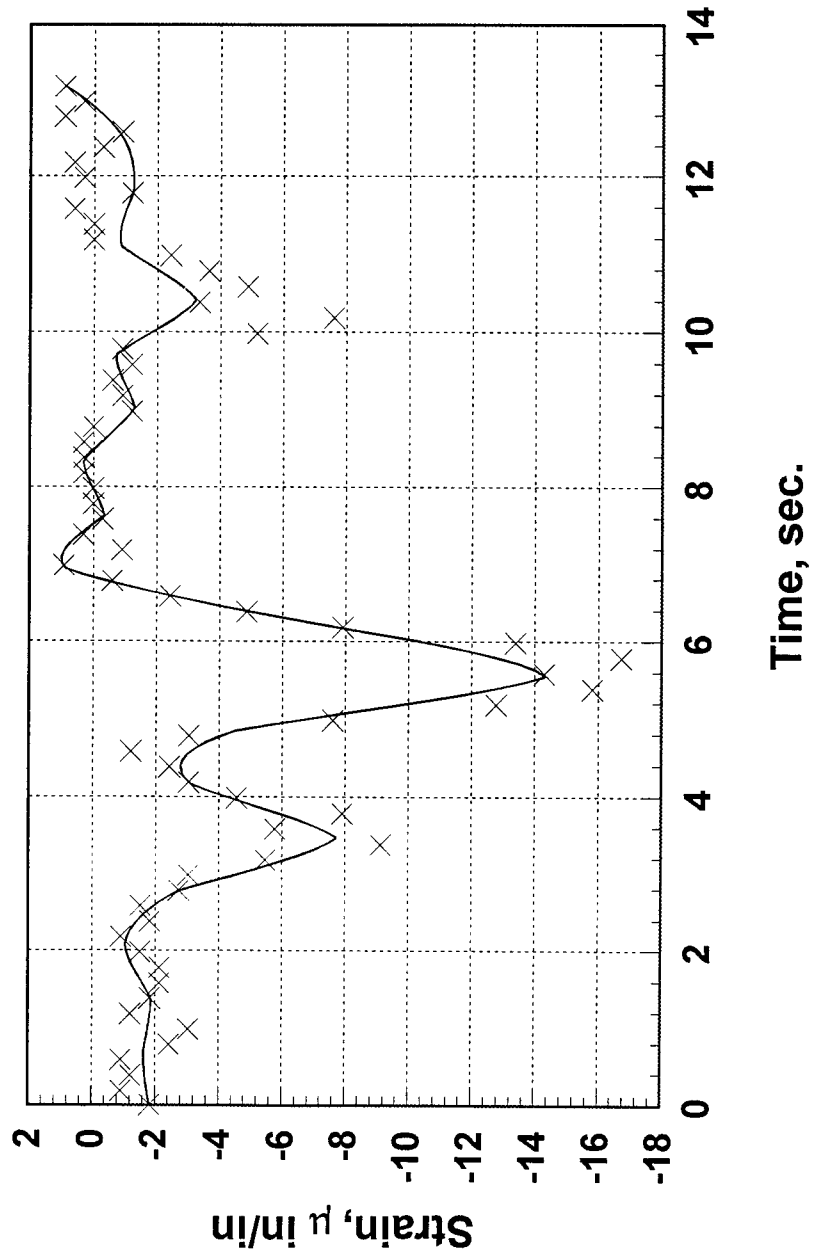
# Test Track #1 Strain vrs. Time



Pass #2  
Gage #1  
Slab C (6' x 6')

Figure 4.89 Strain Results from Strain Gage #1

**Test Track #1  
Strain vrs. Time**



**Figure 4. 90 Strain Results from Gage #2**



## Vertical Middle Span Deflection

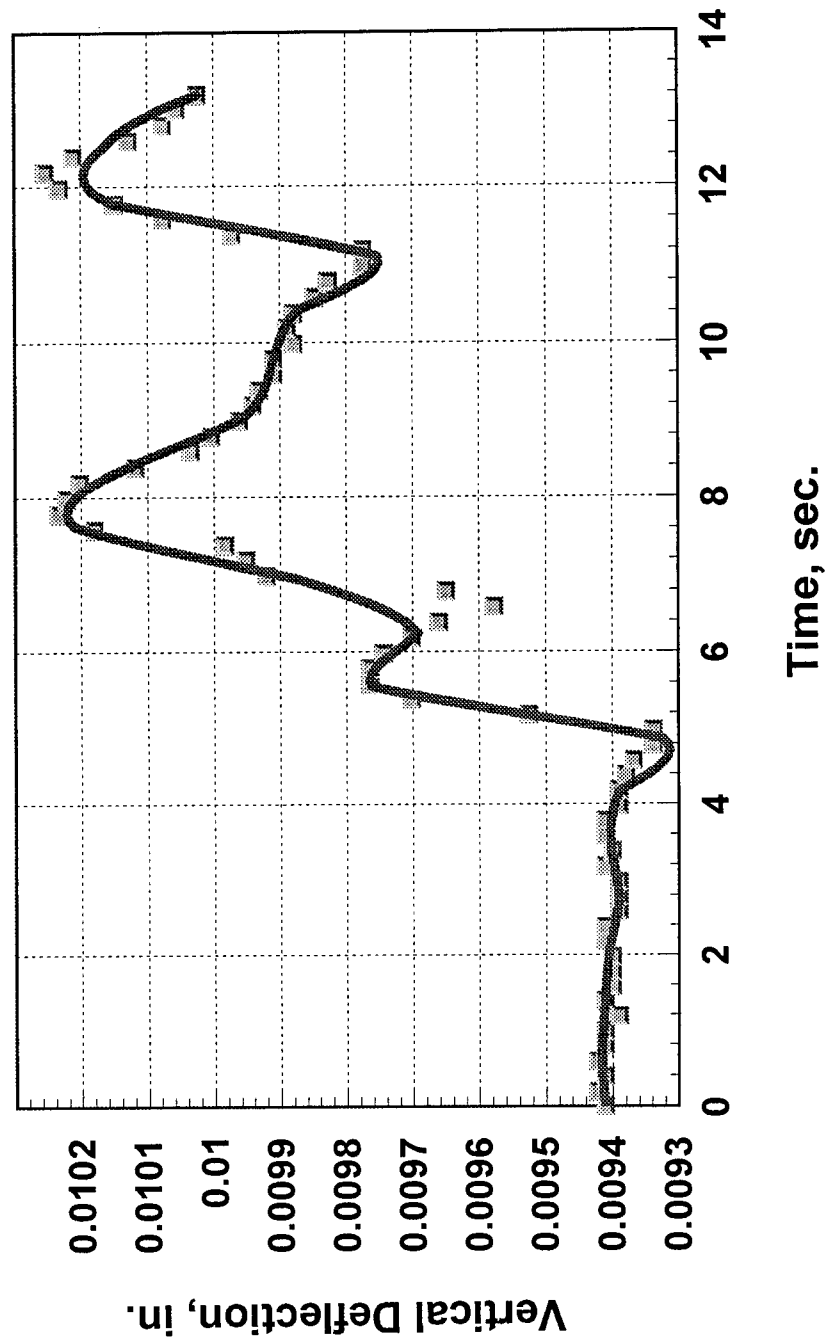
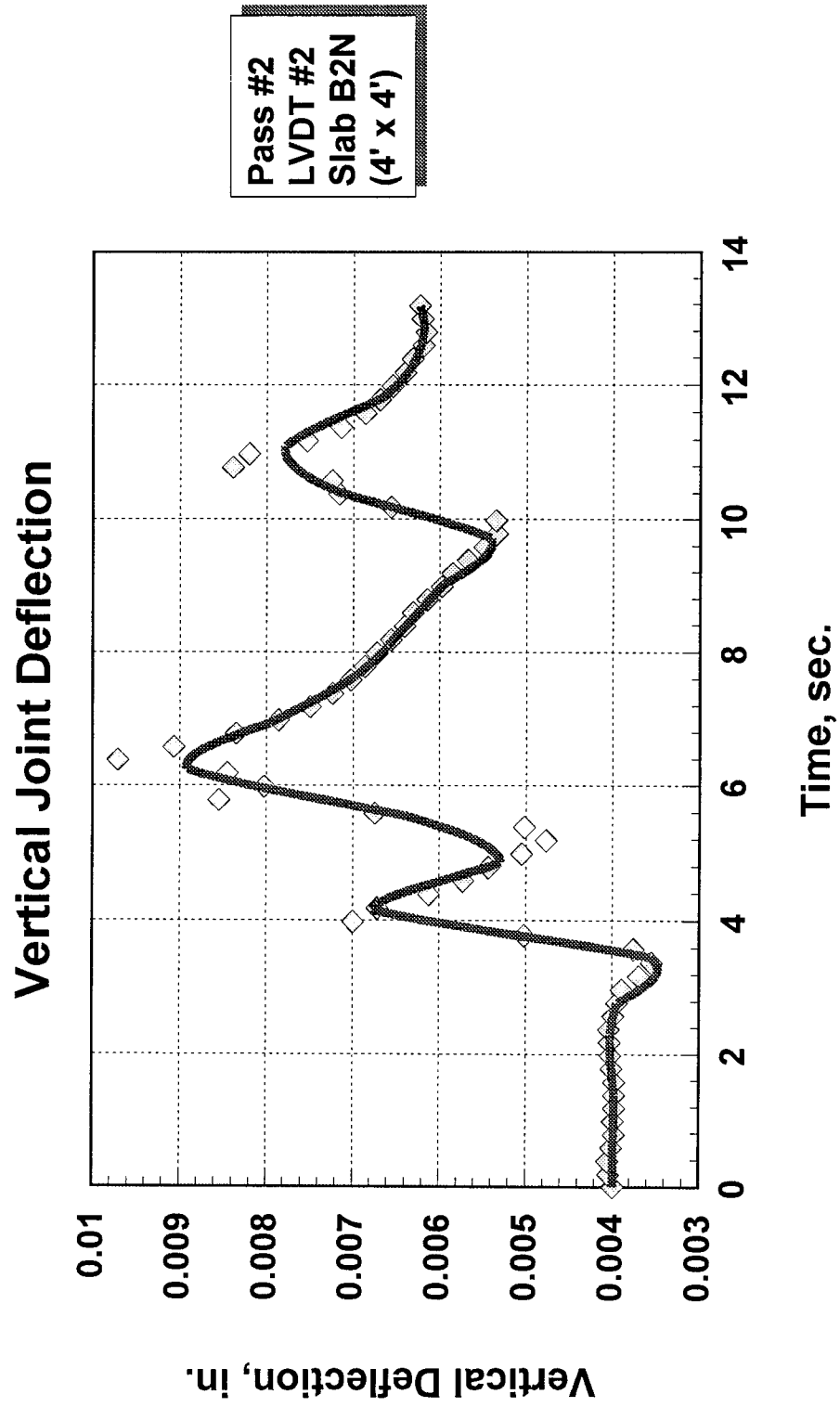
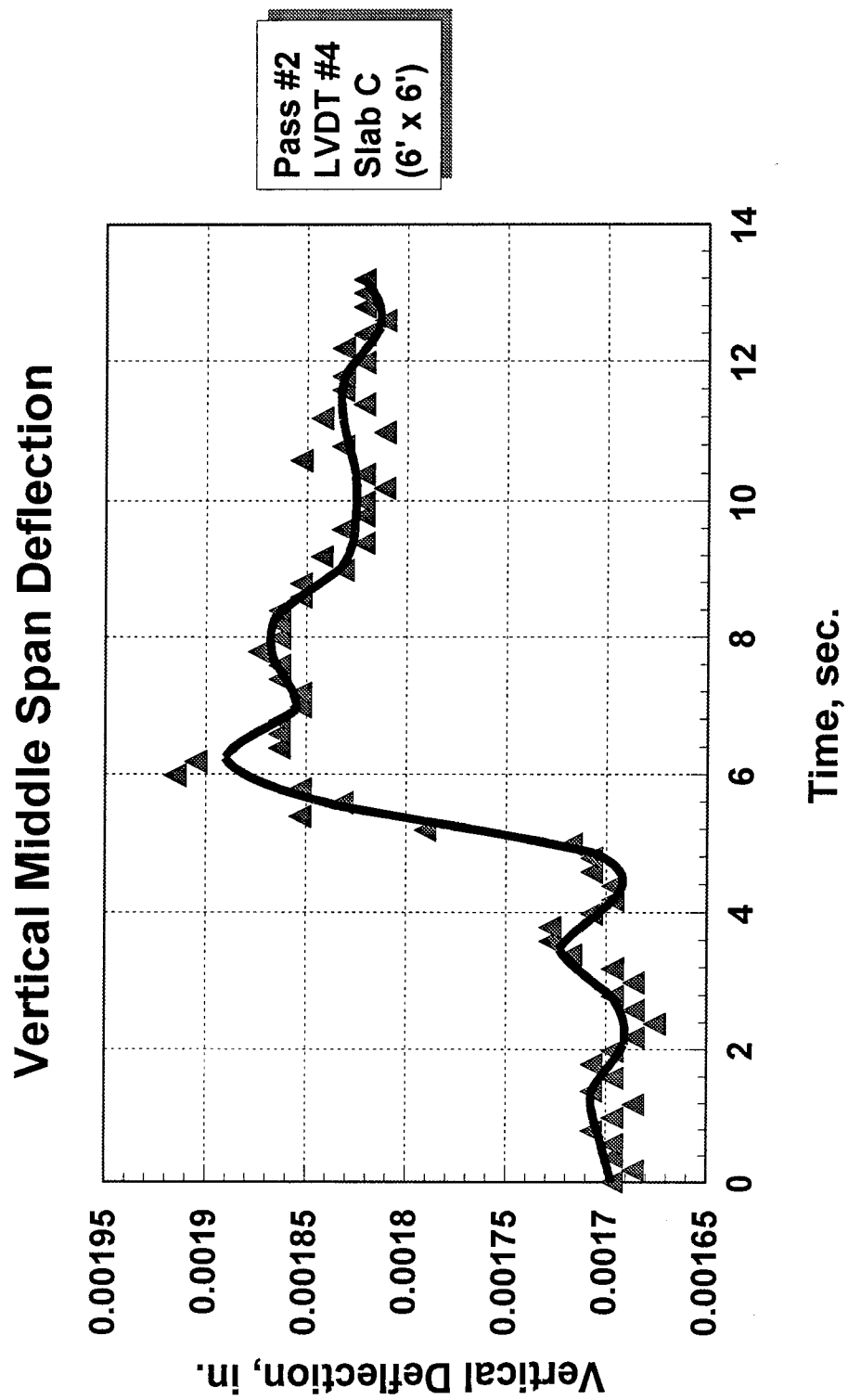


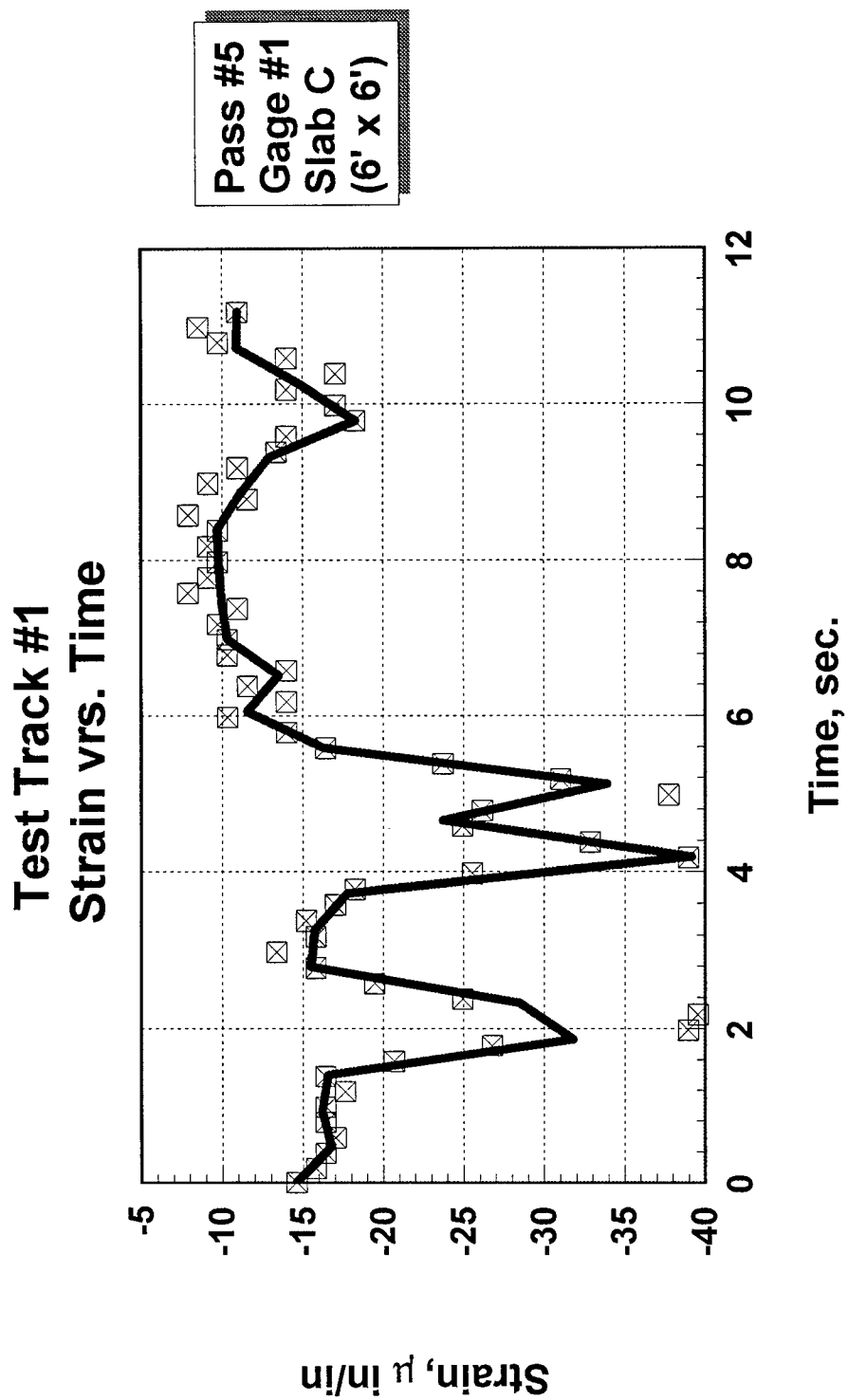
Figure 4.91 Vertical Deflection at Middle Span



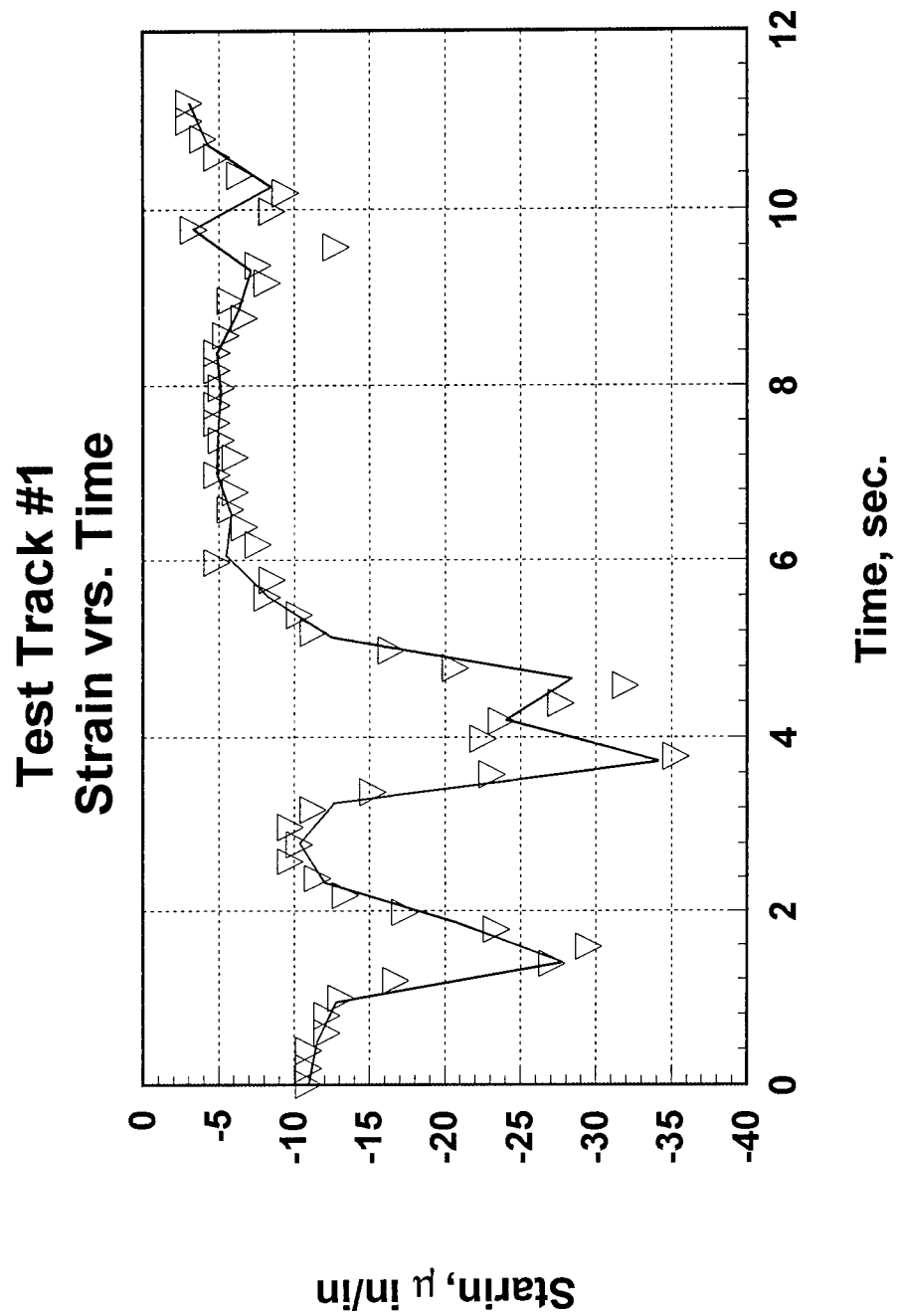
**Figure 4. 92 Vertical Deflection at Joint**



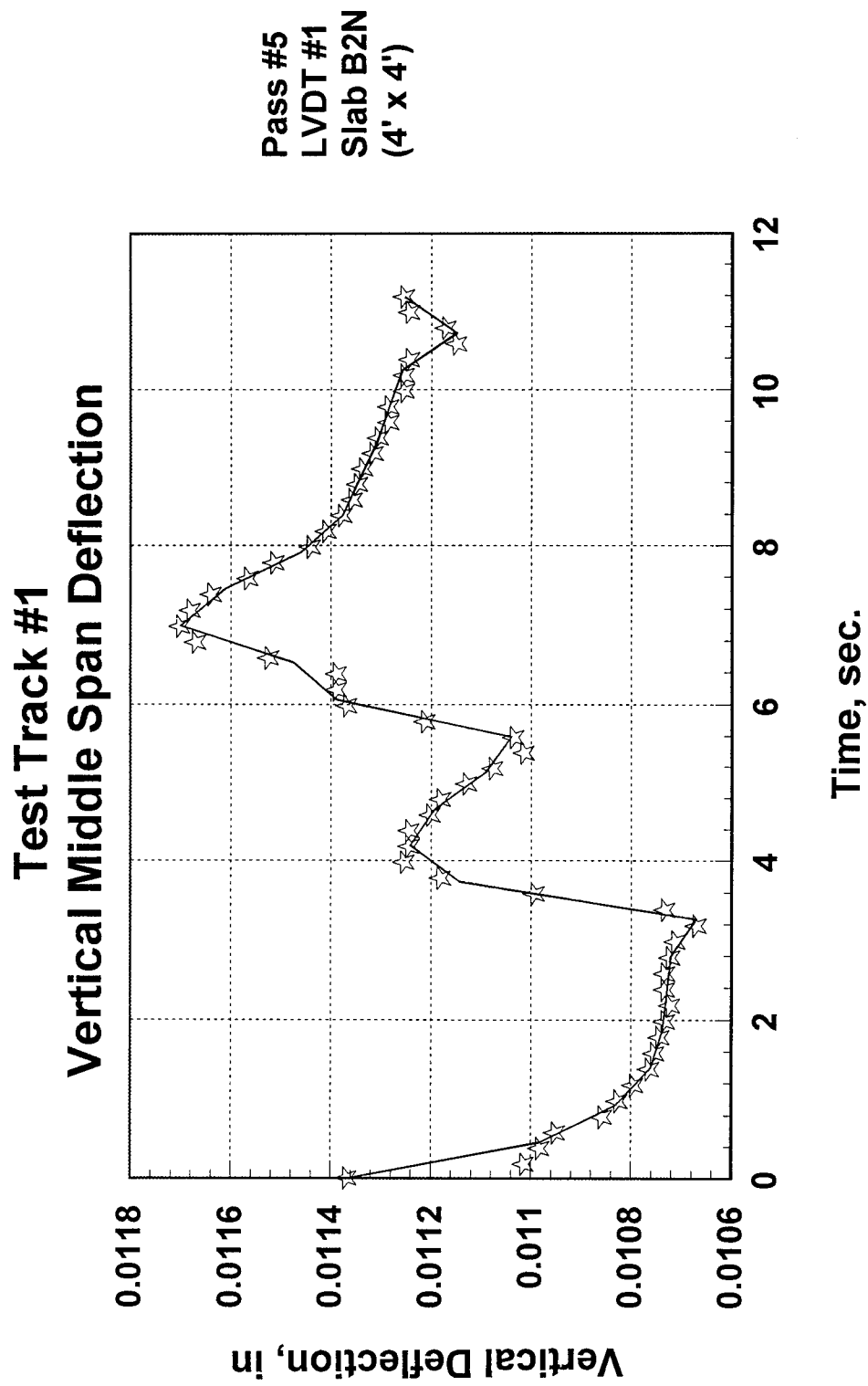
**Figure 4.93 Vertical Middle Span Deflection**



**Figure 4.94 Strain Results from gage #1**



**Figure 4.95 Strain Results from Gage #2**



**Figure 4.96 Vertical Deflection Obtained From LVDT #1**

# Test Track #1 Vertical Joint Deflection

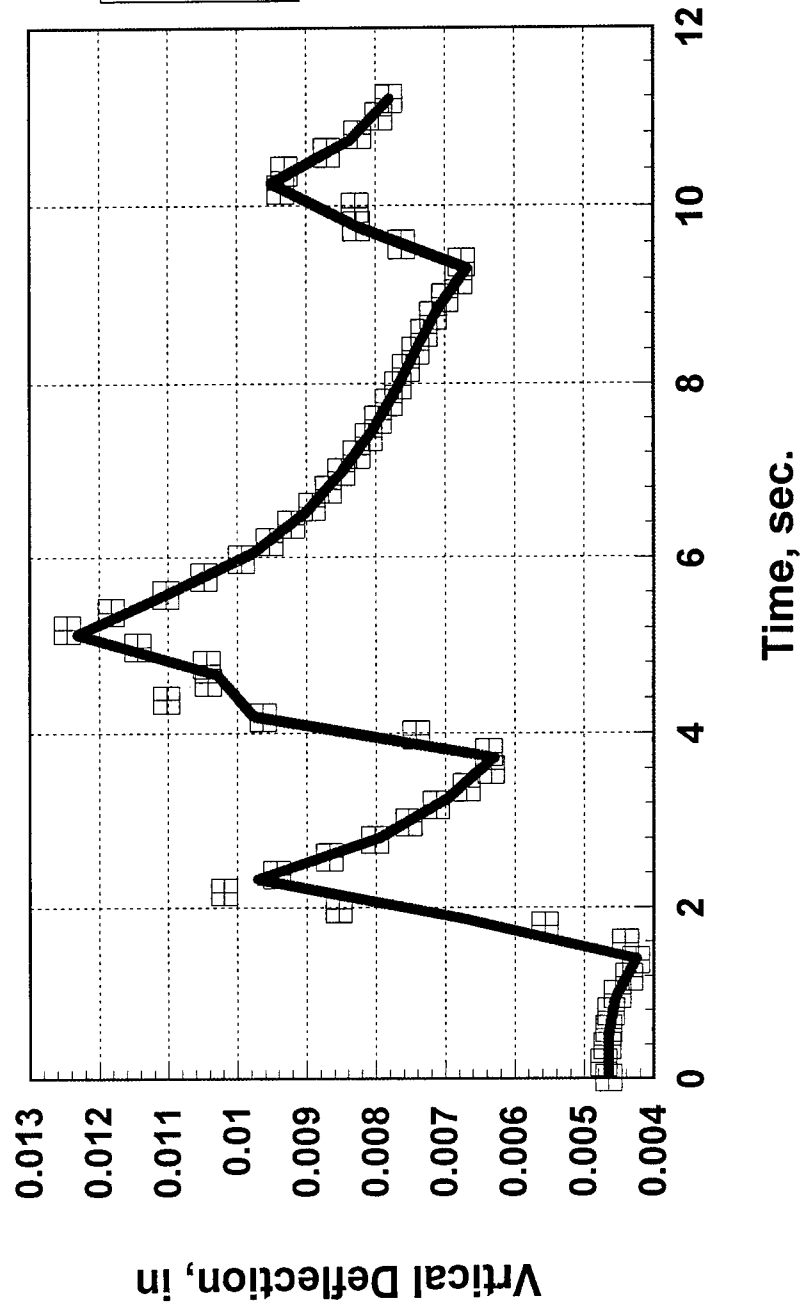


Figure 4.97 Vertical Joint Deflection from LVDT #2



Figure 4.98 Fiber Reinforced Concrete placing over Crack Relief Layer.



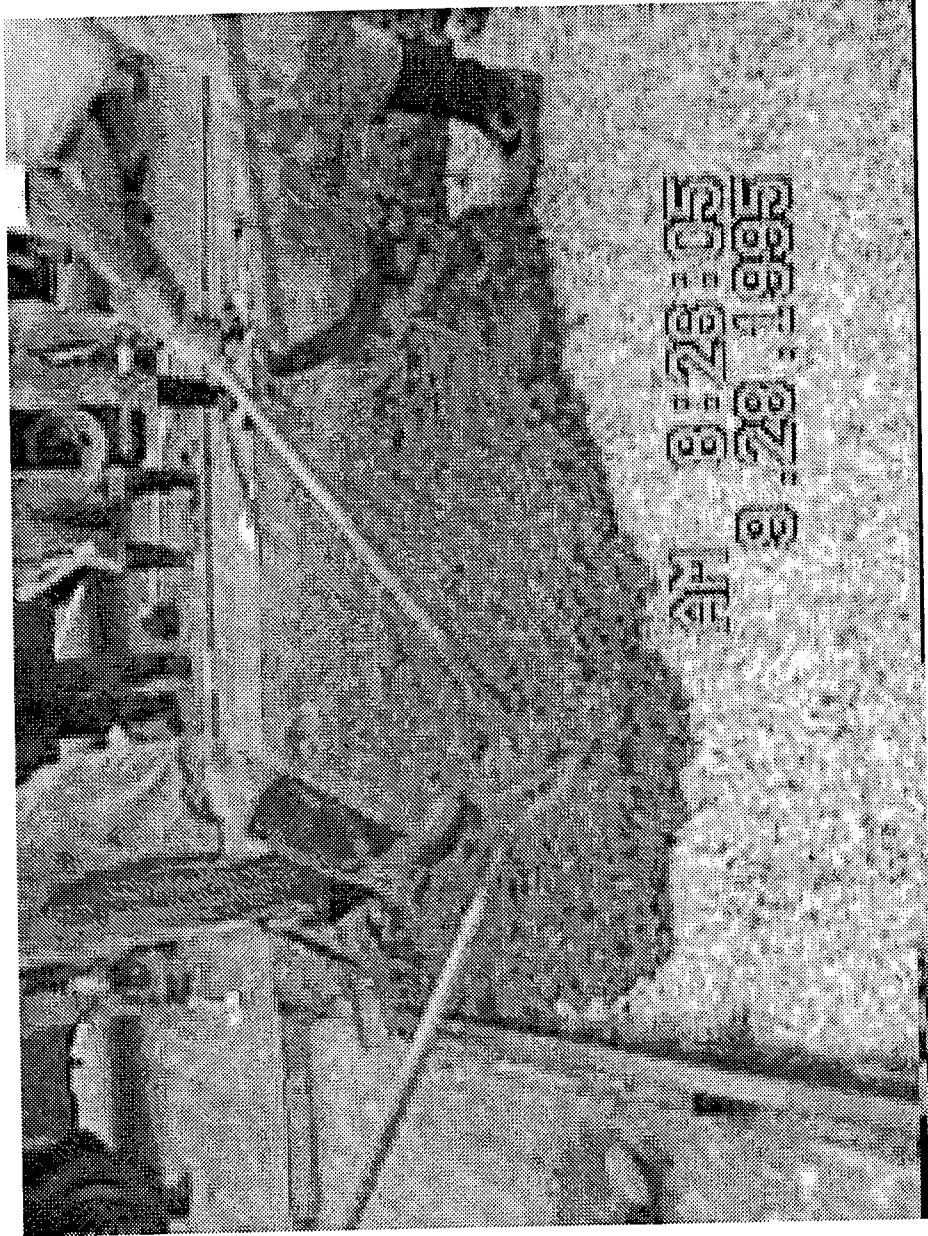


Figure 4.99 Placing of Plain Concrete



Figure 4.100 Preparation of Control Ultra-Thin Concrete Slab



Figure 4.101 Screeding of Fiber Reinforced Concrete

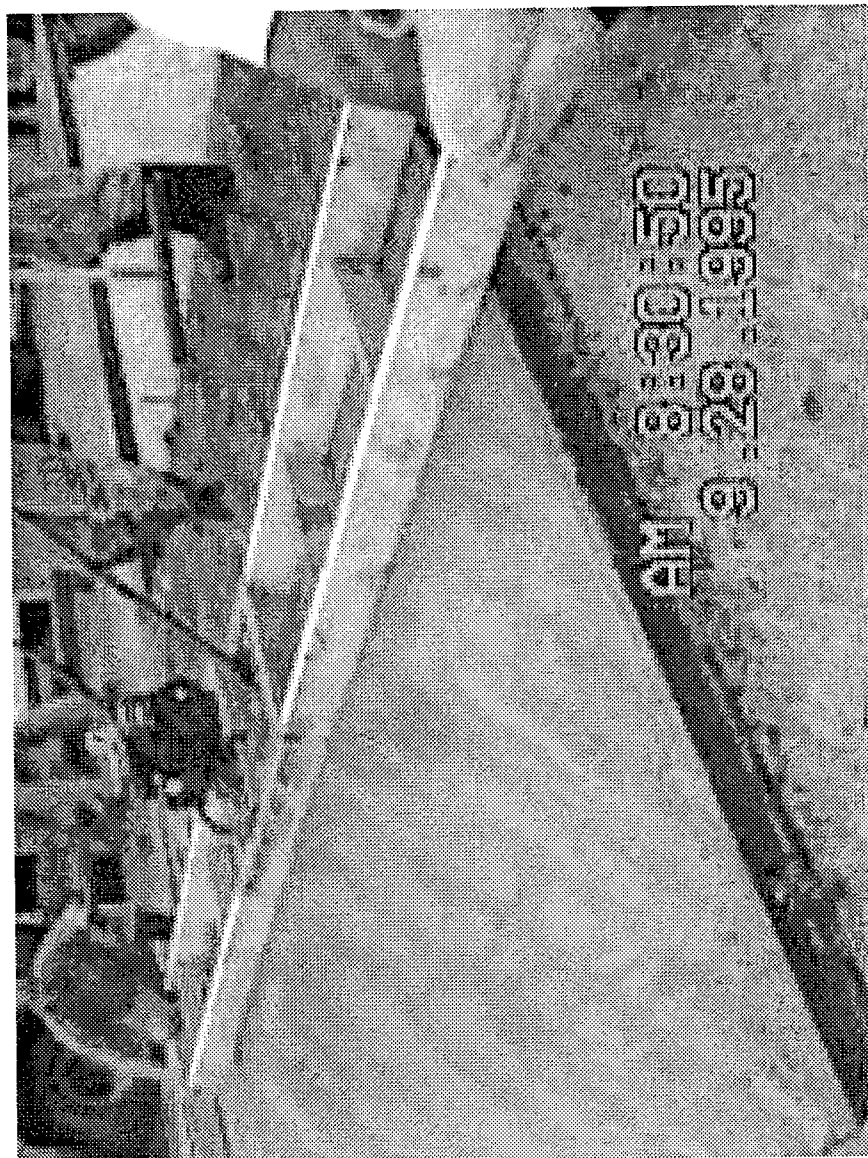


Figure 4.102 Screeding of Fiber Reinforced Concrete





Figure 4.103 Ultra-Thin Pavement Overlay Surface Finishing using Manual Floats

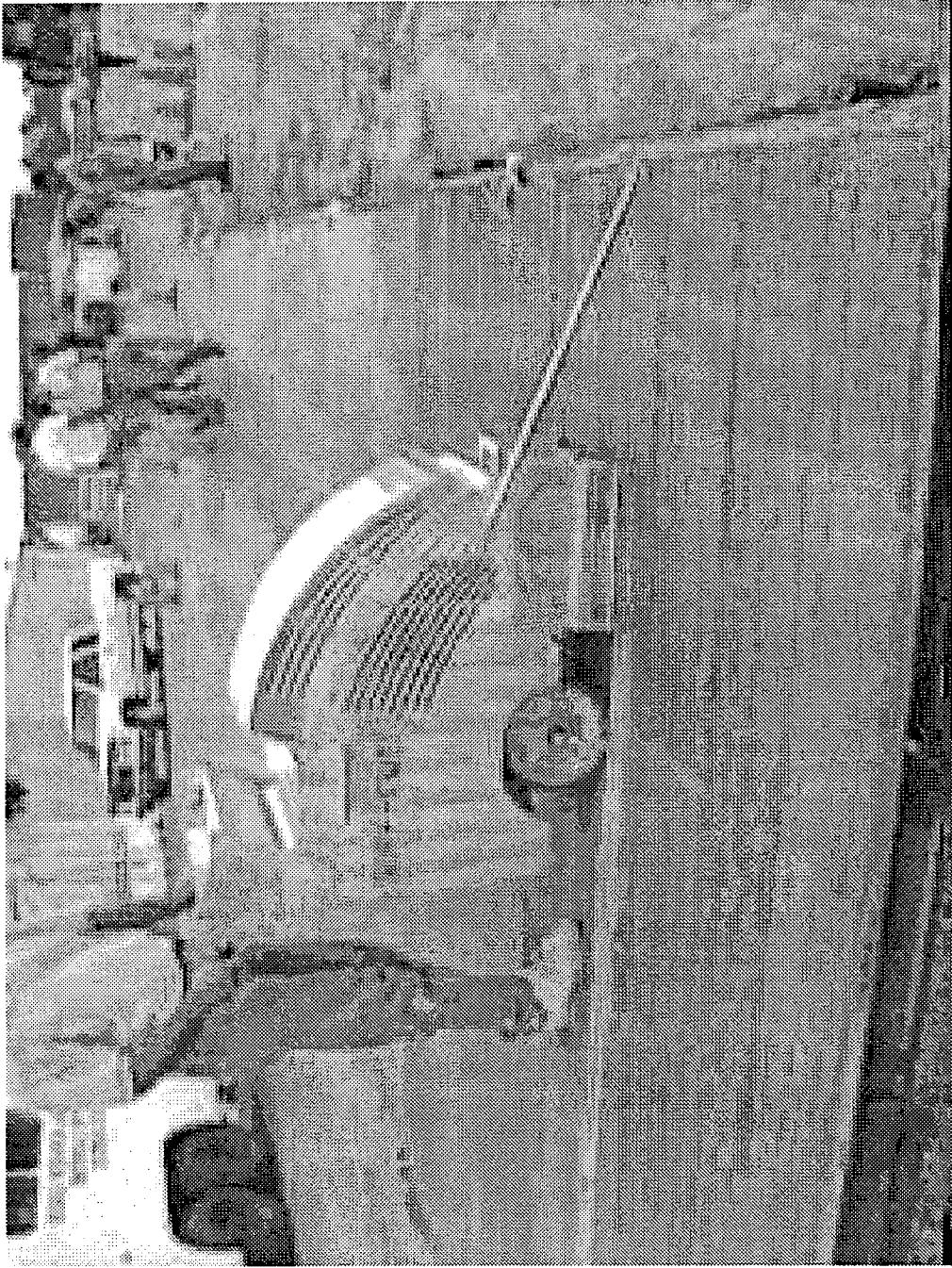


Figure 4.104 Joint Cutting 8 Hours After Placing Concrete

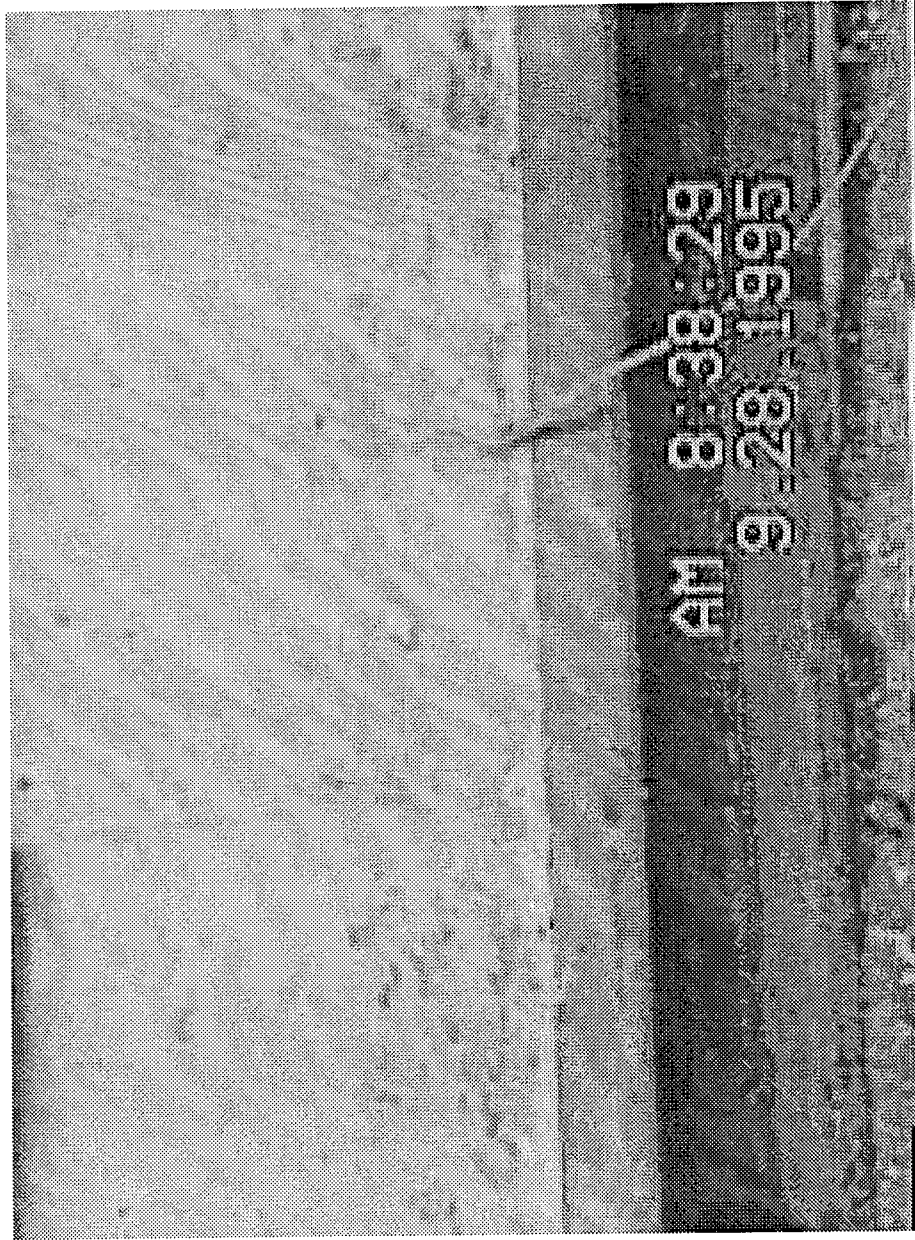


Figure 4.105 Ultra-Thin Pavement Top View and Thermocouple Leadwire

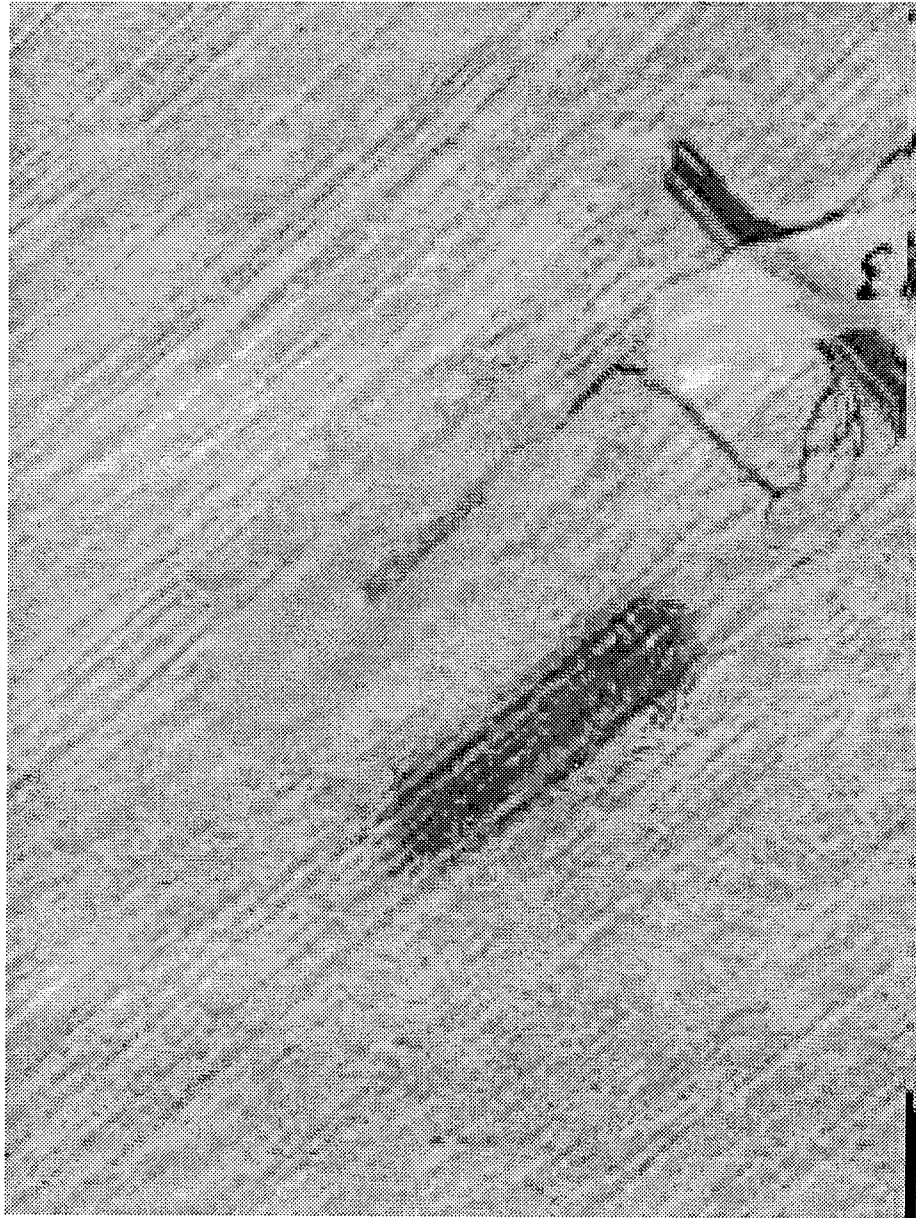


Figure 4.106 Instrumentation of Ultra-Thin Surface using Strain Gauges



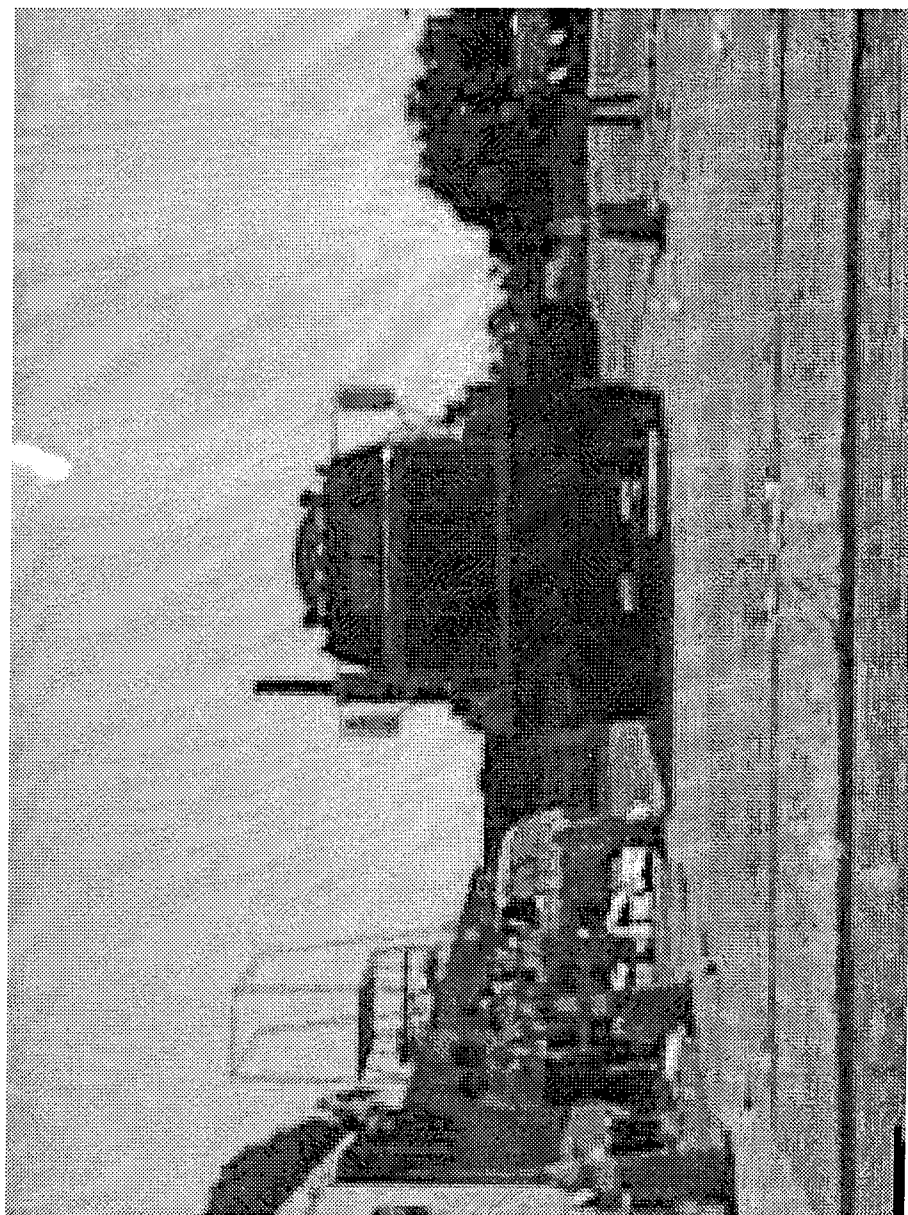


Figure 4.107 Ultra-Thin Pavement Loading using a 20-Kip per Axle Truck

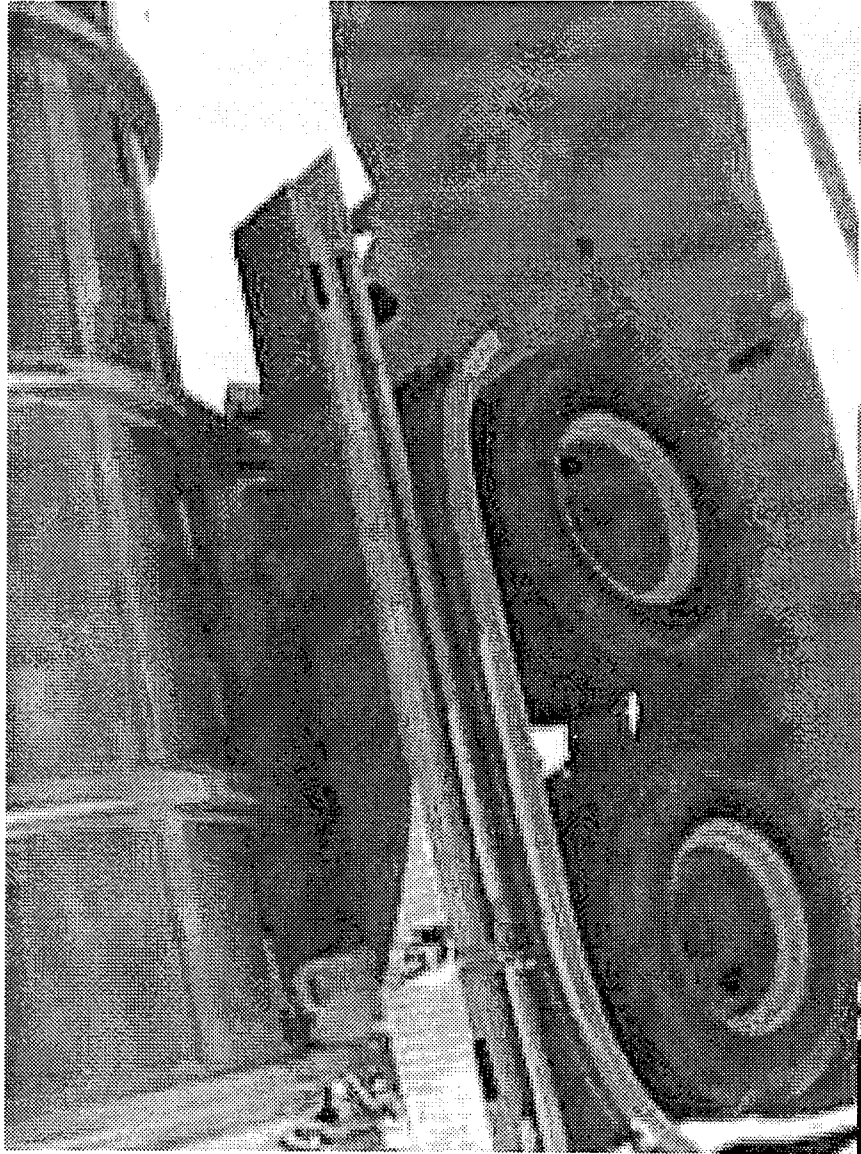


Figure 4.108 Truck Loading Overlay Pavement and Outside Strain Gauge

## **CHAPTER V**

### **CONCLUSIONS AND RECOMMENDATIONS**

#### **5.1 Conclusions:**

The use of plastic fiber as secondary concrete reinforcement has been study in the different stages of concrete preparation, from the fresh concrete properties to the study of static and dynamic properties of hardened concrete. The different plastic properties were presented and the different composite material properties were analyzed using finite element methods. Based on the experimental investigation and analysis, the following conclusions can be made:

1. The workability of fresh fiber reinforced concrete using polypropylene monofilament and collated fibrillated fibers, polyolefin monofilament fibers and post-consumer in-house made recycled polyethylene teraphthalate fiber at the manufacturers recommended ratios is satisfactory.
2. During the mixing process, there was no balling present when using vertical rotation standard drum mixers. Problems with fiber floating on the concrete mix are likely to happen when using horizontal rotation mixers (pan mixers).
3. The amount of water reaching the surface (bleeding ) on the fiber reinforced concrete using virgin and recycled fibers was reduced as well as the amount of aggregate segregation.

4. The addition of fibers did not produce significant changes on the static modulus and compressive strength of the concrete.
5. The tensile strength was improved up to 30 % when using polyolefin monofilament fibers, and increased by 8 to 10% when using collated fibrillated fibers as compared to plain concrete.
6. The flexural strength was improved by 8% when using recycled post-consumer products, and residual strength of up 15 to 25% of the ultimate load were shown.
7. The post-crack energy absorption capacity was increased with the use of fibers. In addition, the failure mode was changed from a brittle failure to a more ductile failure, that is a non-catastrophic failure, in contrast to the catastrophic failure observed in the plain concrete.
8. The fiber-reinforced concrete presented lower strain rate at the initial stage and after load developed, indicating a longer span of the life of concrete.
9. The crack arresting capabilities were proven by the fiber throughout the different crack patten obtained. Plain concrete had an immediate failure, showing a vertical crack pattern, opposite to the alligator crack pattern seen in fiber-reinforced concrete.
10. Fiber reinforced concrete withheld the peak static load for about five to ten seconds before failing in a ductile and non-shattered manner.
11. Three stages were clearly observed during the static testing of fiber reinforced specimens. Crack initiation, **Stage I**, Crack propagation, **Stage II**, and Rapid crack propagation or **Stage III**. The first stage lasted from 0 to 40%, 40 to 90% and 90 to 100% for the cycles to failure were endure by each stage , respectively.

12. Increase in strain was observed as the maximum stress ratio  $S$  decreased. This explains the ductility added to the concrete by the addition of fibers.
13. The cyclic test showed three cracking stages similar to the stages observed in the static test. The addition of fibers clearly marks the delay of crack initiation. This stage initiates as the load is being applied the strain rate increases and stables before changing to the second stage. The first stage was delay up to 20% compared to 6% maximum for the plain concrete. The second stage was greatly improved by the fiber reinforced concrete, by extending this stage from 18% to 90%. Plain concrete extended this stage only up to 80% of the cycles to failure, therefore showing a 10% deficit when compared to the fiber reinforced concrete. The last stage was the shortest of all for both the fiber reinforced concrete and plain concrete. The mode of failure was not catastrophic for the fiber reinforced concrete when compared to the plain concrete.
14. High stress ratio and low compressive strength showed an earlier transition from one cracking stage to the other except when the stress ratios were below 55%.
15. The rate of stiffness degradation was higher for plain concrete during the different stages, this is observed when compared to fiber reinforced concrete.
16. The fiber reinforced concrete always presents higher endurance to failure than plain concrete when using the Wholer diagrams or S-N curves .
17. The crack arresting capabilities of fiber will help to delay severance of cracking, which from an structural point of view, would allow enough time for taking corrective measures , in contrast to the sudden and catastrophic failures present by plain concrete.
18. The three-dimensional finite element models used to simulated fiber reinforced concrete

failure using ASTM 1018 standards can be used to further analyze the cumulative damage and fatigue failure of concrete, since the results were in close agreement with the laboratory work.

19. Fiber orientation has a big effect on the composite mix as concluded from the finite element analysis. The fibers oriented parallel to the axis of bending have the best orientation. This orientation showed the best strength resistance, lowest deflection and best residual strength as well as the lowest strain at any given time.
20. Fiber failure , as indicated by the electron scanning microscopy, is due to fiber pullout and fiber failure in tension. The fiber ends showed an abruptness of the fiber which reflects that the load has been properly transferred from the concrete matrix to the fiber after concrete has failed. The surface of the fiber present calcium formations which are also assumed to help decrease the bond strength between the concrete and the fiber.
21. The pavement overlay have performed well after 20,000 cycles. Almost no cracking has been observed after four month of daily loading with a 20-kip per tandem truck.

As a final conclusion, if fatigue crack formation is consider detrimental to concrete structures, then fiber reinforced concrete should be used instead for its ability to delay crack initiation and prolong the crack propagation interval. Furthermore, the crack arresting capabilities of fibers help to change the failure mode from a catastrophic mode to a more ductile non-shattered failure which will always allow for enough time to take the corrective measures when compared to the sudden, catastrophic failure of plain concrete. Finally, the addition of fiber will always translate into a net increase in cyclic strength and higher

structural strength which will give in the long term, better ductility and durability capabilities to concrete structures.

## **5.2 Recommendations**

This report was elaborated with the purpose of evaluating the fresh and hardened properties of concrete. The main scope was the evaluation and analysis of single-edge-notched beam under constant amplitude loading, followed by an analysis using finite element methods. Based on the findings of this study the following recommendations are presented:

1. The use of fiber reinforce concrete can be recommended for use in pavement construction which is subject to cyclic loading, therefore it would benefit from the net increase in cyclic strength to the concrete.
2. In the analysis and design of concrete structures subjected to fatigue loading conditions, it is advisable not to identify the last stage of cracking (STAGE III) and omit it from the prediction of useful fatigue life of the concrete. This recommendation is based on the fact that concrete micro cracks have already been developed in Stage I and Stage II. The third stage would be useless when adding the effect of the surrounding environment and the possibility of accelerating the deterioration of concrete due to cracking , and therefore this stage should not be included in the final fatigue analysis that use the S-N relationship.
3. The addition of fiber will help to reduce and change the failure modes of plain concrete strength which do fail in a catastrophic and abrupt manner.
4. The use of super plastizicer is needed to obtain a good workability without changing

the water-cement ratio of the mix.

5. The use of pan mixer should be avoided since the specific gravity of the fiber is lower than water, hence floatation of the fiber may be a problem. Use of vertical or standard mixer which rely on gravity mixing should be used.
6. Chemical surface treatment of the fibers should be study to improve the strength of the fiber to matrix bond.
7. The decrease in slump with the use of fiber, should not indicate a loss of workability in the concrete. The decrease in slump is due to the random orientation of the fibers giving fresh concrete a stiffer matrix as the end-product, and therefore a slump reduction which is not representative of the W/C ratio.
8. Equations 4-6 to 4-8 should be used to predict the fatigue life of fiber reinforced concrete subject to constant cyclic loading.
9. The use of recycled post-consumer plastic would produce fiber of equal of better quality than virgin plastics if fibers are produced with better and more modern manufacturing process. The spiral shape should be maintained to improve the strength of the mechanical bonding of the fiber to the concrete.
10. The finite element model prepared in this research should be used to produce concrete pavement analysis under the effect of changing temperature and varying cyclic loading. Furthermore, the debonding and stress analysis of the bonding layers can be performed.



## REFERENCES

1. ACI Committee 215, "*Considerations for Design of Concrete Structures Subjected to Fatigue Loading*," Detroit, Michigan, ACI 215R-74, Revised 1986.
2. ACI Committee 544, "*Measurements of The Properties of Fiber Reinforced Concrete*," (ACI 544-2R-88), American Concrete Institute, Detroit, 1988, pp 329-341.
3. Alliche, A. Francois, D., "*Fatigue Damage of Concrete*," Edited by Shah, S. P. And Swartz, S.E. during SEM-RILEM International Conference on Fracture of Concrete and Rock, June 1987, pp. 88-95.
4. Alwahab, R., and Soroushian, P., "*Characterization of Collated Fibrillated Polypropylene Fibers and Their Application to Concrete*," Report submitted to the College of Engineering, Michigan State University, Dec. 1987, 61 pp.
5. Antrim, J. D., "*The Mechanics of Fatigue in Cement Paste and Plain Concrete*," A Symposium on Concrete Strength, Highway Research Record, National Research Council, 46th Annual Meeting, Jan. 1967.
6. Aziz, R.J., "*Strains and Failure of High-Strength Concrete Under Various Combinations of Sustained and Cyclic Overloads with Comparison to Lower-Strength Concretes*," Ph. D. Dissertation, Cornell University, May 1987.
7. Beaudion, J.J, *Handbook of Fiber Reinforced Concrete*, Noyes Publications, New Jersey, 1990, 332 pp.
8. Bentur, A. And Mindness, S., *Fibre Reinforced Cementitious Composites*, Elsevier Applied Science, New York, 1990, 449 pp.
9. Binsheng, Z., Zhaohong, Z. And Keru, W., "*Fatigue Rupture of Plain Concrete Analyzed by Fracture Mechanics*," Edit by Shah, S.P. and Swartz, S.E. during SEM-RILEM International Conference on Fracture of Concrete and Rock, June 1987, pp 58-63.
10. Brown, W.F. and Strawley, J.E., "*Plain Strain Crack Toughness Testing of High Strength Metallic Materials*," STP 410, ASTM, Philadelphia, 1967, pp 13-14.
11. Do, M.T., Chaallal, O., and Aitcin, P.C., "*Fatigue Behavior of High-Performance Concrete*," Journal of Materials in Civil Engineering, Vol. 5, No. 1, February, 1993, pp 96-111.
12. Espiritu, E., "*Fatigue Strength of Concrete Under Constant Cyclic Loading*," M.S.

Thesis, Florida State University, 1993.

13. Fahmy, M.F. and Lovata, N.L., "Chemical Treatments of Polypropylene Fiber Surfaces Used in Fiber Reinforced Concrete," TRB, No. 1226, 1989, pp 31-35.
14. Galloway, J.W. and Raithby, K.D., "*Effects of Rate of Loading on Flexural Strength and Fatigue Performance of Concrete*," Transport and Road Research Laboratory Report LR 547, 1973.
15. Goldfein, S., "*Plastic Fibrous Reinforcement for Portland Cement*," Technical Report # 1757-TR, U.S. Army Engineer Research and Development Laboratories, Fort Belvoir, Virginia, October 1963, 19 pp.
16. Grzybowski, M. And Meyer, C., "*Damage Accumulation in Concrete With and Without Fiber Reinforcement*," ACI Materials Journal, November-December 1993, pp 594-604.
17. Hilsdorf, H.K. and Kesler, C.E., "*Fatigue Strength of Concrete Under Varying Flexural Stresses*," ACI Journal, Vol. 63, No. 10, Oct. 1966, pp 1059-1075.
18. Holmen, J.O., "*Fatigue of Concrete by Constant and Variable Amplitude Loading*," ACI, SP 75-4, 1982, pp 71-110.
19. Hsiang, W. B., "*Behavior of High-Strength Concrete Subjected to Cyclic Overloads*," Ph. D. Dissertation, Cornell University, 1986.
20. Hsu, T.C., "*Fatigue of Plain Concrete*," ACI Journal, Vol. 78, No. 4, July-Aug. 1981, pp 292-305.
21. Jeng, Y., and Shah, S.P., "*Two Parameter Fracture Model for Concrete*," Journal of Engineering Mechanics, ASCE, Vol. 111, No. 10, Oct. 1985, pp 1227-1241.
22. Johnston, C.D., "*Steel Fiber and Plain Concrete: Factors Influencing Flexural Strength Measurement*," ACI Journal, March-April 1982, pp 131-138.
23. Kelly, J. W., "*Cracks in Concrete: Part I and II*," Concrete Construction, Vol. 26, No. 9, September 1981, pp 725-734.
24. Kesler, C. E., "*Effect of Speed of Testing of Flexural Fatigue Strength of Plain Concrete*," Proceedings, Highway Research Board, Vol. 32, 1953, pp 251-258.
25. Klaiber, F.W. and Lee, D.Y., "*The Effects of Air Content, Water-Cement Ratio and Aggregate Type on the Flexural Fatigue Strength of Plain Concrete*," Fatigue of

Concrete Structures, Publication SP-75, ACI, Detroit, 1982, pp 111-131.

26. McCall, J.T., "***Probability of Fatigue Failure of Plain Concrete,***" ACI Journal, Vol. 55, No. 2, Aug. 1958, pp 233-243.
27. Mindness, S., Lawrence, F.V., and Kesler, C.E., "***The J-Integral as a fracture Criterion for Fiber Reinforced Concrete,***" Cement and Concrete Research, Vol. 7, 1997, pp 731-742.
28. Morris, A.D., Garrett, G.G., "***A Comparative Study of the Static and Fatigue Behavior of Plain and Steel Fiber Reinforced Mortar in Compression and Direct Tension,***" Internal Journal of Cement Composites and Lighthweigh Concrete, Vol. 3, No. 2, may 1981, pp 73-91.
29. Naus, D.J. and Lott, J.L., "***Fracture Toughness of Portland Cement Concretes,***" ACI Journal, Vol. 66, No. 6, June 1969, pp 481-489.
30. Nordby, G.M., "***Fatigue of Concrete- A Review of Research,***" ACI Journal, Vol. 55, No. 2, Aug. 1958, pp 191-219.
31. Ople, F.S. Jr. and Hulsbos, C.L., "***Probable Fatigue Life of Plain Concrete with Stress Gradient,***" ACI Journal, Vol. 63, No. 1, Jan. 1966, pp 59-81.
32. Paramasivam, P., and Nathan, G.K., "***Study of Fiber Reinforced Concrete,***" First Australian Conference on engineering Materials, 1974, pp 333-350.
33. Ramakrishnan, V., "***Materials and Properties of Fiber-Reinforced Concrete,***" Civil Engineering, Vol. 58, No. 4, 1988, pp 29-40.
34. Ramakrishnan, V., Gollapudi, S., and Zellers, R., "***Performance Characterristics and Fatigue Strength of Polypropylene Fiber-Reinforced Concrete,***" Fiber Reinforced Concrete Properties and Applications, ACI Special Publication (SP 105-9), 1990, pp 159-177.
35. Shah, S.P., "***Fatigue Toughness of Cement-Based Materials,***" Edit by Shah, S.P. and Swartz, S.E. during SEM-RILEM International Conference on Fracture of Concrete and Rock, June 1987, pp 1-12.
36. Shah, S.P., "***Do Fibers Increase the Tensile Strength of cemented-Based Matrixes,***" ACI Materials Journal, Vol. 88, No. 6, 1991, pp 595-602.
37. Slate, F.O. and Hoover, K.C., "***Microcracking in Concrete,***" Fracture mechanics of

Concrete, Edit by Carpenteria, A. and Ingrassia, A.R., Nijhoff Publishers, 1984, pp 137-159.

38. ***"Student Manual For Strain Gage technology,"*** reprinted by Measurements Group, Inc., 1991.
39. Swamy, R.N., ***"Fiber-Reinforced Concrete: Mechanics, Properties, and Applications,"*** International Concrete Journal, Vol. 48, No. 1, January 1974, pp 7-16
40. Taylor, H.P.J., and Sharp, J.V., ***"Fatigue in Offshore Concrete Structures,"*** The Structural Engineer, Vol. 56A, No. 3, January 1974, pp 7-16.
41. Zonsveld, J.J., ***"Properties and Testing of Concrete Containing Fibers Other Than Steel,"*** RILEM Symposium on Fiber-Reinforced Cement Concrete, London, U.K., 1975, pp 217-226.